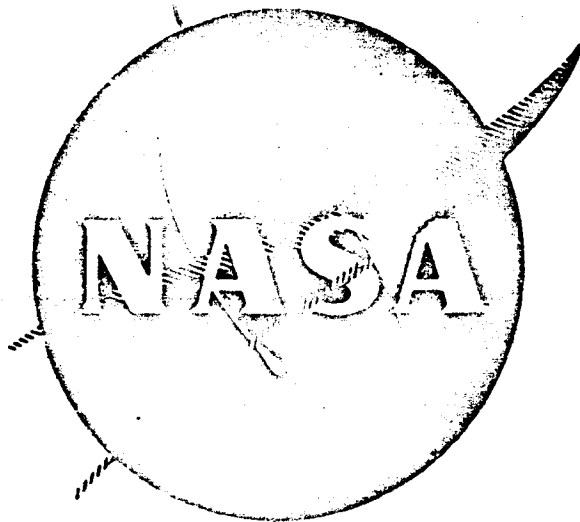


N67-13188



REPORT NO.

NASA-CR-54357

WESTINGHOUSE

WAED 66.11 E

DECEMBER 1965

DEVELOPMENT AND EVALUATION OF MAGNETIC AND ELECTRICAL MATERIALS CAPABLE OF OPERATING IN THE 800° TO 1600°F TEMPERATURE RANGE

Fourth Quarterly Report

by

P. E. Kueser et al

prepared for

NATIONAL AERONAUTICS AND SPACE ADMINISTRATION
LEWIS RESEARCH CENTER
UNDER CONTRACT NAS3-6465



Westinghouse Electric Corporation
AEROSPACE ELECTRICAL DIVISION
LIMA, OHIO

NOTICE

This report was prepared as an account of Government-sponsored work. Neither the United States nor the National Aeronautics and Space Administration (NASA), nor any person acting on behalf of NASA:

- A) Makes any warranty or representation, expressed or implied, with respect to the accuracy, completeness, or usefulness of the information contained in this report, or that the use of any information, apparatus, method, or process disclosed in this report may not infringe privately-owned rights; or
- B) Assumes any liabilities with respect to the use of, or for damages resulting from the use of any information, apparatus, method or process disclosed in this report.

As used above, "person acting on behalf of NASA" includes any employee or contractor of NASA, or employee of such contractor, to the extent that such employee or contractor of NASA or employee of such contractor prepares, disseminates, or provides access to, any information pursuant to his employment or contract with NASA, or his employment with such contractor.

AVAILABILITY NOTICE

Qualified requestors may obtain copies of this report from:

National Aeronautics and Space Administration
Office of Scientific and Technical Information
Washington 25, D. C.
Attn: AFSS-A

Report No. 65.52E

December 1965

DEVELOPMENT AND EVALUATION OF MAGNETIC AND
ELECTRICAL MATERIALS CAPABLE OF OPERATING
IN THE 800° TO 1600°F TEMPERATURE RANGE

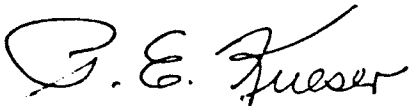
FOURTH QUARTERLY REPORT
(SEPTEMBER 1, 1965 - NOVEMBER 30, 1965)

sponsored by

NATIONAL AERONAUTICS AND SPACE ADMINISTRATION
CONTRACT NAS 3-6465

Project Management
NASA - Lewis Research Center
Space Power Systems Division
R. A. Lindberg

Prepared by:



P. E. Kueser, et al
Manager, NASA Materials Study
and Research Program

Approved by:



N. W. Bucci, Jr.
Manager, Engineering
Systems Research and
Development Department

Westinghouse Electric Corporation
Aerospace Electrical Division
Lima, Ohio

PREFACE

The work reported here was sponsored by the Space Power Systems Division of the NASA Lewis Research Center under Contract NAS 3-6465. Mr. R. A. Lindberg of NASA has provided the Project Management for the program. His review and suggestions as well as those of Mr. T. A. Moss, also of NASA, are gratefully acknowledged. The Westinghouse Aerospace Electrical Division (WAED) is responsible for the Technical Direction of the program. The Westinghouse Research and Development Center (WR & D) is conducting Tasks 1, 2 and 4 of Program I on Optimized Magnetic Materials for Application in the 1000 to 1200°F Range, the Investigation for Raising the Alpha to Gamma Transformation, and Creep Testing of Rotor Materials. Eitel-McCullough (EIMAC) is responsible for the Bore Seal Development, Task 1 of Program III. All other tasks are being conducted at the Westinghouse Aerospace Electrical Division (WAED).

In a program of this magnitude a large group of engineers and scientists are involved in its progress. An attempt to recognize those who are contributing directly, together with their area of endeavor, follows:

Program I - Magnetic Materials for High-Temperature Operation

Task 1 - Optimized Precipitation Hardened Magnetic Materials
for Application in the 1000 to 1200°F Range

Dr. K. Detert (WR & D); J. W. Toth (WAED)

Task 2 - Investigation for Raising the Alpha to Gamma Transformation
Temperature in Cobalt-Iron Alloys

Dr. K. Detert (WR & D); J. W. Toth (WAED)

Task 3 - Dispersion-Strengthened Magnetic Materials for Application
in the 1200 to 1600°F Range

Dr. R. J. Towner (WAED)

Task 4 - Creep Testing

M. Spewock (WR & D); D. H. Lane (WAED)

Program II - High Temperature Capacitor Feasibility

R. E. Stapleton (WAED)

Program III - Bore Seal Development and Combined Material Investigation
Under a Space Simulated Environment

Task 1 - Bore Seal Development

R. C. McRae, Dr. L. Reed (EIMAC); J. W. Toth (WAED)

Tasks 2, 3, 4 - Stator and Bore Seal, Transformer and Solenoid

W. L. Grant, H. E. Keneipp, D. H. Lane, R. P. Shumate,
J. W. Toth (WAED)

Dr. A. C. Beiler (WAED) and Dr. G. W. Wiener (WR&D) are acting as
consultants on Program I.

SUMMARY

This is the fourth quarterly report on Contract NAS 3-6465 for the Development and Evaluation of Magnetic and Electrical Materials Capable of Operating in the Temperature Range from 800 to 1600°F. Advanced space electric power systems are the area of eventual application.

Program I is directed at developing high-temperature magnetic materials with satisfactory strength for use in the solid rotors of electrical generators. Screening results, to date, conducted on martensitic alloys, using additions of tantalum plus tungsten and tantalum plus silicon to a base composition of iron-15% nickel-25% cobalt, indicate that these alloys show promise for meeting the desired creep stress ($> 60,000$ psi at 0.4 percent creep strain), and magnetic saturation (> 13 kilogauss) at 1100°F. In the 1200 to 1600°F range where dispersion strengthening is applied to cobalt and cobalt-iron base alloys, results show the saturation magnetization goal of 12 kilogauss can be met by the 27 cobalt-iron base alloys containing as much as 20 volume percent dispersoid. No problem appears to exist in meeting the goal of a coercive force of less than 25 oersteds at 1200 to 1600°F in either the 27 cobalt-iron base or cobalt base compositions. Creep tests on Nivco alloy at 1100°F are now being conducted at pressures in the $3-5 \times 10^{-9}$ torr range at 1100°F. Design analysis suggests creep strains in excess of one percent should be run above 1050°F. This will provide more reliable design data for rotors in inductor alternators even though the design is based on only a total creep strain of 0.4 percent because this represents the integrated value of a wide range of incremental creep strains.

Program II will determine the feasibility of high-temperature capacitors using high-quality dielectric materials. Comparison of electrical data on boron nitride (boralloy), polycrystalline alumina (Lucalox), polycrystalline beryllia, and single-crystal alumina (Linde sapphire) show that pyrolytic boron nitride has significantly lower a-c losses, higher d-c resistance, and exhibits less change in capacitance with temperature than any other material investigated in the temperature range from room temperature to 1100°F. In addition, the d-c breakdown strength of pyrolytic boron nitride is 7000 v/mil at 1100°F which is several times greater than that obtained for sapphire or beryllia.

Program III incorporates developments on alkali-metal compatible ceramic-to-metal seals and combinations of material designed into stator with a bore seal, a transformer, and a solenoid for investigations of compatibility under

electrical and magnetic stress at elevated temperature and under high vacuum. Ceramic outgassing studies have indicated that the present firing cycles applied to a ceramic using a nitrogen-hydrogen atmosphere followed by the vacuum treatment which they undergo during brazing is sufficient for minimizing oxygen bearing outgassing products. These would add only a few ppm of oxygen to the alkali-metal charge in a typical advanced electric power system. The stator, transformer and solenoid which will provide data on a stability of materials applied to typical electrical designs were installed in the thermal vacuum chamber and stability testing was initiated at 1100°F hot-spot temperature. The chamber pressures were approximately 4×10^{-7} torr at the beginning of the 5000-hour tests and have been decreasing. Minimum cold chamber pressure obtained after system bake-out was 1×10^{-10} torr.

TABLE OF CONTENTS

<u>Section</u>	<u>Page</u>
PREFACE	ii
SUMMARY	iv
 I INTRODUCTION	 1
 II PROGRAM I - MAGNETIC MATERIALS FOR HIGH- TEMPERATURE OPERATION	 3
A. Task 1 - Optimized Precipitation-Hardened Magnetic Materials for Application in the 1000 to 1200°F Range	 4
1. Summary of Technical Progress	4
2. Discussion	4
a. Experimental Procedure	5
b. Results	8
c. Conclusions	55
3. Program for the Next Quarter	65
B. Task 2 - Investigation for Raising the Alpha to Gamma Transformation Temperature in Cobalt- Iron Alloys	 66
C. Task 3 - Dispersion-Strengthened Magnetic Materials for Application in the 1200 to 1600°F Range	 67
1. Summary of Technical Progress	67
2. Discussion	68
a. Prealloyed Atomized Powders	69
b. Internally Oxidized Powders	83
c. Composite Powders	86
d. Supplier Extrusions of Dispersion- Strengthened Cobalt	 90
3. Program for the Next Quarter	98

TABLE OF CONTENTS - Continued

<u>Section</u>	<u>Page</u>
D. Task 4 - Creep Testing	99
1. Summary of Technical Progress.....	99
2. Discussion.....	99
a. Results.....	99
b. Strain Analysis for a Typical Nivco Rotor	101
3. Program for the Next Quarter.....	107
 III PROGRAM II - HIGH TEMPERATURE CAPACITOR FEASIBILITY	108
A. Summary of Technical Progress	108
B. Discussion.....	110
1. Preparation of Single Wafer Capacitors	111
a. Beryllium Oxide.....	111
b. Sapphire.....	114
c. Lucalox	114
2. Sputtered Electrode Adherence.....	114
a. Post Electrode Deposition Heat Treat- ment in Air	115
b. Sputtered Active Metal Base Layer	115
3. Multi-Layer Capacitors (Pyrolytic Boron Nitride)	116
a. Wafer Preparation.....	116
b. Evaluation (Room Temperature Data) ...	121
4. Analysis and Comparison of Electrical Data .	123
a. Capacitance vs. Temperature.....	124
b. Dissipation Factor ($\tan \delta$) vs. Tempera- ture.....	130
c. Capacitance and $\tan \delta$ vs. Frequency and Temperature	130
d. Dielectric "After Working" Effects	142
e. DC Resistance vs. Temperature.....	148
f. DC Breakdown Voltage at 1100° F in Vacuum	150
g. Relative Figure of Merit	151

TABLE OF CONTENTS - Continued

<u>Section</u>	<u>Page</u>
C. Program for the Next Quarter	153
 IV PROGRAM III - BORE SEAL DEVELOPMENT AND COMBINED MATERIAL INVESTIGATIONS UNDER A SPACE-SIMULATED ENVIRONMENT	 154
A. Task 1 - Bore Seal Development.....	155
1. Summary of Technical Progress	155
2. Discussion.....	155
a. Facility Contruction and Check-Out.....	156
b. Ceramic Outgassing Study	158
c. Bore Seal Ceramic Materials	177
d. Active Metal Brazing Alloys	179
3. Program for the Next Quarter	182
B. Task 2 - Stator and Bore Seal.....	183
1. Summary of Technical Progress	183
2. Discussion.....	183
a. Stator Physical and Electrical Design and Construction	 183
b. Stator Assembly.....	186
c. Thermocouple Systems.....	192
d. Thermal Vacuum Chamber Installation .	194
e. Stator Test Circuitry	194
f. Stator Test Procedure	197
g. Data Evaluation	200
3. Program for the Next Quarter	209
C. Task 3 - Transformer	211
1. Summary of Technical Progress	211
2. Discussion.....	211
a. Transformer Physical and Electrical Design and Construction.....	 211
b. Transformer Assembly.....	213
c. Thermocouple System.....	216
d. Thermal Vacuum Chamber Installation..	216

TABLE OF CONTENTS - Concluded

<u>Section</u>	<u>Page</u>
e. Transformer Test Circuitry	218
f. Transformer Test Procedure	218
g. Data Evaluation	221
3. Program for the Next Quarter	221
D. Task 4 - Solenoid	226
1. Summary of Technical Progress	226
2. Discussion	226
a. Solenoid Physical and Electrical Design and Construction	226
b. Solenoid Assembly	226
c. Solenoid Test Circuitry and Test Pro- cedure	232
d. Data Evaluation	232
3. Program for the Next Quarter	237
V REFERENCES	238

LIST OF FIGURES

<u>Number</u>	<u>Title</u>	<u>Page</u>
II-1	Hardness and Coercive Force of Alloy 1-A-33 at Room Temperature After Aging One Hour at Temperature.....	14
II-2	Hardness and Coercive Force of Alloys 1-A-34, 1-A-35, 1-A-36 and 1-A-37 at Room Temperature After Aging One Hour at Temperature .	15
II-3	Hardness and Coercive Force of Alloys 1-A-38, 1-A-42, 1-A-43 and 1-A-44 at Room Temperature After Aging One Hour at Temperature .	16
II-4	Hardness and Coercive Force of Alloys 1-A-45, 1-A-46, 1-A-47 and 1-A-48 at Room Temperature After Aging One Hour at Temperature .	17
II-5	Hardness and Coercive Force of Alloys 1-A-49, 1-A-50, 1-A-51 and 1-A-52 at Room Temperature After Aging One Hour at Temperature .	18
II-6	Hardness and Coercive Force of Alloys 1-B-32, 1-B-33, 1-B-34 and 1-B-35 at Room Temperature After Aging One Hour at Temperature.....	20
II-7	Hardness and Coercive Force of Alloys 1-B-36 and 1-B-37 at Room Temperature After Aging One Hour at Temperature.....	21
II-8	Hardness and Coercive Force of Alloys 1-B-38, 1-B-39, 1-B-40 and 1-B-41 at Room Temperature After Aging One Hour at Temperature.....	22
II-9	Change in Room Temperature Hardness and Coercive Force of Alloys 1-A-33 and 1-A-34 During Isothermal Aging at 1022°F (550°C).....	25
II-10	Change in Room Temperature Hardness and Coercive Force of Alloys 1-A-35 and 1-A-36 During Isothermal Aging at 1022°F (550°C).....	26
II-11	Change in Room Temperature Hardness and Coercive Force of Alloys 1-A-37 and 1-A-42 During Isothermal Aging at 1022°F (550°C).....	27
II-12	Change in Room Temperature Hardness and Coercive Force of Alloys 1-A-43 and 1-A-44 During Isothermal Aging at 1022°F (550°C).....	28

LIST OF FIGURES - Continued

<u>Number</u>	<u>Title</u>	<u>Page</u>
II-13	Change in Room Temperature Hardness and Coer- cive Force of Alloys 1-A-45 and 1-A-46 During Isothermal Aging at 1022°F (550°C).....	29
II-14	Change in Room Temperature Hardness and Coer- cive Force of Alloys 1-A-47 and 1-A-48 During Isothermal Aging at 1022°F (550°C).....	30
II-15	Change in Room Temperature Hardness and Coer- cive Force of Alloys 1-A-49 and 1-A-50 During Isothermal Aging at 1022°F (550°C).....	31
II-16	Change in Room Temperature Hardness and Coer- cive Force of Alloys 1-A-51 and 1-A-52 During Isothermal Aging at 1022°F (550°C).....	32
II-17	Change in Room Temperature Hardness and Coer- cive Force of Alloys 1-B-32 and 1-B-33 During Isothermal Aging at 1292°F (700°C).....	34
II-18	Change in Room Temperature Hardness and Coer- cive Force of Alloys 1-B-35 and 1-B-36 During Isothermal Aging at 1292°F (700°C).....	35
II-19	Change in Room Temperature Hardness and Coer- cive Force of Alloys 1-B-37 and 1-B-38 During Isothermal Aging at 1292°F (700°C).....	36
II-20	Change in Room Temperature Hardness and Coer- cive Force of Alloy 1-B-39 During Isothermal Aging at 1292°F (700°C).....	37
II-21	Change in Room Temperature Hardness and Coer- cive Force of Alloys 1-B-40 and 1-B-41 During Isothermal Aging at 1292°F (700°C).....	38
II-22	Microstructure of Alloy 1-A-33 (54.4Fe-15Ni-25Co- 0.5Be-5Ta-0.1Mn) After 100 Hours Aging at 1022°F (550°C) 500X.....	39
II-23	Microstructure of Alloy 1-A-34 (53.9Fe-15Ni-25Co- 1W-5Ta-0.1Mn) After 100 Hours Aging at 1022°F (550°C) 500X.....	40
II-24	Microstructure of Alloy 1-A-35 (54.4Fe-15Ni-25Co- 0.5Al-5Ta-0.1Mn) After 100 Hours Aging at 1022°F (550°C) 500X.....	41
II-25	Microstructure of Alloy 1-A-36 (53.9Fe-15Ni-25Co- 0.5Al-0.5Ti-5Ta-0.1Mn) After 100 Hours Aging at 1022°F (550°C) 500X.....	42

LIST OF FIGURES - Continued

<u>Number</u>	<u>Title</u>	<u>Page</u>
II-26	Microstructure of Alloy 1-A-37 (53.9Fe-15Ni-25Co-0.5Al-0.5Ti-2Mo-3Ta-0.1Mn) After 100 Hours Aging at 1022°F (550°C) 500 X.....	43
II-27	Microstructure of Alloy 1-A-42 (59.9Fe-5Ni-25Co-5Cr-5Ta-0.1Mn) After 100 Hours Aging at 1022°F (550°C) 500 X	44
II-28	Microstructure of Alloy 1-A-43 (55Fe-15Ni-25Co-2Mo-3Ta) After 100 Hours Aging at 1022°F (550°C) 500 X.....	45
II-29	Microstructure of Alloy 1-A-44 (53Fe-15Ni-25Co-2Cr-5Ta) After 100 Hours Aging at 1022°F (550°C) 500 X.....	46
II-30	Microstructure of Alloy 1-A-45 (57.5Fe-15Ni-25Co-2Cr-0.5Be) After 100 Hours Aging at 1022°F (550°C) 500 X	47
II-31	Microstructure of Alloy 1-A-46 (56Fe-15Ni-25Co-2Cr-2Si) After 100 Hours Aging at 1022°F (550°C) 500 X.....	48
II-32	Microstructure of Alloy 1-A-47 (53Fe-15Ni-25Co-2V-5Ta) After 100 Hours Aging at 1022°F (550°C) 500 X	49
II-33	Microstructure of Alloy 1-A-48 (53Fe-15Ni-25Co-2Si-5Ta) After 100 Hours Aging at 1022°F (550°C) 500 X	50
II-34	Microstructure of Alloy 1-A-49 (56Fe-15Ni-25Co-2Si-2W) After 100 Hours Aging at 1022°F (550°C) 500 X	51
II-35	Microstructure of Alloy 1-A-50 (57Fe-15Ni-25Co-1Si-2V) After 100 Hours Aging at 1022°F (550°C) 500 X	52
II-36	Microstructure of Alloy 1-A-51 (58Fe-15Ni-25Co-1Si-1Ti) After 100 Hours Aging at 1022°F (550°C) 500 X	53
II-37	Microstructure of Alloy 1-A-52 (56Fe-15Ni-25Co-2Mo-2W) After 100 Hours Aging at 1022°F (550°C) 500 X	54

LIST OF FIGURES - Continued

<u>Number</u>	<u>Title</u>	<u>Page</u>
II-38	Microstructure of Alloy 1-B-32 (75.8Co-15Ni-5Fe-2.2Ti-1.5Al-0.5Zr) After 100 Hours Aging at 1292°F (700°C) 500X	56
II-39	Microstructure of Alloy 1-B-33 (70.8Co-15Ni-5Fe-2.2Ti-1.5Al-0.5Zr-5Cu) After 100 Hours Aging at 1292°F (700°C) 500X	57
II-40	Microstructure of Alloy 1-B-35 (73.8Co-15Ni-5Fe-2.2Ti-1.5Al-0.5Zr-2Si) After 100 Hours Aging at 1292°F (700°C) 500X	58
II-41	Microstructure of Alloy 1-B-36 (75.3Co-15Ni-5Fe-2.2Ti-1.5Al-0.5Zr-0.5Be) After 100 Hours Aging at 1292°F (700°C) 500X	59
II-42	Microstructure of Alloy 1-B-37 (70.8Co-15Ni-5Fe-2.2Ti-1.5Al-0.5Zr-5Cr) After 100 Hours Aging at 1292°F (700°C) 500X	60
II-43	Microstructure of Alloy 1-B-38 (70.8Co-15Ni-5Fe-2.2Ti-1.5Al-0.5Zr-5W) After 100 Hours Aging at 1292°F (700°C) 500X	61
II-44	Microstructure of Alloy 1-B-39 (70.8Co-15Ni-5Fe-2.2Ti-1.5Al-0.5Zr-5Ta) After 100 Hours Aging at 1292°F (700°C) 500X	62
II-45	Microstructure of Alloy 1-B-40 (70.8Co-15Ni-5Fe-2.2Ti-1.5Al-0.5Zr-5Mo) After 100 Hours Aging at 1292°F (700°C) 500X	63
II-46	Microstructure of Alloy 1-B-41 (70.8Co-15Ni-5Fe-2.2Ti-1.5Al-0.5Zr-5V) After 100 Hours Aging at 1292°F (700°C) 500X	64
II-47	As-Extruded Rod of Atomized Powder No. 6, Co + 1.2% B + 7.7% Ta, Showing Boride Particles (gray) and Other Particles of Dark Constituent Dispersed in Cobalt Matrix, Longitudinal Section Near Front of Extrusion, 1000X	74

LIST OF FIGURES - Continued

<u>Number</u>	<u>Title</u>	<u>Page</u>
II-48	As-Extruded Rod of Atomized Powder No. 13, Fe + 24.8% Co + 1.1% B + 3.2% Zr, Showing Boride Particles (light) and Other Particles of Dark Constituent Dispersed in Fe-Co Recrystallized Matrix, Grain Boundaries Revealed, Longitudinal Section Near Front of Extrusion, 500 X	75
II-49	As-Extruded Rod of Atomized Powder No. 14, Fe + 25.8% Co + 0.9% B + 4.1% Cb, Showing Boride Particles (light) and Other Particles of Dark Constituent Dispersed in Fe-Co Matrix, Transverse Section Near Front of Extrusion, 1000 X	76
II-50	Tensile Specimen	80
II-51	Composite Powder No. 11, Fe + 23.5% Co + 10.8% ThO ₂ (0.01 - 0.06 micron thoria), From Vitro Labs After Hydrogen Reduction Showing Irregular Shape and Fine Grain Structure of Powder Particles. Thoria Particles Dispersed in Matrix Are Too Small to be Seen, 1000 X....	88
II-52	As-Extruded Rod Supplied by Curtiss-Wright Corp., Supplier Extrusion No. 9, Co + 1.96% ThO ₂ (0.01 - 0.06 micron thoria), Showing Dispersion of Thoria Particles in Cobalt Matrix. Some of the Thoria Particles are Present as Clusters and Stringers. Longitudinal Section Near Front of Extrusion, 1000 X.....	94
II-53	Rod Cold Reduced 85% After Extrusion by Curtiss-Wright Corp., Supplier Extrusion No. 9, Co + 2.05% ThO ₂ (0.01 - 0.06 micron thoria), Showing Dispersion of Thoria Particles in Cobalt Matrix. Longitudinal Section Near Front of Extrusion, 1000 X	95

LIST OF FIGURES - Continued

<u>Number</u>	<u>Title</u>	<u>Page</u>
II-54	As-Extruded Rod Supplied by New England Materials Laboratory, Supplier Extrusion No. 3, Co + 10.4% ThO ₂ (0.01 - 0.06 micron thoria), Showing Dispersion of Thoria Particles in Cobalt Matrix. Some of the Thoria Particles are Present as Clusters and Stringers. Longitudinal Section Near Front of Extrusion, 1000X.....	96
II-55	Creep, Nivco Heat 10-NO2V-1099, Tested in Vacuum at 1100°F and 50,000 psi and 37,500 psi.....	100
II-56	Summary Creep-Stress Rupture Larson-Miller Plot for NIVCO Alloy.....	104
II-57	Creep Strain as a Function of r/r _{OD} for a Typical Solid NIVCO Alloy Inductor Rotor Using a Coolant Temperature of 825°F and a Core Stress of 60,000 psi	105
II-58	Creep Strain as a Function of r/r _{OD} for a Typical Solid NIVCO Alloy Inductor Rotor Using a Coolant Temperature of 825°F, a Core Temperature of 825°F, and a Core Stress of 70,000 psi.....	106
III-1	Fixture for Making Electrical Measurements on Stacked Tabbed Capacitor Wafer.....	120
III-2	Capacitance Change Versus Temperature for BeO Capacitor No. 2 Before and After Heat Treatment in Air (Run No. 1 Versus Run No. 2) Measured in Vacuum at 1-3 x 10 ⁻⁷ torr	125
III-3	Capacitance Change Versus Temperature at 10 kc/sec for Sapphire Capacitor No. 2 Measured in Vacuum at 1-3 x 10 ⁻⁷ torr	126
III-4	Capacitance Change Versus Temperature for Lucalox Capacitor No. 1 in Vacuum (1-3 x 10 ⁻⁷ torr) at 1 kc/sec and 10 kc/sec.....	127

LIST OF FIGURES - Continued

<u>Number</u>	<u>Title</u>	<u>Page</u>
III-5	Change in Capacitance at 1 kc/sec and 10 kc/sec with Temperature for BN Multi-Layer Capacitor No. 1 Measured in Vacuum at $1-3 \times 10^{-7}$ torr	128
III-6	Ratio of $\frac{\Delta C}{C_{72^\circ F}} \times 100$ Versus Temperature at $1-4 \times 10^{-7}$ torr for BN Multi-Layer Capacitor No. 1, Lucalox Capacitor No. 1 and BeO Capacitor No. 2 (Run No. 2) Measured at 1 kc/sec	129
III-7	Dissipation Factor ($\tan \delta$) Versus Temperature for BeO Capacitor No. 2 Showing Hysteresis Effects on Cooling and the Effects of Heat Treatment in Air After Completion of Run No. 1	131
III-8	Dissipation Factor ($\tan \delta$) of Sapphire Capacitor No. 2 at 10 kc/sec and 100 cycles/sec Versus Temperature in Vacuum at $1-4 \times 10^{-7}$ torr ..	132
III-9	$\tan \delta$ Versus Temperature for Lucalox Capacitor No. 1 Showing Hysteresis Effects on Cooling (Measured in vacuum at $1-3 \times 10^{-7}$ torr)	133
III-10	$\tan \delta$ Versus Temperature for BN Multi-Layer Capacitor No. 1 Measured in Vacuum at $1-3 \times 10^{-7}$ torr	134
III-11	Comparison of $\tan \delta$ Versus Temperature for Various Dielectrics Measured at 1 kc/sec and 10 kc/sec (BN Capacitor No. 2) in Vacuum	135
III-12	Capacitance Change Versus Frequency at $72^\circ F$ and $1100^\circ F$ for Pyrolytic Boron Nitride as a Single Wafer Capacitor (BN Capacitor No. 2) and as Three Wafers Stacked and Connected in Parallel (BN Multi-Layer No. 1) Measured in Vacuum at $1-3 \times 10^{-7}$ torr	138
III-13	Ratio of $\frac{\Delta C}{C_{100 \text{ cps}}} \times 100$ Versus Frequency at $72^\circ F$, $1100^\circ F$ and $970^\circ F$ for BN Multi-Layer Capacitor No. 1 and Sapphire Capacitor No. 2 Measured in Vacuum at $1-3 \times 10^{-7}$ torr	139

LIST OF FIGURES - Continued

<u>Number</u>	<u>Title</u>	<u>Page</u>
III-14	Comparison of the Ratio of $\frac{\Delta \tan \delta}{\tan \delta} \times 100$ Versus Frequency for BN Multi-Layer Ca- pacitor No. 1 at 72°F and 1100°F.....	140
III-15	Comparison of Tan δ Versus Frequency at Room Temperature (72°F) and 1100°F for Pyroly- tic Boron Nitride as a Single Wafer Capaci- tor (BN Capacitor No. 2) and as Three Wafers Stacked and Connected in Parallel (BN Multi- Layer No. 1) Measured in Vacuum at 1-3 x 10 ⁻⁷ torr	141
III-16	Tan δ Versus Increasing and Decreasing Tempera- ture for Sapphire Capacitor No. 2 Measured in Vacuum at 1-4 x 10 ⁻⁷ torr, 1 kc/sec	143
III-17	Tan δ Versus Temperature for Sapphire Capacitor No. 1 Showing Hysteresis Effects on Cooling.	144
III-18	Tan δ and Capacitance Versus Time After Heat Treating BeO Capacitor No. 2 in Air to 960°C	145
III-19	Effects of Heating BeO Capacitor No. 2 in Air at 960°C on the Ratio of $\frac{\Delta C}{C} \times 100$ Versus Frequency	146
III-20	Effects of Heating BeO Capacitor No. 2 in Air at 960°C on the Change in the Ratio of $\frac{\Delta \tan \delta}{\tan \delta} \times 100$ Versus Frequency	147
III-21	DC Resistivity (ohm-cm) vs. Temperature in Vacuum (1-4 x 10 ⁻⁷ torr) For Pyrolytic Boron Nitride (BN Capacitor No. 3), Single Crystal Al ₂ O ₃ (Sapphire Capacitor No. 2), Hot Pressed BeO (BeO Capacitor No. 2), and Polycrystalline Al ₂ O ₃ (Lucalox Capacitor No. 1).....	149
III-22	Figure of Merit (M) for Four Different Dielectric Materials Expressed as the Ratio $\frac{M}{M_{BN}} \times 100$.	152

LIST OF FIGURES - Continued

<u>Number</u>	<u>Title</u>	<u>Page</u>
IV-1	Block Diagram of Ceramic Outgassing Analysis System	159
IV-2	Total Pressure Outgassing Curves at 1000°F Furnace Temperature for Sapphire (100% Al ₂ O ₃ , density 3.98 g/cc) Samples for Preconditions 1, 2, and 3	165
IV-3	Total Pressure Outgassing Curves at 1600°F Furnace Temperature for Sapphire (100% Al ₂ O ₃ , density 3.98 g/cc) Samples with Preconditions 1, 2, and 3.....	165
IV-4	Total Pressure Outgassing Curves at 1600°F Furnace Temperature for Lucalox (99.8% Al ₂ O ₃ , density 3.98 g/cc) Samples for Preconditions 1, 2, and 3.....	166
IV-5	Total Pressure Outgassing Curves at 1600°F Furnace Temperature for Thermalox 998 (99.8%BeO, density 2.86 to 2.98 g/cc) Samples for Preconditions 1, 2, and 3	167
IV-6	Total Pressure Outgassing Curves at 1600°F for Sapphire, Lucalox, and Thermalox 998 After Dye Check and Ceramic Cleaning Pro- cedures (PC1).....	168
IV-7	Partial Pressure Curves of Outgassed Products For Sapphire (100% Al ₂ O ₃ , density 3.98 g/cc) Precondition 3, Outgassed at 1600°F.....	169
IV-8	Partial Pressure Curves of Outgassed Products for Lucalox (99.8% Al ₂ O ₃ , density 3.98 g/cc) with Precondition 3, Outgassed at 1600°F....	170
IV-9	Partial Pressure Curves of Outgassed Products for Thermalox 998 (99.8% BeO, density 2.86 to 2.95 g/cc) Precondition 3, Outgassed at 1000°F	171
IV-10	Partial Pressure Curves of Outgassed Products for Thermalox 998 (99.8% BeO, density 2.86 to 2.95 g/cc) with Precondition 1, Outgassed at 1600°F	172
IV-11	Partial Pressure Curves of Outgassed Products for Thermalox 998 (99.8% BeO, density 2.86 to 2.95 g/cc) with Precondition 2, Outgassed at 1600°F	173

LIST OF FIGURES - Continued

<u>Number</u>	<u>Title</u>	<u>Page</u>
IV-12	Partial Pressure Curves of Outgassed Products for Thermalox 998 (99.8% BeO, density 2.86 to 2.95 g/cc) with Precondition 3, Outgassed at 1600°F	174
IV-13	Cutaway View of Stator Without a Bore Seal.....	184
IV-14	Test Stator Stack and Practice Winding Stator Stack.....	187
IV-15	Operator Forming a Winding With Test Wire in Front of the Clean Bench	188
IV-16	Test Winding Installed in Stator Prior to Anadur Bake-Out	189
IV-17	Stator Assembly on Furnace Supports	191
IV-18	Single and Dual Diameter Sheathed Thermocouples	193
IV-19	Cutaway View of Vacuum Furnace Showing the Stator Test Specimen Installed	195
IV-20	Schematic of Stator Electrical Hook-up	196
IV-21	Two Varian Thermal Vacuum Chambers and a Three Element Varian Vac-Sorb Roughing Pump Cart.....	198
IV-22	Varian Thermal Vacuum Chamber Control Consoles and Residual Gas Analyzer	199
IV-23	Chamber Pressure-Time Plot of Stator in Varian Chamber No. 1.....	202
IV-24	Chamber Pressure - Endurance Time Plot for Stator.....	203
IV-25	Stator Cross Section Showing Thermocouple Locations and Junction Positions	206
IV-26	Cutaway View of Transformer	212
IV-27	Transformer Spool Assembly and Windings.....	214
IV-28	Transformer Assembly Less Thermocouples	215
IV-29	Transformer in Position on Furnace Mounting Frame.....	217
IV-30	Cutaway View of a Vacuum Furnace Showing Installation of Two Solenoids and a Transformer	219
IV-31	Electrical Test Schematic for the 1 KVA Rated Transformer.....	220
IV-32	Chamber Pressure-Time Plot of Transformer and Solenoids in Varian Chamber No. 2	222

LIST OF FIGURES - Concluded

<u>Number</u>	<u>Title</u>	<u>Page</u>
IV-33	Transformer Assembly Showing Thermocouple Locations and Junction Positions	224
IV-34	Cutaway View of Solenoid	227
IV-35	Solenoid Winding on Arbor Before Anadur Bake- Out	229
IV-36	Solenoid Winding Assembly and Solenoid Winding on Arbor After Anadur Bake-Out	230
IV-37	Solenoid Housing Assembly	231
IV-38	Solenoid Assemblies Complete Except for Thermocouples	233
IV-39	Transformer and Solenoids on Furnace Mounting Frame	233
IV-40	Solenoid Circuitry	234
IV-41	Solenoid Assembly Showing Thermocouple Loca- tions and Junction Positions	236

LIST OF TABLES

<u>Number</u>	<u>Title</u>	<u>Page</u>
II-1	Composition of Martensitic Alloys 1-A-33 to 1-A-52	6
II-2	Composition of Cobalt-Base Alloys 1-B-32 to 1-B-41	6
II-3	Transformation Temperature of Martensitic Alloys 1-A-33 to 1-A-52	9
II-4	Saturation Magnetic Moment of Martensitic Alloys 1-A-33 to 1-A-52	11
II-5	Saturation Magnetic Moment of Cobalt-Base Alloys 1-B-32 to 1-B-41	11
II-6	Maximum Hardness Obtained by the Isochronal Aging Sequence of Martensitic Alloys 1-A-33 to 1-A-38 and 1-A-42 to 1-A-52	19
II-7	Maximum Hardness Obtained by the Isochronal Aging Sequence of Cobalt-Base Alloys 1-B-32 to 1-B-41	23
II-8	Microstructure of Extrusions, Preliminary Measurements	77
II-9	D-C Magnetic Properties of Hot Extruded Rod ...	83
II-10	Tensile Properties of Hot Extruded Rod	85
II-11	Particle Size, Shape, and Apparent Densities of Composite Powders and Density of Compacts	87
II-12	Supplier Extrusions of Dispersion-Strengthened Cobalt	91
II-13	Chemical Analysis of Supplier Extrusions	93
II-14	Quality Check, Standard Stress-Rupture Test Data for One Specimen from Nivco Heat 10-NO2V-1099 (air test)	102
II-15	Room Temperature Coercive Force Measurements for Nivco Heats AC232 and 10-NO2V-1099 ...	102
III-1	Complete History of Each Capacitor Fabricated and Tested	113
III-2	Properties of Tabbed BN Capacitors No. 1 and No. 2	122

LIST OF TABLES - Concluded

<u>Number</u>	<u>Title</u>	<u>Page</u>
IV-1	Typical Compositions of Nitrogen-Hydrogen Gas Atmospheres in Furnace Hot Zone During 2597°F Firing of Ceramics	161
IV-2	Total Gas Evolved From Sapphire, Lucalox and Thermalox 998 at 1000°F and 1600°F During an Outgassing Period of Twenty Minutes.....	162
IV-3	Ceramic Outgassing Sample Weights and Surfaces Areas	163
IV-4	Silica Analyses (as silicon) of Various Lots of Thermalox 998 Received from Brush Beryllium Co.....	178
IV-5	Summary of Brazing Data for the Selection of Braze Alloys to Join Thermalox 998 Beryllia Ceramic to Columbium-1% Zirconium Metal	180
IV-6	Electrical Measurements of Stator Assembly	205
IV-7	Stator Temperature Distributions.....	208
IV-8	Tabulation of Transformer Electrical Readings ..	223

SECTION I

INTRODUCTION

This is the fourth quarterly report on Contract NAS 3-6465 for the Development and Evaluation of Magnetic and Electrical Materials Capable of Operating in the Temperature Range from 800 to 1600°F. The period of performance is from September 1, 1965 through November 30, 1965. The program consists of three Programs with their related tasks as follows:

- Program I - Magnetic Materials for High-Temperature Operation
 - Task 1 - Optimized Precipitation Hardened Magnetic Materials for Application in the 1000 to 1200°F Range
 - Task 2 - Investigation for Raising the Alpha to Gamma Transformation Temperature in Cobalt-Iron Alloys (completed)
 - Task 3 - Dispersion-Strengthened Magnetic Materials for Application in the 1200 to 1600°F Range
 - Task 4 - Creep Testing
- Program II - High-Temperature Capacitor Feasibility
- Program III - Bore Seal Development and Combined Material Investigation Under a Space Simulated Environment
 - Task 1 - Bore Seal Development
 - Task 2 - Stator and Bore Seal
 - Task 3 - Transformer
 - Task 4 - Solenoid

In Program I, limitations in magnetic material performance at elevated temperature have been recognized from Contract NAS 3-4162 and the development of materials incorporating improved magnetic and mechanical properties is

being pursued. In most cases, high-strength compromises the magnetic properties; therefore, a balance between these two variables is sought.

Program II is directed at determining the feasibility of applying high-quality dielectric materials and their processes to a high-temperature (1100°F) capacitor which is lightweight and suitable for static power conditioning apparatus used in space applications.

Program III incorporates development on ceramic-to-metal seals and on combinations of materials previously evaluated under Contract NAS 3-4162 into a stator with a bore seal, a transformer, and a solenoid for investigations of compatibility under electrical and magnetic stress at elevated temperature and high vacuum.

The three Programs will be reported consecutively in Sections II, III and IV. Section II and Section IV are further divided into their respective tasks. Each task is reported separately and includes a summary of technical progress, a discussion, and the program for the next quarter so the reader may obtain an understanding of each task.

The first, second, and third quarterly reports were issued as NASA-CR-54354, NASA-CR-54355, and NASA-CR-54356 respectively. These reports are extensively referenced in this report. Other references identified by number in the discussion of each task are contained in Section V. These are identified in Section V by the program and task for which the reference is applicable.

SECTION II

PROGRAM I - MAGNETIC MATERIALS FOR HIGH-TEMPERATURE OPERATION

Program I is directed at improvement and furthering the technology of magnetic materials suitable for application in the rotor of a generator or motor in advanced space electric power systems.

Task 1 is concerned with precipitation-hardened magnetic materials in the 1000 to 1200°F range. These materials are of the iron-cobalt-nickel ternary system. The two specific areas of interest are the iron and cobalt corners of the ternary system.

Task 2 is a small research investigation for determining the feasibility of raising the alpha to gamma transformation temperature in the iron-cobalt system; thereby increasing the useful magnetic temperature of this system. This investigation is completed and the final results were given in the third quarterly report. Selected alloy additions of 3 to 5 weight percent increased the transformation temperature approximately 9°F (5°C) for each weight percent added. Magnetic saturation was lowered by each addition. If only a 45°F increase in alpha to gamma transformation temperature is desired, at a slight sacrifice in magnetic saturation, several alloying agents are satisfactory.

Task 3 is directed at applying dispersion-strengthening mechanisms to magnetic materials to achieve useful mechanical and magnetic properties in the 1200 to 1600°F range. Because both variables are influenced differently by particle size and spacing, a compromise is sought thereby tailoring the materials to the need of dynamic electric machines.

Task 4 is a creep program on Nivco alloy (approximately 72 percent cobalt, 23 percent nickel and certain other elements) which will generate 5000 hour design data in a vacuum environment (1×10^{-6} torr or less). This material represents a presently available magnetic material with the highest useful application temperature for stressed applications.

A. TASK 1 - OPTIMIZED PRECIPITATION-HARDENED MAGNETIC MATERIALS FOR APPLICATION IN THE 1000 TO 1200°F RANGE

1. Summary of Technical Progress

- a) Thirty alloys have been tested in the screening program. Twenty alloys were of the martensitic type and ten were of the cobalt base type.
- b) The alloys were melted by the levitation melting technique. Dilatometer tests, magnetic saturation measurements and aging tests with hardness and coercivity measurements and microstructure observations were made.
- c) The test results indicate that some combinations of elements such as tantalum plus tungsten and tantalum plus silicon to a base composition of Fe-15Ni-25Co are promising.

Aluminum and aluminum plus titanium added to tantalum in this base composition decreases the rate of hardness change during aging and increases the maximum Vickers hardness level. However, a much higher increase of coercivity was obtained during aging.

The addition of silicon along with titanium to the Fe-15Ni-25Co base composition kept the coercivity level below 25 oersteds even after 100 hours aging at 1022°F (550°C).

The basic composition Fe-5Ni-5Cr-25Co with addition of tantalum behaved similar to Fe-15Ni-25Co with the additions of tantalum during the aging tests.

- d) In the cobalt base alloys, the beneficial effect of the addition of tantalum to the Co-Ni-Ti-Al base was recognized. The Vickers hardness was increased to a value of 411 which is about twenty percent higher than that of Nivco alloy. The magnetic saturation of the experimental alloy was about ten percent lower than that of Nivco alloy.

2. Discussion

The objective of this program is to find and evaluate an alloy composition which displays high-creep strength and useful ferromagnetic properties at temperatures in the range of 1000 to 1200°F.

The target ultimate tensile strength for the alloy at 1100°F is 125,000 psi or better. The target stress to produce 0.4 percent creep strain in 1000 hours at 1100°F is 76,000 psi or greater. The 10,000 hour stress target at 1100°F is 80 to 90 percent of that at 1000 hours. The target magnetic saturation for the developmental alloy is 13,000 gauss or better at 1100°F and a coercive force less than 25 oersteds.

An alloy screening program is being conducted as the first step in attaining this goal. The purpose of the screening program is to find a certain region of alloy composition where the combination of desirable mechanical and magnetic properties can be attained. Vickers hardness tests, coercivity measurements, and saturation measurements after a suitable heat treatment and dilatometer tests were conducted to provide pertinent data and to determine the thermal stability of the alloy structure. Details of the test methods were reported in the first and second quarterly reports.

a. EXPERIMENTAL PROCEDURE

Martensitic alloys 1-A-33 to 1-A-52 and cobalt-base alloys 1-B-32 to 1-B-41 were studied during this report period. The nominal compositions of the two alloy series are shown in Tables II-1 and II-2. The base composition Fe-15Ni-25Co was used for alloys 1-A-33 to 1-A-37 and 1-A-43 to 1-A-52.

The experimental results which were reported in the second quarterly report showed that precipitation hardening was obtained in this base composition by the addition of the elements tantalum, molybdenum, tungsten, titanium, or beryllium. The single addition of aluminum or silicon raised the alpha to gamma transformation temperature. Chromium and vanadium are believed to reduce the rate of diffusion in ferritic alloys. Combinations of these elements were applied to the base composition for alloys 1-A-33 to 1-A-37 and 1-A-43 to 1-A-52. In alloys 1-A-38 to 1-A-42, the nickel content was substantially decreased in order to determine whether a matrix containing manganese or chromium with reduced or no nickel content would produce a maraging strengthening response when tantalum is added to cause precipitation.

The cobalt alloy compositions 1-B-32 to 1-B-41 were designed on the basis of results which were reported in the third quarterly report. Alloy 1-B-32 with titanium plus aluminum in a matrix of 15Ni-5Fe-bal Co was expected to give the best precipitation hardening while avoiding any discontinuous precipitation. The other alloys contained additional elements to obtain greater strength.

TABLE II-1. Composition of Martensitic Alloys 1-A-33 to 1-A-52

Alloy Number	Nominal Alloy Composition (weight percent)
1-A-33	54.4Fe-15Ni-25Co-0.5Be-5Ta-0.1Mn
1-A-34	53.9Fe-15Ni-25Co-1W-5Ta-0.1Mn
1-A-35	54.4Fe-15Ni-25Co-0.5Al-5Ta-0.1Mn
1-A-36	53.9Fe-15Ni-25Co-0.5Al-0.5Ti-5Ta-0.1Mn
1-A-37	53.9Fe-15Ni-25Co-0.5Al-0.5Ti-2Mo-3Ta-0.1Mn
1-A-38	69.9Fe-25Co-5Ta-0.1Mn
1-A-39	64.9Fe-5Ni-25Co-5Ta-0.1Mn
1-A-40	62Fe-5Ni-25Co-3Mn-5Ta
1-A-41	66Fe-25Co-4Mn-5Ta
1-A-42	59.9Fe-5Ni-25Co-5Cr-5Ta-0.1Mn
1-A-43	55Fe-15Ni-25Co-2Mo-3Ta
1-A-44	53Fe-15Ni-25Co-2Cr-5Ta
1-A-45	57.5Fe-15Ni-25Co-2Cr-0.5Be
1-A-46	56Fe-15Ni-25Co-2Cr-2Si
1-A-47	53Fe-15Ni-25Co-2V-5Ta
1-A-48	53Fe-15Ni-25Co-2Si-5Ta
1-A-49	56Fe-15Ni-25Co-2Si-2W
1-A-50	57Fe-15Ni-25Co-1Si-2V
1-A-51	58Fe-15Ni-25Co-1Si-1Ti
1-A-52	56Fe-15Ni-25Co-2Mo-2W

TABLE II-2. Composition of Cobalt-Base Alloys 1-B-32 to 1-B-41

Alloy Number	Nominal Alloy Composition (weight percent)
1-B-32	75.8Co-15Ni-5Fe-2.2Ti-1.5Al-0.5Zr
1-B-33	70.8Co-15Ni-5Fe-2.2Ti-1.5Al-0.5Zr-5Cu
1-B-34	70.8Co-15Ni-5Fe-2.2Ti-1.5Al-0.5Zr-5Mn
1-B-35	73.8Co-15Ni-5Fe-2.2Ti-1.5Al-0.5Zr-2Si
1-B-36	75.3Co-15Ni-5Fe-2.2Ti-1.5Al-0.5Zr-0.5Be
1-B-37	70.8Co-15Ni-5Fe-2.2Ti-1.5Al-0.5Zr-5Cr
1-B-38	70.8Co-15Ni-5Fe-2.2Ti-1.5Al-0.5Zr-5W
1-B-39	70.8Co-15Ni-5Fe-2.2Ti-1.5Al-0.5Zr-5Ta
1-B-40	70.8Co-15Ni-5Fe-2.2Ti-1.5Al-0.5Zr-5Mo
1-B-41	70.8Co-15Ni-5Fe-2.2Ti-1.5Al-0.5Zr-5V

In order to melt the alloys by the levitation melting technique, small compactions of 20 grams were made as described in the second quarterly report. In most cases, small chips and slugs of the pure metals were compacted together to form the alloy during melting. The small chips or slugs of the added elements were carefully wrapped in nickel or cobalt foil and then inserted in the middle of the compaction. The melting and pouring was done in a high-purity argon atmosphere at slightly reduced pressure.

The specimens for saturation measurements (1/10 inch long, 1/10 inch diameter ~ 0.1 gram) were machined from the tapered, bar-shaped ingots. The dilatometer specimens (1 inch long, 1/4 inch diameter) for the martensitic alloys and the round bars of similar dimension for the cobalt base alloys were also machined from the cast ingots.

The details of measuring magnetic saturation and determining the transformation temperatures were described in the first quarterly report. A description of the hardness tests and coercivity measurements were also included. The round samples were rolled down to small strips of ~ 95 mil thickness prior to the aging treatments. The martensitic specimens were annealed for one hour at 1832 to 1922°F (1000 to 1050°C) in argon flushed tube furnaces, then quenched in oil. The cobalt-base alloys were annealed for one hour at 2012°F (1100°C), then quenched in oil. Before cold rolling, the martensitic alloys were warmed to about 200°F for 30 seconds. Cold rolling was done in the manner described in the second quarterly report.

Samples of the martensitic alloys 1-A-39, 1-A-40 and 1-A-41 broke during cold rolling. Alloys 1-A-33, 1-A-38, 1-A-42 and 1-A-48 developed a few cracks. All other samples including the cobalt-base alloys were rolled down successfully.

After cold rolling, the samples underwent a schedule of heat treatments as outlined in the flow chart on page 19 of the second quarterly report. After annealing at 1832°F (1000°C) in an argon flushed tube furnace, the samples were aged for one hour in salt baths at temperatures successively increased in steps of 90°F (50°C) to obtain the isochronal curve of property change at different temperatures.

After a homogenization treatment, which consisted of two anneals and a slight (5%) deformation between anneals, an isothermal aging treatment was applied at a temperature near that which resulted in the maximum value of hardness determined from the isochronal aging treatment. In the case of the martensitic alloys, the isothermal aging temperature was 1022°F (550°C). In the case of the cobalt-base alloys, the temperature was 1292°F (700°C). However, measurements of property changes such as hardness and coercivity were made at room temperature, thus causing an interruption in the aging treatment. The aging techniques were discussed in detail in the second quarterly report.

Samples for optical metallography were prepared in the manner described in the second quarterly report. The martensitic alloys were mechanically polished, then electrolytically etched in a 10 percent solution of chromic acid. The cobalt alloys were etched at 104°F in a solution of 20 parts HCl and 40 parts HNO₃ in 60 parts of glycerin. Electron microscopy studies of alloys 1-A-26, 1-A-27, and 1-A-28 are in progress.

b. RESULTS

(1) Workability

Difficulties were encountered in a few cases during cold rolling of martensitic alloy samples with reduced nickel content. Further investigation of alloys 1-A-39, 1-A-40, and 1-A-41 were discontinued. A contributing cause may be that a second phase is formed during solidification of the alloy, as observed in alloy 1-A-42, making rolling more difficult. The addition of beryllium, tungsten, and silicon, when suitably combined with other elements, did not result in problems during cold rolling, although some care must be applied.

(2) Dilatometer Tests

The transformation temperatures of alloy samples 1-A-33 to 1-A-52 as determined by dilatometer tests, are shown in Table II-3. One test was made at a high cooling and heating rate of 90°F/min (50°C/min) and another test was made at a slow heating rate of 1.8 to 3.6°F/min (1 to 2°C/min) and a slow cooling rate of 9°F/min (5°C/min).

TABLE II-3. Transformation Temperature of Martensitic Alloys
1-A-33 to 1-A-52

Alloy Number	Nominal Alloy Composition (weight percent)	Transformation On Heating			
		$\alpha \rightarrow \gamma$		$\gamma \rightarrow \alpha$	
		90°F/Min (°F)	50°C/Min (°C)	3.6°F/Min (°F)	2°C/Min (°C)
1-A-33	54.4Fe-15Ni-25Co-0.5Be-5Ta-0.1Mn	1472-1617	800-881	1292-1553	700-845
1-A-34	53.9Fe-15Ni-25Co-1W-5Ta-0.1Mn	1566-1668	852-909	1260-1542	682-839
1-A-35	54.4Fe-15Ni-25Co-0.5Al-5Ta-0.1Mn	1485-1607	807-875	1270-1542	688-839
1-A-36	53.9Fe-15Ni-25Co-0.5Al-0.5Ti-5Ta-0.1Mn	1485-1600	807-871	1292-1539	700-837
1-A-37	53.9Fe-15Ni-25Co-0.5Al-0.5Ti-2Mo-3Ta-0.1Mn	1438-1593	781-867	1256-1553	680-845
1-A-38	69.9Fe-25Co-5Ta-0.1Mn	1764-1780	962-971	1740-1764	949-962
1-A-39	64.9Fe-5Ni-25Co-5Ta-0.1Mn	1659-1740	904-949	1517-1717	825-936
1-A-40	62Fe-5Ni-25Co-3Mn-5Ta	1584-1706	862-930	1292-1645	700-896
1-A-41	66Fe-25Co-4Mn-5Ta	1622-1735	884-946	1416-1699	769-926
1-A-42	59.9Fe-5Ni-25Co-5Cr-5Ta-0.1Mn	1530-1681	832-916	1222-1589	661-865
1-A-43	55Fe-15Ni-25Co-2Mo-3Ta	1411-1578	766-859	1222-1535	661-835
1-A-44	53Fe-15Ni-25Co-2Cr-5Ta	1425-1584	774-862	1112-1485	600-807
1-A-45	57.5Fe-15Ni-25Co-2Cr-0.5Be	1521-1652	827-900	1069-1398	576-759
1-A-46	56Fe-15Ni-25Co-2Cr-2Si	1490-1609	810-876	1041-1420	560-771
1-A-47	53Fe-15Ni-25Co-2V-5Ta	1551-1652	844-900	1222-1508	661-820
1-A-48	53Fe-15Ni-25Co-2Si-5Ta	1569-1652	854-900	1265-1521	685-827
1-A-49	56Fe-15Ni-25Co-2Si-2W	1503-1652	817-900	1218-1472	659-800
1-A-50	57Fe-15Ni-25Co-1Si-2V	1459-1652	793-900	1337-1499	725-815
1-A-51	58Fe-15Ni-25Co-1Si-1Ti	1528-1652	831-900	1308-1615	709-880
1-A-52	56Fe-15Ni-25Co-2Mo-2W	1404-1526	762-830	1175-1472	635-800

Alloy Number	Nominal Alloy Composition (weight percent)	Transformation On Cooling			
		$\gamma \rightarrow \alpha$		$\alpha \rightarrow \gamma$	
		90°F/Min (°F)	50°C/Min (°C)	9°C/Min (°F)	5°C/Min (°C)
1-A-33	54.4Fe-15Ni-25Co-0.5Be-5Ta-0.1Mn	720-509	383-265	786-545	419-285
1-A-34	53.9Fe-15Ni-25Co-1W-5Ta-0.1Mn	721-487	383-253	774-597	412-314
1-A-35	54.4Fe-15Ni-25Co-0.5Al-5Ta-0.1Mn	786-527	419-275	799-667	426-353
1-A-36	53.9Fe-15Ni-25Co-0.5Al-0.5Ti-5Ta-0.1Mn	748-475	398-246	748-536	398-280
1-A-37	53.9Fe-15Ni-25Co-0.5Al-0.5Ti-2Mo-3Ta-0.1Mn	671-369	355-187	673-430	356-221
1-A-38	69.9Fe-25Co-5Ta-0.1Mn	1587-1521	864-827	1726-1713	941-934
1-A-39	64.9Fe-5Ni-25Co-5Ta-0.1Mn	1227-1072	664-578	1351-1218	733-659
1-A-40	62Fe-5Ni-25Co-3Mn-5Ta	1053-837	567-447	1155-972	624-522
1-A-41	66Fe-25Co-4Mn-5Ta	1231-1053	666-567	1330-1166	721-630
1-A-42	59.9Fe-5Ni-25Co-5Cr-5Ta-0.1Mn	833-640	445-338	937-752	503-400
1-A-43	55Fe-15Ni-25Co-2Mo-3Ta	712-475	378-246	747-518	397-270
1-A-44	53Fe-15Ni-25Co-2Cr-5Ta	622-306	328-152	622-392	328-200
1-A-45	57.5Fe-15Ni-25Co-2Cr-0.5Be	675-448	357-231	622-378	328-192
1-A-46	56Fe-15Ni-25Co-2Cr-2Si	619-345	326-174	649-351	343-177
1-A-47	53Fe-15Ni-25Co-2V-5Ta	693-369	367-187	705-478	374-248
1-A-48	53Fe-15Ni-25Co-2Si-5Ta	734-475	390-246	766-597	408-314
1-A-49	56Fe-15Ni-25Co-2Si-2W	727-482	386-250	752-509	400-265
1-A-50	57Fe-15Ni-25Co-1Si-2V	705-437	374-225	775-545	413-285
1-A-51	58Fe-15Ni-25Co-1Si-1Ti	837-512	447-300	894-709	479-376
1-A-52	56Fe-15Ni-25Co-2Mo-2W	721-558	383-292	743-572	395-300

The beginning and end of a noticeable deviation in the slope of the thermal expansion curves are listed in Table II-2 as the beginning and end of transformation.

During slow heating of the martensitic alloys, the transformation into γ started at or below 1112°F (600°C) in alloys 1-A-44, 1-A-45, and 1-A-46 only, which proved again the detrimental effect of chromium addition on the stability of the ferromagnetic α phase even when added in combination with other elements. Except for alloy 1-A-52 which contained molybdenum plus tungsten, all other alloys started to transform above 1202°F (650°C). In the alloys with reduced nickel content, 1-A-38 to 1-A-41, and in alloys 1-A-33, 1-A-36, 1-A-50, and 1-A-51, the beginning of transformation was observed at 1292°F (700°C) or even higher. Alloys 1-A-33, 1-A-36, 1-A-50, and 1-A-51 illustrate the stabilizing effect of beryllium and silicon, and the combination of Al+Ti+Ta on the α phase.

The transformation temperatures measured during cooling showed that the transformation started well above 1112°F (600°C) only in alloys 1-A-38 to 1-A-41. Martensite formation and strengthening cannot be expected during cooling in the alloys with five percent nickel or less except when 5 percent chromium is added.

(3) Saturation Measurements

The results of the saturation measurements are listed in Tables II-4 and II-5. The values after annealing, measured at room temperature, are listed in the third column. The values after aging, measured at room temperature and at 1112°F (600°C), are listed in the fourth and fifth columns. The martensitic alloys had been annealed one hour at 1832°F (1000°C) and aged one hour at 1112°F (600°C). The cobalt-base alloys were annealed one hour at 2012°F (1100°C) and aged one hour at 1292°F (700°C).

The values in the tables were measured as saturation magnetic moment per gram in cgs units (σ). This value may be converted to the approximate saturation in gauss by the equation:

TABLE II-4. Saturation Magnetic Moment of Martensitic Alloys
1-A-33 to 1-A-52

Alloy Number	Nominal Alloy Composition (weight percent)	SATURATION MAGNETIC MOMENT (emu/g) (a)		
		After Annealing One Hour at 1832°F (1000°C)	After Aging One Hour at 1112°F (600°C)	
		Tested at Room Temperature	Tested at Room Temperature	Tested at 1112°F (600°C)
1-A-33	54.4Fe-15Ni-25Co-0.5Be-5Ta-0.1Mn	191	193	160
1-A-34	53.9Fe-15Ni-25Co-1W-5Ta-0.1Mn	192	193	156
1-A-35	54.4Fe-15Ni-25Co-0.5Al-5Ta-0.1Mn	193	194	161
1-A-36	53.9Fe-15Ni-25Co-0.5Al-0.5Ti-5Ta-0.1Mn	188	189	156
1-A-37	53.9Fe-15Ni-25Co-0.5Al-0.5Ti-2Mo-3Ta-0.1Mn	187	186	150
1-A-38	69.9Fe-25Co-5Ta-0.1Mn	222	221	192
1-A-39	64.9Fe-5Ni-25Co-5Ta-0.1Mn	215	214	182
1-A-40	62Fe-5Ni-25Co-3Mn-5Ta	212	209	171
1-A-41	66Fe-25Co-4Mn-5Ta	211	213	174
1-A-42	59.9Fe-5Ni-25Co-5Cr-5Ta-0.1Mn	190	192	152
1-A-43	55Fe-15Ni-25Co-2Mo-3Ta	194	192	147
1-A-44	53Fe-15Ni-25Co-2Cr-5Ta	184	176	122
1-A-45	57.5Fe-15Ni-25Co-2Cr-0.5Be	198	190	137
1-A-46	56Fe-15Ni-25Co-2Cr-2Si	190	177	119
1-A-47	53Fe-15Ni-25Co-2V-5Ta	186	185	145
1-A-48	53Fe-15Ni-25Co-2Si-5Ta	186	190	147
1-A-49	56Fe-15Ni-25Co-2Si-2W	182	181	129
1-A-50	57Fe-15Ni-25Co-1Si-2V	196	192	133
1-A-51	58Fe-15Ni-25Co-1Si-1Ti	204	206	166
1-A-52	56Fe-15Ni-25Co-2Mo-2W	198	197	143
(a) To convert saturation magnetic moment to the approximate induction in gauss, multiply the listed value by 100.				

TABLE II-5. Saturation Magnetic Moment of Cobalt-Base Alloys
1-B-32 to 1-B-41

Alloy Number	Nominal Alloy Composition (weight percent)	SATURATION MAGNETIC MOMENT (emu/g) (a)		
		After Annealing One Hour at 2012°F (1100°C)	After Aging One Hour at 1292°F (700°C)	
		Tested at Room Temperature	Tested at Room Temperature	Tested at 1112°F (600°C)
1-B-32	75.8Co-15Ni-5Fe-2.2Ti-1.5Al-0.5Zr	133	132	103
1-B-33	70.8Co-15Ni-5Fe-2.2Ti-1.5Al-0.5Zr-5Cu	124	125	93
1-B-34	70.8Co-15Ni-5Fe-2.2Ti-1.5Al-0.5Zr-5Mn	122	122	65
1-B-35	73.8Co-15Ni-5Fe-2.2Ti-1.5Al-0.5Zr-2Si	120	118	79
1-B-36	75.3Co-15Ni-5Fe-2.2Ti-1.5Al-0.5Zr-0.5Be	128	128	97
1-B-37	70.8Co-15Ni-5Fe-2.2Ti-1.5Al-0.5Zr-5Cr	99	99	32
1-B-38	70.8Co-15Ni-5Fe-2.2Ti-1.5Al-0.5Zr-5W	117	115	84
1-B-39	70.8Co-15Ni-5Fe-2.2Ti-1.5Al-0.5Zr-5Ta	116	116	90
1-B-40	70.8Co-15Ni-5Fe-2.2Ti-1.5Al-0.5Zr-5Mo	110	107	70
1-B-41	70.8Co-15Ni-5Fe-2.2Ti-1.5Al-0.5Zr-5V	103	97	62
(a) To convert saturation magnetic moment to the approximate induction in gauss, multiply the listed value by 110.				

$$B_S = 4\pi\delta\sigma$$

where:

δ = density in g/cm³

σ = saturation magnetic moment, emu/g

In this report, the value 100 was used as the product of $4\pi\delta$ for the martensitic alloys. In the case of the higher density cobalt alloys, the value 110 was used for $4\pi\delta$.

The martensitic alloy 1-A-38, containing no nickel, showed the highest value of magnetic saturation. In general, all of the alloys with five percent nickel showed higher values of magnetic saturation than the alloys with 15 percent nickel. However, the saturation value of alloy 1-A-42 with five percent nickel plus five percent chromium is approximately the same as some of the better alloys containing 15 percent nickel. The magnetic saturation of all of the 15 percent nickel alloys studied here is lower than that of the simple ternary alloy Fe-15Ni-25Co. (See the first quarterly report.) The (Fe-15Ni-25Co plus x-x) alloys may be categorized according to measured saturation values at 1112°F (600°C). $B_S \geq 15,000$ gauss was attained in experimental alloys 1-A-33, 1-A-34, 1-A-35, 1-A-36, 1-A-37, and 1-A-51. $B_S \leq 13,000$ gauss (the value attained in commercial alloys H-11 and 15% nickel maraging steel) was obtained in experimental alloys 1-A-44, 1-A-45, 1-A-46, 1-A-49, and 1-A-50. This data reflects the deleterious effect of chromium and silicon on magnetic saturation when they are combined with tungsten or vanadium.

Only the cobalt-base alloy 1-B-32 showed a value of magnetic saturation slightly better than that of Nivco alloy (see second quarterly report). All of the other cobalt-base alloys studied which contained additional elements had values of magnetic saturation at 1112°F (600°C) below $B_S = 11,000$ gauss. The addition of 0.5 weight percent of beryllium, five percent copper and five percent tantalum had the least effect on saturation; depressing the value at 1112°F (600°C) by less than 10 percent.

(4) Aging Tests

The isochronal curves of the experimental alloys were plotted showing Vickers pyramid hardness and coercivity at a constant aging time of one hour and at aging temperature increasing in increments of 90°F (50°C).

Figures II-1 to II-5 depict the isochronal curves for the experimental martensitic alloys, with the exception of alloys 1-A-39 to 1-A-41, which broke during rolling. The maximum values of room temperature hardness which were measured during this aging program are listed in Table II-6 together with the aging temperature where maximum hardness was obtained. The room temperature coercivity is listed for the same aging temperature.

The isochronal aging tests show that considerable strengthening occurred in all of the martensitic alloys with one exception, alloy 1-A-38, which did not undergo a martensitic transformation (Figure II-3). If the alloys are listed according to the value of maximum hardness, alloys 1-A-33 with 810 VHN and 1-A-45 with 757 VHN top the list; indicating that beryllium is a strong precipitation hardening element. It appears more useful to list the alloys according to the aging temperature where the maximum hardness is attained. It is desirable that this temperature be as high as possible for anticipated creep strength. It is also desirable that the coercivity associated with the maximum hardness be moderate. The alloys which attained maximum hardness at 1022°F (550°C) and have room temperature coercivity values less than 35 oersteds may be listed as follows: 1-A-34, 1-A-35, 1-A-36, 1-A-37, 1-A-43, 1-A-47, and 1-A-48. The room temperature hardness maximums are between 640 VHN and 695 VHN and the associated coercivity values are between 30 and 35 oersteds. All of these alloys contain tantalum combined with other additions (see Table II-6).

The results of the isochronal aging tests of the cobalt-base alloys 1-B-32 to 1-B-41 are plotted in Figures II-6 to II-8. The maximum values of hardness which were obtained by isochronal aging are listed in Table II-7 together with the temperature at which the maximum value was obtained. The coercivity at this temperature is also listed for each alloy.

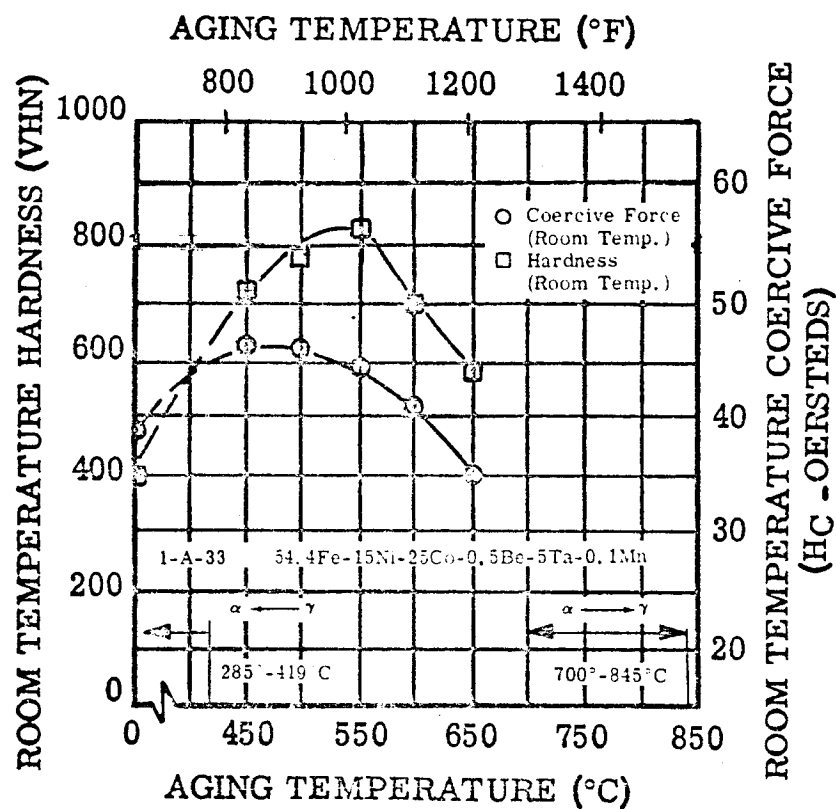


FIGURE II-1. Hardness and Coercive Force of Alloy 1-A-33 at Room Temperature After Aging One Hour at Temperature

Figure II-1. Hardness and Coercive Force of Alloy 1-A-33

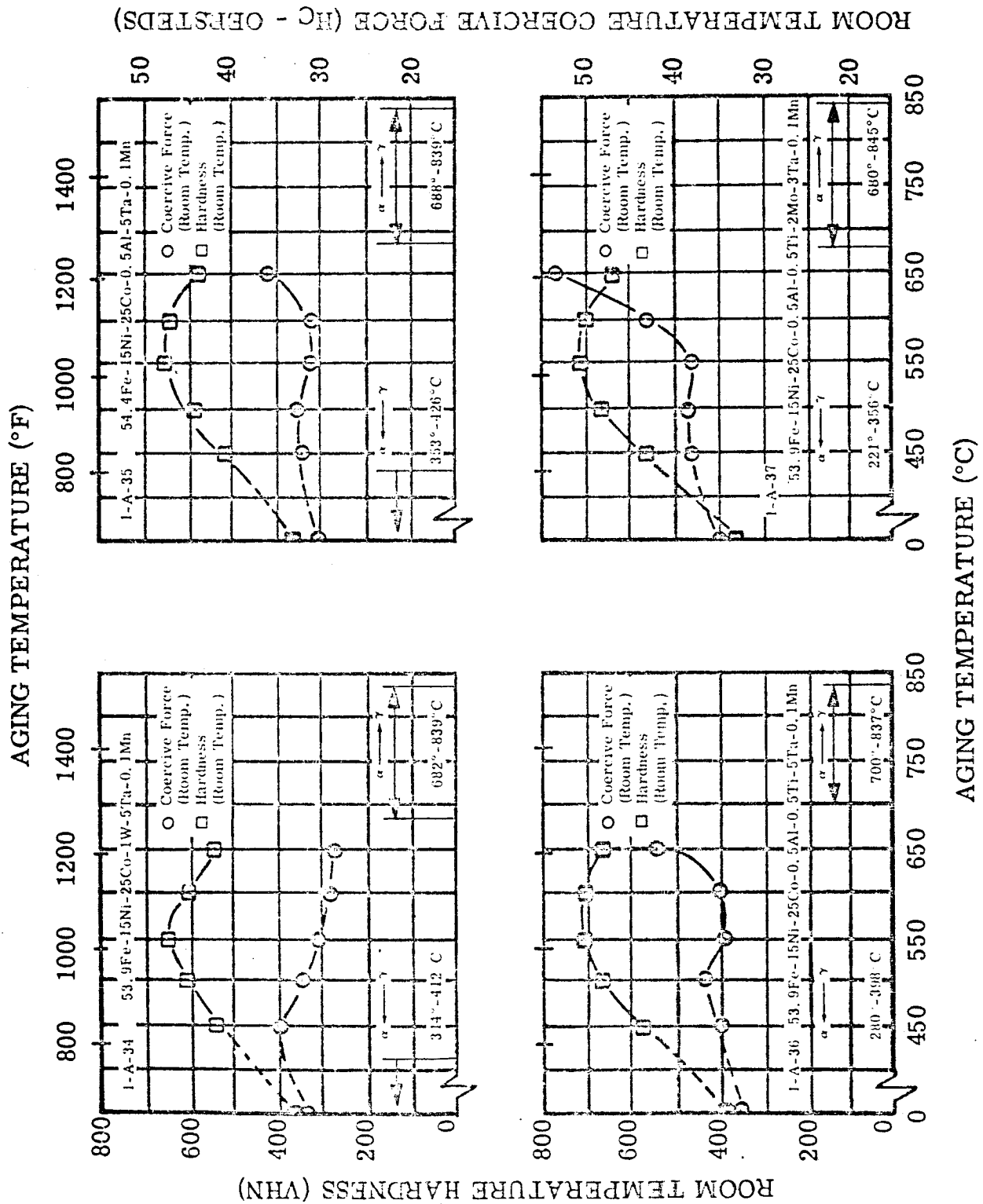


Figure II-2. Hardness and Coercive Force of Alloys 1-A-34, 1-A-35, 1-A-36 and 1-A-37

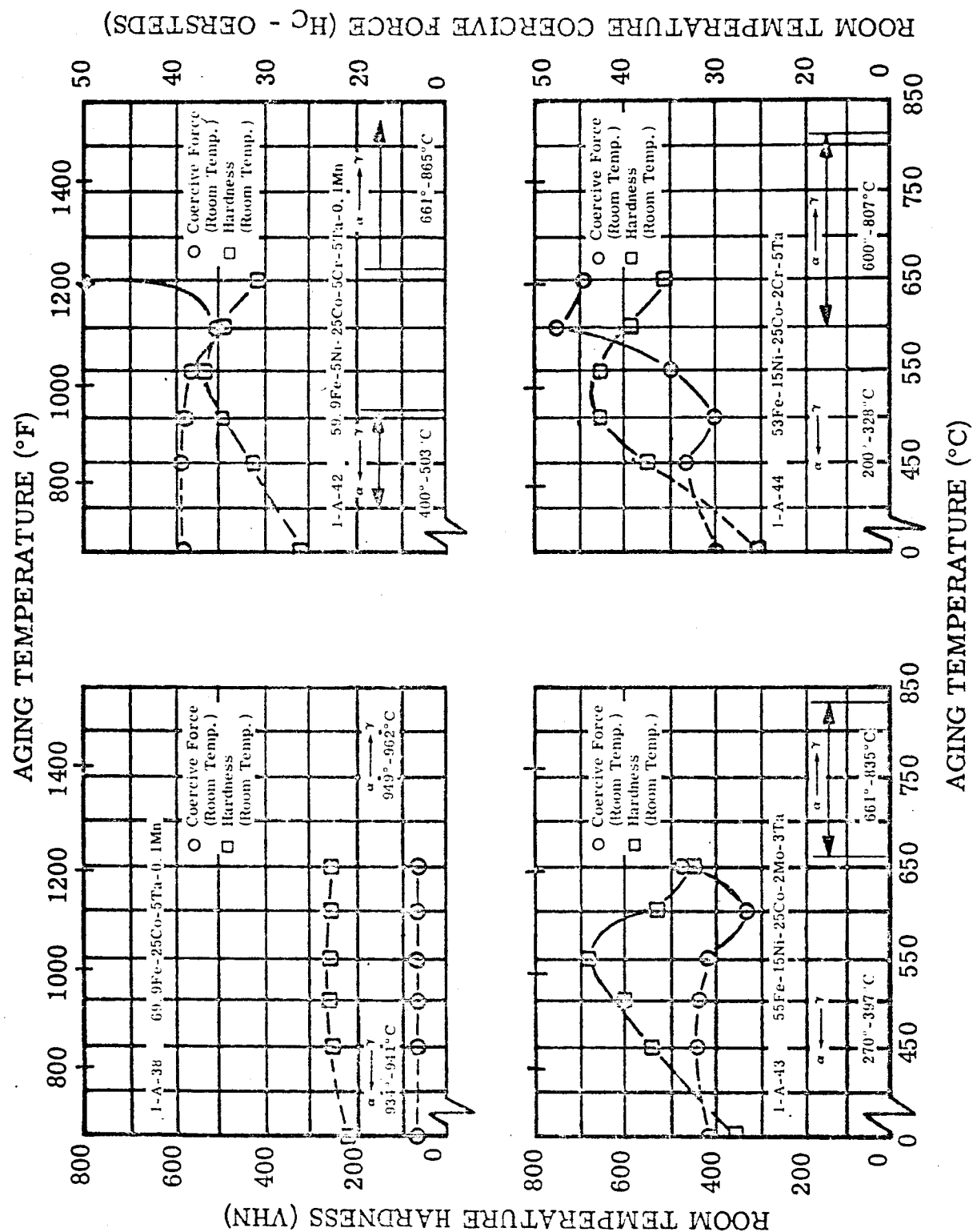


Figure II-3. Hardness and Coercive Force of Alloys 1-A-38, 1-A-42, 1-A-43 and 1-A-44

FIGURE II-3. Hardness and Coercive Force of Alloys 1-A-38, 1-A-42, 1-A-43 and 1-A-44 at Room Temperature After Aging One Hour at Temperature

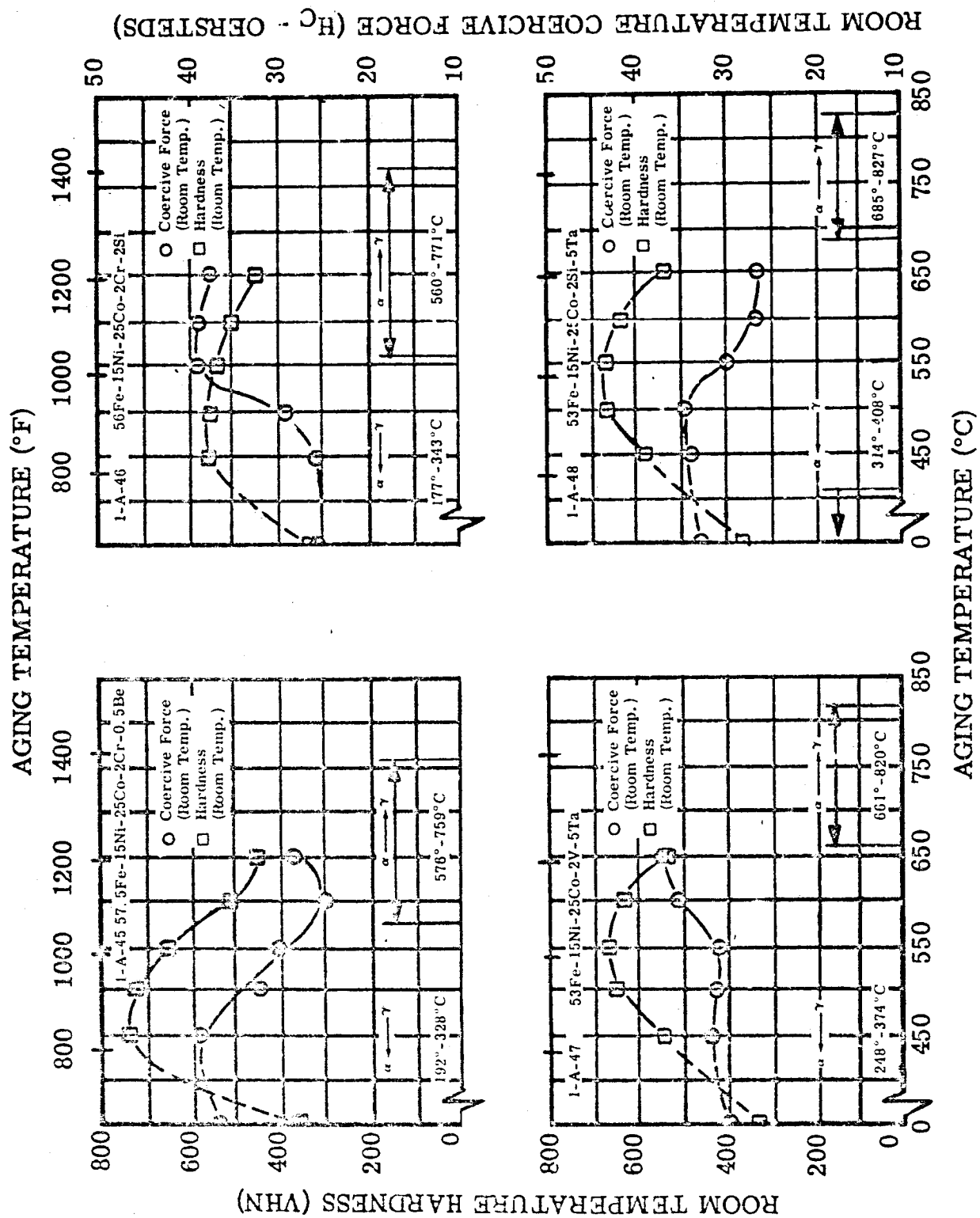


Figure II-4. Hardness and Coercive Force of Alloys 1-A-45, 1-A-46, 1-A-47 and 1-A-48

FIGURE II-4. Hardness and Coercive Force of Alloys 1-A-45, 1-A-46, 1-A-47 and 1-A-48 at Room Temperature After Aging One Hour at Temperature

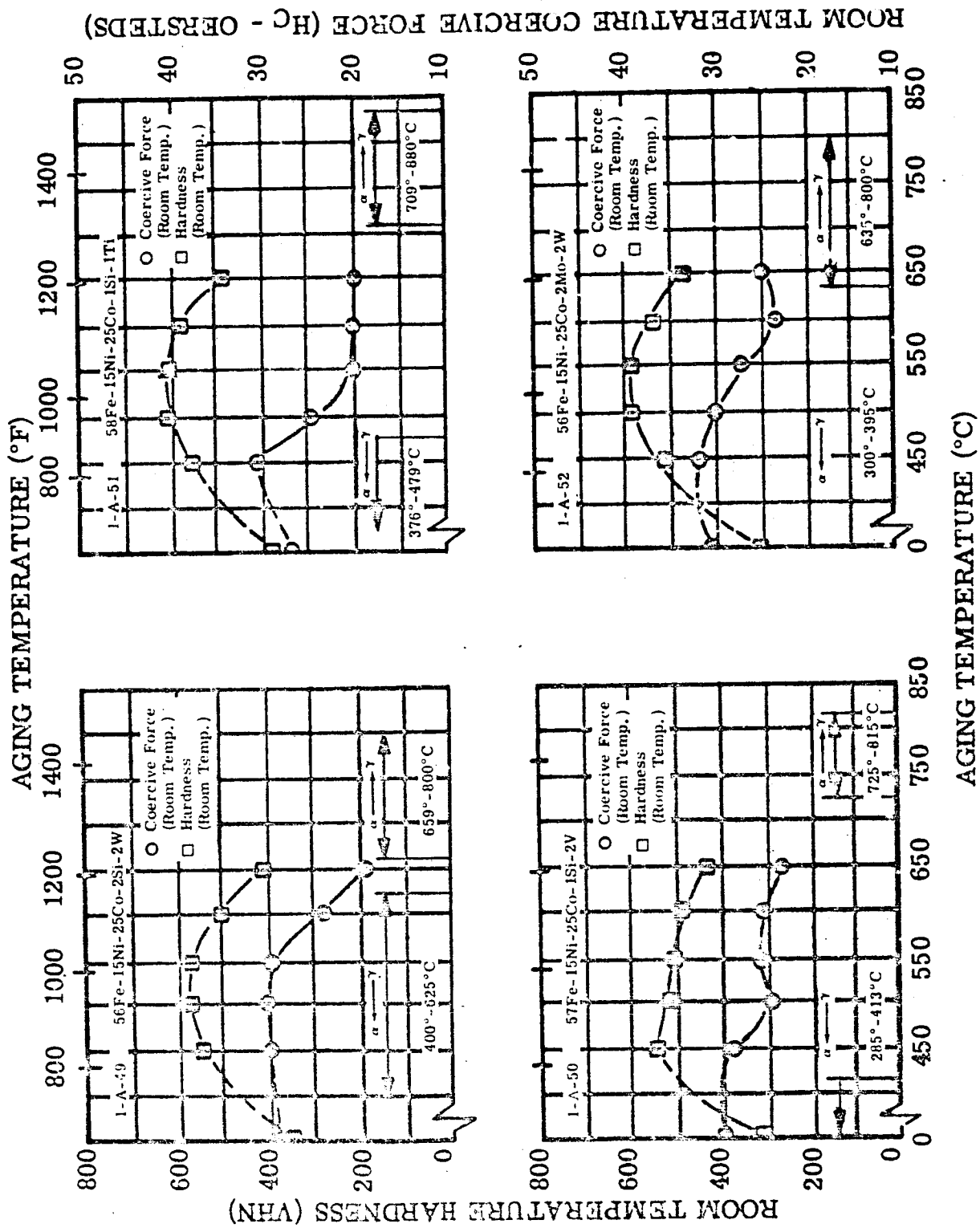


Figure II-5. Hardness and Coercive Force of Alloys 1-A-49, 1-A-50, 1-A-51 and 1-A-52

FIGURE II-5. Hardness and Coercive Force of Alloys 1-A-49, 1-A-50, 1-A-51 and 1-A-52 at Room Temperature After Aging One Hour at Temperature

TABLE II-6. Maximum Hardness Obtained by the Isochronal Aging Sequence of Martensitic Alloys 1-A-33 to 1-A-38 and 1-A-42 to 1-A-52(a)

Alloy Number	Nominal Alloy Composition (weight percent)	Aging Temperature at Which Maximum Room Temperature Hardness was Obtained (°F) (°C)		Total Aging Time (b) (hours)	Maximum Room Temperature Hardness (VHN)	Room Temperature Coercivity at Maximum Hardness (oersteds)
1-A-33	54.4Fe-15Ni-25Co-0.5Be-5Ta-0.1Mn	1022	550	3	810	44.5
1-A-34	53.9Fe-15Ni-25Co-1W-5Ta-0.1Mn	1022	550	3	642	31.0
1-A-35	54.4Fe-15Ni-25Co-0.5Al-5Ta-0.1Mn	1022	550	3	649	31.0
1-A-36	53.9Fe-15Ni-25Co-0.5Al-0.5Ti-5Ta-0.1Mn	1022	550	3	687	34.0
1-A-37	53.9Fe-15Ni-25Co-0.5Al-0.5Ti-2Mo-3Ta-0.1Mn	1022	550	3	674	32.0
1-A-38	69.9Fe-25Co-5Ta-0.1Mn	1022	550	3	259	14.0
1-A-42	59.9Fe-5Ni-25Co-5Cr-5Ta-0.1Mn	1022	550	3	533	36.0
1-A-43	55Fe-15Ni-25Co-2Mo-3Ta	1022	550	3	695	31.0
1-A-44	53Fe-15Ni-25Co-2Cr-5Ta	1022	550	3	663	35.0
1-A-45	57.5Fe-15Ni-25Co-2Cr-0.5Be	842	450	1	757	39.0
1-A-46	56Fe-15Ni-25Co-2Cr-2Si	842	450	1	568	29.5
1-A-47	53Fe-15Ni-25Co-2V-5Ta	1022	550	3	677	31.0
1-A-48	53Fe-15Ni-25Co-2Si-5Ta	1022	550	3	663	30.5
1-A-49	56Fe-15Ni-25Co-2Si-2W	932	500	2	572	30.5
1-A-50	57Fe-15Ni-25Co-1Si-2V	842	450	1	546	29.0
1-A-51	58Fe-15Ni-25Co-1Si-1Ti	932	500	2	616	29.5
1-A-52	56Fe-15Ni-25Co-2Mo-2W	932	500	2	577	30.0

(a) See Figures II-1 through II-5.

(b) Total aging time may be determined by adding one hour aging time for each 90°F(50°C) increment in temperature starting at 842°F (450°C).

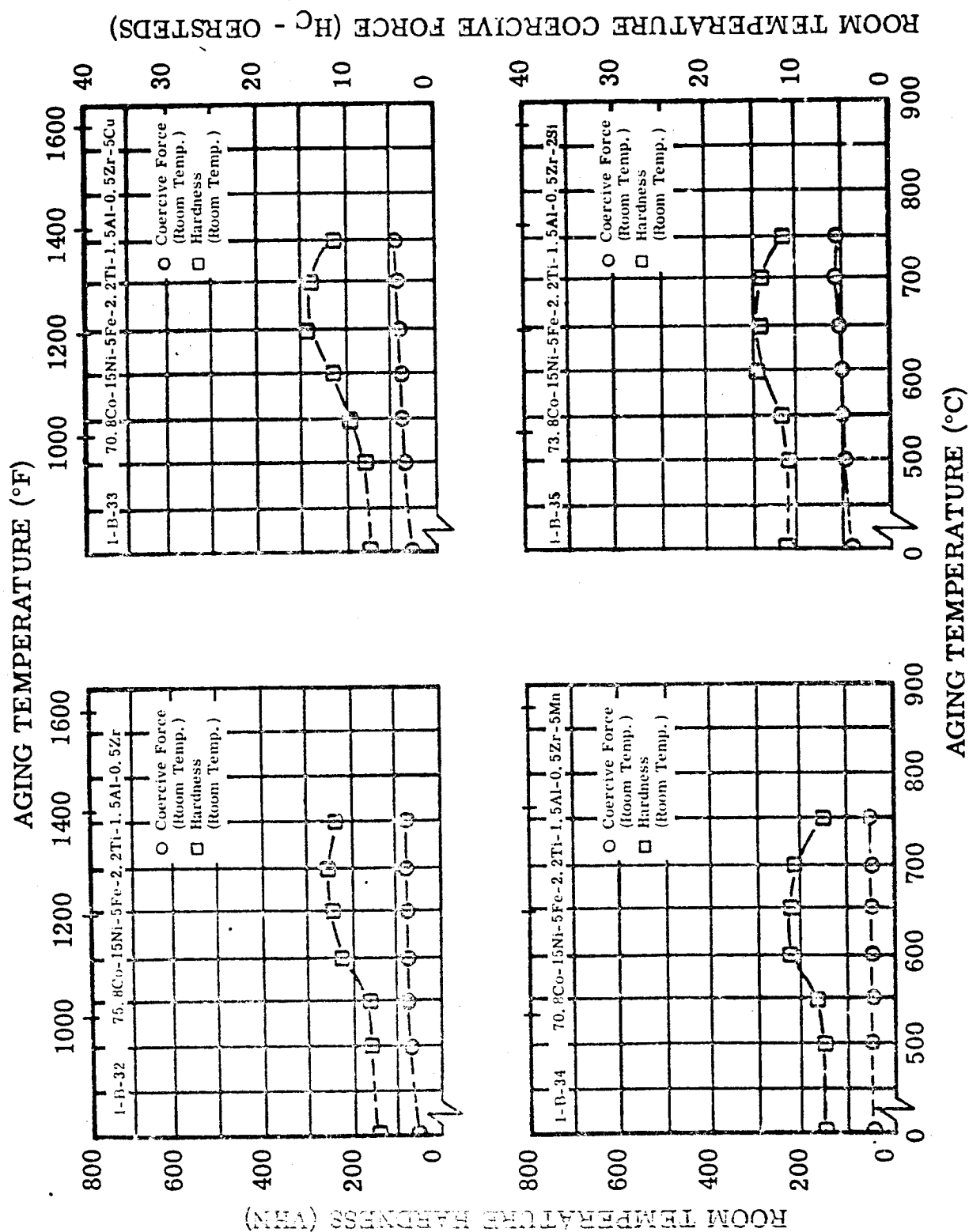


Figure II-6. Hardness and Coercive Force of Alloys 1-B-32, 1-B-33, 1-B-34 and 1-B-35

FIGURE II-6. Hardness and Coercive Force of Alloys 1-B-32, 1-B-33, 1-B-34 and 1-B-35 at Room Temperature After Aging One Hour at Temperature

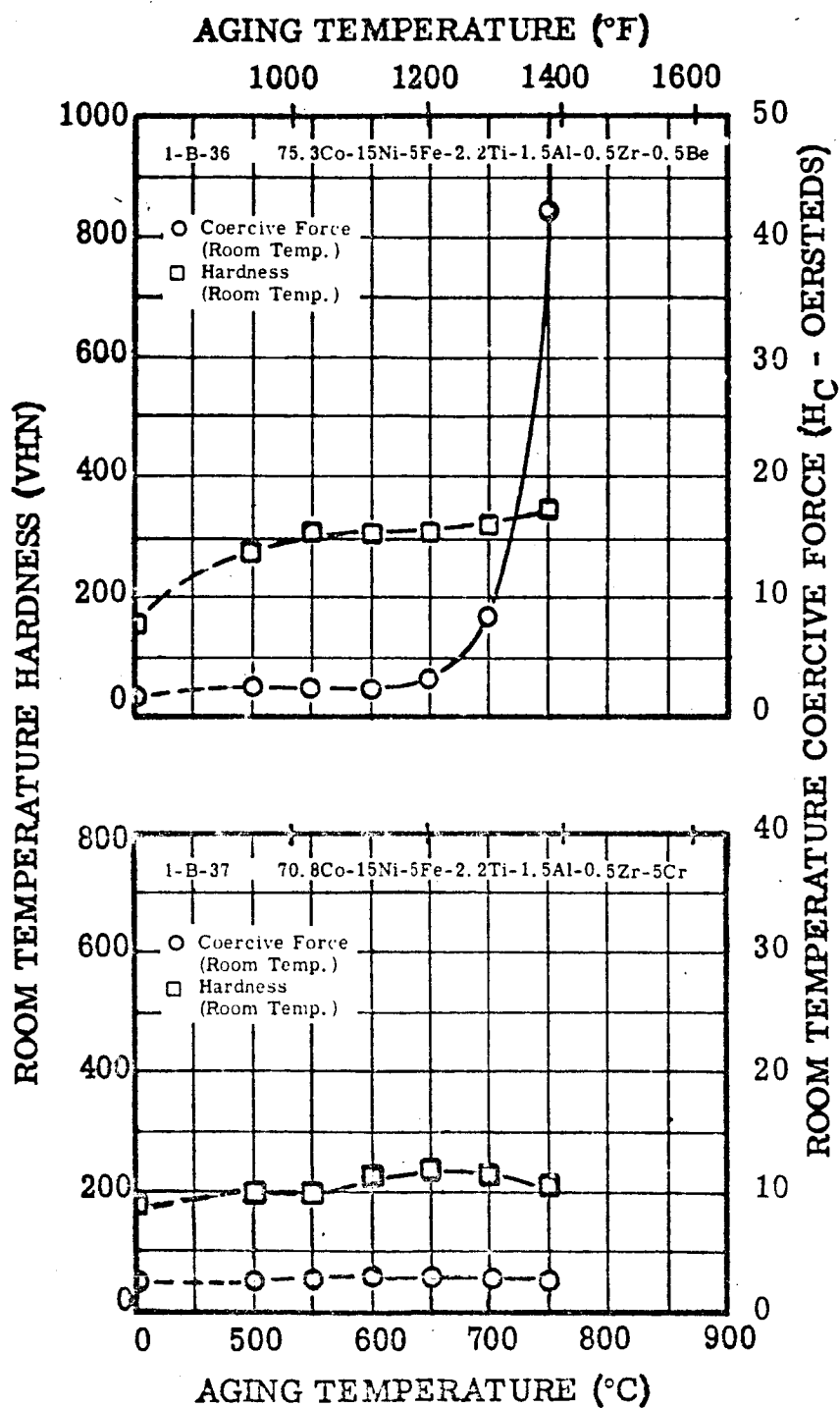


FIGURE II-7. Hardness and Coercive Force of Alloys 1-B-36 and 1-B-37 at Room Temperature After Aging One Hour at Temperature

Figure II-7. Hardness and Coercive Force of Alloys 1-B-36 and 1-B-37

Figure II-8. Hardness and Coercive Force of Alloys 1-B-38, 1-B-39, 1-B-40 and 1-B-41

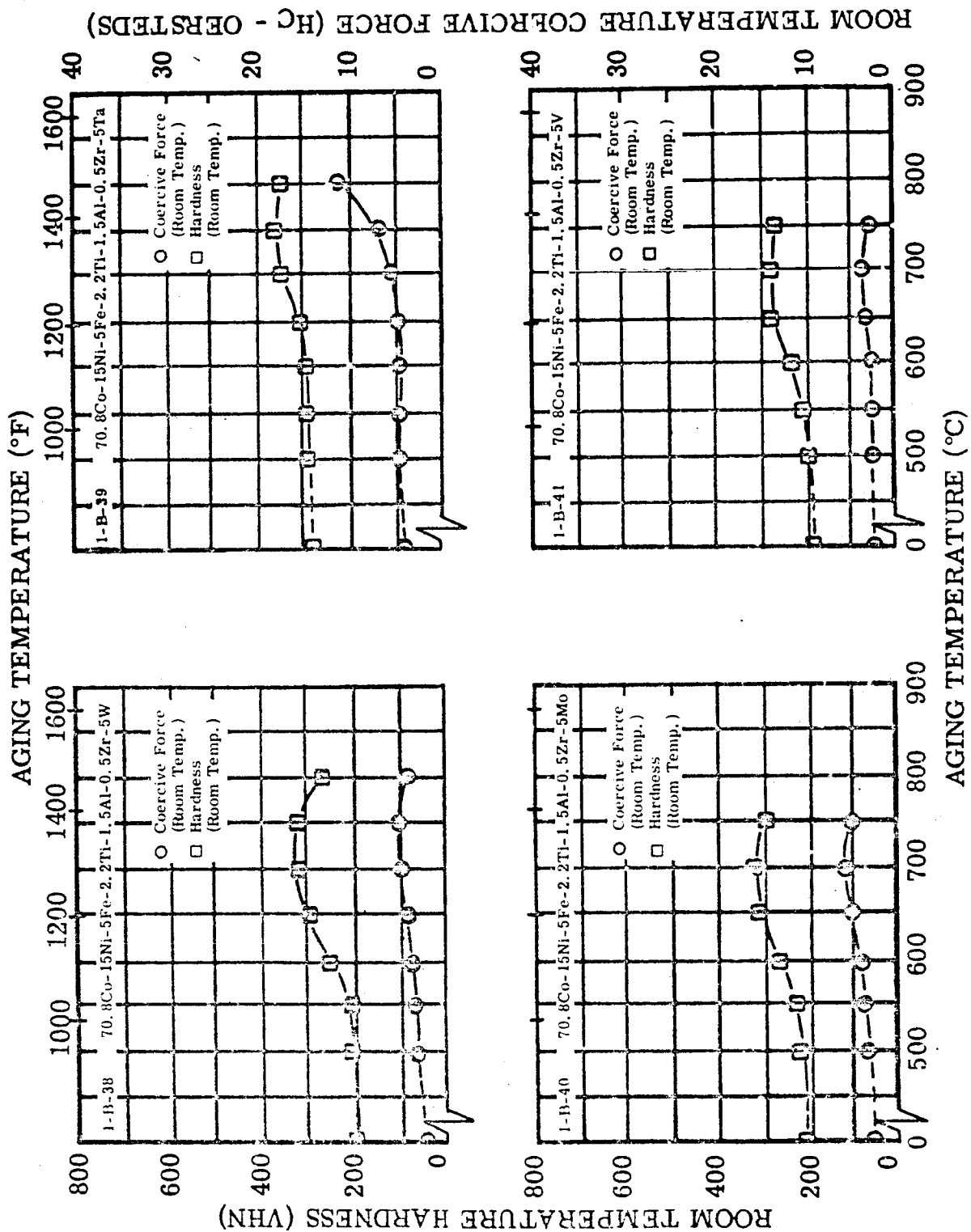


FIGURE II-8. Hardness and Coercive Force of Alloys 1-B-38, 1-B-39, 1-B-40 and 1-B-41 at Room Temperature After Aging One Hour at Temperature

TABLE II-17. Maximum Hardness Obtained by the Isochronal Aging Sequence of Cobalt-Base Alloys 1-B-32 to 1-B-41(a)

Alloy Number	Nominal Alloy Composition (weight percent)	Aging Temperature at Which Maximum Room Temperature Hardness was Obtained (°F)		Total Aging Time (b) (hours)	Maximum Room Temperature Hardness (VHN)	Room Temperature Coercivity at Maximum Hardness (oersteds)
1-B-32	75.8Co-15Ni-5Fe-2.2Ti-1.5Al-0.5Zr	1292	700	5	264	3.8
1-B-33	70.8Co-15Ni-5Fe-2.2Ti-1.5Al-0.5Zr-5Cu	1202	650	4	280	4.0
1-B-34	70.8Co-15Ni-5Fe-2.2Ti-1.5Al-0.5Zr-5Mn	1112	600	3	224	2.5
1-B-35	73.8Co-15Ni-5Fe-2.2Ti-1.5Al-0.5Zr-2Si	1112	600	3	293	5.0
1-B-36	75.3Co-15Ni-5Fe-2.2Ti-1.5Al-0.5Zr-0.5Be	1382	750	6	353	42.0
1-B-37	70.8Co-15Ni-5Fe-2.2Ti-1.5Al-0.5Zr-5Cr	1202	650	4	256	3.0
1-B-38	70.8Co-15Ni-5Fe-2.2Ti-1.5Al-0.5Zr-5W	1382	750	6	328	5.3
1-B-39	70.8Co-15Ni-5Fe-2.2Ti-1.5Al-0.5Zr-5Ta	1382	750	6	383	7.1
1-B-40	70.8Co-15Ni-5Fe-2.2Ti-1.5Al-0.5Zr-5Mo	1292	700	5	330	5.9
1-B-41	70.8Co-15Ni-5Fe-2.2Ti-1.5Al-0.5Zr-5V	1202	650	4	287	3.3

(a) See Figures II-6 through II-13.

(b) Total aging time may be determined by adding one hour aging time for each 90°F (50°C) increment in temperature starting at 932°F (500°C).

The isochronal change of hardness in the cobalt-base alloys indicates an increase of hardness during aging. The increase of hardness in the alloy 1-B-34 is less than that in alloy 1-B-32 indicating that the manganese addition acts as a softener. Maximum hardness is increased in all of the other alloys by the extra elements as compared to alloy 1-B-32. The elements silicon, chromium, tungsten, molybdenum, vanadium and, in particular, tantalum show a substantial increase of hardness, even after cooling from the homogenization treatment, indicating that these elements act as solid solution hardening elements. If one considers only those alloys in which a maximum hardness well above 300 VHN is reached, the list includes alloys 1-B-36, 1-B-38, 1-B-39 and 1-B-40. The hardness maximum of 1-B-36, however, is associated with a very high coercive force. One should, therefore, rule out the addition of beryllium as a useful hardener. The highest value is obtained in the alloy 1-B-39 with 383 VHN at an aging temperature of 1382°F (750°C) indicating that tantalum is the most potent hardener in these alloys.

Isothermal aging tests were conducted at 1022°F (550°C) on the martensitic alloys except for alloy 1-A-38 and alloys 1-A-39 to 1-A-41 which did not show age hardening during the isochronal aging test. The change in hardness and coercivity for the martensitic alloys during isothermal aging are plotted in Figures II-9 to II-16.

These tests show that the properties of most of the martensitic alloys do not change substantially during aging at 1022°F (550°C). However, a rather strong increase of coercivity was observed in the alloys 1-A-35, 1-A-36, 1-A-37, 1-A-43, 1-A-44 and 1-A-47. This indicates that aluminum, chromium and, under certain circumstances, vanadium have an adverse effect on coercivity. A decrease in hardness of more than 20 percent was observed only in 1-A-45 during aging of 100 hours. The hardness remained constant (within 5 percent) in the alloys 1-A-35, 1-A-36 and 1-A-37. However, these three alloys showed a strong increase of coercivity during aging. If one allows a 10 percent decrease in hardness and an increase in coercivity of less than five oersteds, but with absolute values still below 35 oersteds, the alloys 1-A-34, 1-A-42, 1-A-48, 1-A-49, 1-A-50, and 1-A-52 qualify.

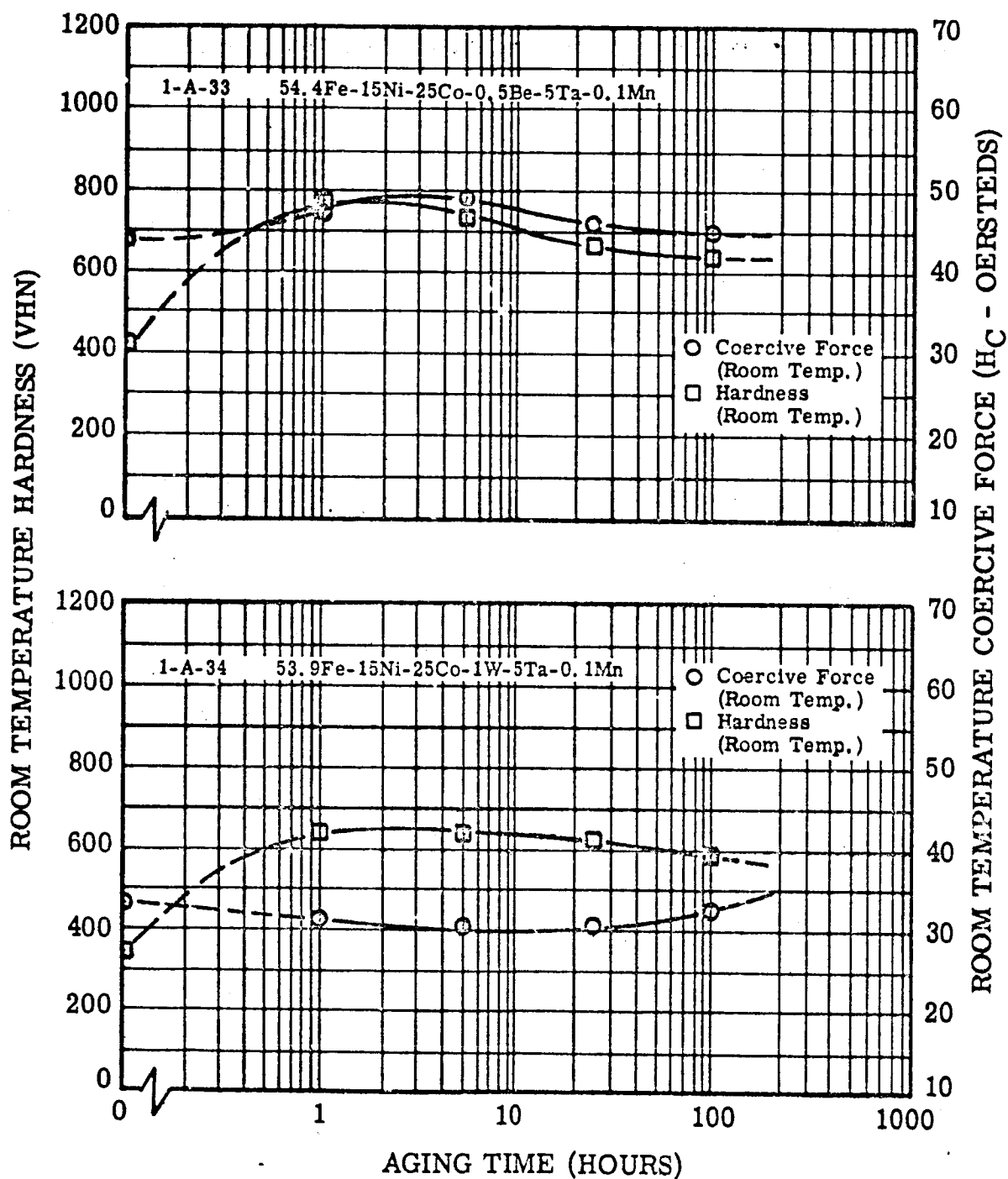


FIGURE II-9. Change in Room Temperature Hardness and Coercive Force of Alloys 1-A-33 and 1-A-34 During Isothermal Aging at 1022°F (550°C)

Figure II-9. Hardness and Coercive Force of Alloys 1-A-33 and 1-A-34 During Isothermal Aging

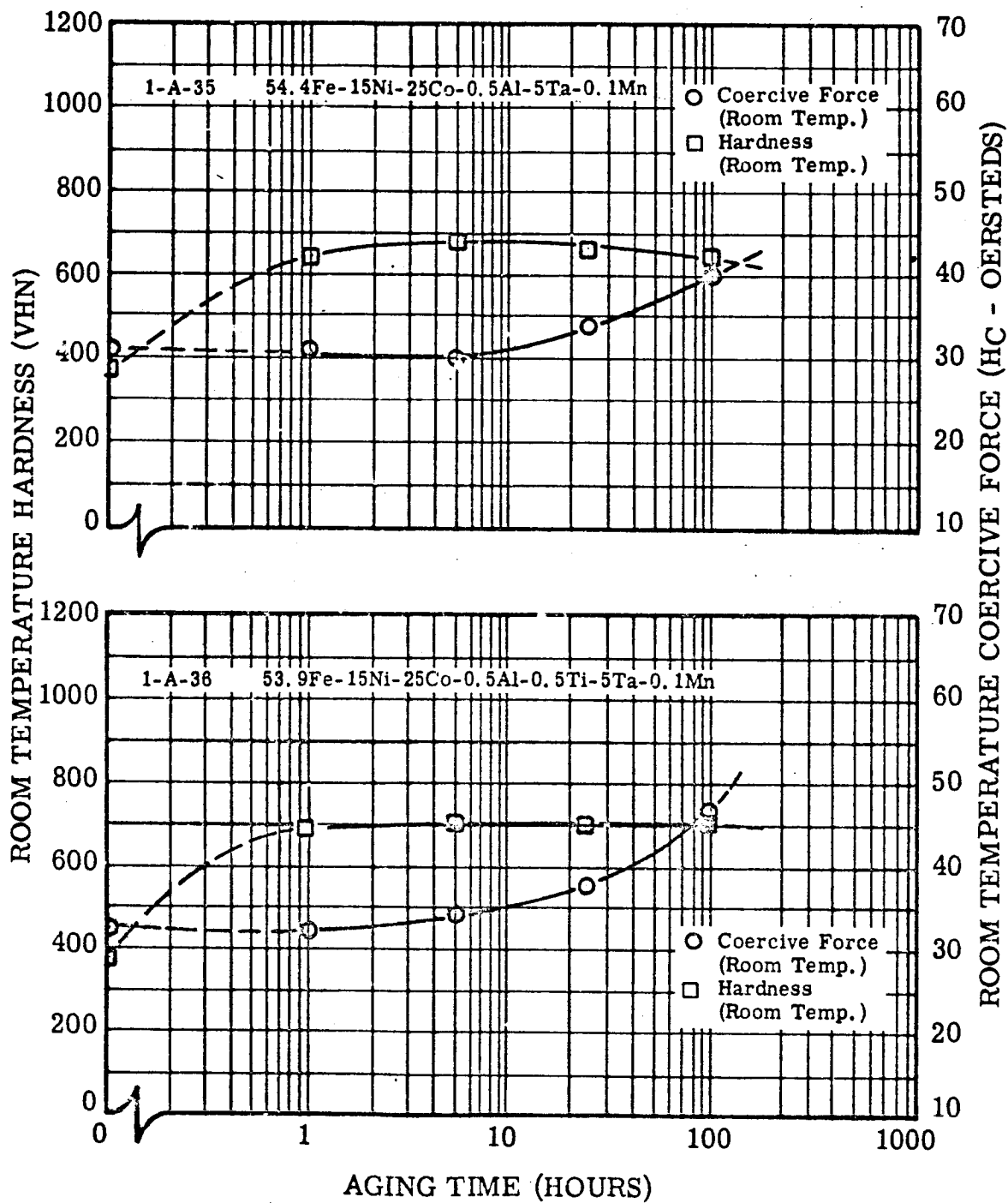


FIGURE II-10. Change in Room Temperature Hardness and Coercive Force of Alloys 1-A-35 and 1-A-36 During Isothermal Aging at 1022°F (550°C)

Figure II-10. Hardness and Coercive Force of Alloys 1-A-35 and 1-A-36 During Isothermal Aging

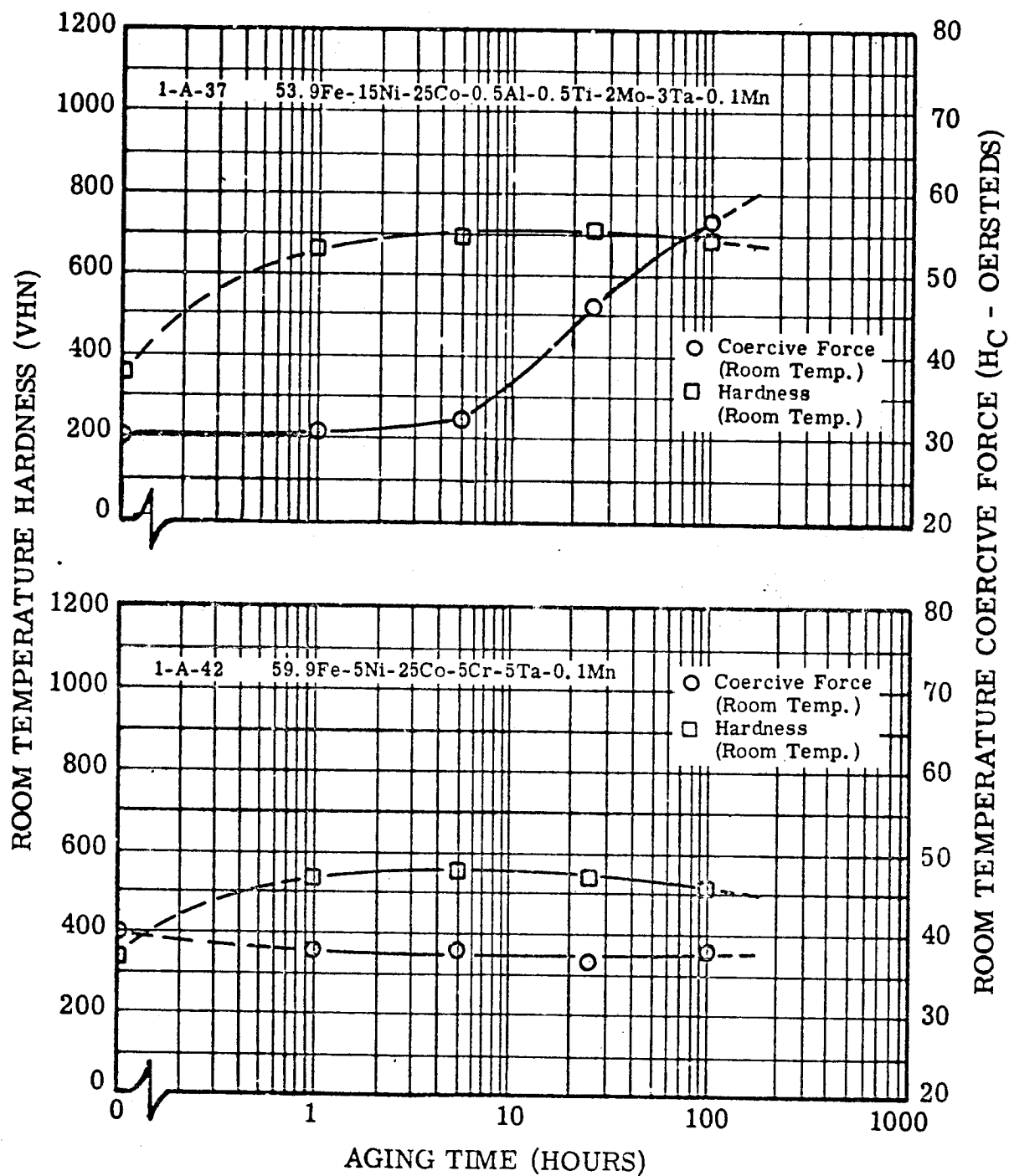


FIGURE II-11. Change in Room Temperature Hardness and Coercive Force of Alloys 1-A-37 and 1-A-42 During Isothermal Aging at 1022°F (550°C)

Figure II-11. Hardness and Coercive Force of Alloys 1-A-37 and 1-A-42 During Isothermal Aging

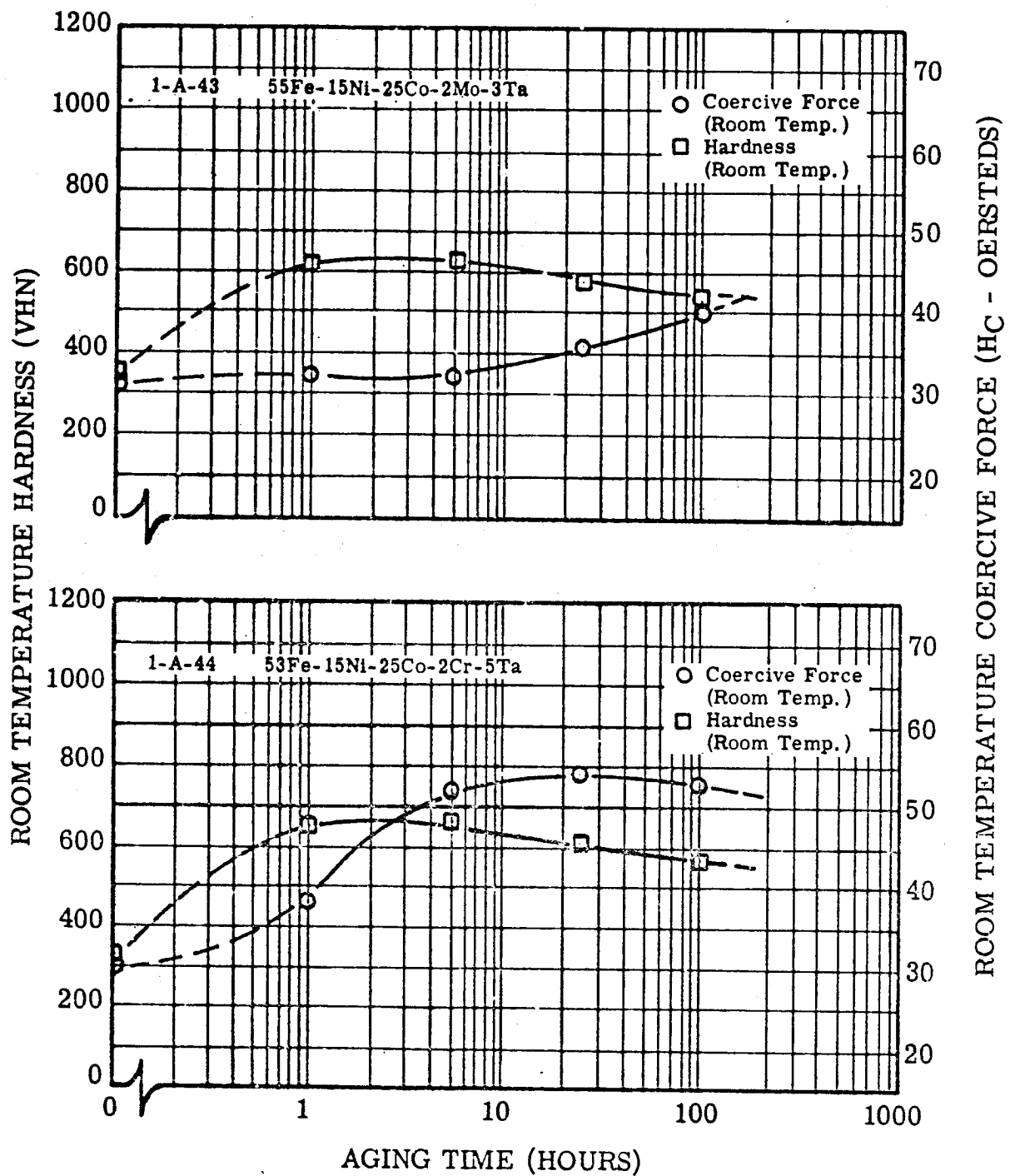


FIGURE II-12. Change in Room Temperature Hardness and Coercive Force of Alloys 1-A-43 and 1-A-44 During Isothermal Aging at 1022°F (550°C)

Figure II-12. Hardness and Coercive Force of Alloys 1-A-43 and 1-A-44 During Isothermal Aging

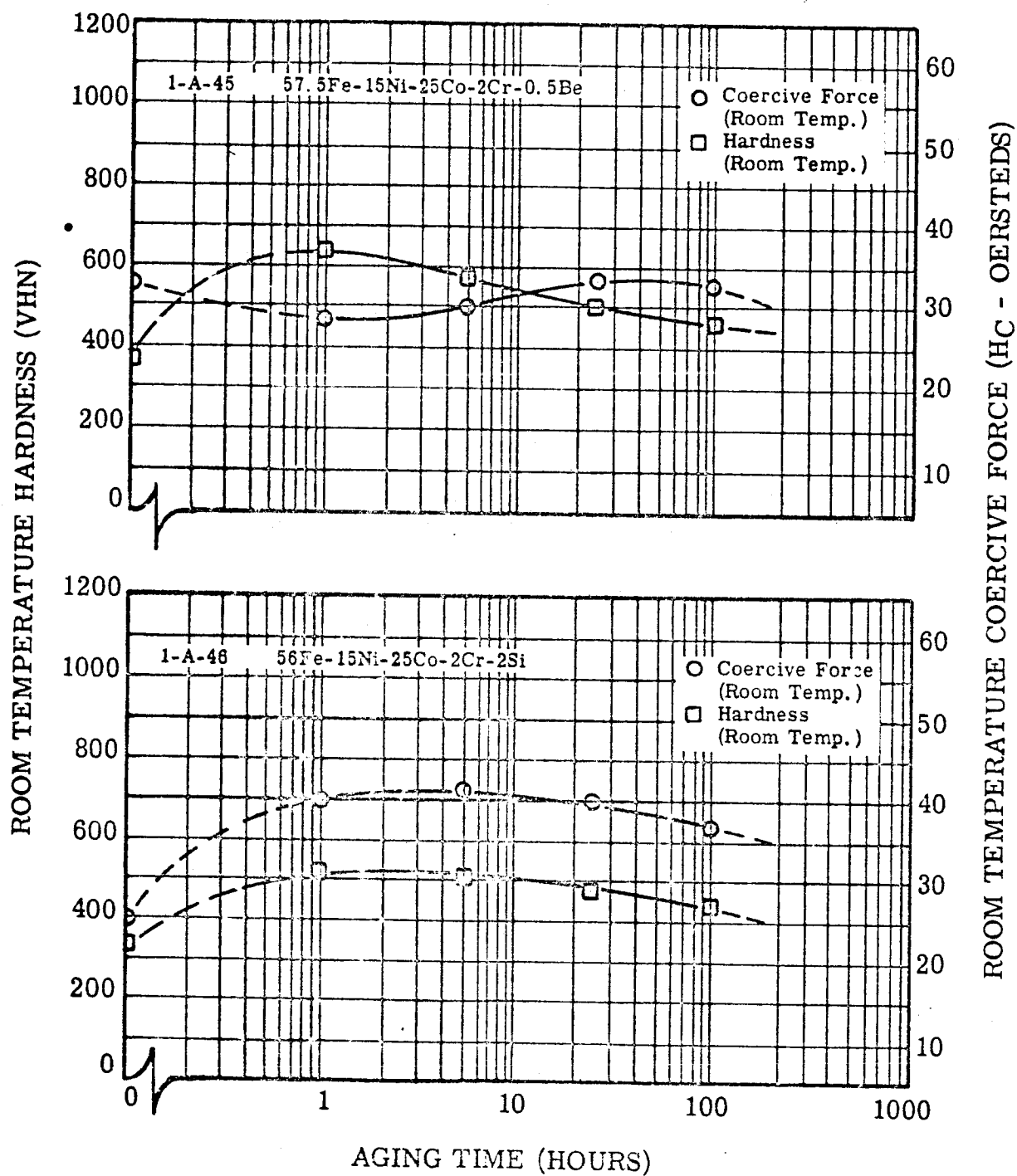


FIGURE II-13. Change in Room Temperature Hardness and Coercive Force of Alloys 1-A-45 and 1-A-46 During Isothermal Aging at 1022°F (550°C)

Figure II-13. Hardness and Coercive Force of Alloys 1-A-45 and 1-A-46 During Isothermal Aging

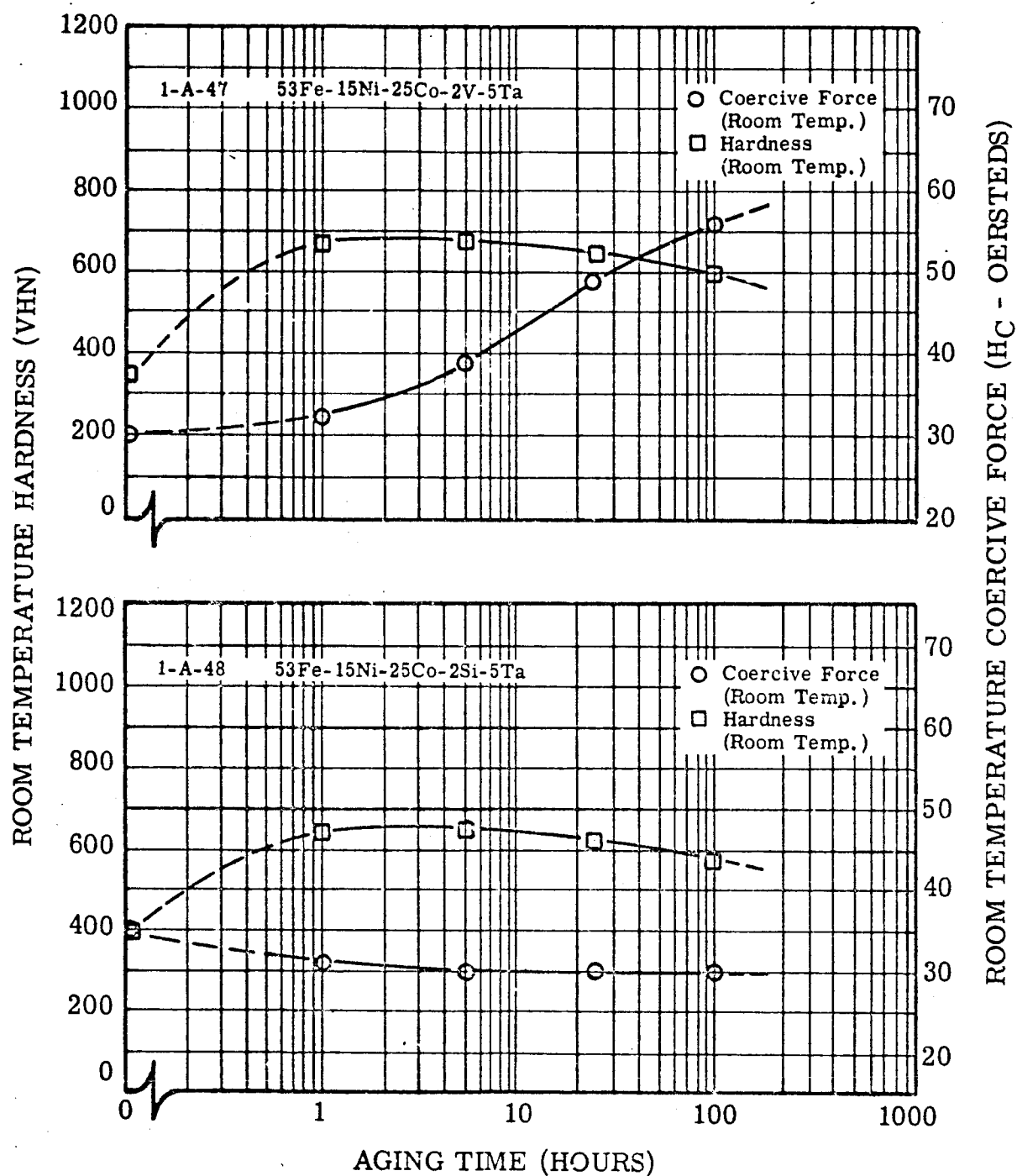


FIGURE II-14. Change in Room Temperature Hardness and Coercive Force of Alloys 1-A-47 and 1-A-48 During Isothermal Aging at 1022°F (550°C)

Figure II-14. Hardness and Coercive Force of Alloys 1-A-47 and 1-A-48 During Isothermal Aging

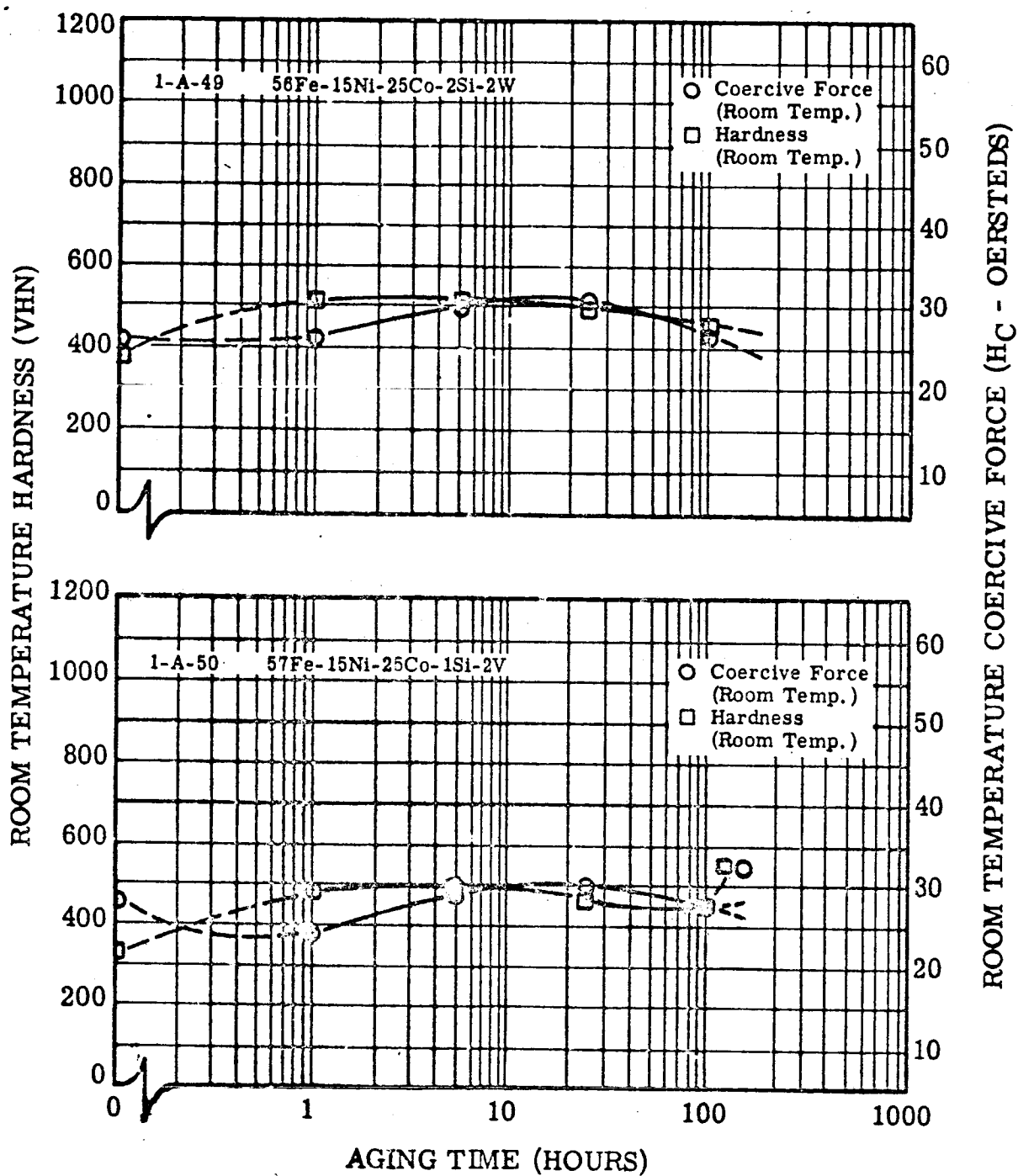


FIGURE II-15. Change in Room Temperature Hardness and Coercive Force of Alloys 1-A-49 and 1-A-50 During Isothermal Aging at 1022°F (550°C)

Figure II-15. Hardness and Coercive Force of Alloys 1-A-49 and 1-A-50 During Isothermal Aging

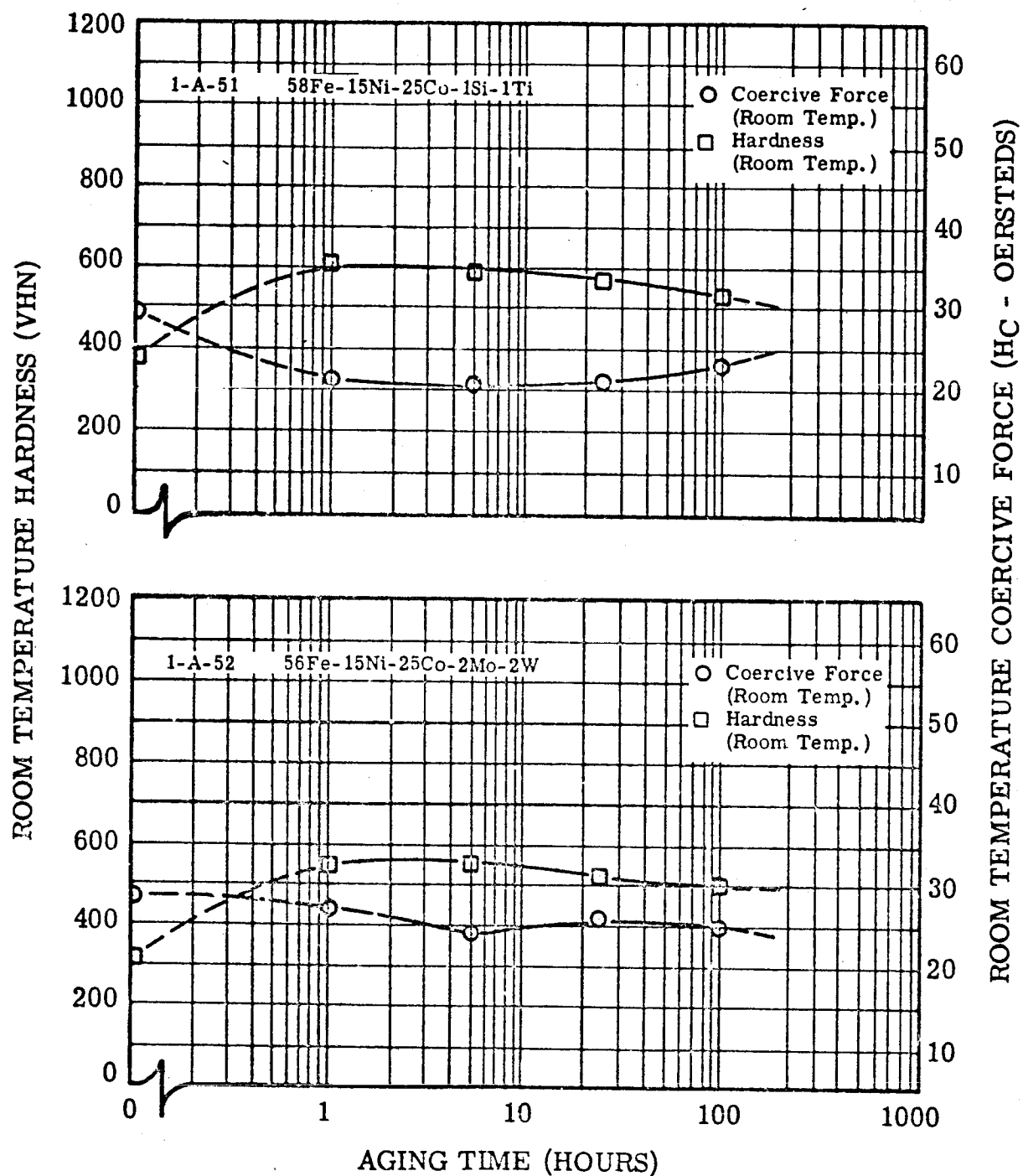


FIGURE II-16. Change in Room Temperature Hardness and Coercive Force of Alloys 1-A-51 and 1-A-52 During Isothermal Aging at 1022°F (550°C)

Figure II-16. Hardness and Coercive Force of Alloys 1-A-51 and 1-A-52 During Isothermal Aging

The aging tests of the martensitic alloys would then suggest the alloys 1-A-34 (53.9Fe-15Ni-25Co-1W-5Ta-0.1Mn) and 1-A-48 (53Fe-15Ni-25Co-2Si-5Ta) as the most promising. Table II-3 shows the α to γ transformation temperature of these alloys to be above 1202°F (650°C).

The results of the 1292°F (700°C) isothermal aging tests of the cobalt-base alloys are plotted in Figures II-17 to II-21. Alloy 1-B-34 was not tested because of the small increase in hardness exhibited during isochronal aging. These tests indicate that both hardness and coercivity increased during aging at 1292°F (700°C). Less than 20 percent increase in hardness was exhibited by the cobalt-base alloys during 100 hours aging. The greatest increase in coercivity was observed in alloy 1-B-36. Nearly all alloys showed a coercivity value near five oersteds after one hour at 1292°F (700°C). An increase of less than 20 oersteds was apparent in alloys 1-B-32, 1-B-37, 1-B-38, and 1-B-39 after 100 hours aging at 1292°F (700°C). Of these alloys, only 1-B-38 and 1-B-39 attained a hardness value in excess of 300 VHN. Therefore, it appears that only alloys 1-B-38 (70.8Co-15Ni-5Fe-2.2Ti-1.5Al-0.5Zr-5W) and 1-B-39 (70.8Co-15Ni-5Fe-2.2Ti-1.5Al-0.5Zr-5W-5Ta) may be useful candidates for stable high-temperature cobalt-base magnetic alloys.

(5) Microstructure

Figures II-22 to II-37 show the light micrographs of the structure of the martensitic alloys after aging for 100 hours at 1022°F (550°C).

Alloy 1-A-42 contains particles of a second phase which may have originated during solidification.

A network of grain boundary precipitate, which may have precipitated along the boundaries when the steel was still austenitic, can be recognized in alloys 1-A-34, 1-A-37, 1-A-44, 1-A-45, 1-A-46, 1-A-49, 1-A-50 and 1-A-51. The alloys 1-A-42, 1-A-47, 1-A-48, 1-A-51, and 1-A-52 showed a very strong attack by the etching solution indicating the presence of a second phase. The attack by the etching solution in the alloys 1-A-35, 1-A-36, 1-A-37, and 1-A-44 was rather light. Alloys 1-A-38 to 1-A-41, which had not been aged isothermally, were not examined.

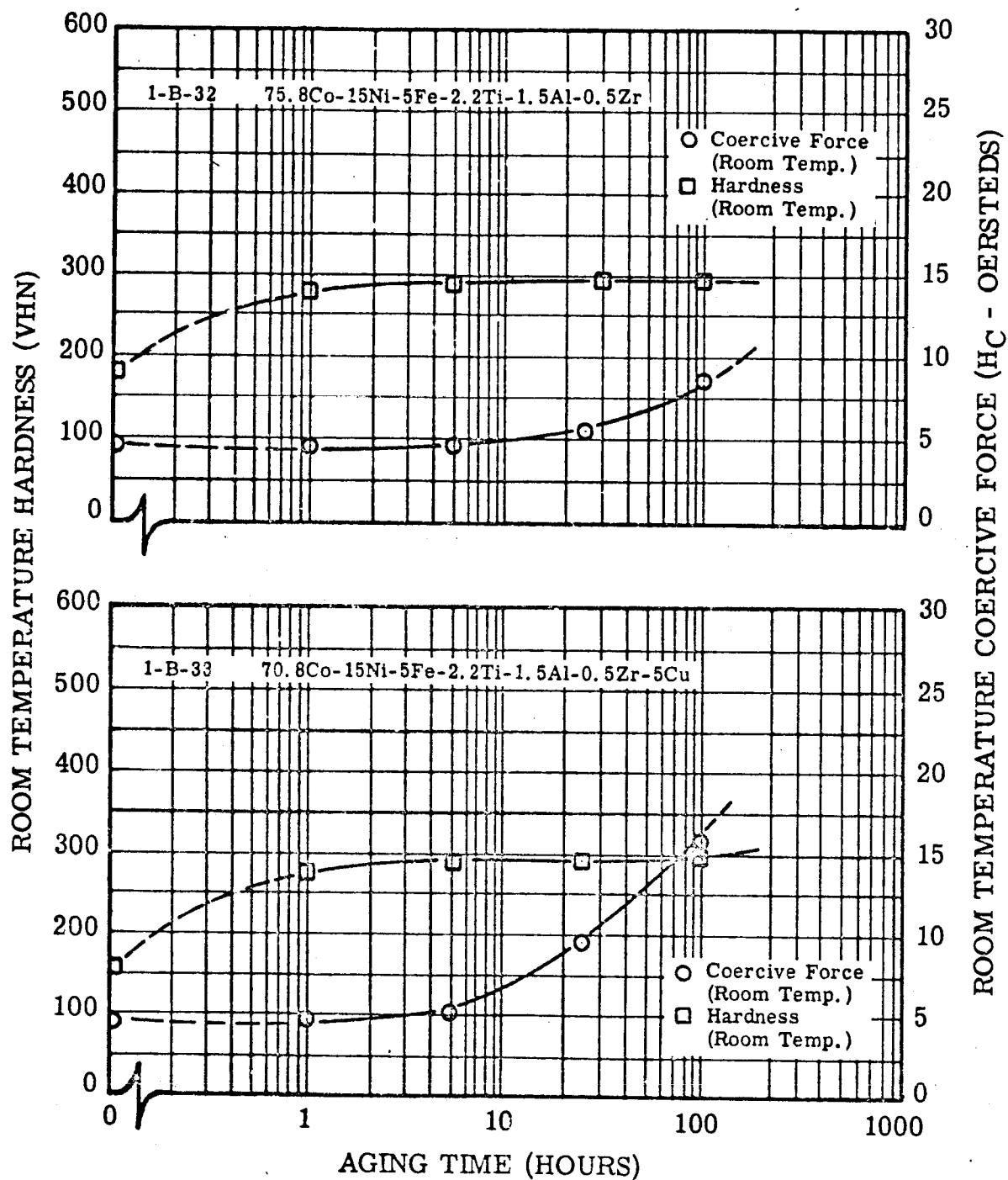


FIGURE II-17. Change in Room Temperature Hardness and Coercive Force of Alloys 1-B-32 and 1-B-33 During Isothermal Aging at 1292°F (700°C)

Figure II-17. Hardness and Coercive Force of Alloys 1-B-32 and 1-B-33 During Isothermal Aging

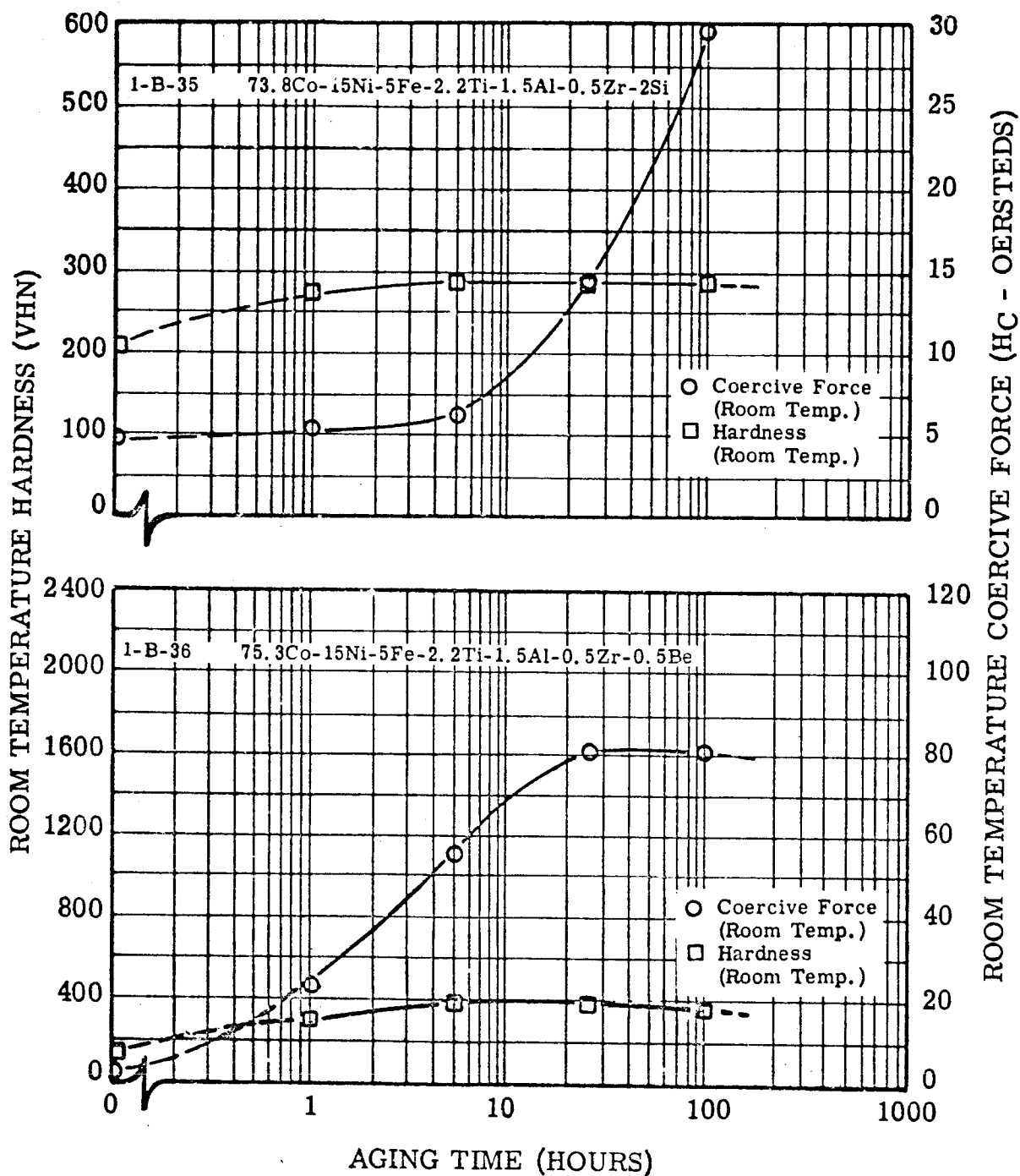


FIGURE II-18. Change in Room Temperature Hardness and Coercive Force of Alloys 1-B-35 and 1-B-36 During Isothermal Aging at 1292°F (700°C)

Figure II-18. Hardness and Coercive Force of Alloys 1-B-35 and 1-B-36 During Isothermal Aging

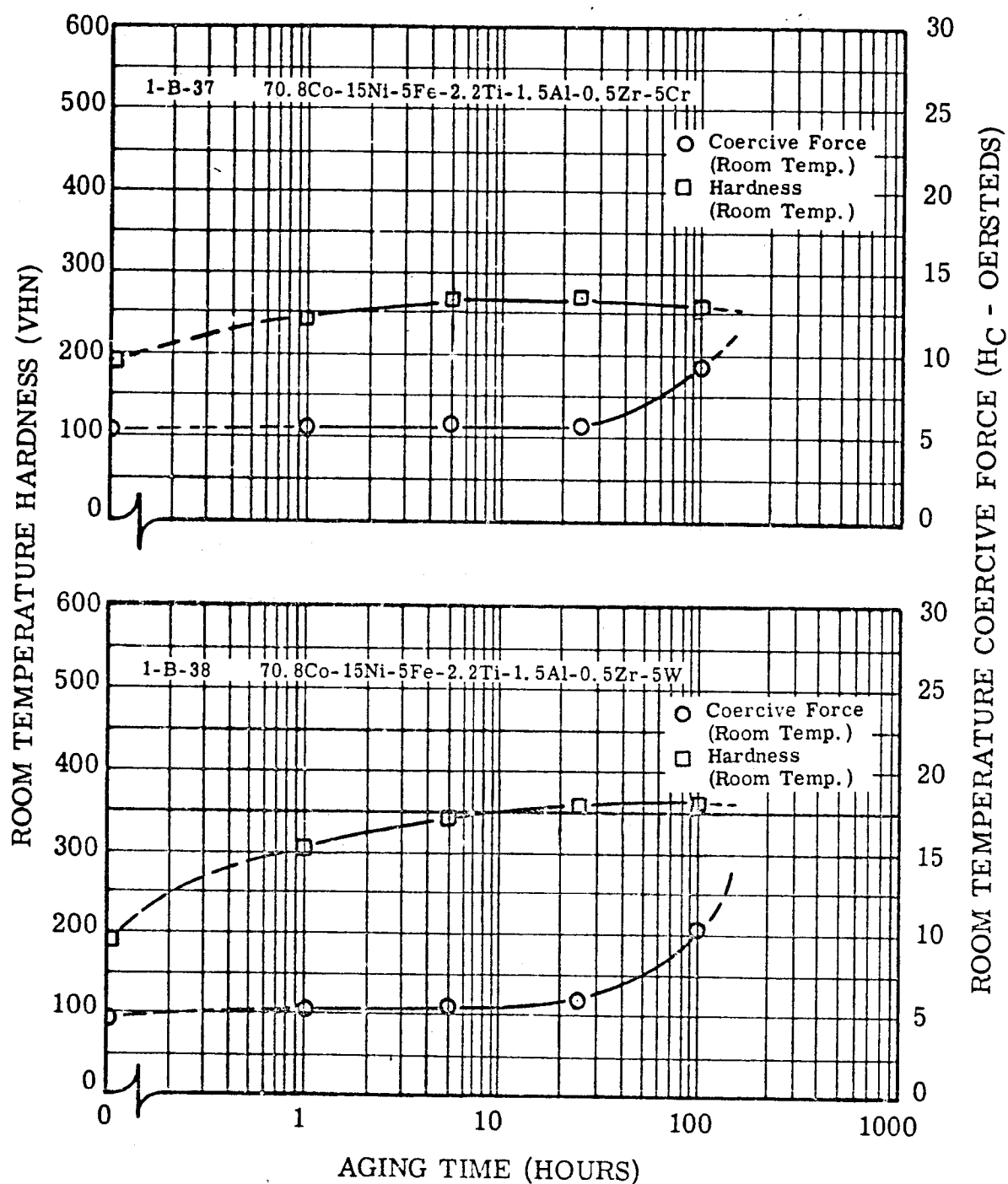


FIGURE II-19. Change in Room Temperature Hardness and Coercive Force of Alloys 1-B-37 and 1-B-38 During Isothermal Aging at 1292°F (700°C)

Figure II-19. Hardness and Coercive Force of Alloys 1-B-37 and 1-B-38 During Isothermal Aging

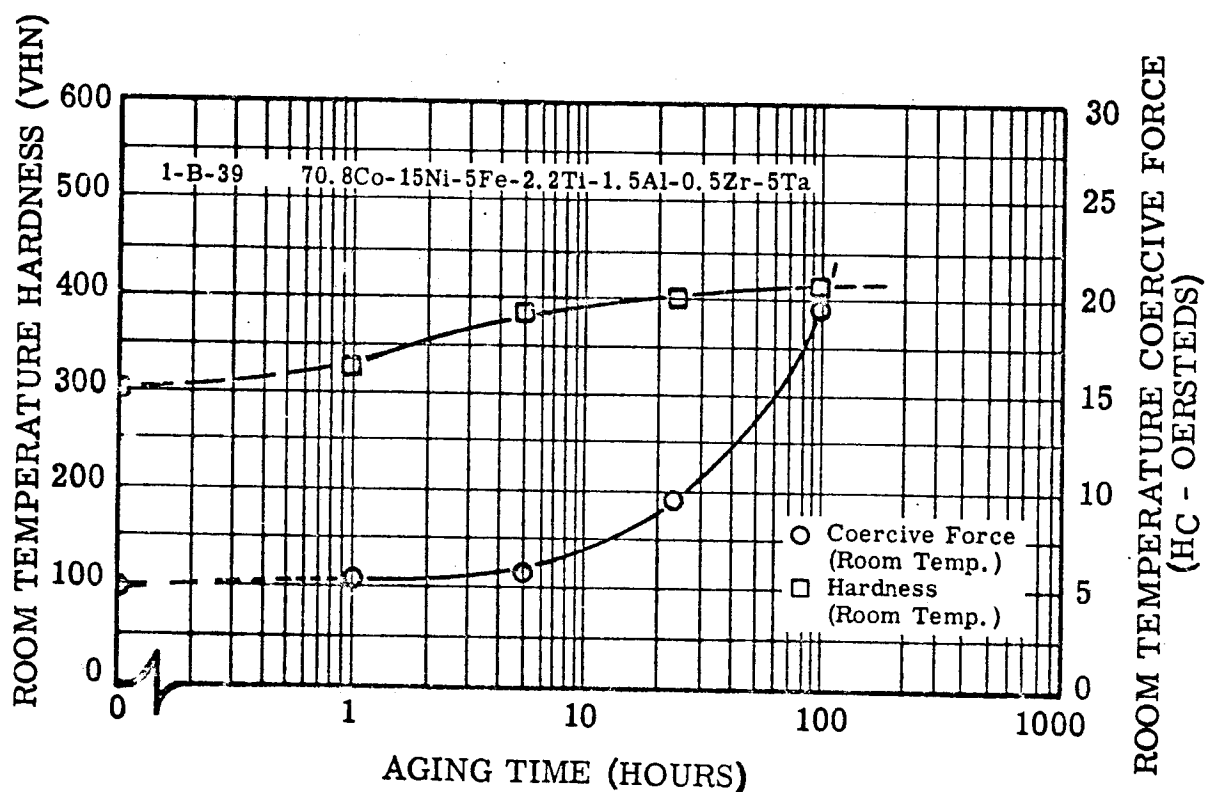


FIGURE II-20. Change in Room Temperature Hardness and Coercive Force of Alloy 1-B-39 During Isothermal Aging at 1292°F (700°C)

Figure II-20. Hardness and Coercive Force of Alloy 1-B-39 During Isothermal Aging

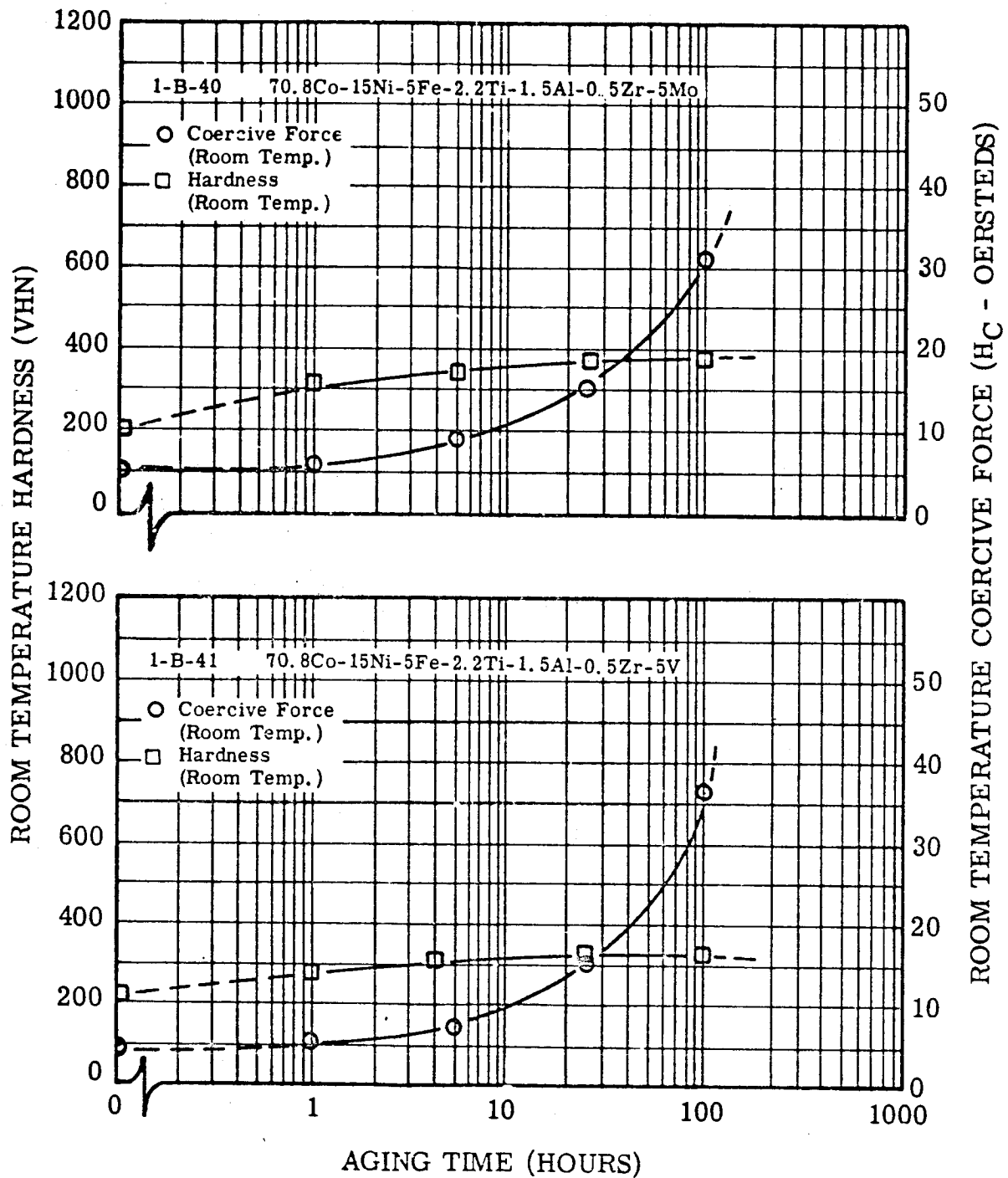
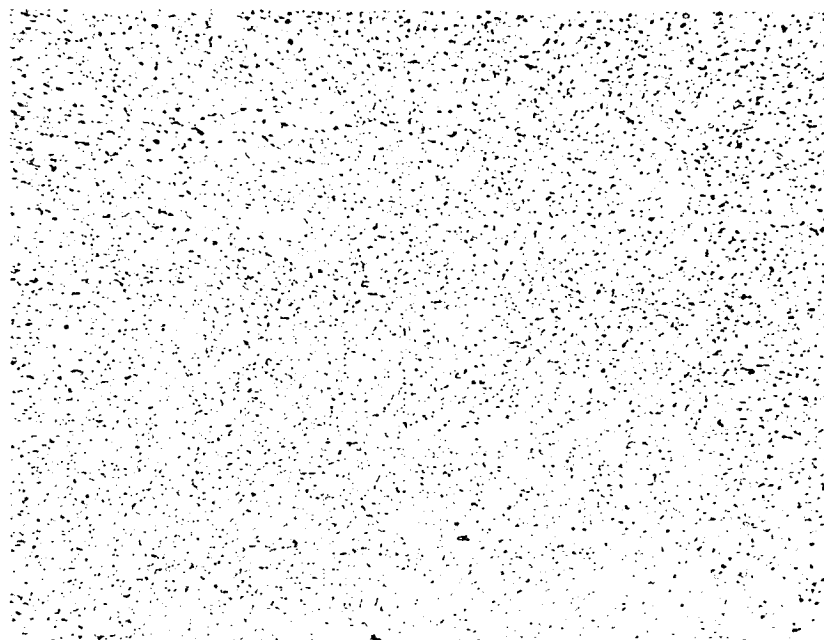


FIGURE II-21. Change in Room Temperature Hardness and Coercive Force of Alloys 1-B-40 and 1-B-41 During Isothermal Aging at 1292°F (700°C)

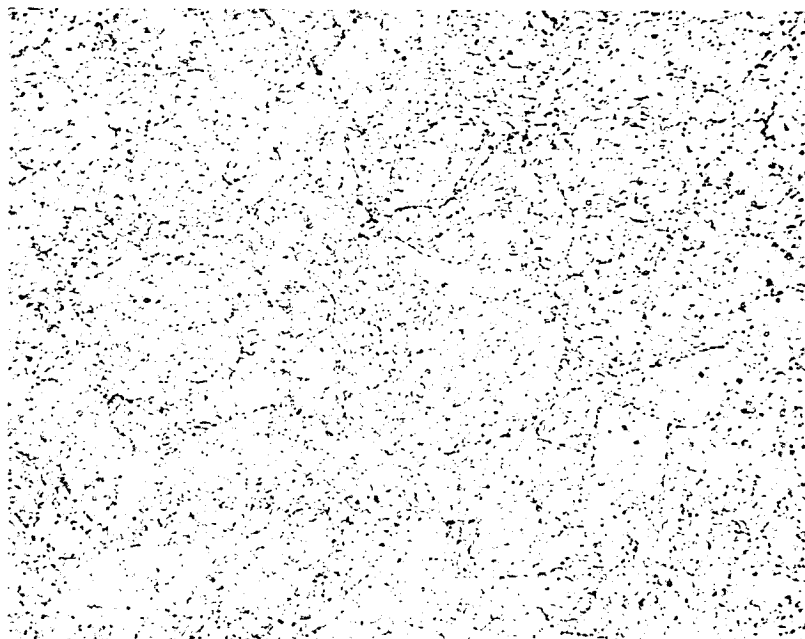
Figure II-21. Hardness and Coercive Force of Alloys 1-B-40 and 1-B-41 During Isothermal Aging



20
10
0
Microns

Electrolytically etched in 10 percent chromic acid.

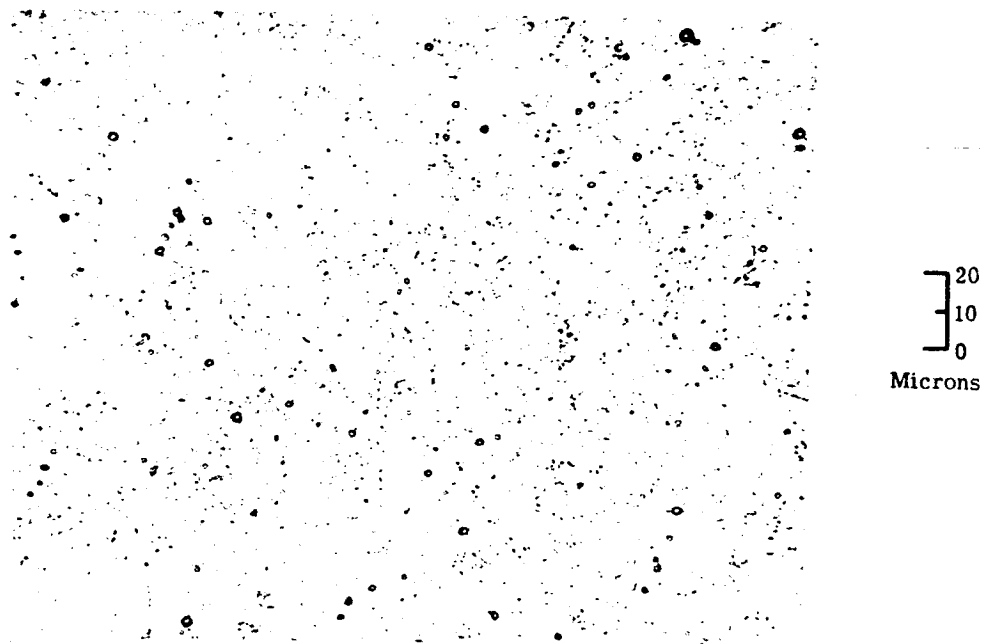
FIGURE II-22. Microstructure of Alloy 1-A-33 (54.4Fe-15Ni-25Co-0.5Be-5Ta-0.1Mn) After 100 Hours Aging at 1022°F (550°C) 500 X



20
10
0
Microns

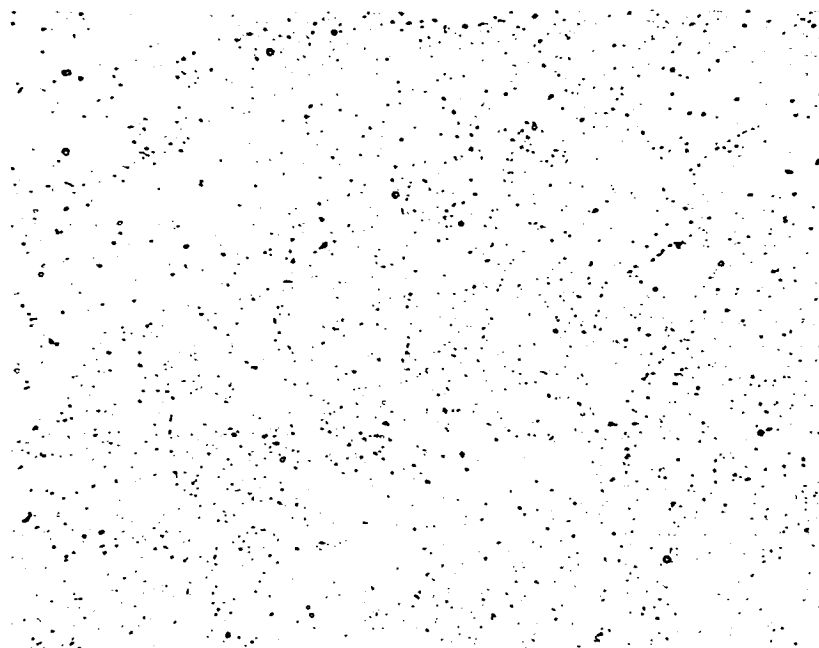
Electrolytically etched in 10 percent chromic acid.

FIGURE II-23. Microstructure of Alloy 1-A-34 (53.9Fe-15Ni-25Co-1W-5Ta-0.1Mn) After 100 Hours Aging at 1022°F (550°C) 500 X



Electrolytically etched in 10 percent chromic acid.

FIGURE II-24. Microstructure of Alloy 1-A-35 (54.4Fe-15Ni-25Co-0.5Al-5Ta-0.1Mn) After 100 Hours Aging at 1022°F (550°C) 500 X



20
10
0
Microns

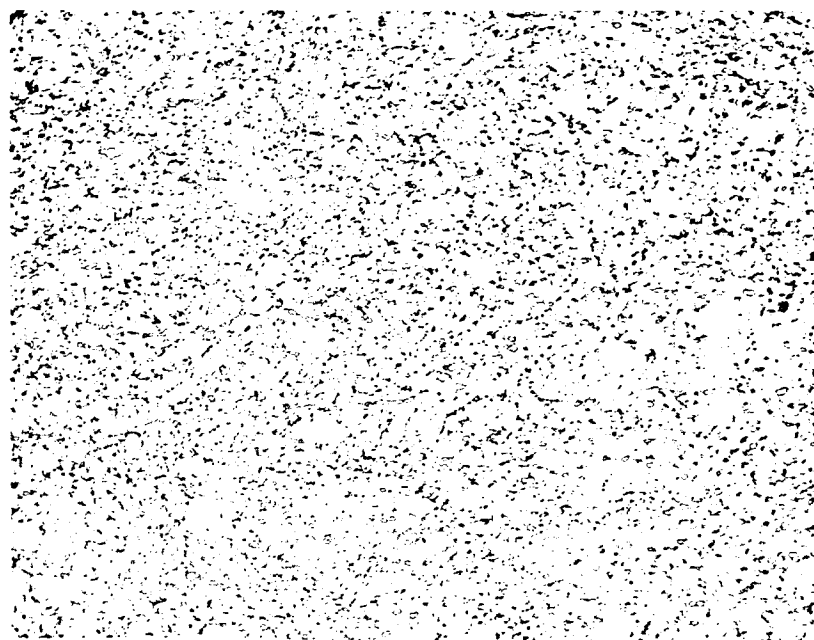
Electrolytically etched in 10 percent chromic acid.

FIGURE II-25. Microstructure of Alloy 1-A-36 (53.9Fe-15Ni-25Co-0.5Al-0.5Ti-5Ta-0.1Mn) After 100 Hours
Aging at 1022°F (550°C) 500 X



Electrolytically etched in 10 percent chromic acid.

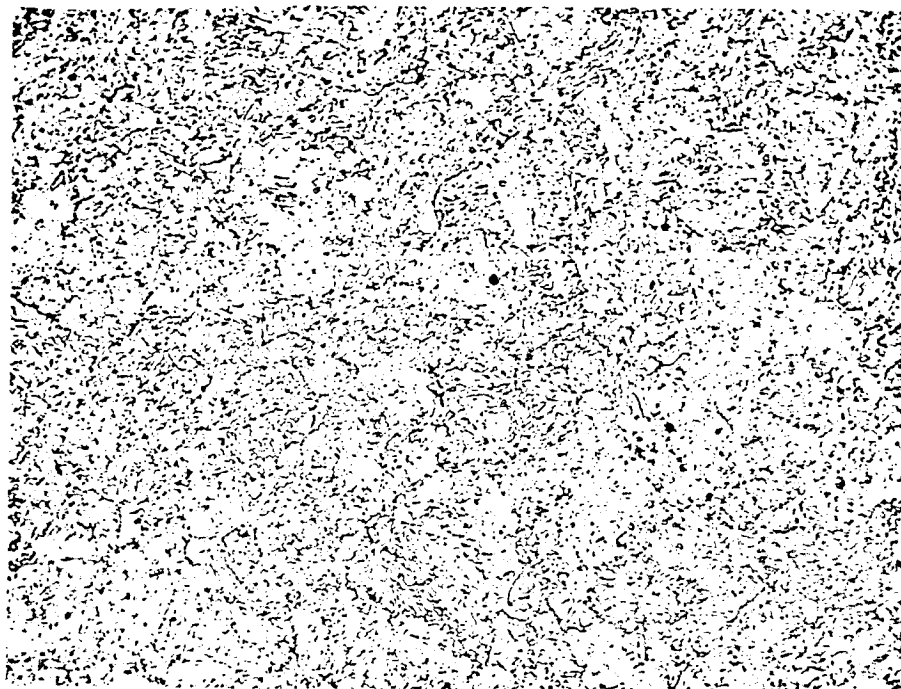
FIGURE II-26. Microstructure of Alloy 1-A-37 (53.9Fe-15Ni-25Co-0.5Al-0.5Ti-2Mo-3Ta-0.1Mn) After 100 Hours Aging at 1022°F (550°C) 500 X



20
10
0
Microns

Electrolytically etched in 10 percent chromic acid.

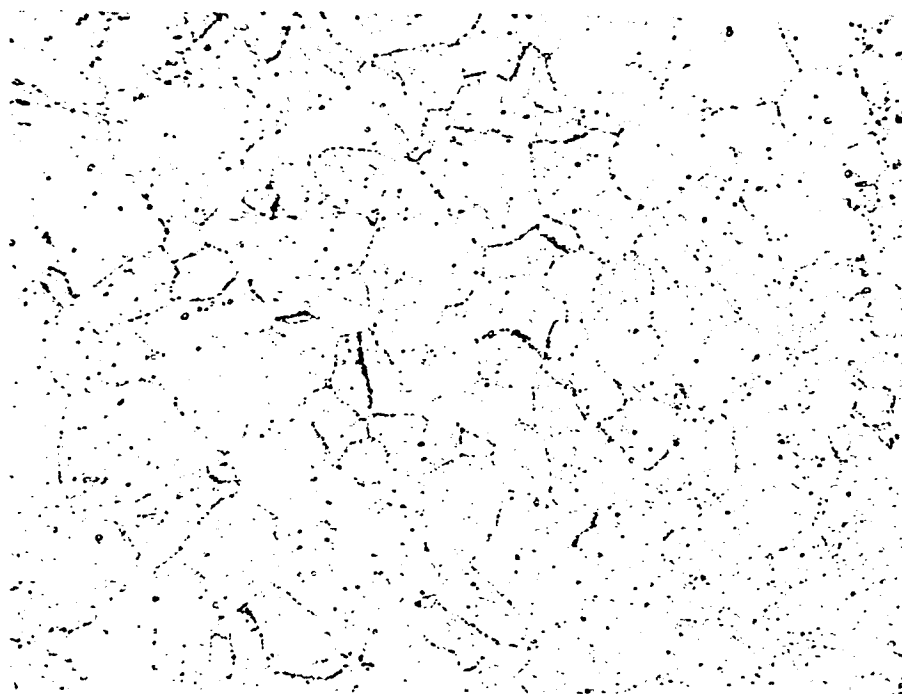
FIGURE II-27. Microstructure of Alloy 1-A-42 (59.9Fe-5Ni-25Co-5Cr-5Ta-0.1Mn) After 100 Hours Aging at 1022°F (550°C) 500 X



20
10
0
Microns

Electrolytically etched in 10 percent chromic acid.

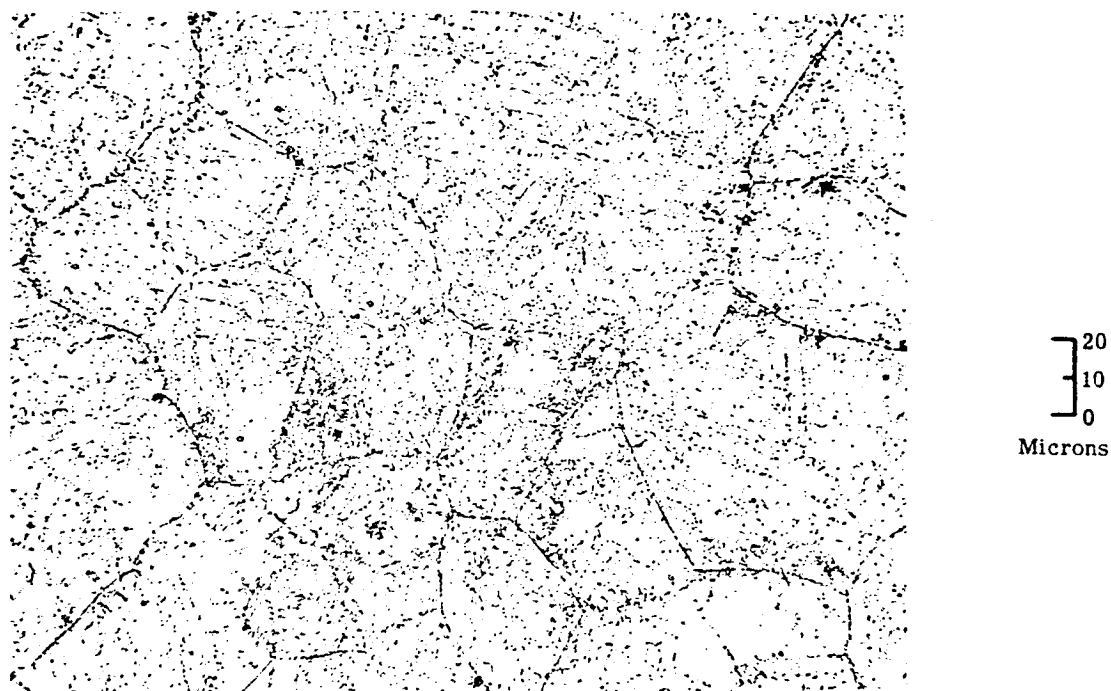
FIGURE II-28. Microstructure of Alloy 1-A-43 (55Fe-15Ni-25Co-2Mo-3Ta)
After 100 Hours Aging at 1022°F (550°C) 500 X



20
10
0
Microns

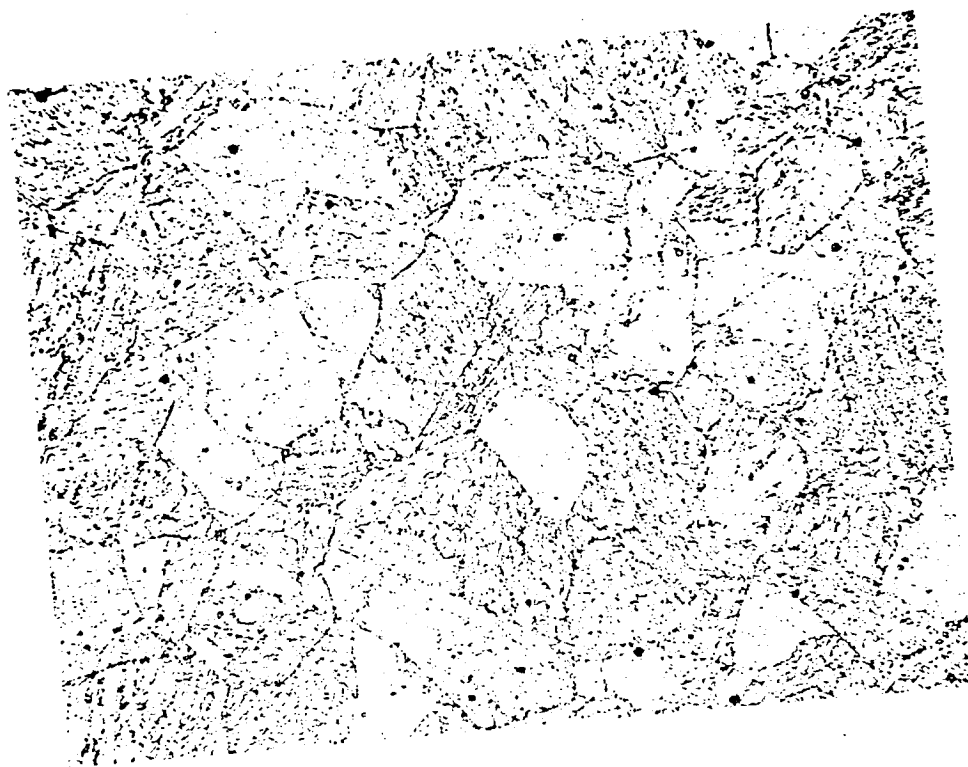
Electrolytically etched in 10 percent chromic acid.

FIGURE II-29. Microstructure of Alloy 1-A-44 (53Fe-15Ni-25Co-2Cr-5Ta)
After 100 Hours Aging at 1022°F (550°C) 500 X



Electrolytically etched in 10 percent chromic acid.

FIGURE II-30. Microstructure of Alloy 1-A-45 (57.5Fe-15Ni-25Co-2Cr-0.5Be) After 100 Hours Aging at 1022°F (550°C) 500X



20
10
0
Microns

Electrolytically etched in 10 percent chromic acid.

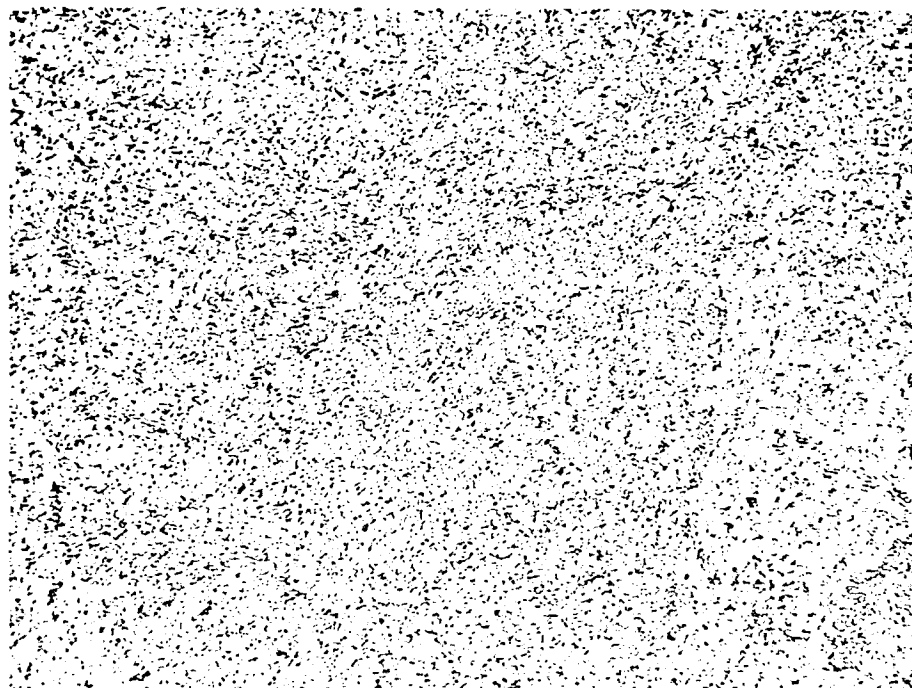
FIGURE II-31. Microstructure of Alloy 1-A-46 (56Fe-15Ni-25Co-2Cr-2Si)
After 100 Hours Aging at 1022°F (550°C) 500 X



20
10
0
Microns

Electrolytically etched in 10 percent chromic acid.

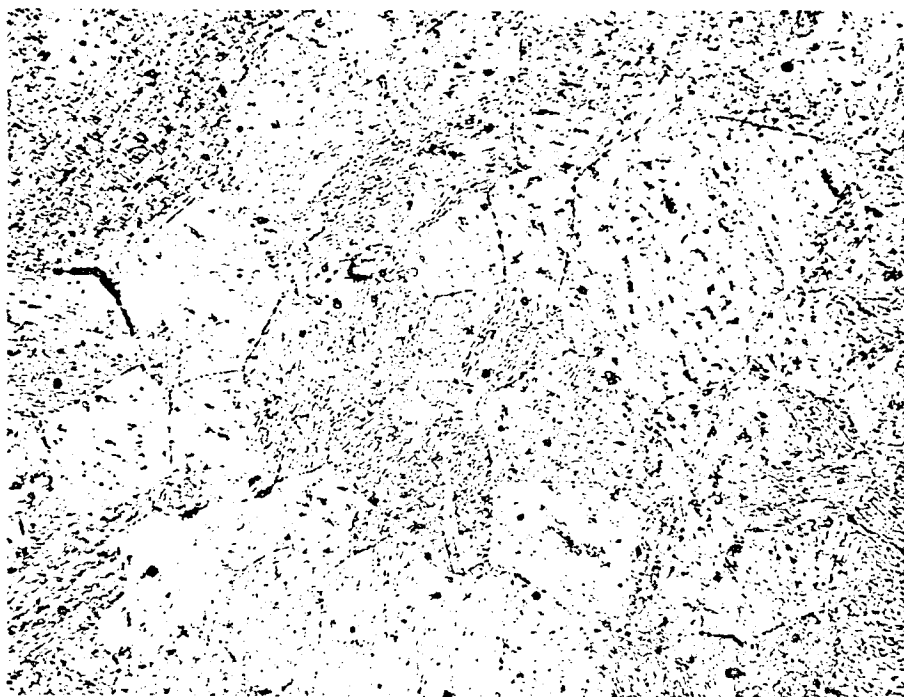
FIGURE II-32. Microstructure of Alloy 1-A-47 (53Fe-15Ni-25Co-2V-5Ta)
After 100 Hours Aging at 1022°F (550°C) 500 X



20
10
0
Microns

Electrolytically etched in 10 percent chromic acid.

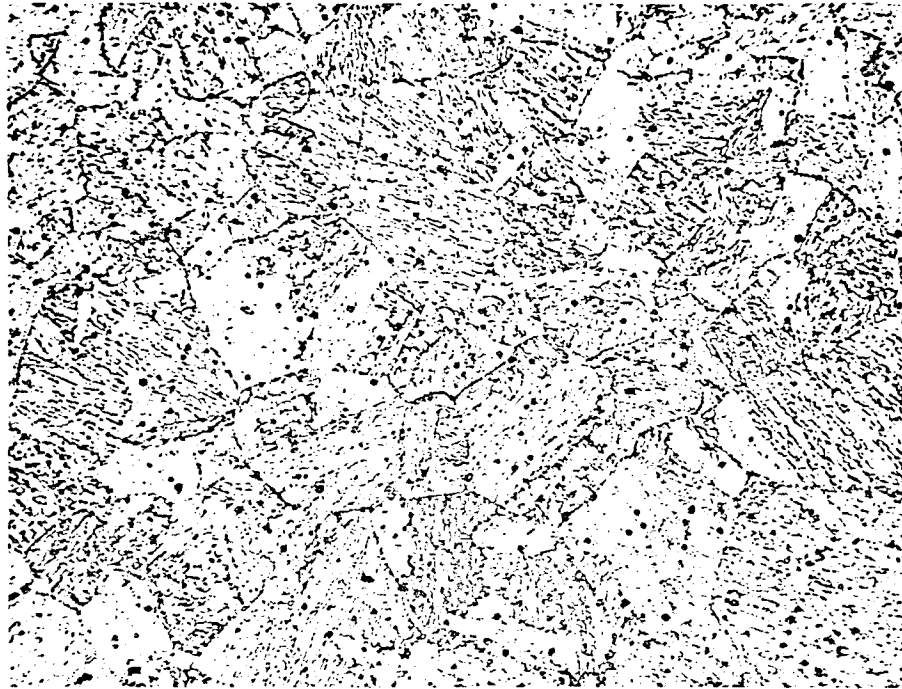
FIGURE II-33. Microstructure of Alloy 1-A-48 (53Fe-15Ni-25Co-2Si-5Ta)
After 100 Hours Aging at 1022°F (550°C) 500 X



20
10
0
Microns

Electrolytically etched in 10 percent chromic acid.

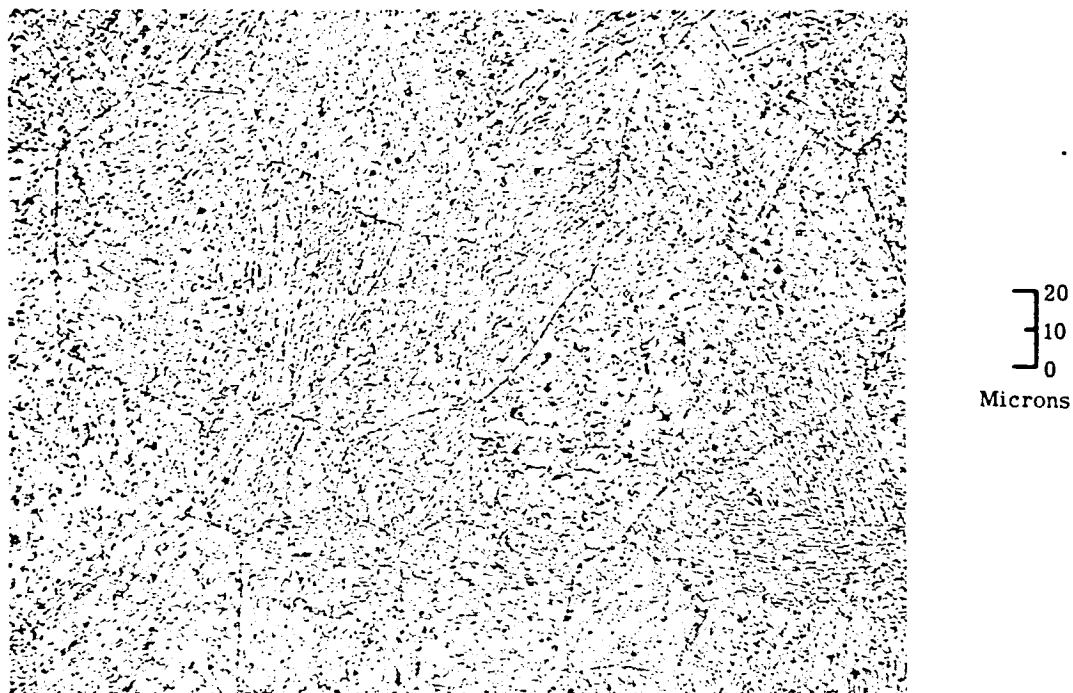
FIGURE II-34. Microstructure of Alloy 1-A-49 (56Fe-15Ni-25Co-2Si-2W)
After 100 Hours Aging at 1022°F (550°C) 500 X



20
10
0
Microns

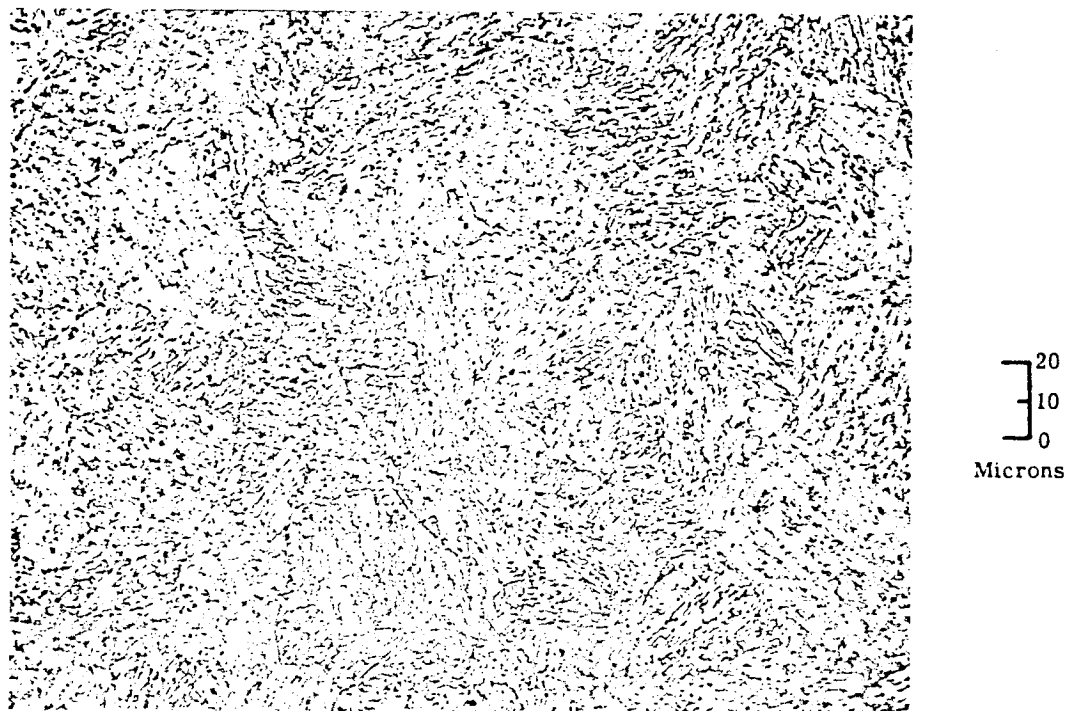
Electrolytically etched in 10 percent chromic acid.

FIGURE II-35. Microstructure of Alloy 1-A-50 (57Fe-15Ni-25Co-1Si-2V)
After 100 Hours Aging at 1022°F (550°C) 500 X



Electrolytically etched in 10 percent chromic acid.

FIGURE II-36. Microstructure of Alloy 1-A-51 (58Fe-15Ni-25Co-1Si-1Ti)
After 100 Hours Aging at 1022°F (550°C) 500 X



Electrolytically etched in 10 percent chromic acid.

FIGURE II-37. Microstructure of Alloy 1-A-52 (56Fe-15Ni-25Co-2Mo-2W)
After 100 Hours Aging at 1022°F (550°C) 500 X

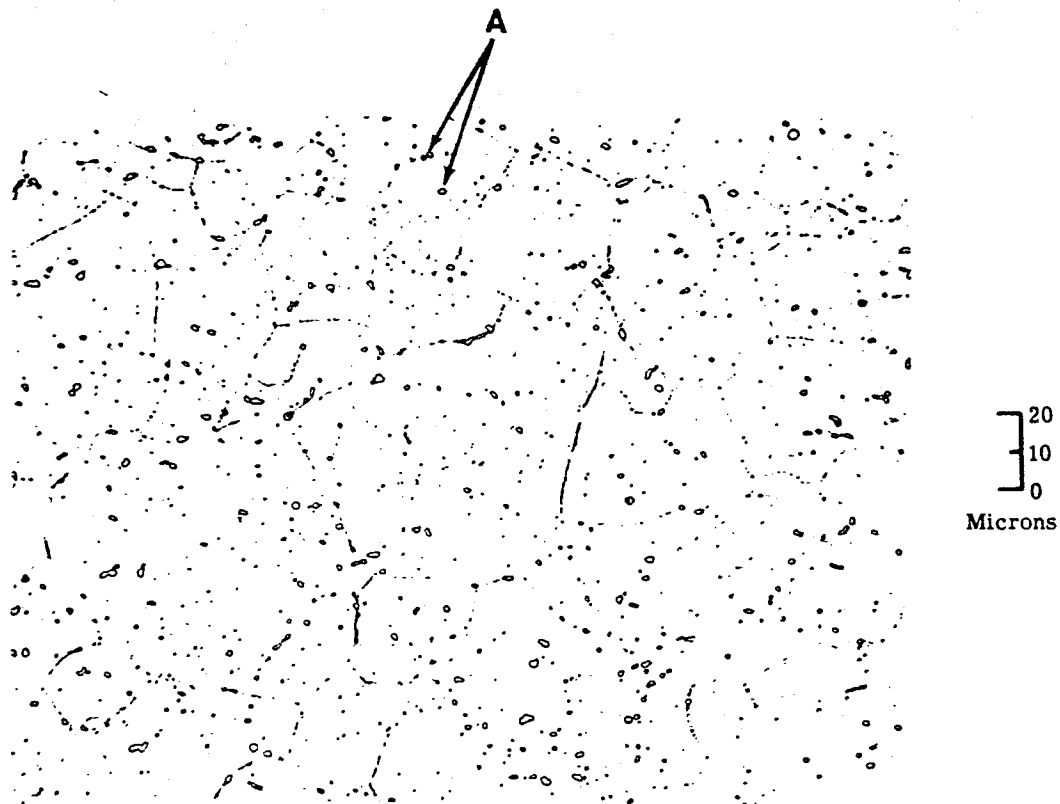
The observation of the microstructure of martensitic alloys indicates no correlation to the measured physical properties. One would expect that the metals which showed a strongly etched structure would also have high values of coercivity. However, this is true for 1-A-47 only. One can, however, conclude that the observed grain boundary precipitate may have an adverse effect on creep strength. Therefore, one should apply some caution in this respect if alloy 1-A-34 is considered a candidate material for a creep resistant alloy based on the results of the aging tests.

Figures II-38 to II-46 show the microstructure of the cobalt-base alloys. The presence of small particles of a second phase can be seen in all of the alloys. These particles may have originated during solidification. In the alloys 1-B-32, 1-B-33, 1-B-35, 1-B-36 and 1-B-39, a fine grain boundary precipitate can be observed. In alloy 1-B-38, one can recognize the start of discontinuous precipitation. About one percent of the structure contains grain boundary seams with discontinuous precipitate. Precipitate within the grains can be observed in alloys 1-B-35 and 1-B-36. The coloring of the grain faces in 1-B-40 and 1-B-41 may point to the existence of submicroscopic precipitate.

It is easier to correlate the observations of the microstructure of the cobalt-base alloys with the measured properties. The high value of coercivity of alloy 1-B-36 after 100 hours aging at 1292°F (700°C) can be associated with the very fine precipitate seen in the light micrograph of this alloy. Evidence of precipitate may also be recognized in the light micrographs of alloys 1-B-35, 1-B-40 and 1-B-41 as indicated above. In these alloys, the coercive force was also higher than 20 oersteds.

c. CONCLUSIONS

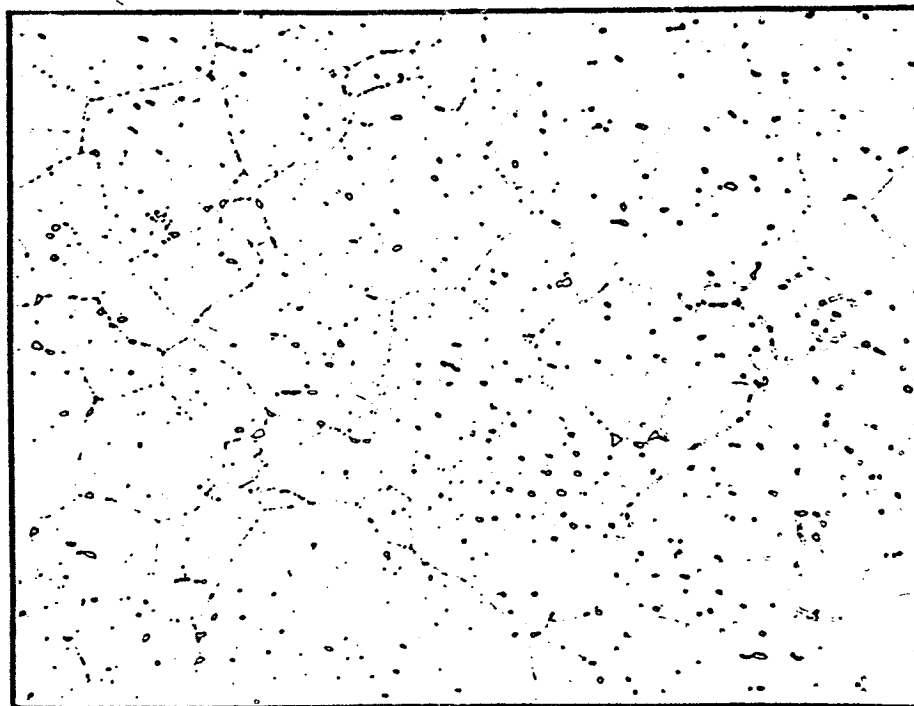
In the martensitic alloys, alloys 1-A-34 and 1-A-48 appear to be promising candidate materials for creep resistant alloys according to the aging tests. The stability of the α phase was sufficient as measured by the dilatometer tests. The magnetic test data at 1112°F (600°C) show that magnetic saturation was quite good for alloy 1-A-48 with B_s a little less than 15,000 gauss; for 1-A-34, B_s is above 15,500 gauss.



A - Second phase particles

Etchant: 20 ml HCl, 40 ml HNO₃, 60 ml glycerin

FIGURE II-38. Microstructure of Alloy 1-B-32 (75.8Co-15Ni-5Fe-2.2Ti-1.5Al-0.5Zr) After 100 Hours Aging at 1292°F (700°C) 500 X



20
10
0
Microns

Etchant: 20 ml HCl, 40 ml HNO₃, 60 ml glycerin

FIGURE II-39. Microstructure of Alloy 1-B-33 (70.8Co-15Ni-5Fe-2.2Ti-1.5Al-0.5Zr-5Cu) After 100 Hours Aging at 1292°F (700°C) 500 X

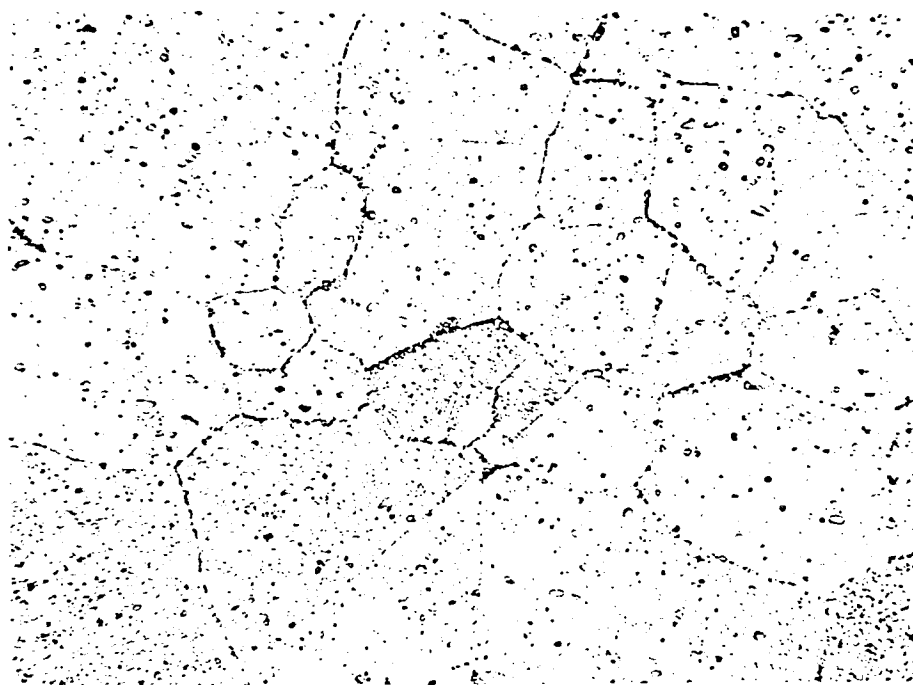


20
10
0
Microns

Etchant: 20 ml HCl, 40 ml HNO₃, 60 ml glycerin

Note extensive precipitate within grains.

FIGURE II-40. Microstructure of Alloy 1-B-35 (73.8Co-15Ni-5Fe-2.2Ti-1.5Al-0.5Zr-2Si) After 100 Hours Aging at 1292°F (700°C) 500 X

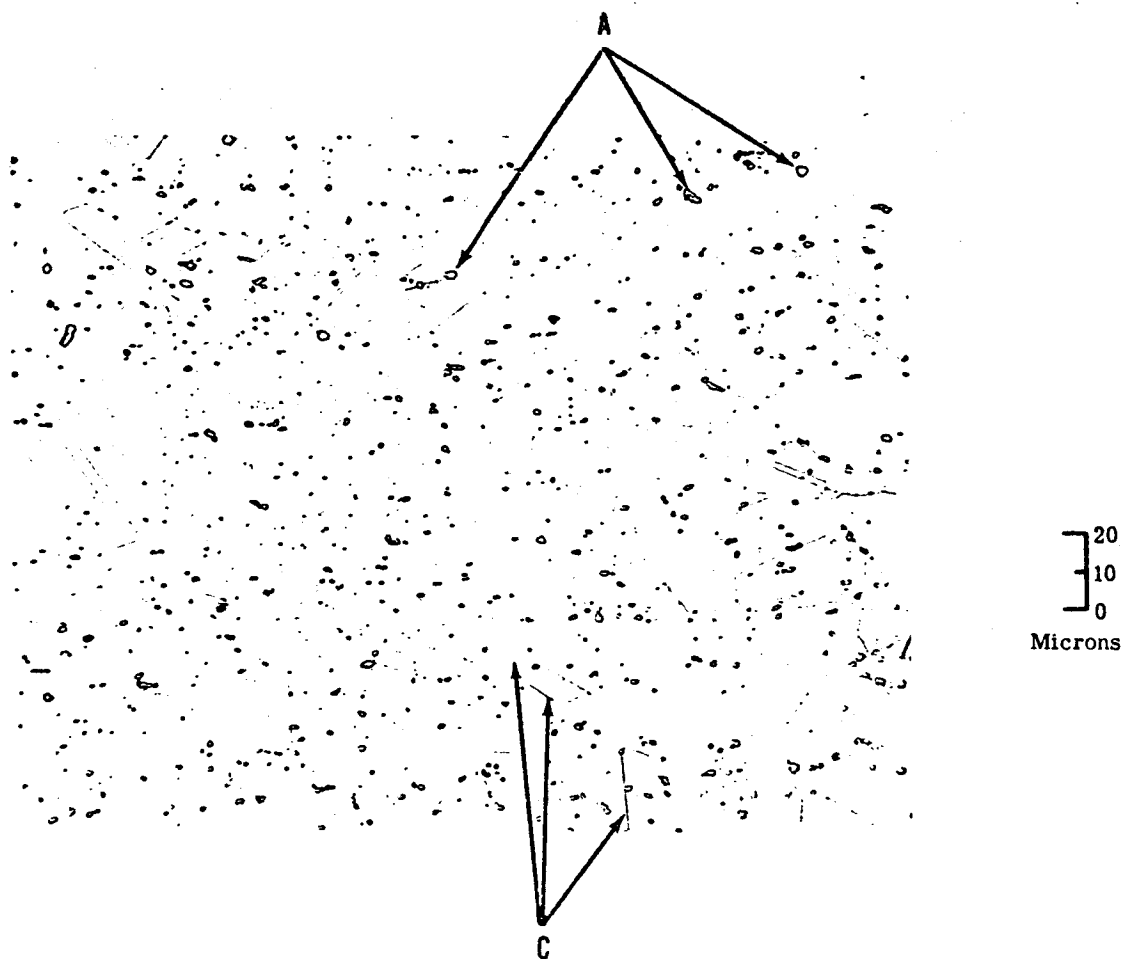


20
10
0
Microns

Etchant: 20 ml HCl, 40 ml HNO₃, 60 ml glycerin

Note extensive precipitate within grains.

FIGURE II-41. Microstructure of Alloy 1-B-36 (75.3Co-15Ni-5Fe-2.2Ti-1.5Al-0.5Zr-0.5Be) After 100 Hours Aging at 1292°F (700°C) 500 X

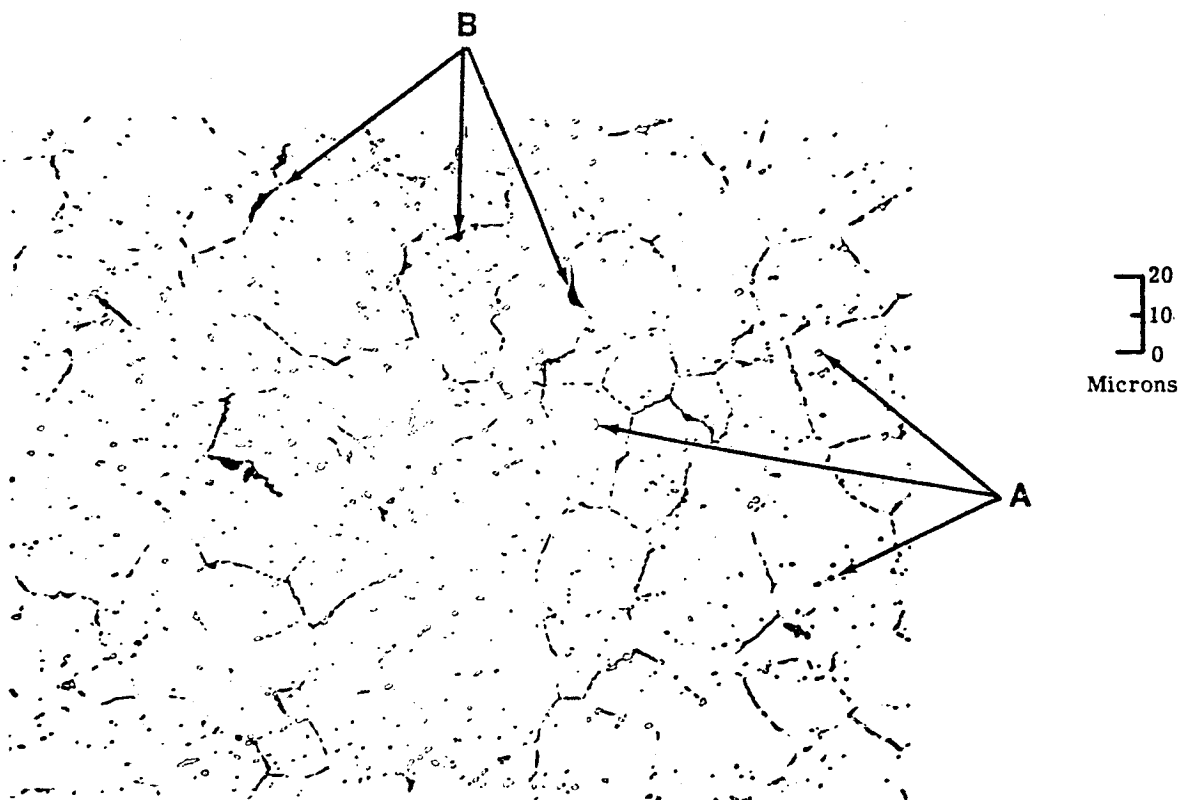


A - Second phase particles

C - Twin boundaries

Etchant: 20 ml HCl, 40 ml HNO₃, 60 ml glycerin

FIGURE II-42. Microstructure of Alloy 1-B-37 (70.8Co-15Ni-5Fe-2.2Ti-1.5Al-0.5Zr-5Cr) After 100 Hours Aging at 1292°F (700°C) 500 X



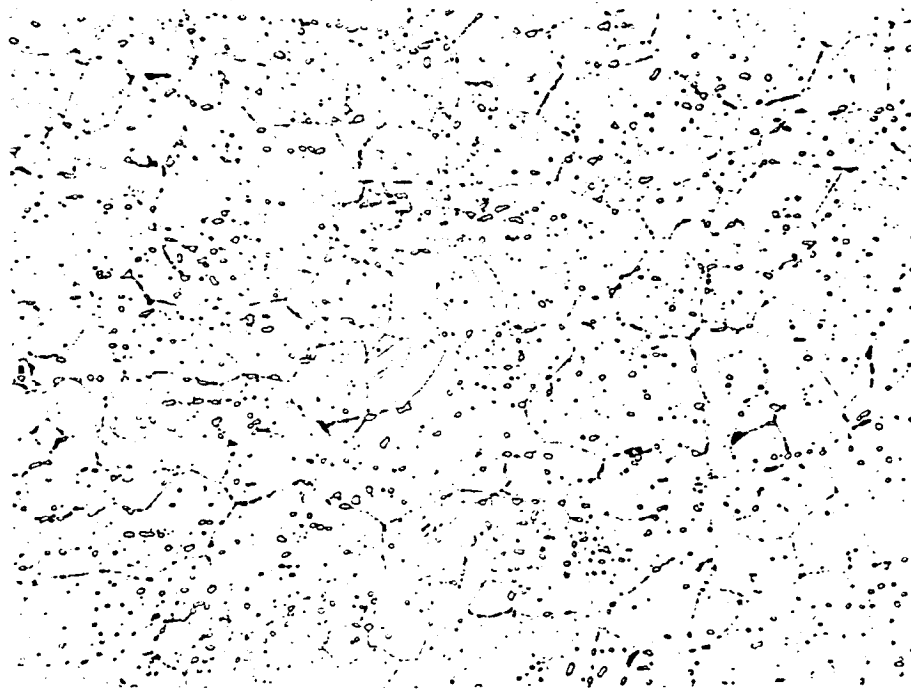
A - Second phase particles

B - Discontinuous precipitate (cellular precipitate at grain boundaries)

Note the beginning of discontinuous precipitation.

Etchant: 20 ml HCl, 40 ml HNO₃, 60 ml glycerin

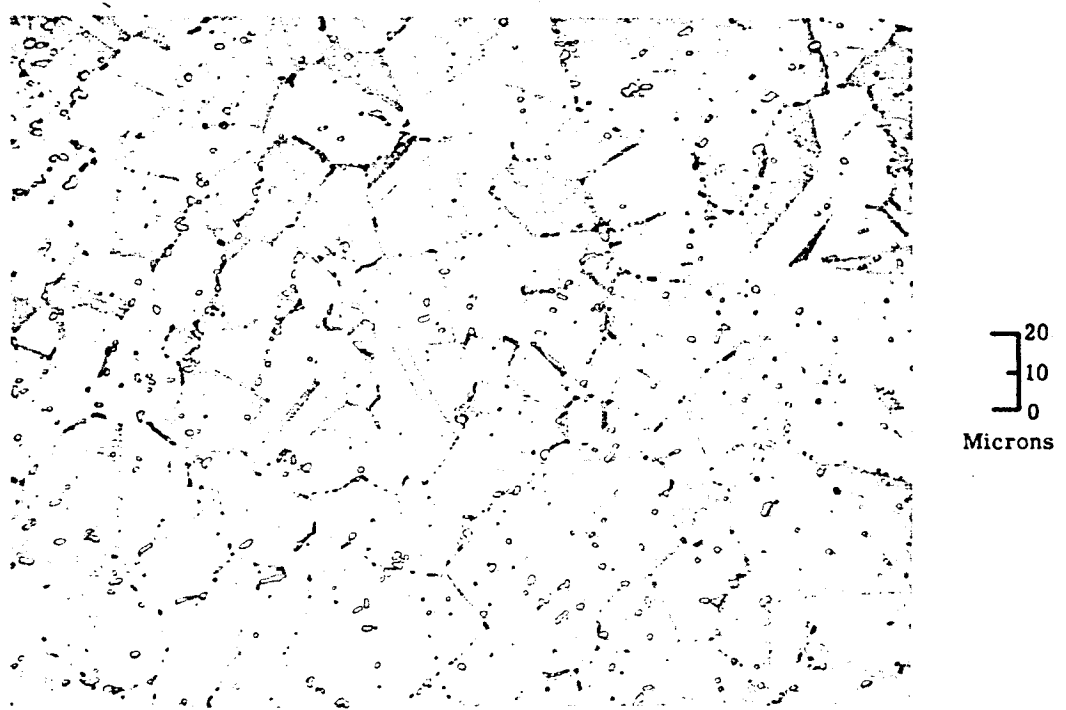
FIGURE II-43. Microstructure of Alloy 1-B-38 (70.8Co-15Ni-5Fe-2.2Ti-1.5Al-0.5Zr-5W) After 100 Hours Aging at 1292°F (700°C) 500 X



20
10
0
Microns

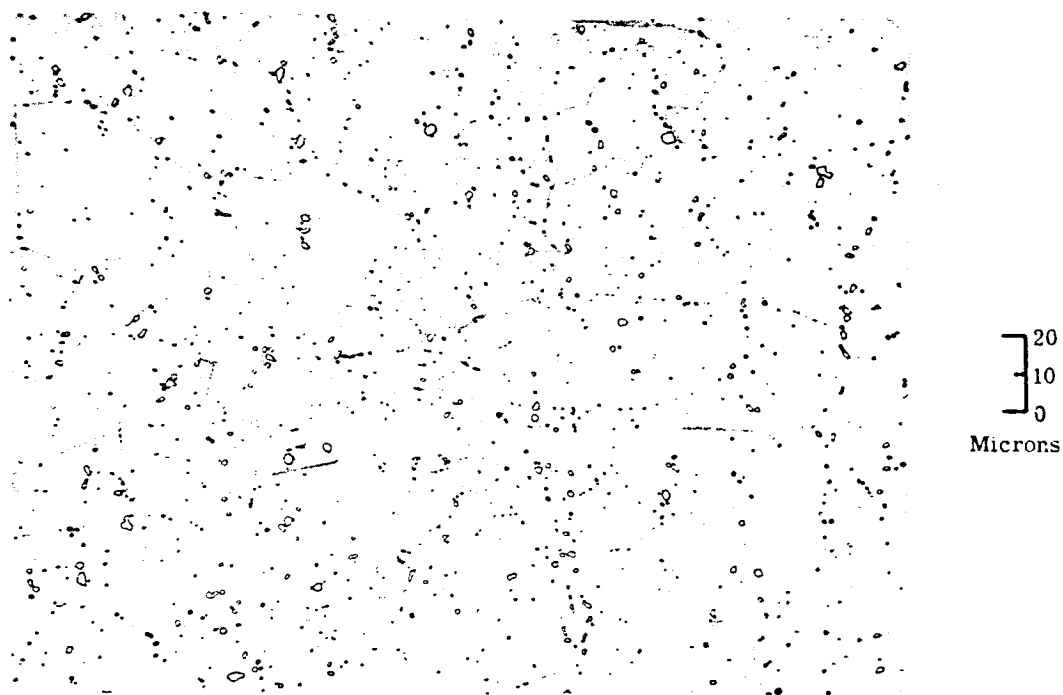
Etchant: 20 ml HCl, 40 ml HNO₃, 60 ml glycerin

FIGURE II-44. Microstructure of Alloy 1-B-39 (70.8Co-15Ni-5Fe-2.2Ti-1.5Al-0.5Zr-5Ta) After 100 Hours Aging at 1292°F (700°C) 500 X



Etchant: 20 ml HCl, 40 ml HNO₃, 60 ml glycerin

FIGURE II-45. Microstructure of Alloy 1-B-40 (70.8Co-15Ni-5Fe-2.2Ti-1.5Al-0.5Zr-5Mo) After 100 Hours Aging at 1292°F (700°C) 500 X



Etchant: 20 ml HCl, 40 ml HNO₃, 60 ml glycerin

FIGURE II-46. Microstructure of Alloy 1-B-41 (70.8Co-15Ni-5Fe-2.2Ti-1.5Al-0.5Zr-5V) After 100 Hours Aging at 1292°F (700°C) 500 X

However, grain boundary precipitate may present a problem in 1-A-34. One can conclude that the combination of one percent tungsten plus five percent tantalum or two percent silicon plus five percent tantalum in an alloy with 15 percent nickel, 25 percent cobalt, balance iron is a favorable combination of elements added to obtain precipitation hardening with stability of the matrix up to 1022°F (550°C) and higher.

The combination of aluminum plus tantalum, aluminum plus titanium plus tantalum, aluminum plus titanium plus tantalum plus molybdenum, as in 1-A-35, 1-A-36, and 1-A-37, proved very interesting. The change of hardness during aging at 1022°F (550°C) was gradual -- less than five percent within 100 hours, but a strong increase of coercivity was observed. The stability of the ferromagnetic α phase and the magnetic saturation was quite good with $B_s = 15,000$ gauss or better at 1112°F (600°C). Faint grain boundary precipitate was present in the microstructure of alloy 1-A-37 only. It might be possible to avoid the undesirable increase of coercivity when the addition of aluminum plus titanium plus tantalum is combined with another addition, which may keep the coercivity low as silicon addition does, or with a modified basic composition with lower coercivity as iron - 12 percent nickel - 25 percent cobalt.

It should be noted that alloy 1-A-42 is low in nickel (only five percent) and behaved quite similar to the 15 percent nickel alloys. Stability of α phase was sufficient. The B_s was higher than 15,000 gauss at 1112°F (600°C). Maraging strengthening could be applied and change of hardness and coercivity during aging for 100 hours at 1022°F (550°C) was less than 10 percent. Only the value of coercivity was slightly high at 38 oersteds. This alloy exhibited exceptional stability during aging.

Based on the results on the cobalt-base alloys, one can conclude that the alloy 1-B-39 deserves attention as a candidate material. The hardness went up to 411 VHN during isothermal aging. Coercivity remained reasonably low. The sacrifice in magnetic saturation of this alloy was less than in the other alloys having a hardness above 300 VHN.

3. Program for the Next Quarter

After evaluation and approval of the experimental alloys by the NASA Project Manager, selected alloys will be melted in the form of larger ingots. Additional mechanical testing will be started.

**B. TASK 2 - INVESTIGATION FOR RAISING THE ALPHA TO GAMMA
TRANSFORMATION TEMPERATURE IN COBALT-IRON ALLOYS**

Work on this task is complete and will be reported in the Final Topical Report.

C. TASK 3 - DISPERSION-STRENGTHENED MAGNETIC MATERIALS FOR APPLICATION IN THE 1200 TO 1600°F RANGE

1. Summary of Technical Progress

- a) Four cobalt-base and four 27 percent cobalt-iron base sintered compacts of prealloyed atomized powders were extruded into rod. Magnetic and tensile properties are being determined on these extrusions which are dispersion-strengthened with boride particles.
- b) Three cobalt-base rods dispersion-strengthened with thorium particles that were purchased from suppliers were tested for magnetic properties, and tensile properties are being determined. Two of these rods (Co + 10 v/o ThO₂ and Co + 2 v/o ThO₂) are being tested in the hot extruded condition, while one rod (Co + 2 v/o ThO₂) was tested after an 85 percent cold reduction by swaging.
- c) Measurements on the microstructure of dispersion-strengthened materials are continuing. Dispersoid parameters such as volume percent of dispersed phase, particle size, and interparticle spacing were measured with the optical microscope and on photomicrographs. (The electron microscope will be used to make more accurate measurements on the dispersoid in extrusions with the best creep and magnetic properties at a later date.)
- d) Data obtained to date on dispersion-strengthened rod indicate that the 27 percent cobalt-iron base compositions have better magnetic properties (lower coercive force and higher saturation) than the cobalt-base. There will be no problem in achieving the program goal of a coercive force of less than 25 oersteds at 1200-1600°F in either 27 percent cobalt-iron base or cobalt-base compositions. A saturation magnetization of 12 kilogauss (the goal is 12 kilogauss minimum at 1200-1600°F) can be met at 1600°F by the 27 percent cobalt-iron base alloys containing as much as approximately 20 v/o dispersoid, while the cobalt-base compositions must contain somewhat less than 10 v/o dispersoid in order to meet this goal at 1600°F. However, the continuing investigation may establish that a much smaller volume percent will suffice for dispersion-strengthening purposes.

- e) Tensile test data were obtained on several compositions at 1200°F, and tests at 1600°F are being initiated. The correlation of tensile properties with the microstructures are, therefore, incomplete. Tests so far at 1200°F (on specimens aged 100 hours at 1200°F at 1×10^{-5} torr or less) indicated that the cobalt-base and 27 percent cobalt-iron base extrusions of prealloyed atomized powders containing boride dispersions have substantially higher ultimate and yield strengths than the cobalt-base extrusions containing thoria dispersions. However, it should be pointed out that the former contained of the order of 20 to 26 v/o dispersed particles, while the latter contained 10 v/o and 2 v/o thoria.
- f) One of the best combinations of magnetic and tensile properties at 1200°F in tests made to date was achieved with an Fe + 24.8 w/o Co + 1.1 w/o B + 3.2 w/o Zr extrusion which had the following properties at 1200°F (creep resistance will be determined at a later date):

Coercive force, $H_C = 8.4$ oersteds

Saturation magnetization, $B_S = 17,200$ gauss

Ultimate Strength = 62,100 psi

Yield strength (0.2% offset) = 31,500 psi

Elongation in 4D = 40 percent

- g) Processing into sintered compacts was nearly completed on four internally oxidized cobalt-base and 27 percent cobalt-iron base atomized powders containing additions of aluminum and beryllium, and six composite powders containing dispersed alumina and thoria particles. The microstructure of the sintered compacts is being evaluated before extrusion.

2. Discussion

The purpose of this project is to develop a dispersion-strengthened, magnetically soft material for use in the 1200-1600°F temperature range for rotor applications. As a goal, the material should have the

following properties at some temperature between 1200 and 1600°F, preferably at 1600°F.

Saturation Magnetization, B_s = 12,000 gauss minimum

Coercive Force, H_c = 25 oersteds maximum

Creep strain in 10,000 hours at 10,000 psi = 0.4 percent maximum

In pursuit of this goal, dispersion-strengthened cobalt-base and 27 percent cobalt-iron-base extrusions are being made from (1) pre-alloyed atomized powders containing boride and cerium intermetallic compound particles, (2) internally oxidized powders containing alumina or beryllia, and (3) composite powders containing both a metal phase and a refractory oxide phase (alumina or thoria) within each powder particle. Also, dispersion-strengthened cobalt-base extrusions containing thoria were purchased from two suppliers. The work done so far is part of the initial evaluation phase of the project which includes determination of saturation magnetization, coercive force, and tensile properties at room temperature and in the 1200-1600°F range. Later on, the intermediate and final evaluation phases of this project will be conducted on the best candidate compositional systems developed in this first phase.

a. PREALLOYED ATOMIZED POWDERS

(1) Extrusion

(a) Machining of Sintered Compacts and Cans

The eight sintered compacts of prealloyed atomized powders containing dispersed boride particles that were described in the third quarterly report were extruded into rod. The compacts, which were approximately two inches in diameter by three inches long after sintering, were machined to 1.95 inches diameter so that they would fit inside 2 inch I. D. x 0.125 inch thick wall mild-steel cans. Care was taken to insure that the compacts remained dry and clean during the machining operation. The mild steel can (SAE 1020) had a 1.5 inch thick nose plug on the front end which was machined on the outside to a 90 degree truncated cone with a 0.75 inch diameter flat section on the nose.

This matched the entrance angle on the die and the die opening of 0.75 inch diameter. The can was made with the back-end open to receive the compact and the 2 inch diameter x 0.25 inch thick end plug of mild steel which later was electron-beam welded flush with the end of the can. The inside length of the can matched the length of each compact plus the 0.25 inch thickness of the end plug. All outside surfaces of the can were sand blasted to promote adherence of the glass lubricant. The total weight of compact, can, and end plug was about four pounds. The compacts themselves weighed two pounds each.

(b) Hermetically Sealing Compacts in Cans

The cans were evacuated to less than 1×10^{-5} torr and tested for helium leak tightness before the compact was inserted and the end sealed. Each open-end can with the compact inside and end plug was baked out for two hours at 1220°F in the 10^{-5} torr range. After cooling to room temperature and back-filling with 99.996 percent purity argon, the cans, compacts, and end plugs were removed from the furnace and carried in a covered container to a Sciaky electron-beam welder (30 kW, Type VX-50 x 30 x 42 with 16 inch diffusion pump), where they were immediately evacuated to the 10^{-5} torr range. Each end plug had eight longitudinal slots 0.063 inches wide x 0.032 inches deep equally spaced around the periphery to facilitate evacuation of the can. The welding conditions were fixed from trial runs so as to give 30 to 50 percent penetration through the 0.25 inch thick end plug. The method had been found by previous experience to give leak tight joints.

(c) Lubrication of Billets and Tools

Before preheating the canned compacts for extrusion, the outside of the can, except for the back-end, was coated with a 0.125 inch thickness of glass slurry consisting of a water soluble, borate-type glass (Code No. 9773, Corning Glass Works, Corning, New York) with collodion and amyl acetate binder, and air dried.

The extrusion tools were made of AISI H-12 hot-work tool steel hardened to Rockwell C 45 to 50 and consisted of an extrusion container 12 inches long with a 2.360 inch diameter bore, a die with a 0.750 inch diameter hole and a conical entrance of 90 degrees included angle, and a ram with a 2.350 inch diameter dummy block attached. The tools were mounted on the horizontal bed of a down acting, 200 ton hydraulic press. The extrusion direction was downward. Preparations for extrusion involved brushing the die, bore of the container, and dummy block while cold with either Sicon Lubricant (colloidal suspension of silicone resin and graphite in water, Lot 11X915, Midland Industrial Finishes Co., Inc., Waukegan, Illinois) or Dag Dispersion No. 99 (colloidal suspension of graphite in organic solvent, Acheson Colloids Co., Port Huron, Michigan). In addition, two glass disks of the borate-type glass weighing 30 grams each and measuring 2.25 inches diameter x 0.5 inch thick were placed inside the bore of the extrusion container on top of the die. Next, 50 grams of loose borate glass powder were poured into the bore of the container on top of the disks. Before the glass was added to the bore, a 0.75 inch diameter x 0.5 inch thick plug of mild steel with a slightly oversize diameter on the top end was placed in the hole of the extrusion die to insure glass was retained until extrusion started. This lubrication practice for extrusion was generally in line with the recent literature on the subject (refs. 1 to 5). The borate-type glass (Corning Code No. 9773) was selected for use because it has a viscosity of between 100 and 300 Poises at 2000°F (the billet extrusion temperature), and could easily be removed from the extrusion, die and other tools since it was soluble in water.

(d) Extrusion Procedure

The extrusion container and die were preheated to approximately 900°F for extrusion. The canned compact previously coated with glass was placed in a Type 304 stainless-steel retort 3.75 inches I.D. x 7.5 inches inside length with the uncoated back end of the billet resting on the bottom of the retort. A matching cover

plate was placed over the top of the retort. Argon of 99.996 percent purity flowed through the retort at five SCFH by means of an inlet tube at the bottom and an outlet tube at the top during preheat. A thermocouple placed inside the retort alongside the canned billet gave temperature readings which corresponded very closely with the indicated furnace temperature. The billet temperature was raised from room temperature to 2000°F and held at 2000°F for approximately one hour. The billet was removed from the furnace and retort, and immediately extruded to 0.75 inch diameter rod with an extrusion speed of 43 feet per minute (8.6 inches per second). The material from the sintered compact was present in the 0.75 inch diameter extrusion as a central core, whose diameter varied from 0.38 to 0.63 inches, surrounded by mild-steel cladding. The minimum extrusion ratio for the alloy core was 11 to 1. The extrusion starting pressures for the compacts varied from 53,000 psi to 91,000 psi. The maximum length of 0.75 inch diameter rod obtained was 33 inches. After scrapping a nine inch length from the front and a four inch length from the back (because of rear-end extrusion defect) the maximum length of core material available for subsequent testing purposes was 20 inches. Even on a billet, which was only about one-third extruded, an eight inch length of core material was obtained.

(2) Testing of Extrusions

(a) Inspection for Defects

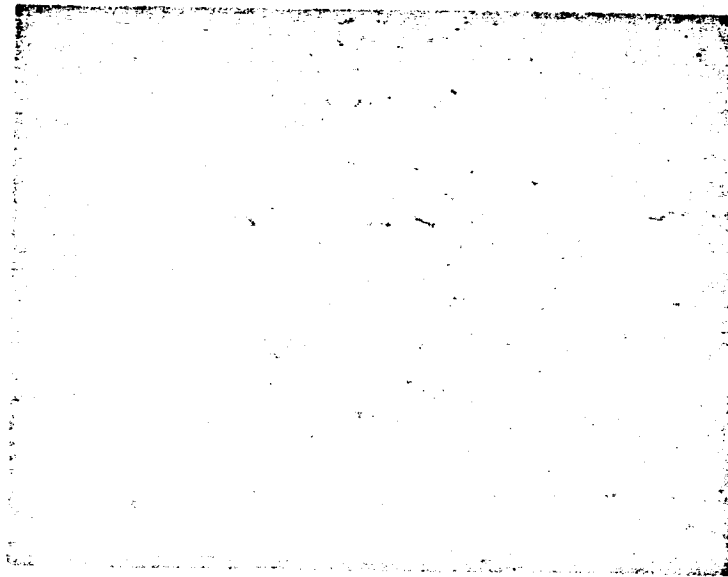
Transverse sections from the front and back of each extrusion were cut off and etched for macroscopic examination in order to locate sound core material before test specimens were taken. Macroetching was performed with the following solutions: 5 percent nital, 50 percent nitric acid in water, and 50 percent hydrochloric acid in water. No gross defects were found in the core material near the front of the extrusion. As a further precaution, transverse and longitudinal sections from the front and back were examined under the

microscope in the as-polished condition and after etching in a solution of acetic-nitric-hydrochloric-water (1:1:4:1 ratio).

(b) Microstructure of Sound Material

The microstructure of the extrusions was revealed by etching in the acetic-nitric-hydrochloric-water solution previously described (Figures II-47, II-48, and II-49). Longitudinal and transverse sections were examined with a Unitron Metallograph Model BN-11 at magnifications up to 1500X. The size of secondary-phase particles dispersed in the cobalt and 27 percent cobalt-iron matrix, their interparticle spacing, and the percent by volume of dispersed phase are being determined in representative areas using a Unitron filar micrometer eyepiece. Also, measurements are being made on photomicrographs using a Norelco Type 52022 film illuminator and measuring device (with millimeter scale and vernier). Lineal analysis and point counting techniques are applied (refs. 6 and 7). The uniformity of the dispersion, the amount of porosity, and possible indications of lack of bonding between the dispersoid and the matrix were noted. X-ray diffraction back reflection Laue patterns were obtained from various regions on the metallographic specimens to indicate the degree of recrystallization and grain size (refs. 8 and 9). The initial results of the microstructural examinations are presented in Table II-8.

The identity of the secondary-phase particles seen in the extrusions has not been determined yet. In the cobalt-base alloys, some of these constituent particles may belong to the family of ternary borides called tau which have the Cr_{23}C_6 structure (D_{84} structure type) and are represented by $\text{T}_{23-\text{m}}\text{M}_{\text{m}}\text{B}_{\text{n}}$, where T is Co, and M is one of the following: Ti, Zr, Cb or Ta, (refs. 10 and 11). Roughly, m ranges from 2 to 3.5 and n from 5 to 12. The composition of the cobalt-tantalum boride is $\text{Co}_{21}\text{Ta}_2\text{B}_6$ at 800°C (1472°F) and in the isothermal section no tie lines run in the direction Co to TaB_2 . No D_{84} type borides have been reported with iron, although ternary iron carbides and an iron carboboride with this structure have been reported in the



20
10
0
Microns

FIGURE II-47. As-Extruded Rod of Atomized Powder No. 6, Co+1.2% B+ 7.7% Ta, Showing Boride Particles (gray) and Other Particles of Dark Constituent Dispersed in Cobalt Matrix, Longitudinal Section Near Front of Extrusion, 1000 X. Etched in Acetic-Nitric-Hydrochloric-Water. (1:1:4:1 Ratio)

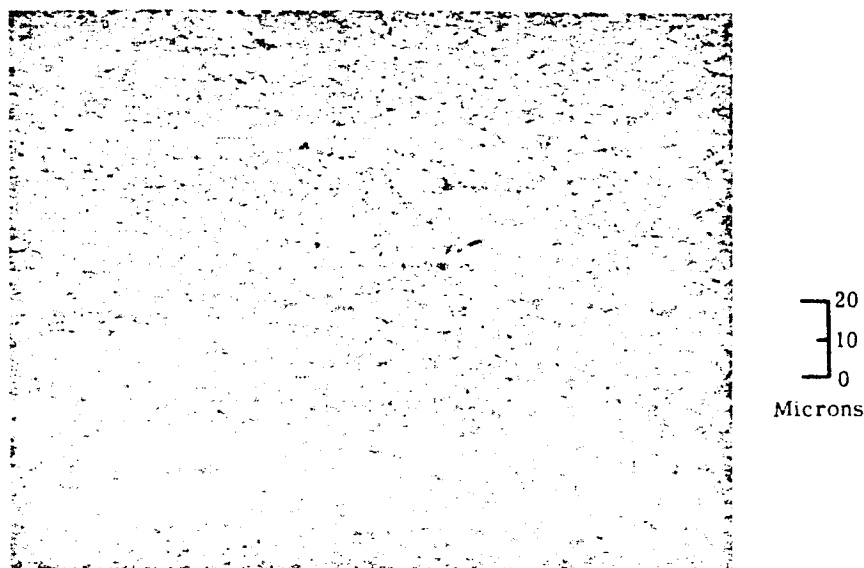


FIGURE II-48. As-Extruded Rod of Atomized Powder No. 13, Fe+24.8% Co+1.1% B+3.2% Zr, Showing Boride Particles (light) and Other Particles of Dark Constituent Dispersed in Fe-Co Recrystallized Matrix, Grain Boundaries Revealed, Longitudinal Section Near Front of Extrusion, 500 X. Etched in Acetic-Nitric-Hydrochloric-Water.(1:1:4:1 Ratio)

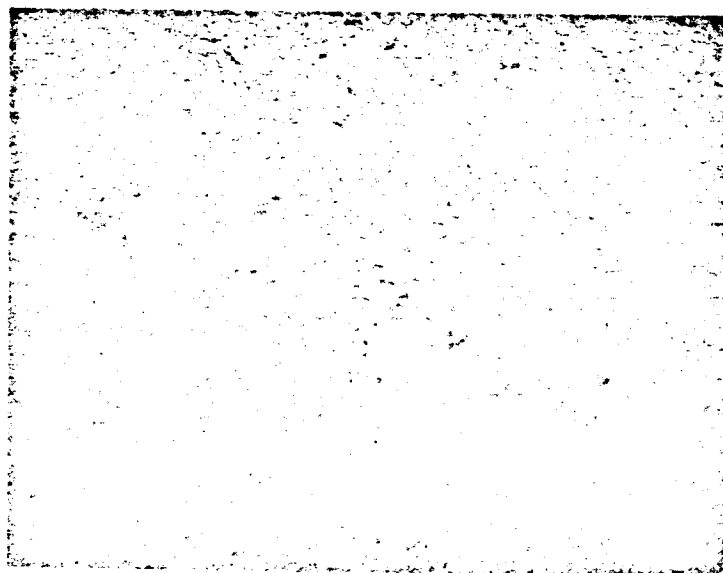


FIGURE II-49. As-Extruded Rod of Atomized Powder No. 14, Fe+25.8% Co+0.9% B+4.1% Cb, Showing Boride Particles (light) and Other Particles of Dark Constituent Dispersed in Fe-Co Matrix, Transverse Section Near Front of Extrusion, 1000 X. Etched in Acetic-Nitric-Hydrochloric-Water. (1:1:4:1 Ratio)

TABLE II-8. Microstructure of Extrusions, Preliminary Measurements

Powder or Extrusion No.	Nominal Composition (weight percent)	Amount of Dispersed Phase (percent by volume)	Average Size of Dispersed Particles (f) (microns)	Average Interparticle Spacing (microns)	Degree of Recrystallization (percent)	Average Grain Size (Approx.) (microns)	Amount of Porosity (g) (percent)
Prealloyed Aluminized Powders (Extruded)							
3	Co+1.3B+1.6Ti	(e)	(e)	(e)	(d)	5	(e)
4	Co+1.3B+3.4Zr	26	0.95	2.7	(d)	5	2
5	Co+1.1B+4.4Cb	(e)	(e)	(e)	(d)	5	(e)
6	Co+1.2B+7.7Ta	(e)	(e)	(e)	(d)	5	(e)
12	Fe+26.5Co+0.9B+1.8Ti	(e)	(e)	(e)	Complete	20	(e)
13	Fe+24.8Co+1.1B+3.2Zr	20	0.90	3.6	Complete	20	2
14	Fe+25.8Co+0.9B+4.1Cb	(e)	(e)	(e)	Complete	20	(e)
15	Fe+24.1Co+1.0B+7.0Ta	(e)	(e)	(e)	Complete	20	(e)
Supplier Extrusions of Dispersion-Strengthened Cobalt							
3(b)	Co+10.4ThO ₂ (0.01-0.06 μ ThO ₂)	10	(e)	(e)	(d)	2	2
9(c)	Co+2.0ThO ₂ (0.01-0.06 μ ThO ₂)	2	(e)	(e)	(d)	5	0-1
9(a)(c)	Co+2.0ThO ₂ (0.01-0.06 μ ThO ₂)	2	(e)	(e)	(d)	-	0-1
<p>Note:</p> <p>(a) Given 85 percent cold reduction by swaging after hot extrusion. All other material in hot extruded condition.</p> <p>(b) Extrusion supplied by New England Materials Laboratory, Inc., Medford, Massachusetts.</p> <p>(c) Extrusion supplied by Curtiss-Wright Corp., Metals Processing Division, Buffalo, New York.</p> <p>(d) Cobalt undergoes phase transformation at 783°F from cubic to hexagonal structure on cooling. These materials were partially transformed and contained a mixture of hexagonal and cubic cobalt at room temperature.</p> <p>(e) Not determined to date.</p> <p>(f) No evidence of lack of bonding between the dispersed phase and the matrix was found. An essentially uniform distribution of dispersed phase was achieved.</p> <p>(g) Determined by comparison with theoretical density and/or observations under microscope.</p>							

TABLE II-8. Microstructure of Extrusions, Preliminary Measurements

Powder or Extrusion No.	Nominal Composition (weight percent)	Amount of Dispersed Phase (percent by volume)	Average Size of Dispersed Particles (f) (microns)	Average Interparticle Spacing (microns)	Degree of Recrystallization (percent)	Average Grain Size (Approx.) (microns)	Amount of Porosity (g) (percent)
Prealloyed Atomized Powders (Extruded)							
3	Co+1.3B+1.6Ti	(e)	(e)	(e)	(d)	5	(e)
4	Co+1.3B+3.4Zr	26	0.95	2.7	(d)	5	2
5	Co+1.1B+4.4Cb	(e)	(e)	(e)	(d)	5	(e)
6	Co+1.2B+7.7Ta	(e)	(e)	(e)	(d)	5	(e)
12	Fe+26.5Co+0.9B+1.8Ti	(e)	(e)	(e)	Complete	20	(e)
13	Fe+24.8Co+1.1B+3.2Zr	20	0.90	3.6	Complete	20	2
14	Fe+25.8Co+0.9B+4.1Cb	(e)	(e)	(e)	Complete	20	(e)
15	Fe+24.1Co+1.0B+7.0Ta	(e)	(e)	(e)	Complete	20	(e)
Supplier Extrusions of Dispersion-Strengthened Cobalt							
3(b)	Co+10.4ThO ₂ (0.01-0.06 μ ThO ₂)	10	(e)	(e)	(d)	2	2
9(c)	Co+2.0ThO ₂ (0.01-0.06 μ ThO ₂)	2	(e)	(e)	(d)	5	0-1
9(a)(c)	Co+2.0ThO ₂ (0.01-0.06 μ ThO ₂)	2	(e)	(e)	(d)	-	0-1
<p>Note:</p> <p>(a) Given 85 percent cold reduction by swaging after hot extrusion. All other material in hot extruded condition.</p> <p>(b) Extrusion supplied by New England Materials Laboratory, Inc., Medford, Massachusetts.</p> <p>(c) Extrusion supplied by Curtiss-Wright Corp., Metals Processing Division, Buffalo, New York.</p> <p>(d) Cobalt undergoes phase transformation at 783°F from cubic to hexagonal structure on cooling. These materials were partially transformed and contained a mixture of hexagonal and cubic cobalt at room temperature.</p> <p>(e) Not determined to date.</p> <p>(f) No evidence of lack of bonding between the dispersed phase and the matrix was found. An essentially uniform distribution of dispersed phase was achieved.</p> <p>(g) Determined by comparison with theoretical density and/or observations under microscope.</p>							

literature. The ternary borides, tau, crystallize congruently from the melt and are reported to have microhardness values somewhat above hardened steel (ref. 10).

(c) Effect of Thermal Treatment on Dispersoid and Properties

An attempt to correlate the dispersoid parameters (chemical composition of the dispersed phase, size of particles, interparticle spacing, and volume percent) with the magnetic and tensile properties, which will be discussed later, is continuing for the various materials investigated on this program. Insufficient data have been obtained to make a correlation yet.

In the case of extrusions made from atomized powders, there are four stages in processing where thermal treatments have been applied:

- 1) Hydrogen reduction of powders for six hours at 1220°F.
- 2) Hydrogen sintering of compacts for two hours at 1800°F.
- 3) Vacuum bake-out of compacts and cans for two hours at 1220°F.
- 4) Preheating of canned compacts for extrusion for one hour at 2000°F.

Although all of these steps are desirable in the processing of the powders into extrusions, the 1800°F and 2000°F temperatures are well above the intended service temperature range of 1200°F to 1600°F. Processing temperatures and times could be decreased if the tensile data presently being generated indicate that the particle size and interparticle spacing of the dispersed phase are consistently too large as a result of thermal treatment to achieve the desired strength levels. Also, once a stronger correlation between strength at elevated temperatures and dispersoid parameters has been achieved, there may be justification for screening out some remaining compositions on the basis of instability.

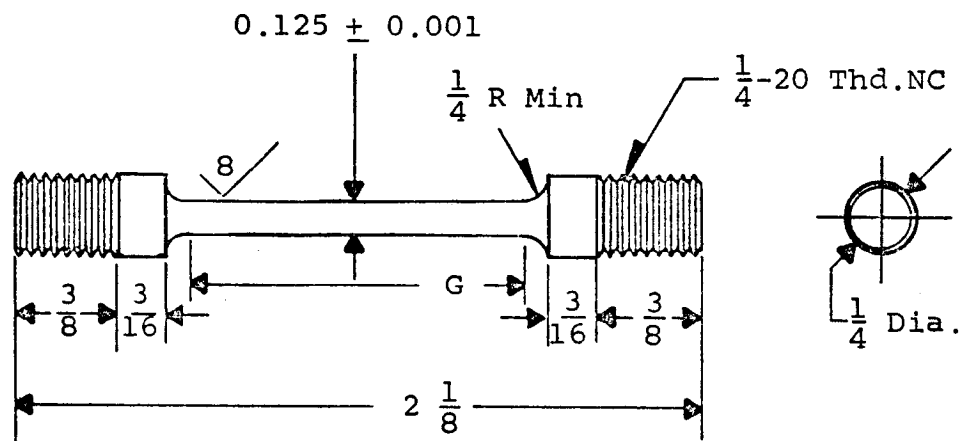
and agglomeration of the dispersed phase after hydrogen reduction and sintering without carrying them as far as the extrusion stage.

(d) Location and Preparation of Test Specimens From Extrusions

After the macroscopic and microscopic examinations of sections from the front and back of the extrusions had located the intermediate core material of high quality, samples were taken for testing starting near the front of the extrusion. The d-c magnetic test specimens were taken first. The magnetic saturation specimen was machined to 0.1 inch diameter x 0.1 inch long, and the coercive force specimens to 0.25 inch diameter x 1.0 inch long. Next, the tensile specimens which were 2.125 inches long with 0.25 inch diameter ends and a 0.125 inch diameter reduced section, as shown in Figure II-50, were obtained. Actually the tensile specimens were rough machined in a lathe and left with an 0.020 inch oversize diameter on the reduced section. Those specimens to be aged 100 hours at elevated temperatures in a vacuum of 1×10^{-5} torr before testing were given their aging treatments before grinding the threads on the ends and the diameter of the reduced section to final size. Coolant was used in all machining and grinding operations.

(e) D-C Magnetic Properties

Magnetic testing was conducted at the Westinghouse Research and Development Center under the supervision of Dr. K. Detert and the following description of test procedure was provided by him (ref. 12). The coercive force H_c , was measured directly using a Precision Coercive Force Meter, Manufactured by Institute Dr. Forster, Reutlingen, West Germany (ref. 13). The 0.25 inch diameter x 1.0 inch long specimen was magnetized in a field of 1300 oersteds in a large field coil. After switching off the field, the remanent field of the specimen was picked up by



NOTE: Taper gauge length "G" to center so that the dia. at the ends of the gauge length exceeds the dia. at the center of the gauge length by not less than 0.0005 inch nor more than 0.001 inch. "G" and total length are nominal.

Westinghouse Dwg. No. Ref. EDSK 326749

FIGURE II-50. Tensile Specimen

a sensitive field probe and a reverse field gradually applied until the field probe measured no remanent field coming from the specimen. For tests at 1200 to 1600°F, a tube furnace with electrical resistance heating coil of platinum - 10 percent rhodium wire, bifilar wound, was placed inside the field coil of the coercive force meter. A flow of 99.996 percent purity argon was maintained through the tube to protect the specimen against oxidation. The specimen was held at temperature for five minutes before its coercive force was measured. Alternating current was supplied to the furnace during measurements. The accuracy of the coercive force values at all temperatures was plus or minus two percent or better, while the temperature was held within plus or minus 10°F of that intended, as indicated by a thermocouple. Measurements were made on standard specimens at the start and end of each series of tests for verification of test procedure.

The specific saturation was measured on a 0.1 inch diameter x 0.1 inch long specimen weighing approximately 0.1 gram. The length was short in order to avoid too high demagnetizing forces. The saturation was measured by means of a magnetic balance in a field gradient of 975 oersteds per centimeter with a mean applied magnetizing field of 11,500 oersteds (refs. 12 and 14). Actually, even this high a field is not enough to reach saturation in cobalt alloys at room temperature. It has been reported that 17,000 oersteds are required for pure cobalt (ref. 15). The magnet was supplied by Varian Associates, Model V-4007. The specimen was sealed in a quartz tube which was evacuated and back-filled with 99.996 percent purity argon to a pressure of 100 mm. of mercury. The quartz tube was attached to a transducer gauge supplied by Statham Transducer Inc. The force acting on the specimen due to the applied magnetic field was determined. For measurements above room temperature, a small furnace slightly under 1 inch O.D. x 0.25 inch I. D. x 3 inches long, bifilar wound with platinum - 10 percent rhodium wire was used.

During saturation measurement, alternating current was supplied to the furnace. The temperature was checked by placing a separate thermocouple inside the furnace at the position of the specimen to be measured. The temperature was controlled to better than plus or minus 10°F. The accuracy of the saturation values was plus or minus one percent. The holding time at elevated temperature before testing was five minutes. A standard iron or cobalt specimen was measured at the start and end of each series of experimental compositions for calibration purposes. The saturation magnetization, B_s , in gauss was calculated from the specific saturation, (saturation magnetic moment), σ_s , in emu per gram from the equation:

$$B_s = 4 \pi \delta \sigma_s$$

where:

δ = density in g/cm³

σ_s = saturation magnetic moment, emu/g

The results of the coercive force and saturation measurements are presented in Table II-9. The tentative goals set up at the start of this program, in regard to magnetic properties, were a coercive force, H_c , of less than 25 oersteds and a saturation magnetization, B_s , of not less than 12,000 gauss at some temperature between 1200 and 1600°F, preferably at 1600°F. It may be seen from Table II-9 that the cobalt-base extrusions of prealloyed atomized powders did not quite meet the saturation goal, even at 1200°F. On the other hand, the 27 percent cobalt-iron base alloys made from atomized powder did have a saturation above 12,000 gauss in the entire range from 1200 to 1600°F. The supplier extrusions of cobalt-base material with 2 v/o thoria likewise meet this saturation goal, while the supplier extrusion with 10 v/o thoria does at all temperatures except 1600°F. In respect to coercive force, all extrusions tested had values less than 25 oersteds from 1200 to 1600°F.

TABLE II-9. D-C Magnetic Properties of Hot Extruded Rod

Powder or Extrusion No.	Nominal Composition (weight percent)	Coercive Force, H _c (oersteds)							Magnetic Saturation										Room Temp. Density of Material (g/cc)
		At Room Temperature		After Testing at 1200-1600°F					Saturation Magnetic Moment, σ (emu/gram)										
		Initial	Testing at 1200-1600°F	At 1200°F	At 1400°F	At 1500°F	At 1600°F	Approximate Saturation Magnetization, B _g (kilogauss)											
								At Room Temp.	At 1200°F	At 1400°F	At 1500°F	At 1600°F	At Room Temp.	At 1200°F	At 1400°F	At 1500°F	At 1600°F		
Prealloyed Atomized Powders (Extruded)																			
3	Co-1.3B+1.6Ti	25.0	27.0	6.3	4.8	4.0	3.3	132 (c)	95.7	89.2	83.5	77.4	13.7 (c)	9.9	9.3	8.7	8.0	8.26	
4	Co-1.3B+3.4Zr	48.0	53.0	9.2	7.1	5.8	4.7	132 (c)	99.9	92.6	86.9	80.6	14.0 (c)	10.6	9.8	9.2	8.5	8.43	
5	Co-1.1B+4.4Cb	42.3	-	-	-	-	7.0 (b)	-	-	-	-	-	-	-	-	-	-	8.58	
6	Co-1.2B+7.7Ta	41.0	45.0	11.6	9.4	8.4	6.3	134 (c)	95.3	87.5	82.8	78.8	14.8 (c)	10.6	9.7	9.2	8.7	8.81	
12	Fe+26.5Co+0.9B+1.8Ti	12.8	12.1	5.5	4.1	3.4	2.3	216	179	156	144	129	20.9	17.3	15.1	13.9	12.5	7.70	
13	Fe+24.8Co+1.1B+3.2Zr	18.8	17.6	8.4	6.4	4.9	3.6	212	175	152	142	127	20.9	17.2	15.0	14.0	12.5	7.84	
14	Fe+25.8Co+0.9B+4.1Cb	19.6	19.0	8.7	6.8	5.3	3.7	211	165	152	140	127	20.8	16.3	15.0	13.8	12.5	7.86	
15	Fe+24.1Co+1.0B+7.0Ta	21.0	19.0	10.4	8.6	6.2	4.4	200	159	145	135	121	20.5	16.2	14.9	13.8	12.4	8.15	
Supplier Extrusions of Dispersion-Strengthened Cobalt																			
3 (d)	Co+10.4ThO ₂ (0.01-0.06%ThO ₂)	49.0	49.0	19.4	16.7	14.8	13.4	144 (c)	125	116	110	103	15.7 (c)	13.6	12.6	12.0	11.2	8.66	
9 (e)	Co+2.0ThO ₂ (0.01-0.06%ThO ₂)	68.0	62.0	8.4	7.3	6.1	5.3	155 (c)	137	127	119	112	17.2 (c)	15.2	14.1	13.2	12.4	8.82	
9 (a)(e)	Co+2.0ThO ₂ (0.01-0.06%ThO ₂)	114.0	71.0	9.3	7.1	5.7	4.8	155 (c)	138	128	121	112	17.2 (c)	15.3	14.2	13.5	12.5	8.85	

Note:

(a) Given 85 percent cold reduction by swaging after hot extrusion. All other material is hot extruded condition.

(b) Not an accurate value. Test specimen too long (1.875 inches) for uniform temperature distribution.

(c) Measured values are presumably 5 percent too low because it was not possible to saturate the specimens at room temperature.

(d) Extrusion supplied by New England Materials Laboratory, Inc., Medford, Massachusetts.

(e) Extrusion supplied by Curtiss-Wright Corp., Metals Processing Division, Buffalo, New York.

Note:

- (a) Given 85 percent cold reduction by swaging after hot extrusion. All other material in hot extruded condition.
- (b) Not an accurate value. Test specimen too long (1.875 inches) for uniform temperature distribution.
- (c) Measured values are presumably 5 percent too low because it was not possible to saturate the specimens at room temperature.
- (d) Extrusion supplied by New England Materials Laboratory, Inc., Medford, Massachusetts.
- (e) Extrusion supplied by Curtiss-Wright Corp., Metals Processing Division, Buffalo, New York.

(f) Tensile Properties

The 0.125 diameter x 2.125 inches long threaded end tensile specimens were tested in an Instron Universal Testing Instrument, Model TTC. For the elevated temperature tests, a Satec Power Positioning Furnace, Model RA-1800 with a Kanthal-Al heating element was used to heat the specimen under vacuum to temperature. The specimens were tested in a vacuum of $0.9 - 2.6 \times 10^{-5}$ torr using a liquid nitrogen trap after stabilizing at the test temperature for half an hour. A strain rate of 0.005 inch per inch per minute was used up to the yield stress (0.2 percent offset) and 0.05 inch per inch per minute beyond that to fracture. Prior to tensile testing, all elevated temperature test specimens were rough machined and aged 100 hours at the test temperature in a vacuum of 1×10^{-5} torr or better (mainly 1×10^{-6} torr). One specimen from each extrusion was tested at each temperature.

In this preliminary evaluation phase of the program, the tensile properties are to be determined at room temperature, 1200°F, and 1600°F on all compositions. Those determined to date are presented in Table II-10.

b. INTERNALLY OXIDIZED POWDERS

The following four prealloyed powders were screened through 325 mesh and given internal oxidation treatments over a period of six hours at 1830°F in oxygen of 99.5 percent minimum purity, which had passed through a Drierite Drying Apparatus, at a pressure of one atmosphere.

<u>Atomized Powder Number</u>	<u>Composition (weight percent)</u>
8	Co + 2.5Al
9	Co + 1.9Be
17	Fe + 26.5Co + 2.3Al
18	Fe + 27.9Co + 1.4Be

TABLE II-10. Tensile Properties of Hot Extruded Rod

Powder or Extrusion No.	Nominal Composition (weight percent)	At Room Temperature				At 1200°F (a)			
		Ultimate Strength (1000 psi)	0.2% Offset Yield Strength (1000 psi)	Elongation in 4D (percent)	Reduction in Area (percent)	Ultimate Strength (1000 psi)	0.2% Offset Yield Strength (1000 psi)	Elongation in 4D (percent)	Reduction in Area (percent)
Prealloyed Atomized Powders (Extruded)									
3	Co+1.3B+1.6Ti	123.1	117.0	6.0	2.1	51.2	26.4	27	25
4	Co+1.3B+3.4Zr	162.4	144.3	1.0	0.7	75.7	38.9	20	24
5	Co+1.1B+4.4Cb	172.8	116.2	10.0	4.1	80.3	41.9	23	27
6	Co+1.2B+7.7Ta	175.6	136.1	9.8	8.4	73.6	42.0	24	25
12	Fe+26.5Co+0.9B+1.8Ti	132.1	87.8	7.0	6.3	56.4	27.6	50	53
13	Fe+24.8Co+1.1B+3.2Zr	147.1	88.9	10.0	11.8	62.1	31.5	40	44
14	Fe+25.8Co+0.9B+4.1Cb	146.5	101.5	10.0	9.1	67.2	31.5	34	34
15	Fe+24.1Co+1.0B+7.0Ta	129.0	79.3	8.0	7.8	62.8	31.5	34	28
Supplier Extrusions of Dispersion-Strengthened Cobalt									
3	Co+10.4ThO ₂ (0.01-0.06μThO ₂)	129.4	97.3	0.2	0.0	25.1	18.3	4.0	2.1
9	Co+2.0ThO ₂ (0.01-0.06μThO ₂)	120.5	82.5	3.5	10.6	25.8	13.8	30	24
9 (b)	Co+2.0ThO ₂ (0.01-0.06μThO ₂)	104.6	80.8	1.3	3.8				
Note:									
(a) Specimens aged 100 hours at 1 x 10 ⁻⁵ torr or less at the elevated tensile test temperature before testing.									
(b) Cold reduction in area of 85 percent by swaging after hot extrusion. All other materials tested in hot extruded condition.									

The retort and equipment used were described in the second quarterly report. The experimental details will be described in the next quarterly report when hydrogen reduction of the cobalt and iron oxides, isostatic compacting and extrusion have been completed, and the microstructure has been studied.

c. COMPOSITE POWDERS

(1) Measurements on Powders

The seven composite powders produced by three different suppliers that were ordered for this program were listed in the third quarterly report. The nominal oxide content of all powders was ten percent by volume of alumina or thorium. The powder particle size, particle shape, apparent density, and other information concerning powder compact density, which will be discussed later, are indicated in Table II-11.

The Fisher Sub-Sieve Sizer (ASTM Method B 330-58T) was used to determine the average particle diameters (APD) of the composite powders which were not screened before processing started. The powder particle size of all composite powders was smaller than that of the minus 325 mesh atomized powders given in the third quarterly report. The powder particle size, shape, and microstructure were examined under the microscope after mounting in plastic, polishing, and etching. Composite powder Nos. 3, 4, and 11 from Chas. Pfizer, which were recently examined, had a general appearance similar to that of composite powder Nos. 1 and 2 from the same source (see photomicrograph in the third quarterly report.) Figure II-51 shows the microstructure of composite powder No. 11 from Vitro Labs after hydrogen reduction. (The chemical analysis reported by the powder supplier was given in the third quarterly report). The apparent density, which is the weight of powder that fills a standard volume under free-flowing conditions (without jarring) has been expressed in terms of grams per cubic centimeter (ASTM Method B 212-48) in Table II-11, and also as percent of the theoretical density of each composition. The composite powders tended to have lower apparent densities than the minus 325 mesh atomized powders listed in the third quarterly report.

TABLE II-11. Particle Size, Shape, and Apparent Densities of Composite Powders and Density of Compacts

Composite Powder No.	Supplier	Supplier's Lot No.	Nominal Composition (a) (weight percent)	Particle Size of Oxide (microns)	Powder Particle Size- Fisher APD (microns)	Powder Particle Shape	Apparent Density of Powder		Density of Compact			
							(g/cc)	(percent)(b)	Green-pressed at 50 000 psi (g/cc)	(percent)(b)	Sintered - 2 hrs., 1800° F. in H ₂	
											(g/cc)	(percent)(b)
3	Sherritt Gordon	951	Co+11.2ThO ₂	0.01-0.06	2.6	Irregular	2.40	26.8	6.16	69	6.03	67
11	Vitro Labs	38, 39	23.7Co+64.2Fe+12.1ThO ₂	0.01-0.06	1.3 (c)(d)	Irregular	1.58 (c)	19.4 (c)	4.63	57	6.48	79
1	Chas. Pfizer	RX2002	Co+4.75Al ₂ O ₃	0.01-0.06	2.6	Equiaxed	2.53	30.3	5.85	70	5.97	71
2	Chas. Pfizer	RX2003	Co+4.75Al ₂ O ₃	0.1-0.6	3.9	Equiaxed	2.60	31.1	5.50	66	5.81	69
3	Chas. Pfizer	RX2044	Co+11.2ThO ₂	0.01-0.06	3.6	Equiaxed	2.69	30.0	6.37	71	6.49	73
4	Chas. Pfizer	RX2045	Co+11.2ThO ₂	0.1-0.6	3.6	Equiaxed	2.63	29.4	6.51	73	6.53	73
11	Chas. Pfizer	RX2059	23.7Co+64.2Fe+12.1ThO ₂	0.01-0.06	1.6	Equiaxed	1.35	16.5	6.10	75	6.10	75

Note:

(a) Oxide content corresponds to 10 percent by volume.

(b) Percent of theoretical density.

(c) After hydrogen reduction of 6 hours at 1220°F.

(d) Estimated by supplier to be 0.5 micron before hydrogen reduction.

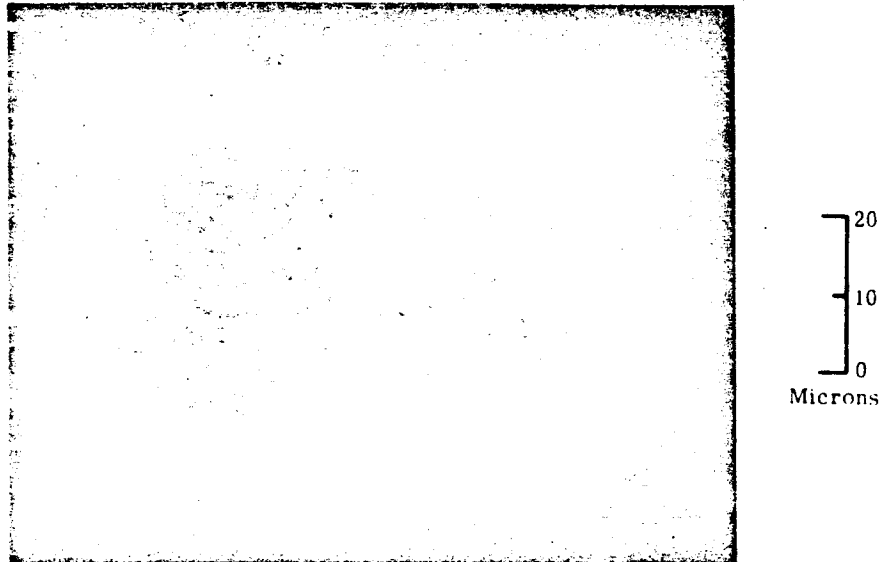


FIGURE II-51. Composite Powder No. 11, Fe+23.5%Co+10.8% ThO₂ (0.01 - 0.06 micron thoria), From Vitro Labs After Hydrogen Reduction Showing Irregular Shape and Fine Grain Structure of Powder Particles. Thoria Particles Dispersed in Matrix Are Too Small to be Seen, 1000 X. Etched in Acetic-Nitric-Hydrochloric-Water. (1:1:4:1 Ratio)

(2) Hydrogen Reduction Treatments for Powders

Six of the seven composite powders have been hydrogen reduced for six hours at 1220°F in hydrogen of 99.95 percent guaranteed purity. The hydrogen used for reduction and the 99.996 percent guaranteed purity argon used for pre-purge and post-purge of the retort flowed from their respective cylinders through an attached Deoxo Hydrogen Catalytic Purifier (Model 10-50) and thence through a Drierite Drying Apparatus. The dew point of the hydrogen, after passing through the Deoxo Purifier and Drierite, was measured to be lower than minus 90°F. These gases, flow rates, equipment, and procedure were the same as reported in the third quarterly report for the hydrogen reduction of atomized powders.

Since composite powder No. 11 from Vitro Labs was reported by them to be submicron (estimated 0.5 micron) size and pyrophoric, the entire four pound quantity received was removed under argon from two hermetically sealed cans in which it was shipped and spread out to a depth of 0.5 inches in 15 shallow, rectangular trays (150 mm. long x 65 mm. wide x 19 mm. high) of impervious, recrystallized 99 percent alumina (Coors AD 99) placed inside the Inconel 600 retort. This work was performed inside a 30 inches I. D. x 48 inches long Vacuum Industries glove box which had been evacuated to less than one micron of mercury before back-filling with argon. After sealing the retort lid, and inlet and outlet tubes, the retort and powder were removed from the glove box and placed in an electrical resistance furnace where a hydrogen reduction treatment was applied in the normal manner. The powder was not pyrophoric after hydrogen reduction because of a sintering together of individual powder particles, thus effectively increasing their size.

(3) Isostatic Pressing of Powders

After hydrogen reduction, each composite powder was placed in a high-speed food blender for breaking up any lumps which might be present (no caking occurred during hydrogen reduction). Each powder passed completely through a 28 mesh sieve and was loaded into a rubber bag for isostatic pressing which was conducted in the same

manner as described in the third quarterly report. A pressure of 50,000 psi was held for one minute. The two pound (approximately) green compacts of composite powders tended to be of smaller diameter and greater length than those of the atomized powders pressed under the same conditions, reflecting the generally lower apparent densities of the composite powders and the greater volume occupied when a given weight was loaded into a rubber bag for pressing. The compacts of the composite powders were approximately 1.5 to 1.8 inches diameter x 4 inches long, while the green compacts of atomized powders were approximately 2 inches diameter x 3 inches long. The densities of the green and sintered compacts of composite powders are listed in Table II-11.

(4) Sintering of Compacts

Sintering for two hours at 1800°F in hydrogen was carried out in the same manner as described for the atomized powders in the third quarterly report.

d. SUPPLIER EXTRUSIONS OF DISPERSION-STRENGTHENED COBALT

(1) Description of Materials

The extruded compositions listed in Table II-12 were obtained for the initial evaluation phase of this program. The cobalt plus 10 volume percent thoria composition (No. 3) from the New England Materials Laboratory was received in the hot extruded condition. The Metals Processing Division of Curtiss-Wright Corporation supplied the cobalt plus two volume percent thoria composition (No.9) in two conditions: hot extruded and 85 percent cold worked by swaging (after hot extrusion). According to the specifications that the suppliers worked toward, the purity of the cobalt and ThO_2 was to have been 99.5 percent or greater.

The New England Materials Laboratory supplied two 42 inch long pieces of extrusion designated CR-68-1 and CR-68-2 with an alloy core and mild-steel cladding on the surface. The core diameter was 0.375 to 0.400

TABLE II-12. Supplier Extrusions of Dispersion-Strengthened Cobalt

Extrusion Number	Nominal Composition (weight percent)	Particle Size of Oxide (microns)	Supplier's Process of Manufacture	Supplier	Supplier's Lot Number
3	88.8Co+11.2ThO ₂	0.01-0.06	The ThO ₂ is introduced by the thermal decomposition of a thorium salt onto the cobalt powder, followed by hydrogen reduction, pressing, sintering, and extrusion, (ref. 16)	New England Materials Laboratory	CR-68-1 and CR-68-2
9	97.7Co+2.3ThO ₂	0.01-0.06	Prepared by co-dissolving the desired elements in a volatile solvent, flash-drying, heating, grinding, and reduction of cobalt oxide. Compacting, sintering, and extrusion are then performed, (ref. 17)	Curtiss-Wright, Metals Processing Division	PP1-18A-1
9(a)	97.7Co+2.3ThO ₂	0.01-0.06	Same as above plus cold working.	Same as above	Same as above
<p>Note: (a) Supplied in cold worked condition. Cold reduction of 85 percent by swaging given to hot extruded rod. All other material supplied in hot extruded condition.</p>					

inches and the overall diameter was 0.562 inches. The material was reported to have been extruded at 1850°F with a 25 to 1 reduction ratio. The extrusion direction was indicated on the rods. The chemical analysis of the extruded alloy core reported by the supplier is indicated in Table II-13. The carbon content is slightly higher than the desired target limit, while sulphur content exceeded the target limit by a considerable amount.

Curtiss-Wright Corporation sent three pieces of hot extruded rod (24-1/8, 28-15/16, and 31-1/16 inches long) having a total length of 84-1/8 inches. Four pieces of cold swaged rod (16-1/16, 23-3/16, 20-1/4 and 24 inches long) with a length totaling 83-1/2 inches were supplied from their Lot No. PP1-18A-1. Table II-13 shows that the ThO₂ content was slightly lower than the target limit.

(2) Testing of Extrusions

(a) Inspection for Defects

Transverse sections from the front and back of each extruded rod were examined for defects both macroscopically and microscopically in the manner described earlier for extrusions made from prealloyed atomized powders. In this way, sound material representative of the product was insured for testing. No gross defects were seen. However, the Curtiss-Wright rod contained some stringers of non-metallic material which they stated were clusters of thorium oxide particles, Figure II-52.

(b) Microstructure of Representative Material

Table II-8 gives the results of the examination of microstructure under the light microscope. Figures II-52, II-53, and II-54 show the dispersion of thorium particles in the cobalt matrix.

(c) Location and Preparation of Test Specimens from Extrusions

This operation was carried out in the same manner

TABLE II-13. Chemical Analysis of Supplier Extrusions^(a)

Element	New England Materials Lab. Supplier Extrusion No. 3, 88.8Co+11.2ThO ₂ (weight percent)			Curtiss-Wright Supplier Extrusion No. 9, 97.74Co+2.26ThO ₂ (weight percent)			
	Westinghouse Specification Target Limits	Analysis	Precision of Analysis	Westinghouse Specification Target Limits	Hot Extruded Analysis (f)	85% Cold Reduction Analysis (g)	Precision of Analysis
Mn	0.04 maximum	< 0.01	(b)	0.04 maximum	0.002	0.001	(Not reported)
Si	0.04 maximum	< 0.03	(b)	0.04 maximum	0.001	0.002	
C	0.020 maximum	0.023	+0.0002	0.020 maximum	0.0085	0.0092	
S	0.006 maximum	0.028	+0.0003	0.006 maximum	< 0.001	< 0.001	
P	0.010 maximum	< 0.001	--	0.010 maximum	0.0003	0.0004	
Ni	0.70 maximum	< 0.01	(b)	0.70 maximum	0.49	0.46	
Cr	0.10 maximum	< 0.01	(b)	0.10 maximum	0.079	0.070	
Co	Remainder	---	---	Remainder	---	---	
Fe	---	0.06	+0.001	---	0.10 (e)	0.01 (e)	
ThO ₂	9.7 - 12.7	10.4	+0.23 (c)	2.11 - 2.41	1.96	2.05	
O (other than as ThO ₂)	---	0.21	--	---	0.00	0.00	
O (total)	---	1.47 (d)	--	---	---	---	
N	---	0.004 (d)	--	---	0.0010	0.0028	
H	---	0.0182 (d)	--	---	0.0019	0.0011	

Note:

(a) Reported by the extrusion supplier.

(b) Wet chemical analyses were inconclusive and, therefore, spectrographic analyses were conducted for these elements.

(c) Precision on analysis of thorium (9.16% thorium as analyzed which is equivalent to 10.4% ThO₂).

(d) Vacuum fusion at 1700°C.

(e) Spectrographic analysis.

(f) Designated by supplier as Lot No. PP1-18A-1, Ext. #15.

(g) Designated by supplier as Lot No. PP1-18A-1, Ext. #5.

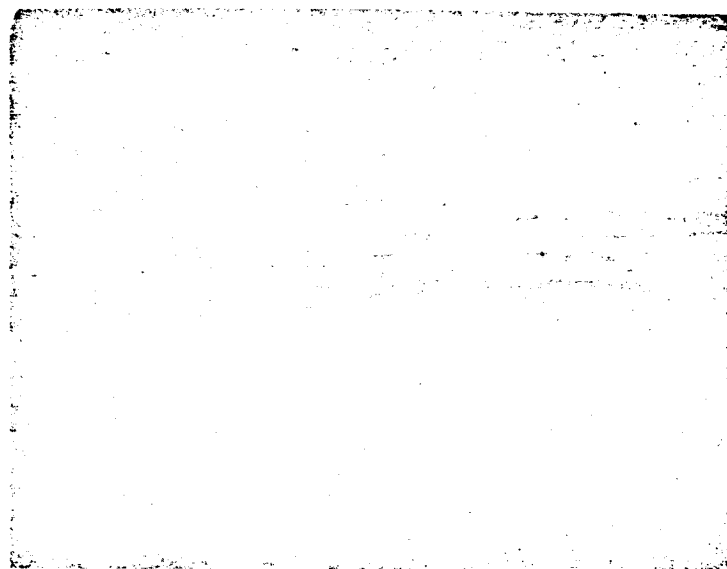


FIGURE II-52. As-Extruded Rod Supplied by Curtiss-Wright Corp., Supplier Extrusion No. 9, Co+1.96%ThO₂ (0.01 - 0.06 micron thoria), Showing Dispersion of Thoria Particles in Cobalt Matrix. Some of the Thoria Particles are Present as Clusters and Stringers. Longitudinal Section Near Front of Extrusion, 1000 X. Lightly Etched in Acetic-Nitric-Hydrochloric-Water. (1:1:4:1 Ratio)

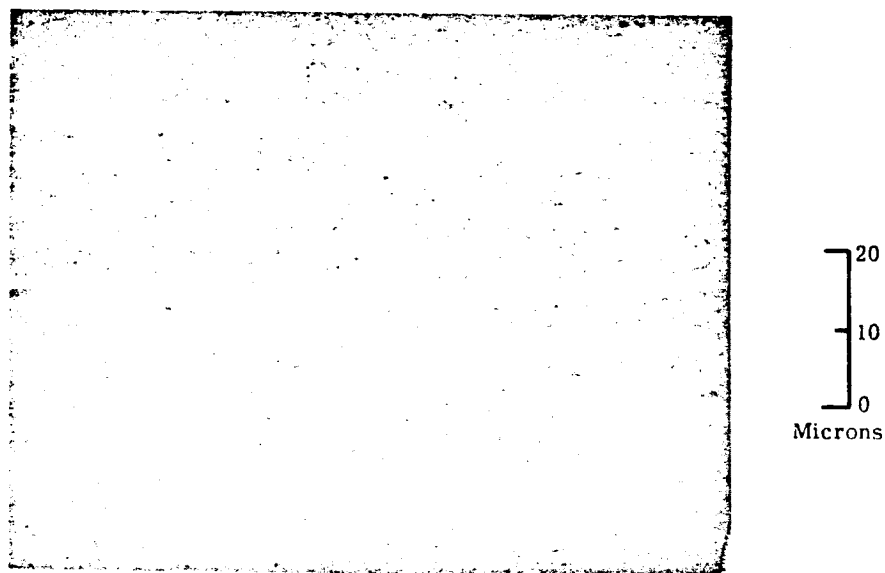


FIGURE II-53. Rod Cold Reduced 85% After Extrusion by Curtiss-Wright Corp., Supplier Extrusion No. 9, Co+2.05% ThO₂ (0.01-0.06 micron thoria), Showing Dispersion of Thoria Particles in Cobalt Matrix. Longitudinal Section Near Front of Extrusion, 1000 X. Lightly Etched in Acetic-Nitric-Hydrochloric-Water. (1:1:4:1 Ratio)

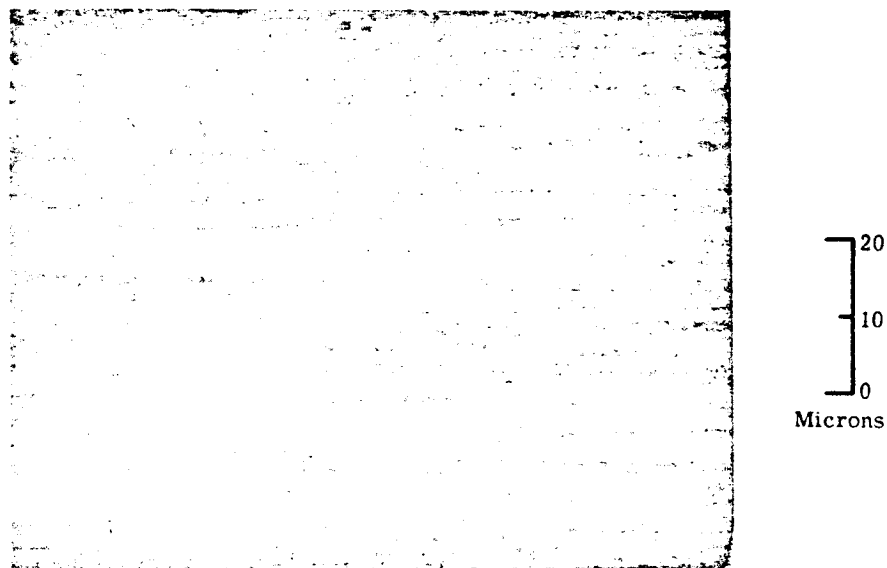


FIGURE II-54. As-Extruded Rod Supplied by New England Materials Laboratory, Supplier Extrusion No. 3, Co+10.4% ThO₂ (0.01-0.06 micron thoria), Showing Dispersion of Thoria Particles in Cobalt Matrix. Some of the Thoria Particles are Present as Clusters and Stringers. Longitudinal Section Near Front of Extrusion, 1000 X. Lightly Etched in Acetic-Nitric-Hydrochloric-Water.(1:1:4:1 Ratio)

previously described for rod extruded from pre-alloyed atomized powders. Specimens from the front of the rod relative to the extrusion direction were tested.

(d) D-C Soft Magnetic Properties

The coercive force and saturation measurements are presented in Table II-9. The coercive force values at room temperature for the cobalt-base supplier extrusions were higher than for the extrusions of cobalt-base atomized powders. This was related to the greater proportion of hexagonal cobalt and smaller proportion of cubic cobalt in the supplier's extrusions. Cold working further increased the amount of hexagonal cobalt at the expense of cubic cobalt and, therefore, increased the coercive force at room temperature. The tests at 1200 to 1600°F show that the coercive force decreased considerably. At these temperatures the hexagonal cobalt phase had transformed to cubic. The coercive force values of the supplier's extrusions at elevated temperatures were less than 25 oersteds, but tended to remain as high or higher than those of the extruded atomized powders, even though the latter contained the greater amount of dispersed phase. Perhaps the reason for this is that the average particle size of the dispersed phase was smaller in the supplier's extrusions, and therefore, more nearly of the proper size (relative to the magnetic domain wall thickness) to promote "sticking" and retard domain wall movement.

The magnetic saturation of the supplier's extrusions at all temperatures was higher than that of the cobalt-base extrusions of atomized powders due to the dilution effect of the greater amount of non-magnetic dispersed phase in the latter class of materials.

After more dispersion-strengthened materials have been magnetically tested and the results analyzed, a quantitative explanation of the relation of magnetic properties to structure will be provided.

(e) Tensile Properties

Not enough tensile tests have been completed to date for comparison and analysis purposes. The data available are given in Table II-10.

3. Program for the Next Quarter

- a) Magnetic and tensile testing will be continued on old and new extrusions.
- b) Measurements on dispersoid parameters will be continued in order to correlate properties with microstructure, and to develop recommendations concerning compositions and processing conditions for the intermediate evaluation phase of this program.

D. TASK 4 - CREEP TESTING

1. Summary of Technical Progress

- a) One standard stress rupture test was completed as a check on the quality of the new heat of Nivco alloy (10-NO2V-1099). Rupture occurred at 192 hours which exceeds the Westinghouse 100 hour minimum life requirement for Nivco when loaded to 65,000 psi at 1150°F in air.
- b) The first specimen from the new heat has been on test 2009 hours at 1100°F and 50,000 psi. Pressure is 5.8×10^{-9} torr and total extension is 1.5 percent.
- c) Specimen No. 2 from the new heat has been on test 1818 hours at 1100°F and 37,500 psi. Pressure is 3.4×10^{-9} torr and total extension is 0.16 percent. Strain time plots for these two specimens is shown in Figure II-55.

2. Discussion

Long-term creep data are needed on high-strength rotor materials suitable for electric alternators. Nivco alloy (23Ni-1.7Ti-0.4Al-0.2Zr-Balance Co) is presently the highest temperature rotor material available. Five thousand hour tests are planned at temperatures to 1150°F in vacuum (1×10^{-6} torr) to complement short-time data run on NAS3-4162.

An unexpected, low-ductility failure of the first heat of material has required the substitution of a second heat. The second heat represents the latest processing methods now used for the Nivco alloy. It results in a smaller grain size. The new processing methods had not been put into practice when the Task began and the original heat represented current practice as of that date. The discussion of the material change and the metallurgical interpretations was given in the third quarterly report.

a. RESULTS

Both high-vacuum test specimens from heat 10-NO2V-1099 were brought to temperature slowly so that the pressure would not exceed 5×10^{-6} torr. When the pressure reached 9×10^{-7} torr, the samples were loaded. After 48 hours, capsule pressure had fallen to 1.8×10^{-7} torr. Pressures of 5.8 and 3.4

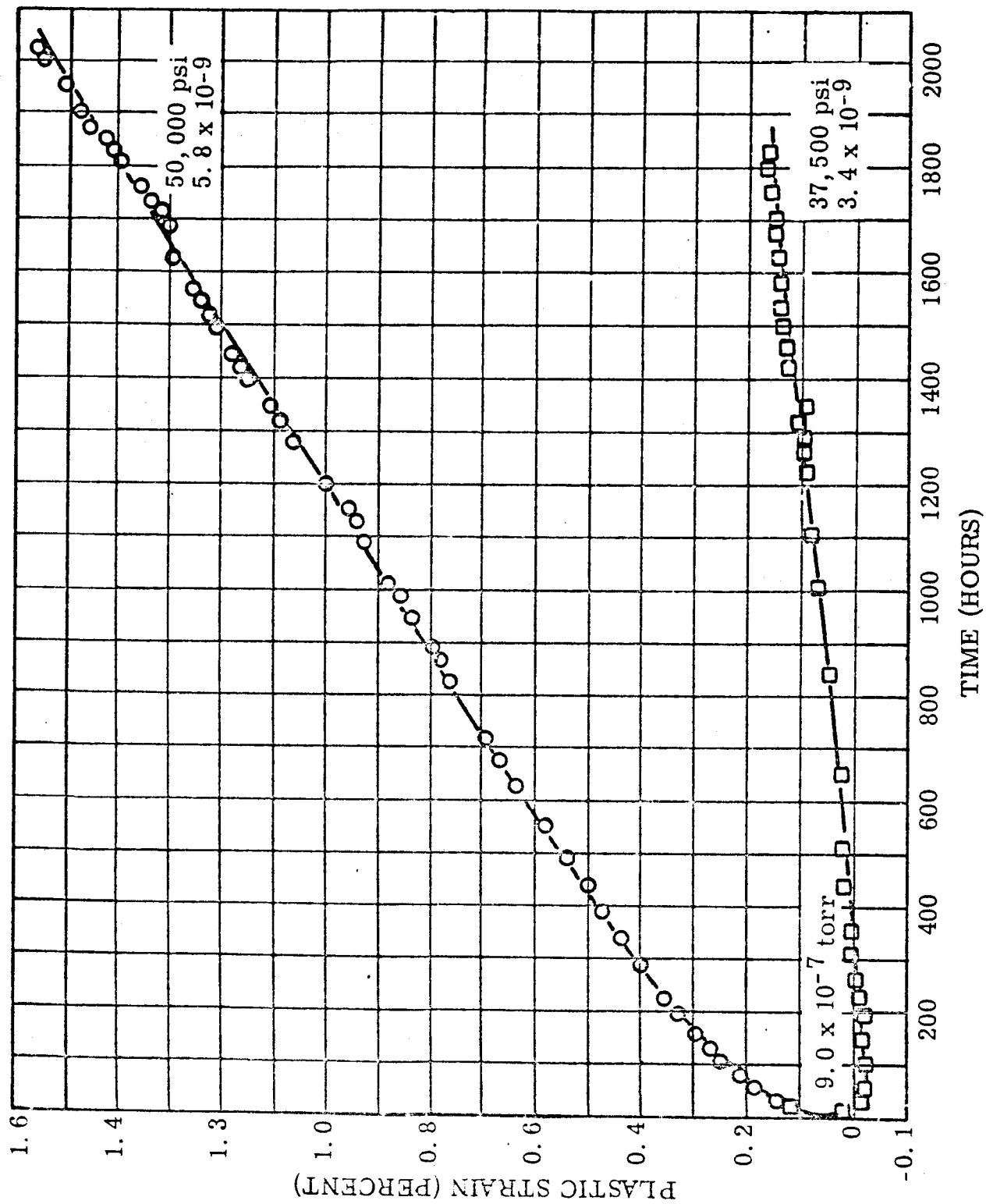


Figure II-55. Creep - Nivco Bar

FIGURE II-55. Creep, Nivco Heat 10-NO2V-1099, Tested in Vacuum at 1100°F and 50,000 psi and 37,500 psi

$\times 10^{-9}$ torr were reached after approximately 2000 hours of testing. The single stress-rupture test in air on Nivco alloy was required as a quality check. The alloy must withstand a 65,000 psi stress at 1150°F for a minimum of 100 hours before it is considered satisfactory for use. Good rupture ductility would be 20 percent elongation. The sample from heat 10-NO2V-1099 ruptured at 192 hours with 33.1 percent elongation (see Table II-14 for data). The rupture was located in the plain bar section of the combination smooth and notched bar specimen. An ASTM grain size of seven was measured on the new material. It is concluded that this particular lot of material is suitable for long-time vacuum creep testing.

The first vacuum test specimen from the new heat of Nivco has reached 1.5 percent extension after 2000 hours at 50,000 psi and 1100°F. Limited vacuum creep data obtained on NAS3-4162 placed the Larson-Miller extrapolated 10,000 hour stress for 1.0 percent strain at about 50,000 psi. Production Nivco alloy, however, was modified since testing started to improve long-time rupture ductility and transverse tensile ductility as mentioned previously. These modifications have resulted in a modest reduction in the creep strength. The lower creep curve of Figure II-55 was obtained from the 37,500 psi specimen and shows a small contraction in the first 100 hours of test which is indicative of stress induced precipitation normally obscured by testing at a higher creep rate. Room temperature coercive force measurements made on heat 10-NO2V-1099 are given in Table II-15. Included are the coercive force measurements on the previous heat (AC232) for reference purposes. The differences in the coercivity of the different samples are the cumulative effects of minor chemistry variations, instrument error, measuring technique and operator variables. The observed differences are not considered significant.

b. STRAIN ANALYSIS FOR A TYPICAL NIVCO ROTOR

A limited temperature-stress-creep strain analysis has been made on a model Nivco alloy rotor. A typical solid rotor design was selected for the analysis and was taken from the work sponsored by the Air Force on SPUR/SNAP50. The stress and rotor temperature profiles were taken from a SPUR Development Report (ref. 18) and converted into dimensionless ratios of stress and temperature as a function of rotor radius. Next,

TABLE II-14. Quality Check, Standard Stress-Rupture Test
Data for One Specimen from Nivco Heat
10-NO2V-1099 (air test)

Test Temperature (°F)	1150
Stress (psi)	65,000
Rupture Time (hours)	192
Minimum Creep Rate (percent/hour)	0.030
Time to 0.5 Percent Strain (hours)	0.50
Time to 1.0 Percent Strain (hours)	7.0
Time to 3.0 Percent Strain (hours)	67.0
Transition Time (hours)	72.0
Transition Strain (percent)	3.0
Plastic Strain on Loading	0.0
Rupture Elongation (percent)	33.1
Hardness Before Test (DPH)	371
Hardness After Test (DPH)	385

TABLE II-15. Room Temperature Coercive Force Measurements
for Nivco Heats AC232 and 10-NO2V-1099

Coercive Force (Oersteds) (a)			
Sample No.	Heat AC232 (Previous Heat)	Sample No.	Heat 10-NO2V-1099 (Present Heat)
1	9.5	9	8.7
2	9.6	10	9.0
3	9.0	11	8.6
4	8.6	12	10.1
5	6.9	13	10.4
6	7.2	14	8.0
7	9.3	15	9.0
8	8.0	16	8.9
Average	8.5	Average	9.2
(a) Each value is the average of 4 readings.			

all existing Nivco creep and rupture data taken over a period of several years were reduced, with the aid of a computer, to equations for the Larson-Miller parameter by the least squares method. These are plotted on Figure II-56 for 0.2, 0.4, and 1.0% creep strain and for rupture. No data points are shown for clarity since the curves were plotted from the equations which are based on over 200 test points. These curves were then used to estimate the amount of creep which would occur under varying conditions of stress and temperature in 10,000 hours. These values were used with the dimensionless ratios of temperature and stress mentioned previously for a typical rotor to identify the incremental creep strain which a rotor would undergo at various operating conditions. Figures II-57 and II-58 present this incremental strain as a function of the dimensionless radius ratio r/r_{OD} (r_{OD} is defined on Figure II-57 at 825°F and two stresses. Integrating the incremental creep strain then defines the total creep strain for a typical application. The integrated value is also given on the two figures.

The significance of the results is as follows:

- (1) While the design limits for total creep strain over the rotor diameter may be only 0.20 to 0.40 percent, the localized creep may amount to several percent in typical designs. Therefore, creep testing should be done to as much as two to four percent creep strain to provide sufficient design information on the Nivco alloy.
- (2) Using the criterion of (1) above, only a small amount of creep will occur at the rotor inner radius where the stresses are the highest but the temperatures are the lowest.
- (3) Most of the creep will then occur at the outer rotor radius where the temperatures exceed 1050°F to 1075°F. The sharp rise in the slope of the curves of Figures II-57 and II-58 show this plainly.

In making the foregoing analysis, it was assumed that the magnetic properties and thermal conductivity of Nivco were similar to those of H-11 alloy used in the SPUR rotor design calculations.

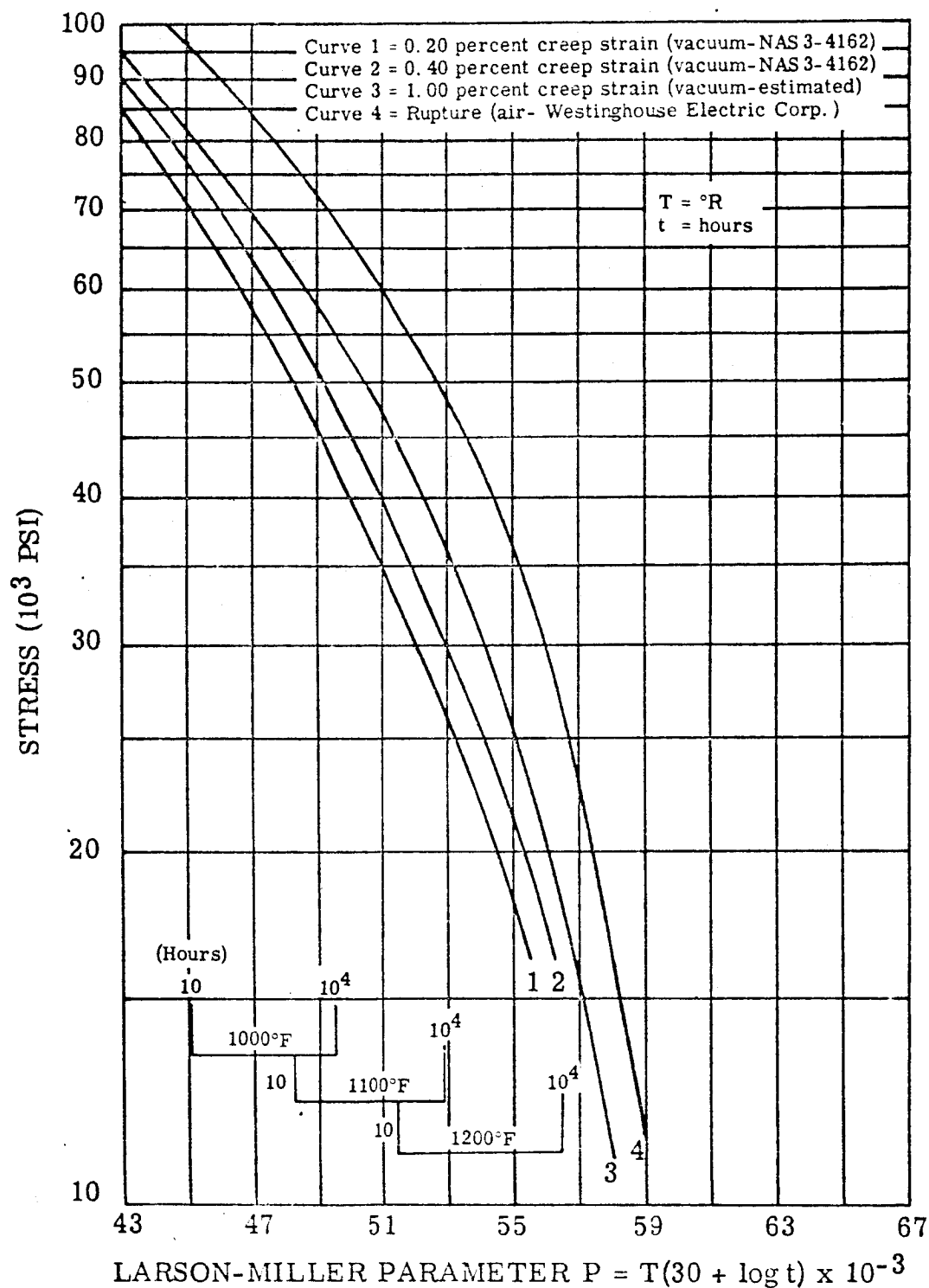


FIGURE II-56. Summary Creep-Stress Rupture Larson-Miller Plot for NIVCO Alloy (Curves are least squares fit of over 200 test points which have been omitted for clarity)

Figure II-56. Summary Creep - Larson-Miller Plot - Nivco

Figure II-57. Creep Strain - As Function of r/r_{OD} at 60,000 psi

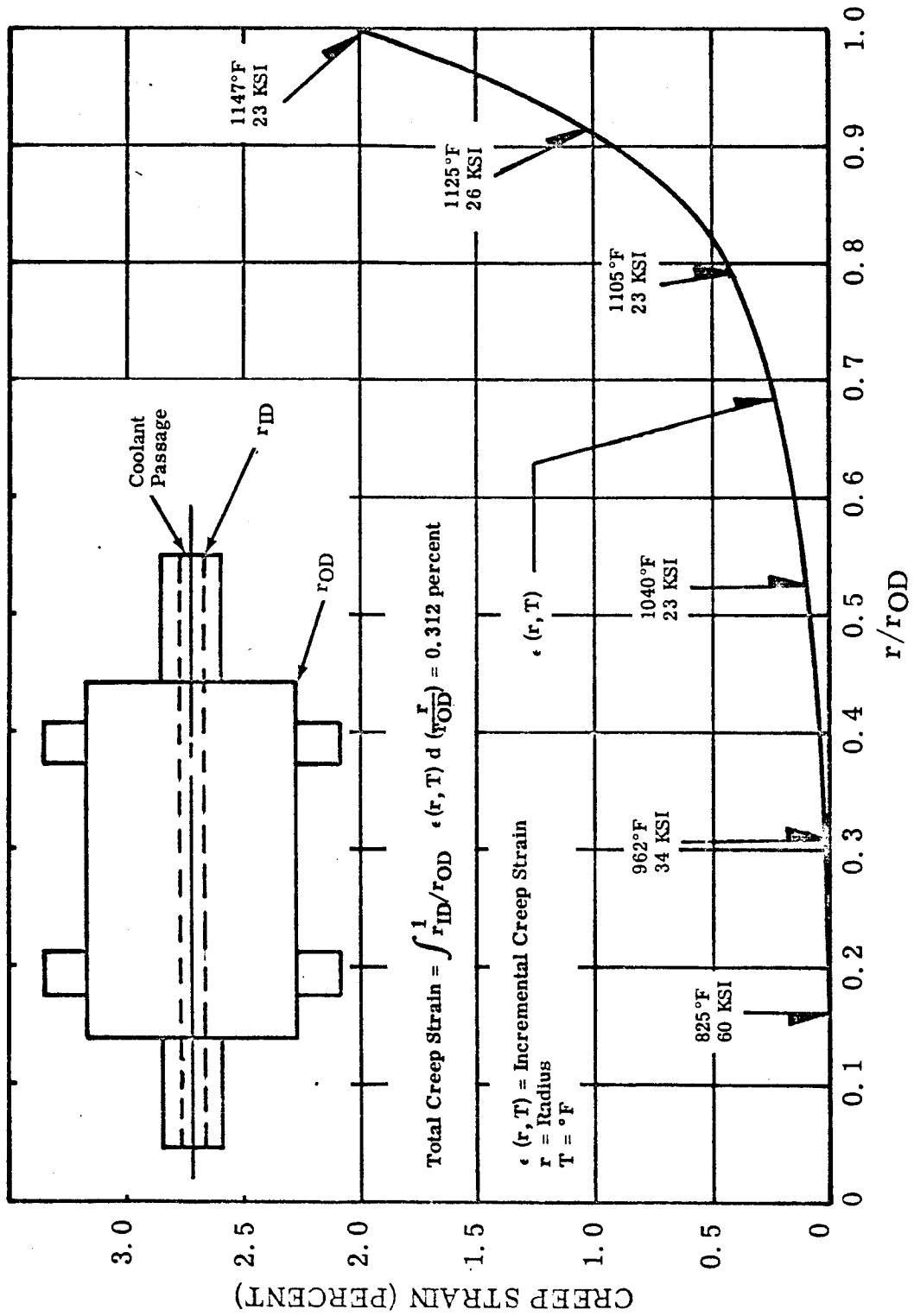


FIGURE II-57. Creep Strain as a Function of r/r_{OD} for a Typical Solid NIVCO Alloy
 Inductor Rotor Using a Coolant Temperature of 825°F and a Core
 Stress of 60,000 psi

Figure II-58. Creep Strain - As Function of r/r_{OD} at 70,000 psi

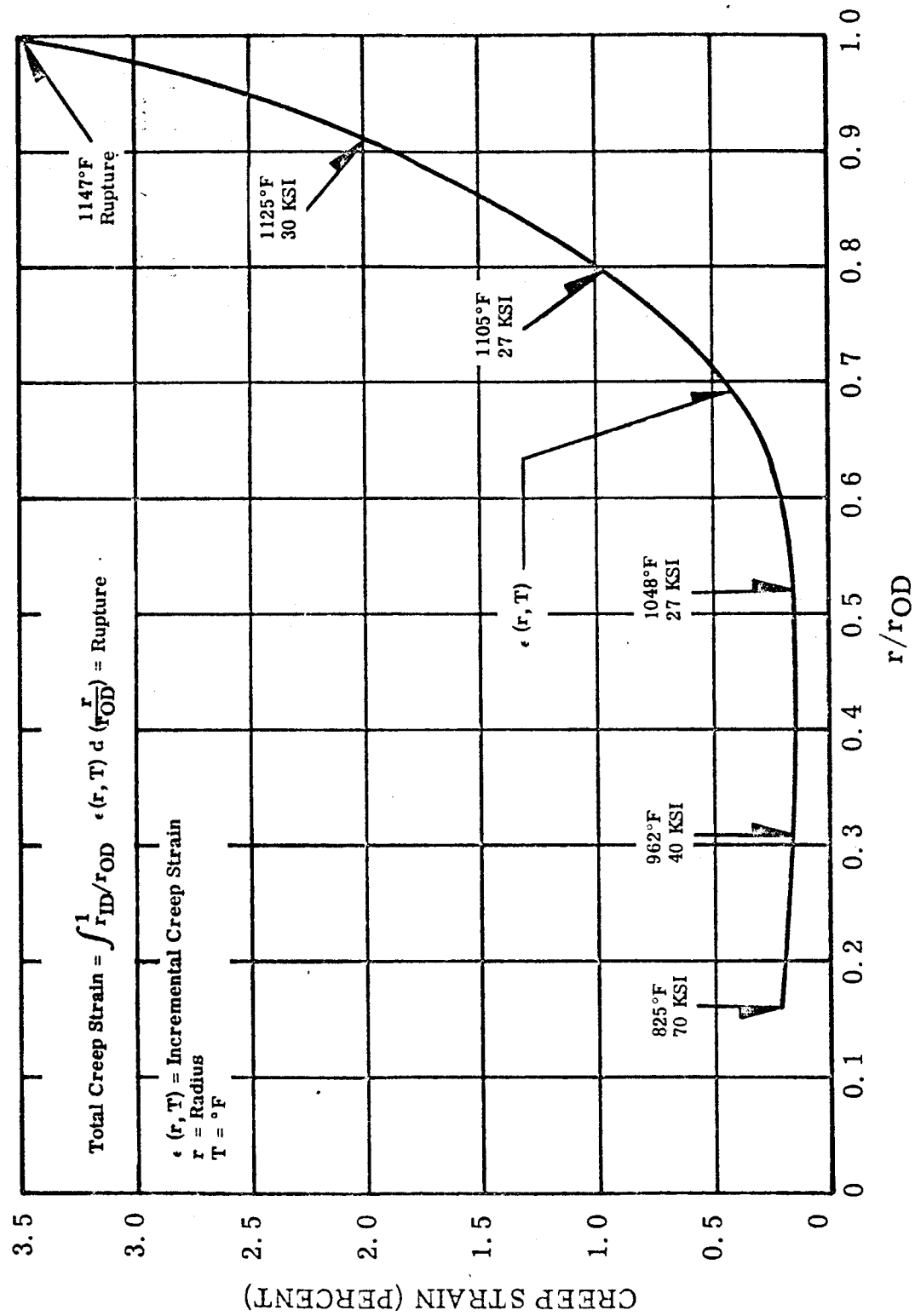


FIGURE II-58. Creep Strain as a Function of r/r_{OD} for a Typical Solid NIVCO Alloy Inductor Rotor Using a Coolant Temperature of 825°F, a Core Temperature of 825°F, and a Core Stress of 70,000 psi

These properties are slightly different for Nivco alloy, but even with the difference, the same general trends will occur. These calculations are based upon the stresses in the rotor at zero time. The stress pattern will shift with time as creep causes a redistribution of the stress pattern.

As a result of this analysis, the four remaining creep tests will be run at temperatures above 1000°F and at creep strains in excess of one percent to better define creep strain at the more critical portion of the rotor.

3. Program for the Next Quarter

Two additional tests will be started on heat 10-NO2V-1099 utilizing two new Vacion pumps recently purchased by Westinghouse.

SECTION III

PROGRAM II - HIGH TEMPERATURE CAPACITOR FEASIBILITY

This program will study the feasibility of building a lightweight capacitor suitable for operation up to 1100°F. It will utilize high-purity dielectric materials and specialized fabrication methods. The ultimate application is in lightweight, high-temperature, power conditioning-equipment suitable for space application.

A. SUMMARY OF TECHNICAL PROGRESS

- 1) Room and elevated temperature electrical measurements (dissipation factor ($\tan \delta$), capacitance and d-c resistance to 1100°F) in vacuum have been completed on four different types of dielectric materials. These include pyrolytic boron nitride (Boralloy), polycrystalline Al_2O_3 (Lucalox), polycrystalline BeO, and single crystal Al_2O_3 (Linde Sapphire).
- 2) A comparison of electrical data for each of these materials shows that pyrolytic boron nitride has significantly lower a-c losses, higher d-c resistance, and exhibits less change in capacitance with temperature than any other material investigated over the temperature range from room to 1100°F. In addition, the d-c breakdown strength of pyrolytic boron nitride is in the range of 7000 volts/mil at 1100°F. This value is several times greater than that obtained for sapphire or BeO at 1100°F.
- 3) Based on elevated temperature electrical measurements and a volume parameter (MF/IN^3) a "figure of merit" has been calculated for each dielectric material. These calculations show that pyrolytic boron nitride is the prime material candidate for fabricating a high temperature capacitor by a factor of at least 100 over single crystal Al_2O_3 (Sapphire), its nearest competitor.
- 4) D-C voltage breakdown measurements were made on three single wafer capacitors at 1100°F in vacuum. (BN Capacitor No. 3, Sapphire Capacitor No. 1, and BeO Capacitor No. 2). The results show the need for improved instrumentation in future tests because of the "self healing" effect of thin film electrodes. These electrodes volatilize at each breakdown point which prevents the capacitor from actually shorting or drawing enough current to trip the power supply relay at the first breakdown indication.

- 5) An analysis of the electrical data has shown the significance of substrate surface roughness, sputtering parameters (electrode thickness) and the electrode material (bulk resistivity) on the equivalent series resistance of a test capacitor with thin film electrodes. The series resistance effect causes an increase in the measured dissipation factor which is not an intrinsic property of the dielectric material.
- 6) Several interesting effects were observed in the measurement of capacitance and $\tan \delta$ vs. temperature primarily for the metal oxide type dielectrics. These effects can be described as a hysteresis or dielectric "after working" phenomena on measuring $\tan \delta$ and capacitance during heating and then during cooling from an elevated temperature. In addition, a marked aging (decrease) of $\tan \delta$ and capacitance was recorded for a BeO capacitor after it had been heated in air to 970°C (1778°F). An attempt has been made to account for these observations.
- 7) A series of preliminary experiments were performed to determine the effects of heat treatment and a sputtered active metal base coat on electrode adherence. The results indicate that titanium and tungsten base coats and post electrode deposition heat treatments in air have a marked effect on the adherence of Pt-20% Rh electrodes on metal oxides (Sapphire, BeO and Lucalox) but no detectable effect on pyrolytic boron nitride.
- 8) Lapping methods have been substantially improved in preparing one mil thick wafers of pyrolytic boron nitride. Wax bonding of wafers to a holding fixture has been found to be unnecessary in order to achieve satisfactory wafers in the one mil thickness range (see Section IIIB. 3. (1)(a), (b)). Fifteen one inch square wafers have been produced by these methods.
- 9) Five tabbed pyrolytic boron nitride wafers in the thickness range from 0.5 to 1 mil have been prepared and electroded. Three of these wafers have been stacked into a three layer capacitor and the capacitance and dissipation factor of this multi-layered unit has been measured at room and elevated temperatures (to 1100°F) in vacuum ($1-3 \times 10^{-7}$ torr).

B. DISCUSSION

One of the basic objectives of this program is to demonstrate methods of fabricating single layer capacitors from a group of candidate high temperature dielectric materials in bulk form and to establish a basis for selecting the most promising material for further investigation in a multi-layered capacitor configuration. These results can then be related to a determination of feasibility for high temperature capacitors which are lightweight and suitable for static power conditioning apparatus for space applications.

A lightweight high temperature capacitor capable of operating in the 800 to 1100°F temperature range without supplemental cooling must have low losses, high capacitance stability and a volume parameter (MF·volts/IN³) comparable to equivalent capacitor types designed for much lower operating temperatures. In terms of specific goals these capabilities include:

- 1) Volume Parameter (MF·volts/IN³): 50 to 150
- 2) Dissipation Factor (max.) at 1100°F: 0.005 to 0.03 (60 cps to 50 kc/sec)
- 3) Capacitance Change: $\pm 5\%$ (room temperature to 1100°F)

The three earlier quarterly reports that have been issued on this program have discussed in detail the results achieved and the methods and materials used to prepare thin (< 5 mil) dielectric wafers. These wafers have been considered as candidate materials and processed into single wafer capacitors by slicing, lapping and polishing techniques followed by electroding with sputtered thin film electrodes. Electrical properties have been measured at room and elevated temperatures (to 1100°F) in vacuum (< 1×10^{-6} torr).

These data have been reported for single wafer capacitors of pyrolytic boron nitride (Boralloy) and single crystal Al₂O₃ (Sapphire). In this report similar data are included for hot pressed beryllium oxide and polycrystalline Al₂O₃ (Lucalox) as well as additional data for pyrolytic boron nitride and sapphire.

One of the objectives of this program is to determine which of these candidate materials can be fabricated from its bulk form into a thin capacitor wafer. To make a valid comparison concerning the "fabricability" of these materials a determined effort has been made to achieve the thinnest practical thickness for each type of material consistent with satisfactory electrical properties at room and elevated temperatures. The ratio of the measured capacitance (MF) to volume (IN³) is an indicator of this "fabricability" since the measured capacitance is inversely proportional to the dielectric thickness and the volume of dielectric between the plates is, of course, less for thinner material. In this report, a "figure of merit" (M) has been deter-

ed for each dielectric material investigated based on its fabricability and elevated temperature electrical properties. This "figure of merit" clearly shows the superiority of pyrolytic boron nitride over the other materials evaluated for high temperature (1100°F) capacitor applications.

Also included in this report are the results that have been achieved in preparing and testing pyrolytic boron nitride material for multi-layered capacitors. The individual wafers in this type of capacitor are stacked one on top of the other and their electrodes are interconnected in parallel to obtain higher capacitance values.

Preparation of Single Wafer Capacitors

a. BERYLLIUM OXIDE

Two electroded BeO capacitors have been prepared from a group of six hot pressed BeO specimens received from Atomics International with "as ground" or lapped surface finishes. The wafers were 0.470 inch diameter with a thickness ranging from 5 to 6 mils. These wafers were sliced (in a direction perpendicular to the pressing axis) from a core sample taken from the center of a hot pressed slug three inches in diameter by one inch thick. The hot-pressed slug was pressed in a graphite die from Minox AAA powder (99.95% purity). An analysis of Minox AAA (Mineral Concentrates and Chemical Co.) is given in the first quarterly report.

R. L. McKisson of Atomics International has reported that the material is > 99.9% dense with an average grain size of 12 microns. The purity of the hot pressed material is probably very close to the purity of the starting raw material except for any impurities that may have diffused into the charge during hot pressing. However, since the sample wafers were obtained from a core sample this source of contamination would be minimal.

An effort was made to lap and polish these wafers to a minimum practical thickness. The techniques and equipment used are the same as those that have been described in previous reports for Lucalox and Sapphire wafers except as noted in the following discussion.

Two BeO wafers were wax bonded to individual metal holders (\approx 1 lb. each) and lapped and polished on the Syntron machine with nine micron diamond on a nylon lap surface. Periodic inspection of the wafers was made. After about 10 hours on the machine circumferential cracks were noted at the wafer edges. Two additional wafers were selected and each wafer

was gently hand lapped on both sides with six micron diamond on a glass plate. These wafers were then remounted on metal holders (~1 lb. each) and lapped and polished on the Syntron machine with nine micron diamond on a nylon lap surface. One of these wafers was successfully polished (semi-polish-grain pull outs were evident) on both sides. The other wafer was polished on one side but developed circumferential cracks around its edge during polishing on the reverse side. The final thickness of the polished wafer was about three mils.

Pt-20% Rh electrodes were applied to the three mil semi-polished wafer by sputtering. Details of the sputtering processing conditions are listed in Table III-1 under Group 4. During loading of this wafer between sputtering masks a short hair line crack appeared at one edge of the disk even though special precautions were taken to avoid such an occurrence. Pyrolytic boron nitride masks were used and a modified clamping method was employed to obtain soft bearing surfaces and light uniform pressures. This crack, however, was masked with a narrow thin strip of pyrolytic boron nitride and electrodes were sputtered on both surfaces in the usual manner.

Another BeO wafer was prepared for electroding but no attempt was made to polish its surfaces. Both surfaces were lightly lapped with six micron diamond on glass and then cleaned. The cleaning procedure used is the same as that reported in the third quarterly report for sapphire. Details of the sputtering process for this wafer are also listed in Table III-1 under Group 5. No difficulties were encountered in mounting and sputtering electrodes on this wafer apparently due to a minimum amount of mechanical working, and its increased thickness (~4.5 mils). The two wafers with sputtered electrodes are designated BeO Capacitor No. 1 and No. 2 for identification and cross reference in subsequent testing.

Comparing the workability of hot-pressed BeO wafers with Lucalox, hot pressed Linde A or synthetic sapphire, indicates that BeO is mechanically weaker than the various forms of aluminum oxide and cannot be lapped and polished to thin sections much less than about four to six mils. This observation is based on similar lapping and polishing techniques used for each of these materials.

TABLE III-1. Complete History of Each Capacitor Fabricated and Tested

Capacitor Materials, Dimensions, Electrical Tests																	Sputtered Electrodes - Process History										Sputtering Data		
Group No.	Substrate Wafer Material	Substrate Surface Finish	Substrate Dimensions	Capacitor Test Designation Number	Electrical Tests Performed at 7 x 10 ⁻⁸ to 4 x 10 ⁻⁷ torr	Other Tests	Electrode	Electrode Diameter	Substrate Mask	Target Geometry	Target to Substrate Distance	System Pressure Before Backfill	Glow Discharge Cleaning Time	Target Voltage	Time On (minutes)	Anode	Magnet (amps)												
1	Pyrolytic Boron Nitride (Boralloy)	Polished	0.750" dia. ~ 1.1 mils thick	BN capacitor No. 2	3 Test Runs: RT to 1100°F, Tan δ & capacitance versus temperature & frequency	Microstructure	PT-20%Rh 99.9% purity	0.683"	Glass microscope slides 1" x 3" (Corning Brand)	Rectangular: 1-1/2" x 3"	3/4"	4 x 10 ⁻⁷ torr	53 min. at 4 to 0.5 microns argon pressure	900 V. at 60 ma	35	34 V. at 3.6 amps	3												
2	Sapphire - Single Crystal Al ₂ O ₃ (Linde Co.)	Polished	~ 1.0" dia. 3.25 mils thick (0.383" electrode dia.)	Sapphire capacitor No. 1	2 Test Runs: RT to 1100°F, Tan δ & capacitance versus temperature & frequency: Breakdown voltage at 1100°F	Heat treat in air at 1652°F (900°C) before electrical tests in vacuum	PT-20%Rh 99.9% purity	0.383"	Glass microscope slides 1" x 3" (Corning Brand)	Rectangular: 1-1/2" x 3"	3/4"	4.5 x 10 ⁻⁷ torr	58 min. at 4 to 1 micron argon pressure	700 V. at 70 ma	9	35 V. at 3.5 amps	1.3												
3	Sapphire - Single Crystal Al ₂ O ₃ (Linde Co.)	Polished	~ 1.1" dia. 3.2 mils thick (0.683" electrode dia.)	Sapphire capacitor No. 2	1 Test Run: RT to 1100°F, Tan δ & capacitance versus temperature & frequency & d-c resistance	----	PT-20%Rh 99.9% purity	0.683"	Pyrolytic BN mask clamped with 7059 glass (Corning) & SS screws	Rectangular: 1-1/2" x 3"	3/4"	3 x 10 ⁻⁷ torr	57 min. at 4.8 to 0.2 micron argon pressure	600 V. at 68 ma	6	47 V. at 3.5 amps	1.0												
4	Beryllium Oxide - Hot Pressed (Atomics International)	Semi-polished	0.470" dia. ~ 3.0 mils thick	BeO capacitor No. 1	1 Test Run: RT to 1100°F, Tan δ & capacitance versus temperature & frequency	----	PT-20%Rh 99.9% purity	0.383"	Pyrolytic BN mask clamped with 7059 glass (Corning) & SS screws	Rectangular: 1-1/2" x 3"	3/4"	4.5 x 10 ⁻⁷ torr	82 min. at 5 to 0.3 micron argon pressure	600 V. at 65 ma	15	53 V. at 3.5 amps	1.1												
5	Beryllium Oxide - Hot Pressed (Atomics International)	As Lapped	0.470" dia. ~ 4.5 mils thick	BeO capacitor No. 2	2 Test Runs: RT to 1100°F, Tan δ, capacitance, d-c resistance & d-c voltage breakdown at 1100°F	Heat treat in air at 1760°F (960°C)	PT-20%Rh 99.9% purity	0.383"	Pyrolytic BN mask clamped with 7059 glass (Corning) & SS screws	Rectangular: 1-1/2" x 3"	3/4"	5.6 x 10 ⁻⁷ torr	55 min. at 5 to 0.5 micron argon pressure	700 V. at 50-70 ma	10	45 V. at 4 amps	1												
	Pyrolytic Boron Nitride (Boralloy)	As Lapped (Matte)	0.750" dia. ~ 1.0 mils thick	Tabbed BN capacitor No. 2	No measurement made	Heat to 1100°F in vacuum, RT electrical measurements		0.683"	Corning 7059 glass 2" x 3"																				
6	Lucalox-Poly-crystalline Al ₂ O ₃ (General Electric Co.)	As Lapped	0.750" dia. 5 mils thick	Lucalox capacitor No. 1	1 Test Run: RT to 1100°F, Tan δ, capacitance, d-c resistance	Heat treat in air at 1652°F (900°C)	PT-20%Rh 99.9% purity	0.683"	Corning 7059 glass 2" x 3". Clamped with SS screws	Rectangular: 1-1/2" x 3"	3/4"	7 x 10 ⁻⁷ torr	81 min. at 5 to 0.5 micron argon pressure	700 V. at 50-70 ma	11	49 V. at 36 amps	1.3												
	Pyrolytic Boron Nitride (Boralloy)	Polished	0.750" dia. ~ 0.7 mils thick	Tabbed BN capacitor No. 1	No measurement made	RT, Tan δ & capacitance																							
7	Lucalox-Poly-crystalline Al ₂ O ₃ (General Electric Co.)	Semi-polished	0.750" dia. ~ 5 mils thick	None	None	Electrode adherence	PT-20%Rh top layer & titanium base layer	0.383"	Corning 7059 glass 2" x 3"	1-1/2" x 3" PT-20%Rh (Target No. 2)	3/4"	4.6 x 10 ⁻⁷ torr	62 min. at 1 to 0.5 micron argon pressure	500 V. at 26 to 31 ma (Target No. 2)	10	42 V. at 3.5 amps	1.4												
	Pyrolytic Boron Nitride (Boralloy)	Polished	0.750" dia. ~ 1.5 mils thick	None	None	Electrode adherence		0.383"	Pyrolytic BN	2" x 3" Titanium (Target No. 1)	1-1/4"			500 V. at 70 to 80 ma (Target No. 1)	10														
8	Sapphire Single Crystal Al ₂ O ₃ (Linde Co.)	Polished	Broken piece 3 mils thick	None	None	Electrode adherence	PT-20%Rh top layer & tungsten base layer	0.200"	Corning 7059 glass 2" x 3"	1-1/2" x 3" PT-20%Rh (Target No. 2)	3/4"	1.4 x 10 ⁻⁷ torr	43 min. at 10 to 0.5 micron argon pressure	600 V. at 35 ma (Target No. 2)	7	47 V. at 3.5 amps	2												
	Pyrolytic Boron Nitride (Boralloy)	Polished	0.750" dia. ~ 1.0 mils thick	BN capacitor No. 3	DC voltage breakdown at 1100°F	Electrode adherence		0.383"	0.060" dia. wire spiral (Target No. 1)	0.060" dia. wire spiral (Target No. 1)	1-1/4" (No. 2)			600 V. at 60 ma (Target No. 1)	5														
9	Three Tabbed Pyrolytic Boron Nitride Wafers (Boralloy)	As Lapped (Matte)	0.750" dia. 0.7 mils avg. thickness of three wafers	BN multi-layer No. 1 (3 wafers)	1 Test Run: RT to 1100°F, Tan δ & capacitance.	----	Platinum 99.95% purity	0.683"	Corning 7059 glass 2" x 3" (8 wafers per mask)	Rectangular: 3" x 3"	1-1/4"	5 x 10 ⁻⁷ torr	80 min. at 2 to 1 micron argon pressure	600 V. at 83 ma	24	44 V. at 3.5 amps	2												

b. SAPPHIRE

A discussion of lapping, polishing and cleaning methods used to prepare the sapphire wafers for application of sputtered electrodes was included in the third quarterly report. One additional sapphire capacitor has been prepared during this report period using similar methods. This wafer has an overall diameter slightly greater than one inch with an average thickness of 3.2 mils. Standard 0.683 inch diameter Pt-20% Rh electrodes were sputtered on the central portion of the wafer. The sputtering process conditions are shown in Table III-1 under Group 3.

A comparatively long polishing time (~ 100 hours) was required on the Syntron machine using nine and three micron diamond on nylon to polish both sides of this wafer. However, the surface polish was such that mirror-like reflecting electrodes were produced. This wafer is designated Sapphire Capacitor No. 2.

c. LUCALOX

A number of thin Lucalox wafers were prepared during the first and second quarterly report periods in the three to six mil thickness range. These wafers have semi-polished surfaces due to a large number of grain pull-outs. As previously reported, the pull-outs could not be eliminated even though a number of variations in polishing and lapping methods were tried and evaluated.

One five mil wafer from this group was electroded with a sputtered Pt-20% Rh alloy deposit. The sputtering process conditions are shown in Table III-1 under Group 6.

2. Sputtered Electrode Adherence

The adherence of sputtered Pt-20% Rh alloy electrodes has proven to be satisfactory for all elevated temperature electrical tests performed to date. However, when a pointed steel scribe is run across the electrode surface the metal is sometimes separated from the substrate under the scribe line (100X magnification). Using this basis of comparison for electrode adherence the following process variations were investigated.

a. POST ELECTRODE DEPOSITION HEAT TREATMENT IN AIR

(1) Pyrolytic Boron Nitride

No definite effect was observed for Pt-20% Rh electrodes on pyrolytic boron nitride after heating in air in the 600°C (1112°F) temperature range. Since the hardness of boron nitride is only two (2) on the Mohs scale, the scribe penetrates the substrate surface as well as the metal electrode making a comparison difficult.

(2) Aluminum and Beryllium Oxides

A definite improvement in adherence was observed after electroded wafers of sapphire, Lucalox and hot pressed BeO were heated in air in the 800 to 1000°C (1472 to 1832°F) temperature range. Table III-1 lists the capacitors that were heat treated in this manner following electrode deposition. The most important effect observed is the change in electrical properties which are discussed later.

b. SPUTTERED ACTIVE METAL BASE LAYER

A sapphire wafer and a pyrolytic BN wafer were prepared with multi-layered electrodes consisting of a thin-base coating of sputtered tungsten overcoated with Pt-20% Rh. The scribe tests showed no difference in adherence for pyrolytic BN; however, the adherence of the electrodes on the sapphire wafer appeared to be significantly improved over Pt-20% Rh electrodes without the tungsten base layer. Sputtering process conditions are shown in Table III-1 under Group 8.

Titanium was sputtered on a Lucalox and a pyrolytic BN wafer followed by an overcoating of Pt-20% Rh. Again, the adherence was apparently unchanged on the pyrolytic BN substrate but was improved on Lucalox. Refer to Table III-1 under Group 7 for sputtering details.

The preparation and evaluation of these multi-layered electrodes has only been preliminary and the effect on electrical properties is inconclusive. In general; however, it appears that titanium and tungsten have little or no effect in promoting adherence between noble metals and boron nitride. The bond between Pt-Rh and metal oxide type substrates is improved probably because the interface energy is lowered by the formation of an oxide transition zone at the substrate and titanium or tungsten interface.

3. Multi-Layer Capacitors (Pyrolytic Boron Nitride)

a. WAFER PREPARATION

In terms of fabricating thin wafers of high-purity, high-temperature dielectrics from bulk material, pyrolytic boron nitride has yielded the most promising results. Thin wafers can now be routinely made in the one to two mil thickness range and, when carefully handled, satisfactory capacitors can be prepared with one mil wafers which have electrical properties at high temperatures in vacuum superior to any other material tested.

Previous quarterly reports have outlined the slicing, lapping, and polishing methods used to prepare one mil boron nitride wafers. The work performed during this report period has been directed towards improving the lapping and polishing methods to:

- 1) reduce rejects,
- 2) improve thickness uniformity,
- 3) reduce the depth and number of surface scratches on polished wafers,
- 4) eliminate unnecessary process steps/simplify techniques, and
- 5) reduce preparation time.

The results of this work have indicated at which stages in the process the reject rate can be reduced. Thickness uniformity has increased to the point where no variation in thickness can be detected across a one inch square wafer one mil thick using a hand held micrometer. The overall process has been simplified and preparation time has been reduced primarily by eliminating the need to wax bond wafers to a holding fixture during lapping. The only phase of the process which has not yielded to improvement, thus far, is the polishing step.

(1) Lapping Square Wafers

The most promising method recently developed to lap wafers to the one mil thickness range is as follows:

- (a) Cleaved wafers with uneven surfaces (third quarterly report, page 107) are wax bonded to a metal holder and lapped with 400 grit alumina abrasive (Norton Co.) on a glass plate until a flat uniform surface is obtained. The wafers are reverse mounted and the opposite face is lapped until flat and uniform. Wafer thicknesses at this point range from five to seven mils. This step is unnecessary for wafers that have been sliced completely through.
- (b) From five to seven mils down to one mil, the need to bond the wafers to holding fixtures has been found to be unnecessary. A series of fixtures are now used that have different thickness steel shim strips resistance welded to their flat sides. Each fixture consists of a solid steel disk 3 inches in diameter and $1/2$ to 1 inch thick. The surfaces of these disks have previously been surface ground and then lapped flat and smooth. The shim strips are $1/2$ inch wide by 12 inches long and are cut into short lengths to form a square opening slightly larger than the wafer to be lapped (about $1/16$ inch on a side). These strips are then laid out on the flat surface of a steel disk and resistance welded at a number of points to the disk. A four mil thick shim strip, for example, forms a raised stop on the surface of the lapping fixture whose height difference is very close to four mils and uniform at all points after the cutting burrs have been lapped off. In this manner, a number of lapping fixtures have been made with four, three, two, and one mil shim stops.
- (c) Starting with a six mil thick, one inch square wafer, the wafer is first set into a four mil shim opening with a small amount of lapping fluid applied to the interface between the wafer and the fixture. The fixture and wafer are then carefully set on a glass lap plate (wafer side down) mounted on the Mazur Lapping/Polishing Machine. The machine is started at its slowest speed setting and the wafer is lapped (figure 8 motion) until it reaches the thickness of the raised stop (4 mils). A 400 grit size alumina abrasive plus Dymo lapping fluid is used for all lapping down to four mils. From four mils down to one mil, 10 micron alumina (S. S. White Co.) and deionized water is used. After a wafer is lapped to four mils, it is reset into a three mil fixture and the procedure is repeated until a final thickness in the one mil range is achieved.

The results using this technique have been very satisfactory. One mil wafers are flat and do not exhibit the type of camber or warping characteristic of one mil wafers produced by the "wax bonding method". Yield is high (estimated at about 90%) and the tedious and time consuming task of squeezing out air bubbles (necessary for "wax bonding") at the wafer-holder interface is eliminated.

A matte wafer surface finish is produced by this method and all attempts to date to generate a polished surface on unbonded or "floating" one mil wafers has been unsuccessful. Therefore, it was decided to evaluate the electrical properties of one mil unpolished wafers for comparison purposes with polished wafer capacitors. These results are discussed later.

(2) Tabbed Capacitors

A total of about 15 one inch square by one mil wafers have been made with matte surfaces. Three or four of these wafers have thicknesses of about 0.7 mils and one wafer has a thickness of 0.5 mils. These thinner wafers were produced with the first one mil thick shim fixture which had worn down to these thinner thicknesses.

Ten tabbed wafers (refer to third quarterly report) have been fabricated from this group by two different methods.

- (a) Ultrasonic cutting with a "cutting" tool machined into the mirror image or "female" outline of the wafer, and
- (b) Airabrasive (S.S. White Unit) cutting using a steel mask to cover the wafer outline.

Either of these methods is satisfactory although the "airabrasive" method is more convenient for small quantities. This operation is the final machining step prior to cleaning before deposition of sputtered electrodes.

The cleaning procedure is one of the most critical phases of the process and to date it is believed that an entirely satisfactory method has not been developed. Ultrasonic agitation of one mil wafers in the various cleaning solutions (Triclorethylene, Alconox and water, methyl alcohol and acetone - see second quarterly report for details) requires very careful control of the energy input. At least seven tabbed wafers were rejected because small whitish spots were visible after cleaning. It is believed these spots are delaminations caused by excessive ultrasonic agitation. Since it is difficult to determine a "safe" energy level with a limited number of specimens, it has been decided to eliminate ultrasonic cleaning in future processing.

It is planned to investigate acid cleaning and/or air and vacuum heat treatments to oxidize and/or volatilize as much adsorbed and absorbed organics and other impurities as possible prior to application of electrodes. The effects on elevated temperature electrical properties will be compared with previous results for capacitor substrates that have been heated in air to about 900°C (1652°F) and then heated in vacuum in the 10⁻⁶ torr range to 1000 to 2000°C (1832 to 3632°F).

From the group of ten tabbed wafers that have been fabricated in the one mil thickness range, five of these wafers have been electroded. Two wafers have sputtered Pt-20% Rh electrodes and three wafers have sputtered pure platinum (99.95%) electrodes. The third quarterly report shows the mask geometry (Figure III-10) and discusses the deposition approach. Table III-1 under groups 5, 6, and 9 shows the details of the sputtering processes used.

The two tabbed wafers with sputtered Pt-20% Rh electrodes were prepared primarily to establish the feasibility of the parallel interconnection scheme as outlined and illustrated in Figure III-9 in the third quarterly report. The next three tabbed wafers with sputtered platinum electrodes were prepared to check out the test fixture shown in Figure III-1. This fixture is designed to align tabbed wafers when stacked on top of each other and to make external connections to the tab extensions. The component parts of the fixture are made from 1 x 1 x 1/8 inch blocks of pyrolytic boron nitride.

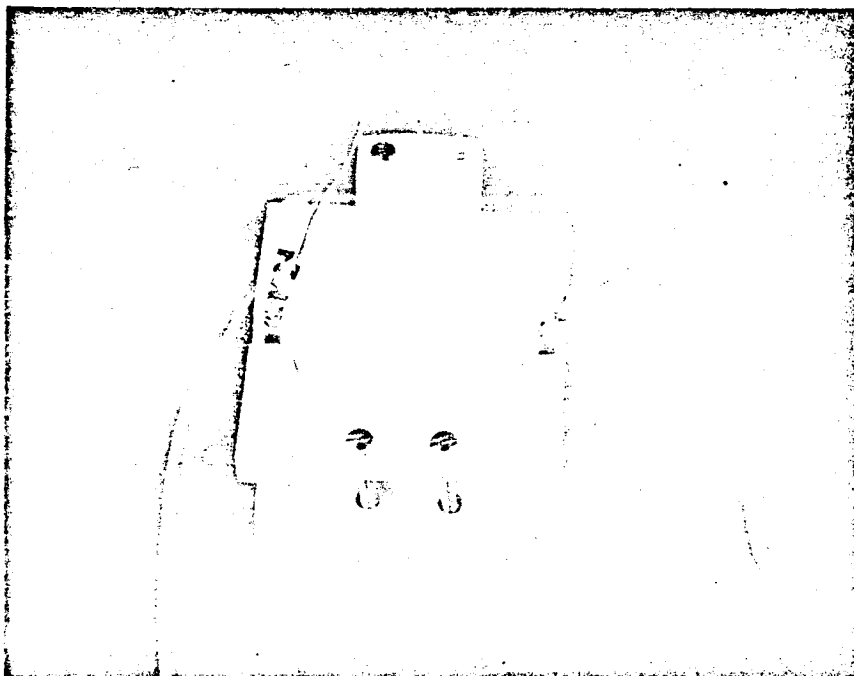


FIGURE III-1. Fixture for Making Electrical Measurements on
Stacked Tabbed Capacitor Wafer

The first test run at elevated temperatures in vacuum was made using this fixture and a three layer stacked capacitor composed of the three tabbed wafers with platinum electrodes. This particular three stack capacitor is designated BN multi-layer Capacitor No. 1 and the electrical data obtained for this unit is discussed later in this section.

b. EVALUATION (ROOM TEMPERATURE DATA)

Table III-2 shows the individual capacitance and dissipation factors for the two tabbed wafers with Pt-20% Rh electrodes. In addition, similar data are shown for these two capacitors stacked one on top of the other and interconnected in parallel. All measurements were made via the tab contact points. The arithmetic sum of the individual wafer capacitances is shown in Table III-2 for comparison with the measured capacitance of the two layer unit. This value is within 0.01% of the arithmetic sum indicating that a satisfactory interconnection can be achieved using "wrap around" sputtered electrodes.

One of these tabbed wafer capacitors (Tabbed BN Capacitor No. 2) was subsequently heated to 1100°F at $1-3 \times 10^{-7}$ torr for about 1/2 hour. As shown in Table III-2 there are no significant changes in electrical properties before and after the test when measurements were made via the tab contact points. This test was performed as a preliminary step in evaluating the capability of sputtered electrodes to maintain electrical continuity around the tabs after heating to the maximum test temperature (1100°F).

The three tabbed wafers with sputtered platinum electrodes were also stacked and interconnected in parallel. Room temperature measurements obtained for this three layer unit are shown below (designated: BN Multi-Layer Capacitor No. 1) for three different frequencies.

Capacitance	Dissipation Factor ($\tan \delta$)	Frequency
1134.4 pF	0.000520	50 cps
1133.3 pF	0.000605	1 kc/sec
1132.4 pF	0.001140	10 kc/sec

TABLE III-2. Properties of Tabbed BN Capacitors No. 1 and No. 2

	Electrical Data 72° F - Air					Characteristics of Substrate (Boralloy: Pyrolytic Boron Nitride)				
	Capacitance pF		Tan δ			Wafer Thickness (calculated)	Surface Finish	Electrodes	Sputtering Process	
	1 kc/sec	10 kc/sec	1 kc/sec	10 kc/sec	10 kc/sec				Sputter Time & Volts	Cross Reference
Tabbed BN Capacitor No. 1	507.529	507.052	0.000777	0.000980	0.000980	0.55 Mils	Polished	Pt-20% Rh	11 min. at 700 volts	Group 6 Table III-1
Tabbed BN Capacitor No. 2	321.549	321.151	0.000998	0.00194	0.00194	0.86 Mils	As lapped (Matte)	Pt-20% Rh	10 min. at 700 volts	Group 5 Table III-1
Arithmetic sum of capacitor No. 1 and No. 2 (capacitance)	829.078	828.203								
Measured value of stacked unit capacitor No. 1 and No. 2	829.183	828.344								
Tabbed BN Capacitor No. 2 after heating to 1100° F at 2×10^{-7} torr	323.964	323.599	0.000926	0.00141	0.00141					

These are three terminal measurements made in a shielded metal box to minimize stray capacitance effects. The fixture used to align the wafers and make external electrical contact to the tab extensions is shown in Figure III-1.

Further inspection of Table III-2 shows a correlation between wafer surface finish and dissipation factor. For example, tabbed BN Capacitor No. 1 has a polished surface whereas tabbed BN Capacitor No. 2 has an "as lapped" surface and it can be assumed that both wafers have equal thickness electrodes since the sputtering conditions were almost identical (11 minutes at 700 V for No. 1 and 10 minutes at 700 V for No. 2). Comparing the dissipation factor shown in Table III-2 for these two capacitors shows that a lower dissipation factor was measured at 1 kc/sec and 10 kc/sec for the capacitor with polished surfaces. This indicates that the increased loss is caused by an equivalent series resistance introduced by the electrodes on Capacitor No. 2. The high series resistance is apparently the result of an increase in the effective resistivity or ohms/square resistance of the thin film electrodes deposited on the capacitor wafer whose surfaces have a higher degree of roughness.

A similar effect is indicated by the increase in $\tan \delta$ with frequency for the data previously shown for BN Multi-Layer Capacitor No. 1. The individual capacitors in this unit have "as lapped" or matte surface finishes. The $\tan \delta$ value for this capacitor is somewhat lower at 1 kc/sec and 10 kc/sec than the $\tan \delta$ values for the first two tabbed wafers with Pt-20% Rh electrodes shown in Table III-2. This is probably due to: 1) the thicker electrodes (longer sputtering time) and 2) the lower bulk resistivity of platinum vs. the platinum-rhodium alloy.

These results show the need for further investigations of sputtering parameters, electrode materials, and surface roughness and their effect on $\tan \delta$. Possibly an order of magnitude reduction in $\tan \delta$ can be achieved over much of the frequency range of interest in this program. This work is planned for the next report period.

4. Analysis and Comparison of Electrical Data

All capacitance and dissipation factor measurements reported in this section were made with a General Radio Type 1620-A Capacitance

Measuring Assembly. Three terminal coaxial lead bridge connections were used. Elevated temperature measurements in vacuum ($1 - 4 \times 10^{-7}$ torr) were made in a small resistance heated furnace insulated with tantalum radiation shields. The furnace and the associated vacuum system is described in the second quarterly report. The thermocouple junction shown in Figure III-2 in the second quarterly report has been repositioned so that it is embedded in the columbium disk used to support single wafer capacitors, thus minimizing any temperature differential between the indicated temperature and the actual specimen temperature. In addition, a thin platinum disk (99.95% purity) has been resistance welded to the top surface of the columbium disk to reduce any contact resistance that might be introduced by an oxide film on the columbium. This setup has not been modified during the course of collecting the data reported in this section and the comparative results should have significance.

D-C resistance measurements were made with Keithly Model 610B Electrometer and a Keithly Model 240 Regulated D-C Power Supply. The d-c resistance of the test furnace insulators (less test specimen) was measured at 1000 V d-c in vacuum (3×10^{-7} torr) up to 1100°F and found to be in the range 10^{17} to 10^{14} ohms from 72 to 1100°F .

a. CAPACITANCE VS. TEMPERATURE

Figures III-2, III-3, III-4, and III-5 show capacitance change with temperature in vacuum for BeO Capacitor No. 2, Sapphire Capacitor No. 2, Lucalox Capacitor No. 1 and BN Multi-Layer Capacitor No. 1, respectively. These data are shown in two forms, actual capacitance readings vs. temperature and the ratio of $\Delta C/C_{72^{\circ}\text{F}} \times 100$. Casual inspection of the figures does not reveal the comparative capacitance changes, therefore Figure III-6 shows the ratio of $\Delta C/C_{72^{\circ}\text{F}} \times 100$ for each of the above capacitors plotted on equivalent coordinate points. Pyrolytic boron nitride has a negative capacitance change of only 1.7% at 1 kc/sec and 1100°F . This value is almost an order of magnitude less than BeO or Lucalox which increase in capacitance with increasing temperature. Sapphire has a positive ratio of $\Delta C/C_{72^{\circ}\text{F}} \times 100$ of about eleven percent over the same temperature range.

The negative value of the ratio of $\Delta C/C_{72^{\circ}\text{F}} \times 100$ for pyrolytic boron nitride at 1100°F is very close to the value that would be expected from the decrease in capacitance due entirely to thermal expansion since pyrolytic boron nitride has a reported thermal

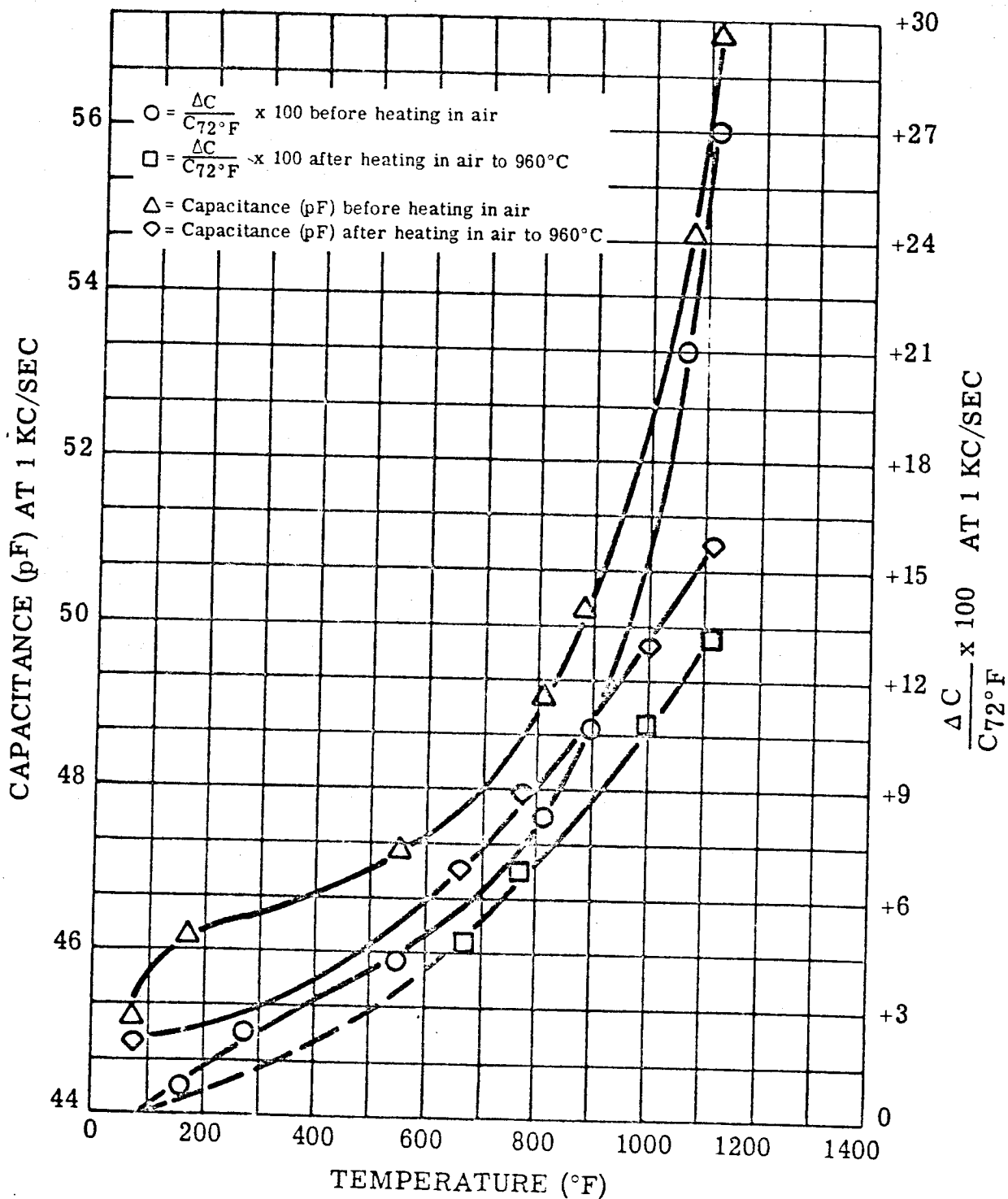


FIGURE III-2. Capacitance Change Versus Temperature for BeO Capacitor No. 2 Before and After Heat Treatment in Air (Run No. 1 Versus Run No. 2) Measured in Vacuum at $1-3 \times 10^{-7}$ torr

Figure III-2. Capacitance Change versus Temperature for BeO Capacitor Before and After Heat Treatment

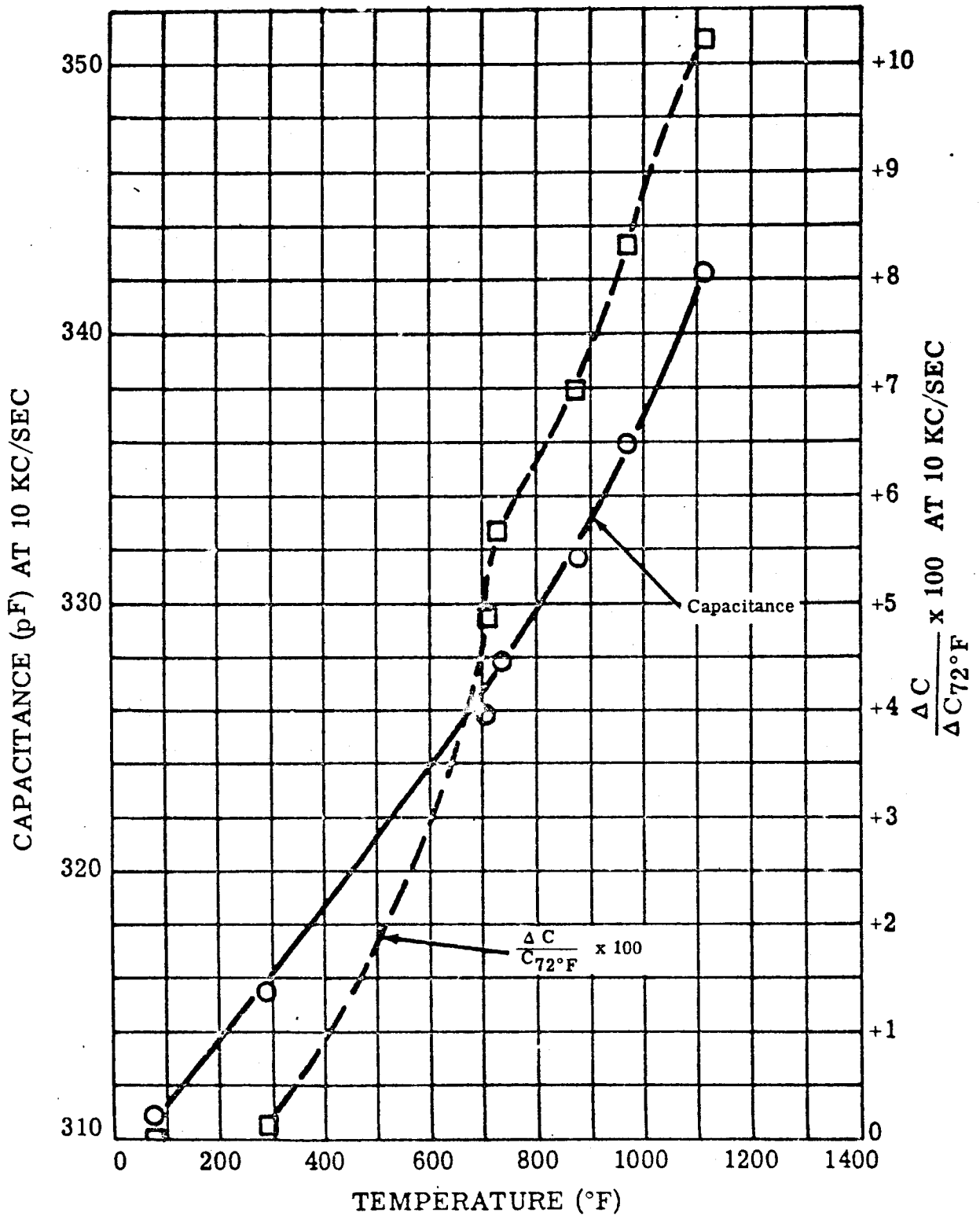
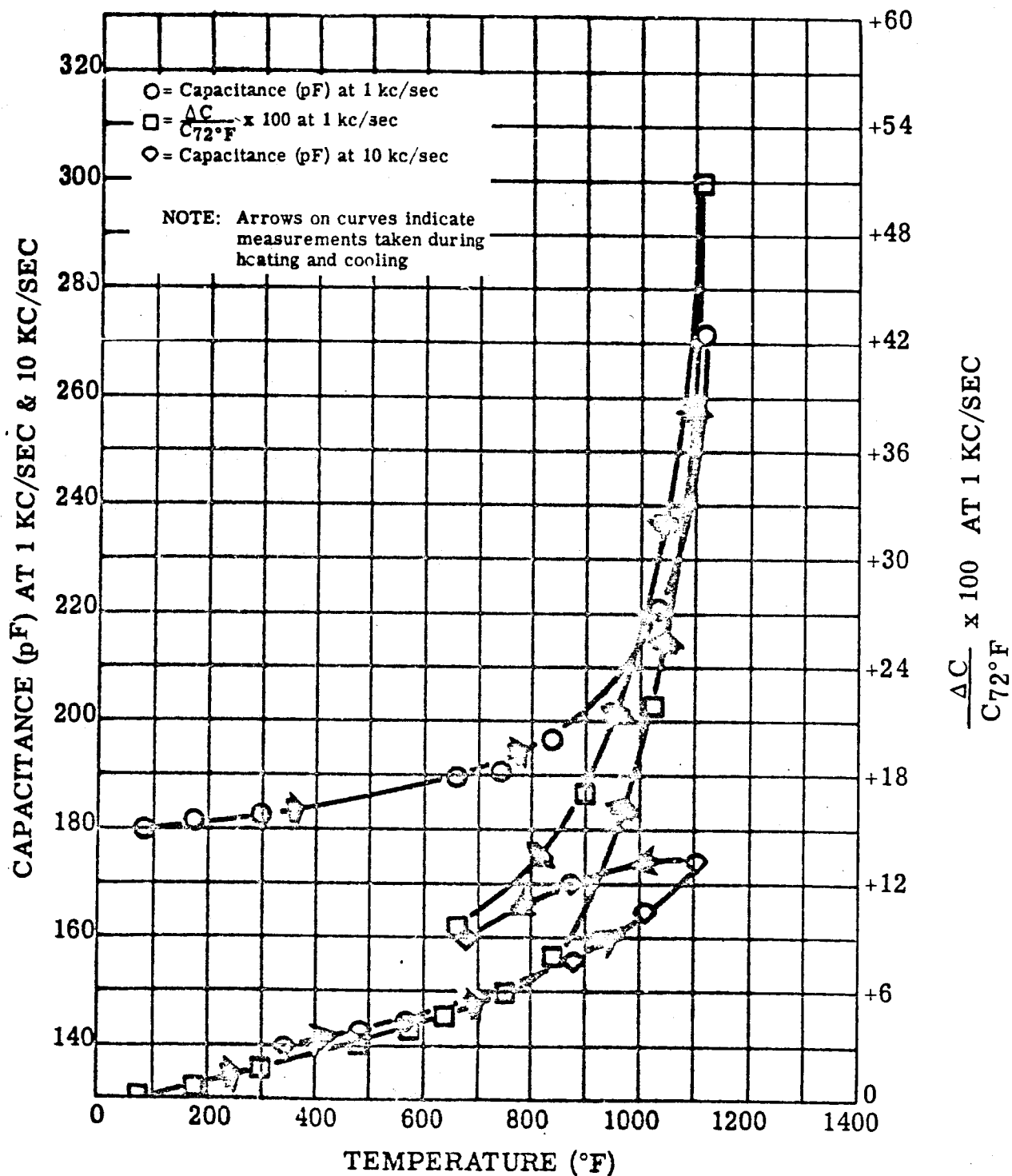


FIGURE III-3. Capacitance Change Versus Temperature at 10 kc/sec for Sapphire Capacitor No. 2 Measured in Vacuum at $1-3 \times 10^{-7}$ torr

Figure III-3. Capacitance Change versus Temperature for Sapphire Capacitor No. 2



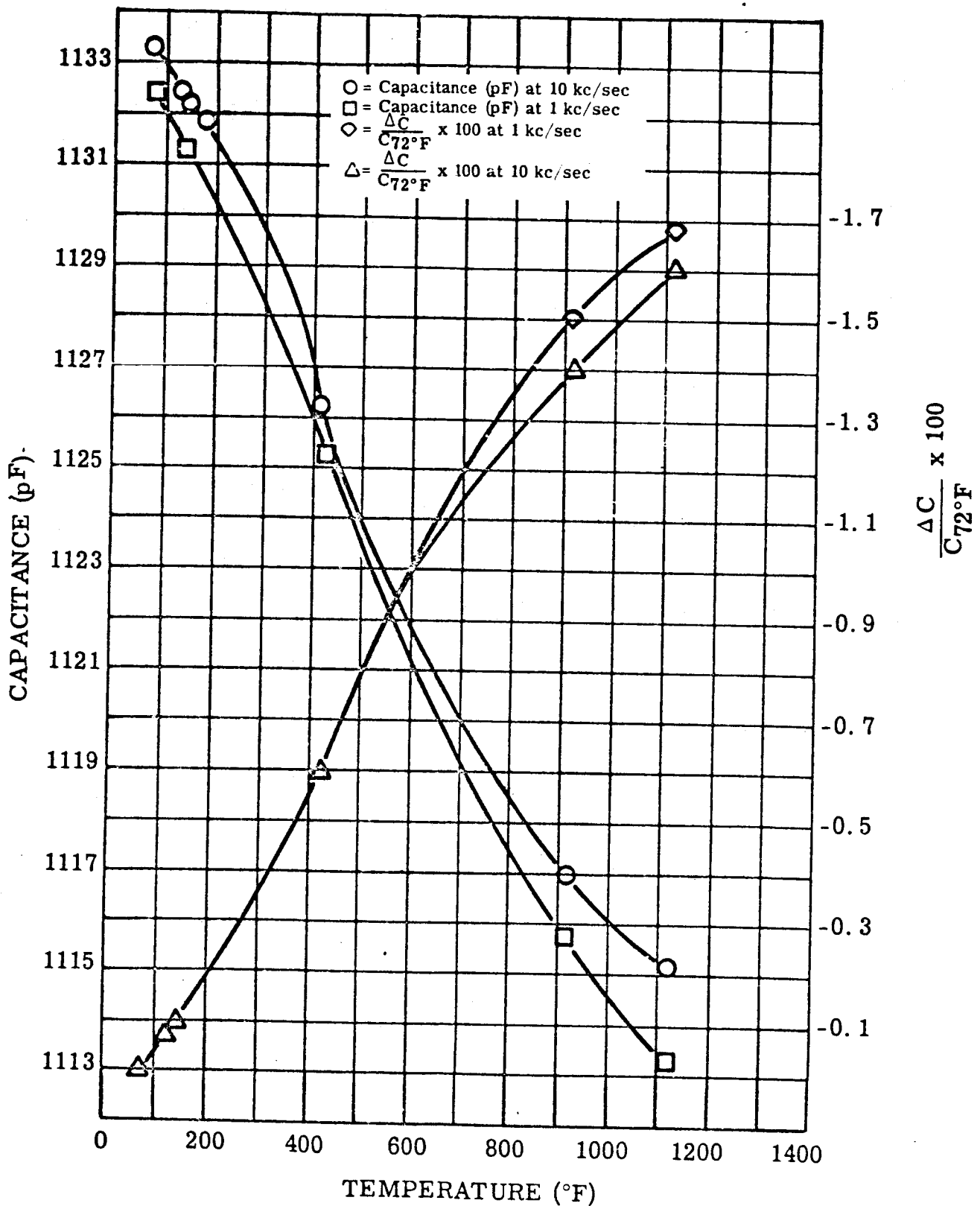


FIGURE III-5. Change in Capacitance at 1 kc/sec and 10 kc/sec with Temperature for BN Multi-Layer Capacitor No. 1 Measured in Vacuum at $1-3 \times 10^{-7}$ torr

Figure III-5. Capacitance Change versus Temperature for Pyrolytic Boron Nitride Multi-Layer Capacitor No. 1

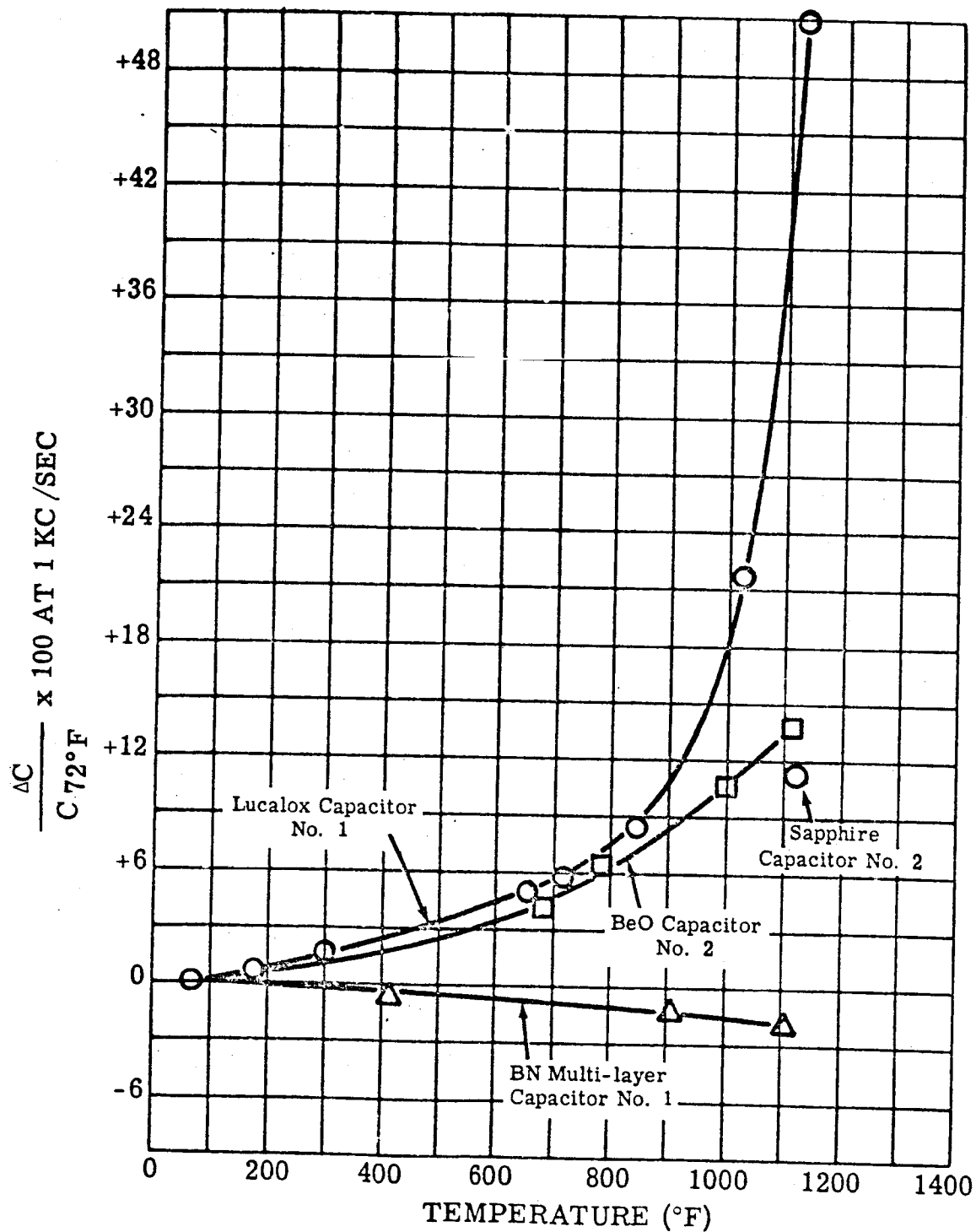


FIGURE III-6. Ratio of $\frac{\Delta C}{C_{72^\circ F}} \times 100$ Versus Temperature at $1-4 \times 10^{-7}$ torr for BN Multi-Layer Capacitor No. 1, Lucalox Capacitor No. 1 and BeO Capacitor No. 2 (Run No. 2) Measured at 1 kc/sec

Figure III-6. Comparison of Percent Capacitance Change Versus Temperature for Three Different Capacitor Materials

expansion ($\Delta L/L$ in/in) at 1100°F of 0.020 (2%) measured in the c direction from 32 to 1100°F. Since capacitance is inversely proportional to thickness, the correlation is very good.

These results are consistent with the extremely low impurity level reported for pyrolytic boron nitride. An ideal dielectric would show no change in dielectric constant or capacitance with temperature. If the dielectric contains impurities they can act as charge carriers and increase the polarizability (measured dielectric constant) of the material. At higher temperatures ion mobility, for example, is increased causing increased polarization effects and, therefore, an increase in the measured capacitance. It would appear that pyrolytic boron nitride is approaching the characteristics of an ideal dielectric over a wider temperature range than any other solid dielectric material presently available.

b. DISSIPATION FACTOR ($\tan \delta$) VS. TEMPERATURE

$\tan \delta$ values vs. temperature for BeO Capacitor No. 2, Sapphire Capacitor No. 2, Lucalox Capacitor No. 1 and BN Multi-Layer Capacitor No. 1 are shown in Figures III-7, III-8, III-9, and III-10. These data show that pyrolytic boron nitride has substantially lower a-c losses over most of the temperature range up to and including 1100°F.

Figure III-11 shows these data plotted together for a frequency of 1 kc/sec. The losses for the Multi-Layer BN Capacitor are somewhat higher than those previously measured for a single wafer capacitor (BN Capacitor No. 2) with polished surfaces. These results are attributed to series resistance effects which were briefly discussed earlier. A more detailed discussion is included in the next section dealing with the data on frequency vs. $\tan \delta$ at room and elevated temperatures.

c. CAPACITANCE AND $\tan \delta$ VS. FREQUENCY AND TEMPERATURE

An ideal dielectric material would have a dielectric constant independent of frequency. But any real capacitor with a solid dielectric deviates from ideal performance (ref. 1) and has an

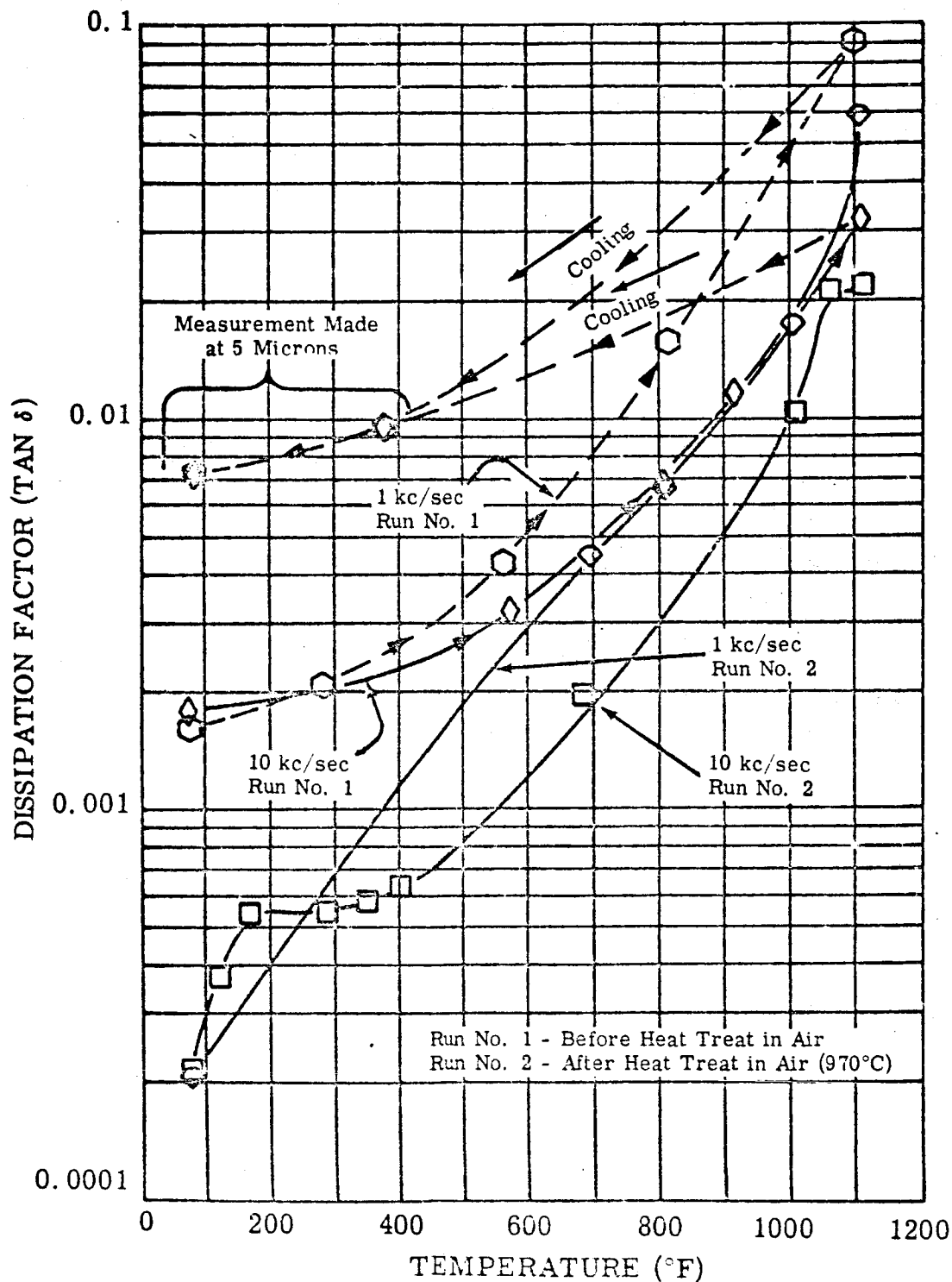


FIGURE III-7. Dissipation Factor ($\tan \delta$) Versus Temperature for BeO Capacitor No. 2 Showing Hysteresis Effects on Cooling and the Effects of Heat Treatment in Air After Completion of Run No. 1 (All measurements made at 1 to 3×10^{-7} torr except as noted)

Figure III-7. $\tan \delta$ versus Temperature for BeO Capacitor No. 2 Before and After Heat Treatment

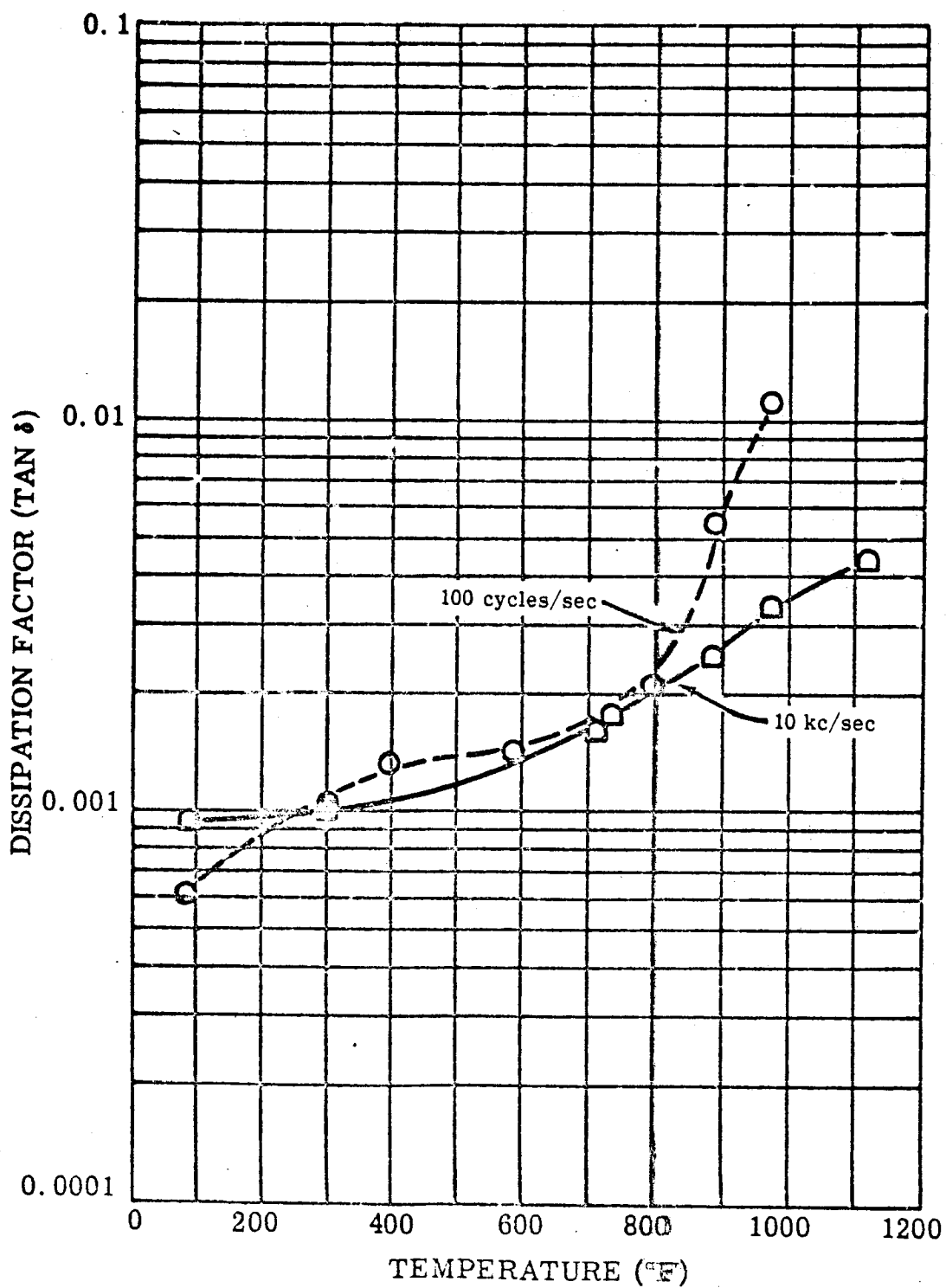


FIGURE III-8. Dissipation Factor ($\tan \delta$) of Sapphire Capacitor No. 2 at 10 kc/sec and 100 cycles/sec Versus Temperature in Vacuum at $1-4 \times 10^{-7}$ torr

Figure III-8. $\tan \delta$ Versus Temperature for Sapphire Capacitor No. 2

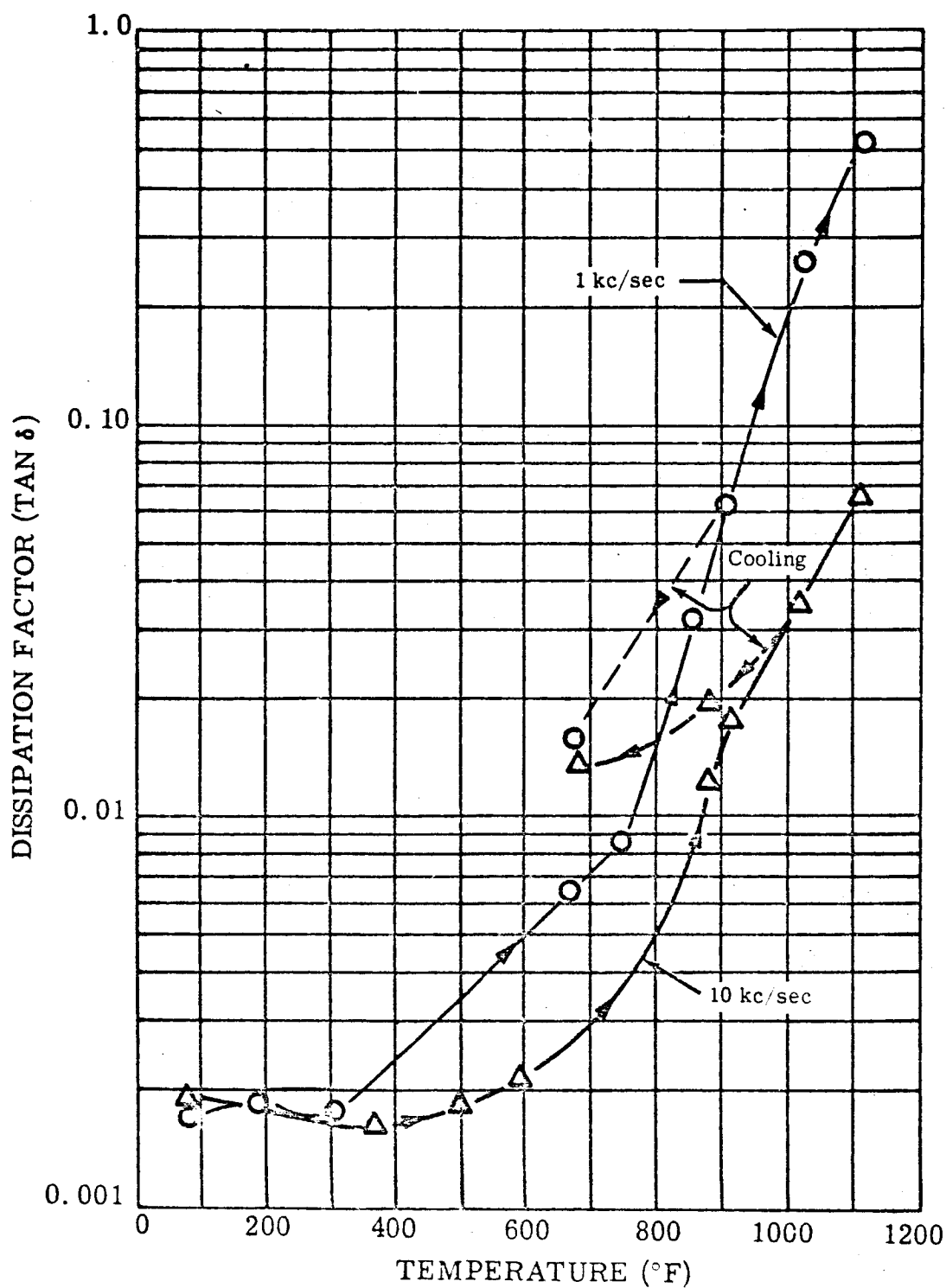


FIGURE III-9. Tan δ Versus Temperature for Lucalox Capacitor No. 1
Showing Hysteresis Effects on Cooling
(Measured in vacuum at $1-3 \times 10^{-7}$ torr)

Figure III-9. Tan δ versus Temperature for Lucalox Capacitor No. 1

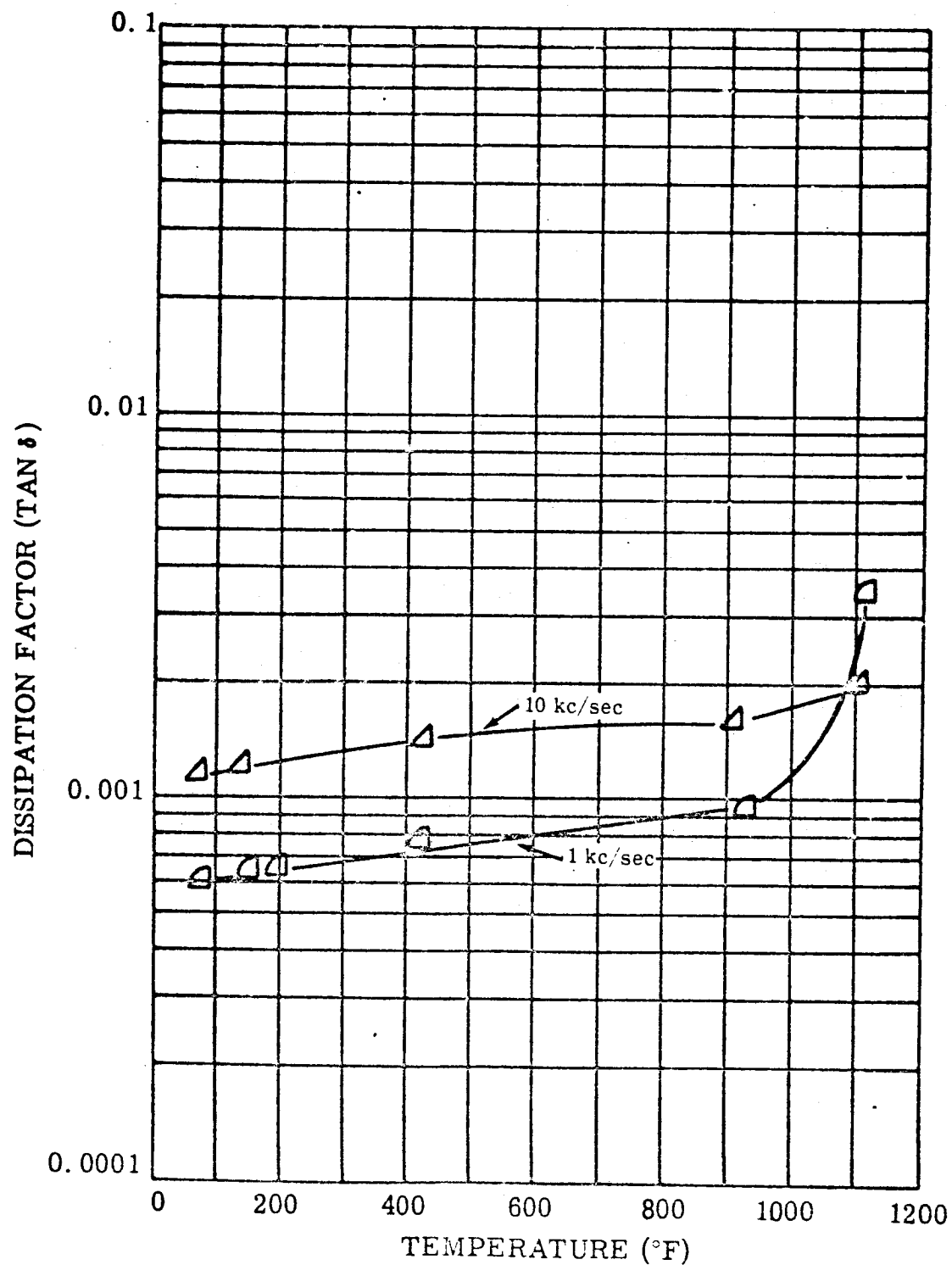


FIGURE III-10. Tan δ Versus Temperature for BN Multi-Layer Capacitor No. 1 Measured in Vacuum at $1-3 \times 10^{-7}$ torr

Figure III-10. Tan δ versus Temperature for Pyrolytic Boron Nitride Multi-Layer Capacitor No. 1

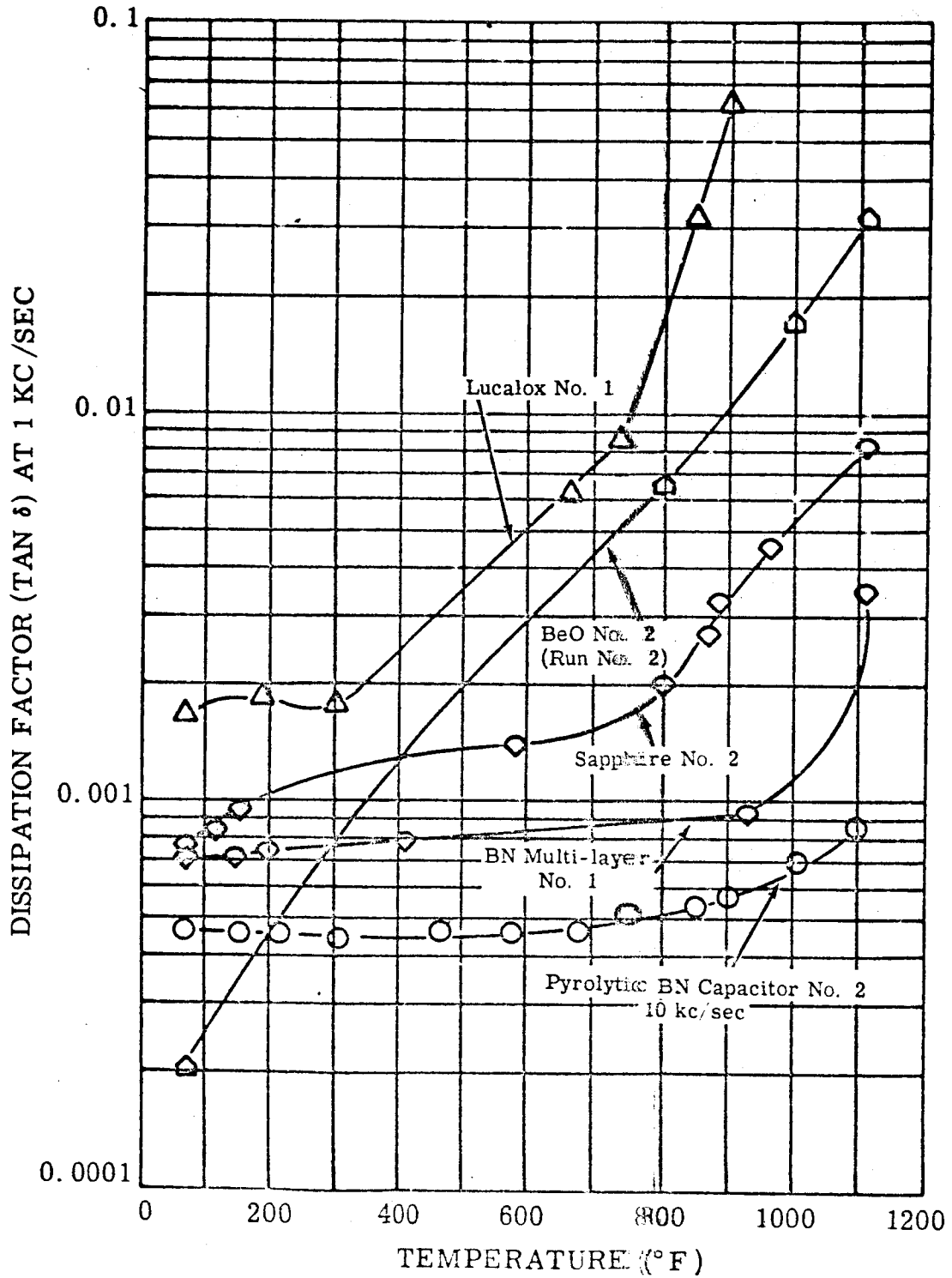
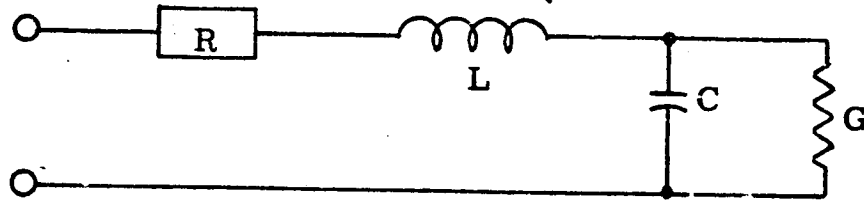


FIGURE III-11. Comparison of Tan δ Versus Temperature for Various Dielectrics Measured at 1 kc/sec and 10 kc/sec (BN Capacitor No. 2) in Vacuum

Figure III-11. Tan δ Versus Temperature for Four Different Capacitor Materials

equivalent circuit as shown below,



where:

R = metallic resistance (leads, supports, electrodes)

L = series inductance of leads, supports and electrodes

C = capacitance between electrodes

G = conductance (dielectric losses of supporting insulators, solid dielectric between capacitor electrodes and d-c leakage conductance)

The measured capacitance increases, therefore, from the zero frequency capacitance, C_0 , as frequency, f , increases because of series inductance as shown in equation (1).

$$(1) \quad \frac{\Delta C}{C_0} \approx 2 \pi f L C_0$$

A tendency for capacitance to decrease with increasing frequency due to space charge polarization produces a negatively sloped curve over part of the frequency range. The sum of these two effects (polarization and series inductance) generally results in a U-shaped curve for a capacitance versus frequency relationship.

Similarly, the total dissipation factor ($\tan \delta$) varies with frequency in accordance with equation (2).

$$(2) \quad \tan \delta = \frac{G}{2 \pi f C} + 2 \pi f^{3/2} R C$$

At sufficiently high frequencies, $\tan \delta$ will begin to increase as the $3/2$ power of the frequency due to the losses represented by the series resistance, R , in the equivalent circuit. In the lower

frequency ranges $\tan \delta$ decreases with increasing frequency due to conductance losses (G). The sum of these two terms in equation (2) results in a U-shaped curve with a negative slope up to frequencies ranging from 1 kc/sec to 1 Mc/sec depending on capacitance values.

Figures III-12 and III-13 show the variations in capacitance and the ratio of $\Delta C/C_{100 \text{ cps}} \times 100$ with increasing frequency for BN Multi-Layer Capacitor No. 1, BN Capacitor No. 2 (single wafer), and Sapphire Capacitor No. 2. These particular capacitors were selected for illustrative purposes because they show the least variations in capacitance with frequency of any of the capacitors tested. The curve for BN Capacitor No. 2 at 72°F in Figure III-12 shows only a slight decrease in capacitance ($\sim 0.2\%$) from 10^2 to 10^4 cps. Thus, it appears that there is no appreciable tendency for the capacitance to increase because of series inductance. If a space charge polarization mechanism were predominant (due to mobile charges from impurities) over this frequency range, it would show a decreasing contribution to the total polarizability or measured capacitance as the frequency was increased. This effect is not apparent in Figure III-12 or III-13 for the 72°F data. However, since series inductance and space charge polarization are competing effects, they could cancel each other depending on relative magnitudes.

At 1100°F the change in capacitance for BN Multi-Layer Capacitor No. 1 shows a greater rate of decrease with increasing frequency (Figure III-12 and III-13) due to space charge polarization (ion jump orientation and increased concentration of charge carriers).

Above a frequency of about 4×10^4 cycles/sec the residual inductance appears to override polarization effects and the capacitance begins to increase with frequency (equation (1)).

Figures III-14 and III-15 show comparisons of $\tan \delta$ versus frequency for single and multi-layer boron nitride capacitors. These data are shown for 72°F and 1100°F measurements. A characteristic U-shape curve is evident for BN Multi-Layer Capacitor No. 1 only at 1100°F. This is apparently because the conductance term in equation (2) is of sufficient magnitude at this temperature to control the slope (negative) of the curve at frequencies up to about 10^4 cycles/sec. At higher frequencies the series resistance term in equation (2) increases ($f^{3/2}$) at a greater rate and the slope of the curve has a positive value.

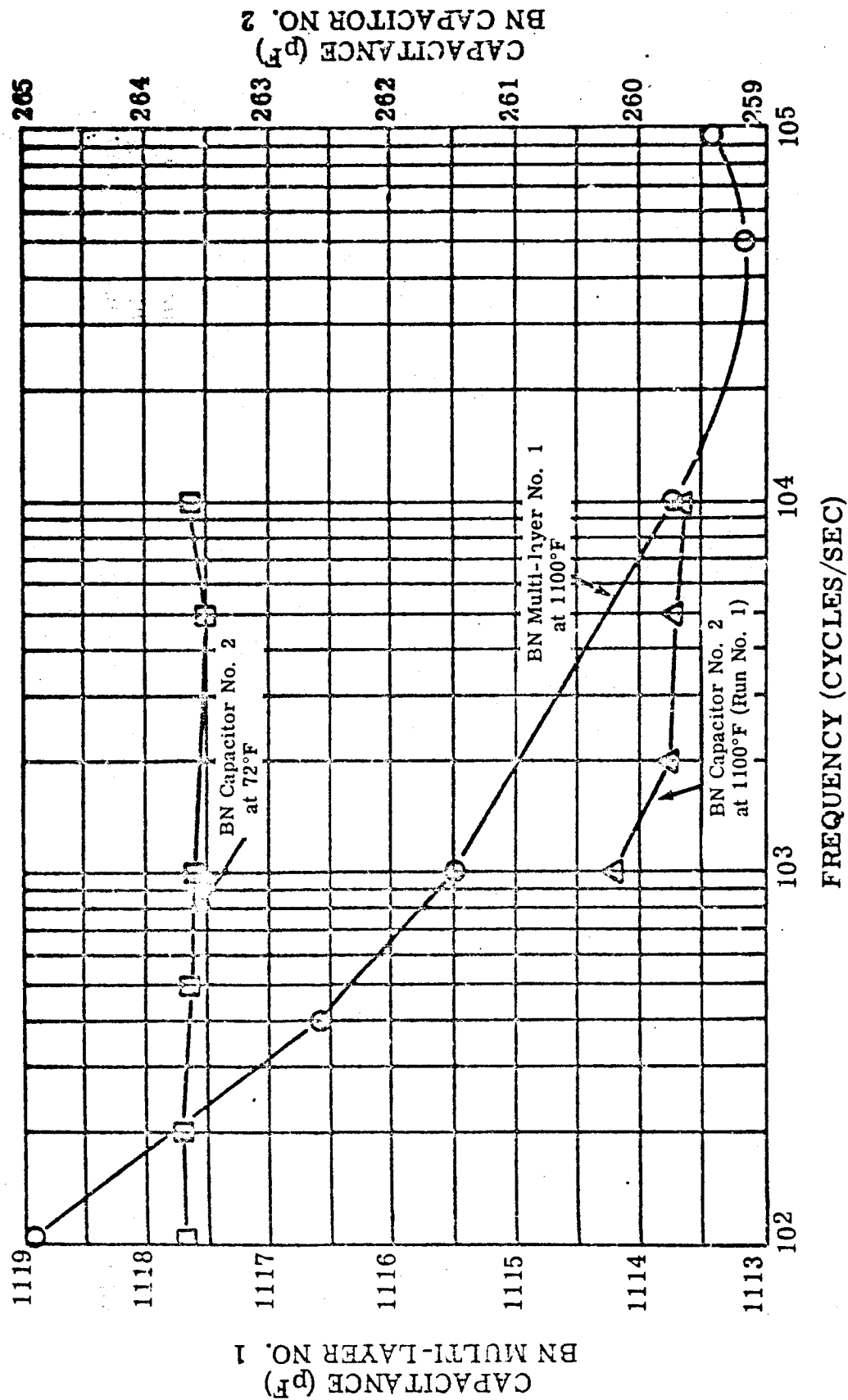


FIGURE III-12. Capacitance Change Versus Frequency at 72°F and 1100°F for Pyrolytic Boron Nitride as a Single Wafer Capacitor (BN Capacitor No. 2) and as Three Wafers Stacked and Connected in Parallel (BN Multi-Layer No. 1) Measured in Vacuum at 1-3 x 10⁻⁷ torr

Figure III-12. Capacitance Change versus Frequency for Two Types of Pyrolytic Boron Nitride Capacitors

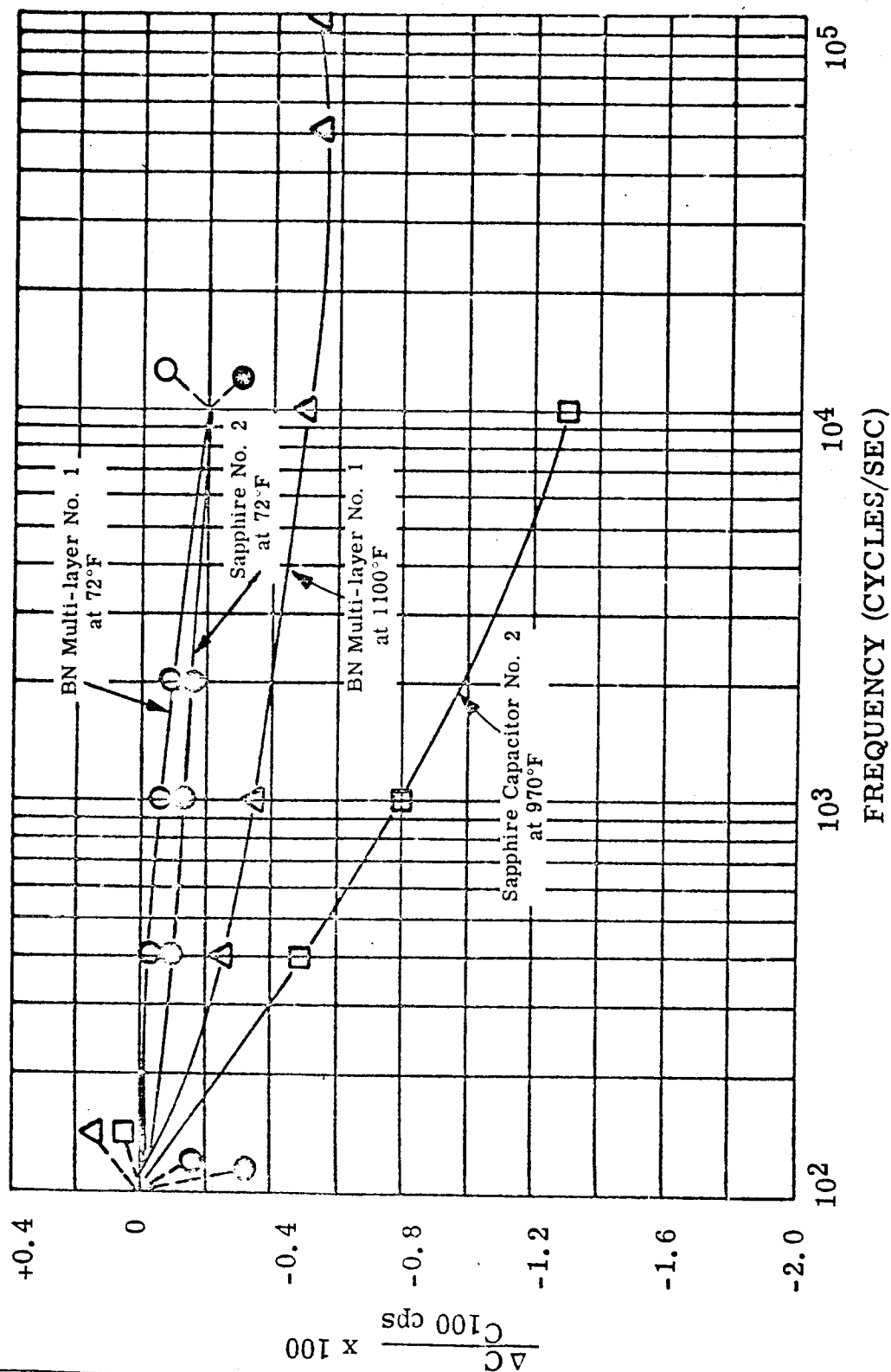


FIGURE III-13. Ratio of $\frac{\Delta C}{C_{100 \text{ cps}}} \times 100$ Versus Frequency at 72°F, 1100°F, and 970°F for BN Multi-Layer Capacitor No. 1 and Sapphire Capacitor No. 2 Measured in Vacuum at 1-3 x 10⁻⁷ torr

Figure III-13. Comparison of the ratio of $\frac{\Delta C}{C_{100 \text{ cps}}} \times 100$ Versus Frequency for a Sapphire and Pyrolytic Boron Nitride Capacitor

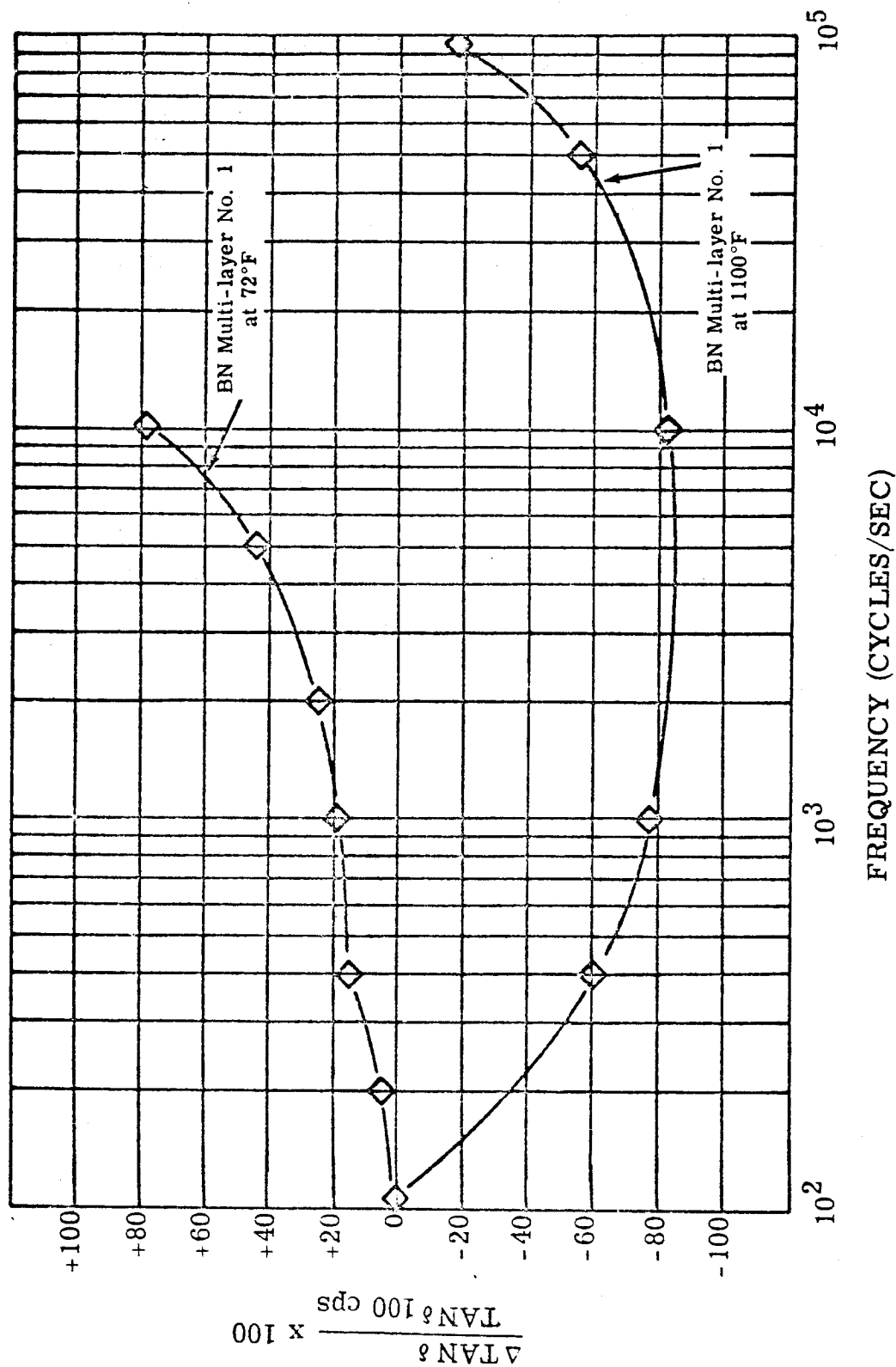


FIGURE III-14. Comparison of the ratio of $\frac{\Delta \tan \delta}{\tan \delta 100 \text{ cps}} \times 100$ Versus Frequency for BN Multi-Layer Capacitor No. 1 at 72°F and 1100°F (measured in vacuum at 1-3 x 10⁻⁷ torr)

Figure III-14. Comparison of the Ratio of $\frac{\Delta \tan \delta}{\tan \delta 100 \text{ cps}} \times 100$ Versus Frequency for a Multi-Layer Pyrolytic Boron Nitride Capacitor

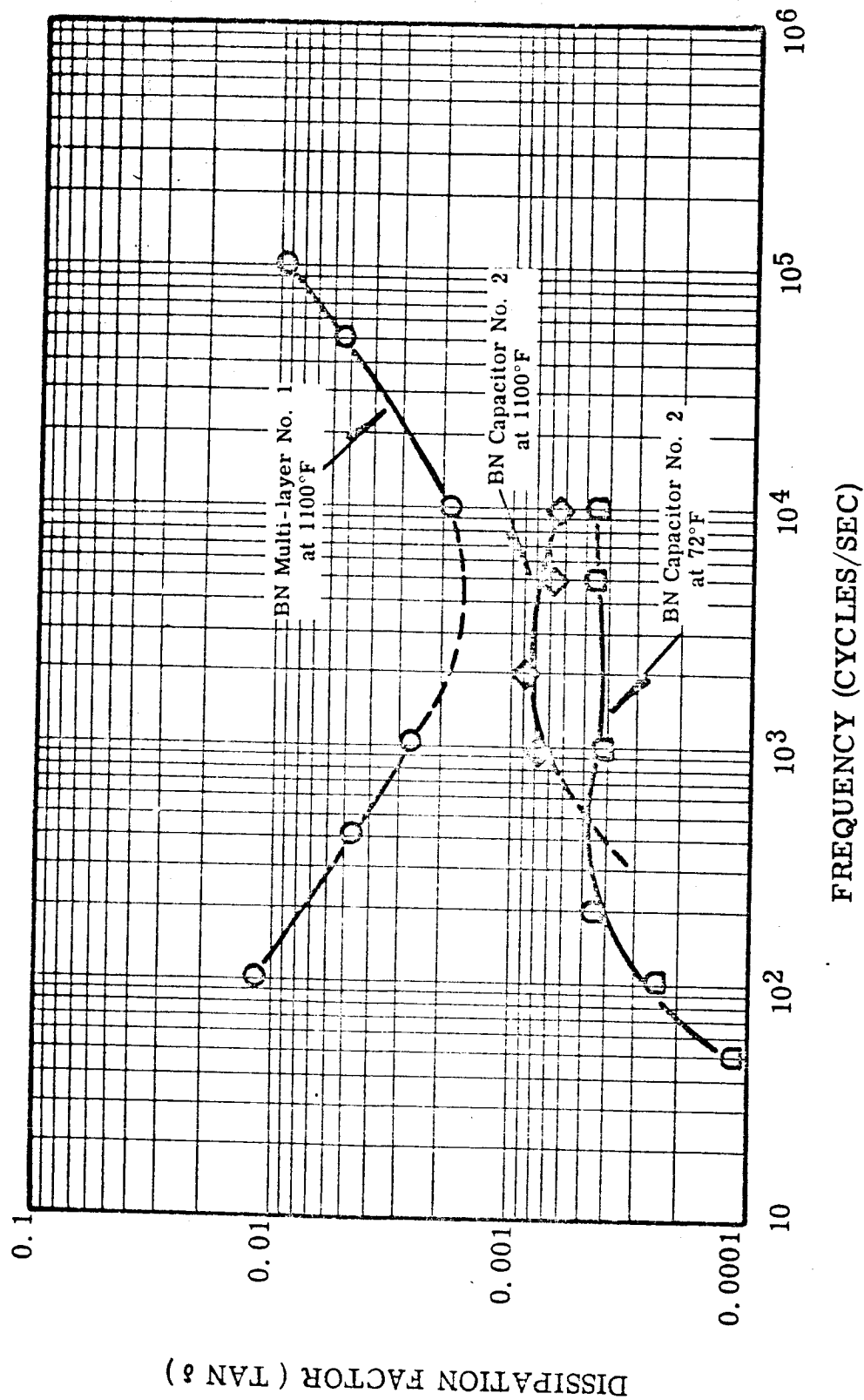


FIGURE III-15. Comparison of $\tan \delta$ Versus Frequency at Room Temperature (72°F) and 1100°F for Pyrolytic Boron Nitride as a Single Wafer Capacitor (BN Capacitor No. 2) and as Three Wafers Stacked and Connected in Parallel (BN Multi-Layer No. 1) Measured in Vacuum at $1-3 \times 10^{-7}$ torr

Figure III-15. Comparison of $\tan \delta$ Versus Frequency for Single and Multi-Layer Pyrolytic Boron Nitride Capacitors

d. DIELECTRIC "AFTER WORKING" EFFECTS

Several of the curves presented for $\tan \delta$ and capacitance changes with temperature show what appears to be a hysteresis effect after measurements were made during increasing temperature vs. those recorded during cooling. In all instances, the measured capacitance and $\tan \delta$ values were higher on the cooling curve than on the corresponding heating curve. This effect was not observed to any significant extent with pyrolytic boron nitride but appeared to be most noticeable for metal oxide type dielectrics (Lucalox, BeO).

Several explanations have been considered to explain this effect. The one that seems reasonable at present is somewhat analogous to spontaneous polarization in ferroelectric materials and/or to the concept of an electret. An electret (ref. 2) results from a "frozen in" polarization and can be made synthetically by cooling molten wax under an applied field. For the measurements shown in this section $\tan \delta$ and capacitance readings were made alternately with d-c resistance measurements. A d-c voltage ranging from 100 to 1000 volts was applied to the specimens at temperatures up to 1100°F. It seems reasonable to expect that some degree of orientation polarization occurred particularly at the higher temperatures where charge carriers (from impurities etc.) are more mobile. On cooling, this induced polarization persists in a non-equilibrium state and then gradually relaxes possibly by bulk or grain boundary diffusion or surface absorption. Examples of these effects are shown in Figures III-2, III-4, III-7, III-9, III-16, and III-17 for Sapphire, BeO and Lucalox Capacitors at different measuring frequencies. These effects will be studied in more detail with pyrolytic boron nitride capacitors.

Figure III-18 shows an aging effect on $\tan \delta$ and capacitance for BeO Capacitor No. 2 after it was heated in air to 960°C (1760°F). A very marked decrease in $\tan \delta$ is evident after 200 hours of aging time at room temperature (72°F). The capacitance is also shown to decrease with time. This effect is similar to that observed in ferroelectric barium titanate.

Figures III-19 and III-20 show the effect of heat treatment on the ratio of $\frac{\Delta C}{C_{50 \text{ cps}}} \times 100$ and the ratio of $\frac{\Delta \tan \delta}{\tan \delta_{50 \text{ cps}}} \times 100$ as a function of frequency for BeO Capacitor No. 2. Volatilization of impurities is indicated by a flattening of the ΔC curve after heating the capacitor to 960°C (1760°F) in air (Figure III-19) and the

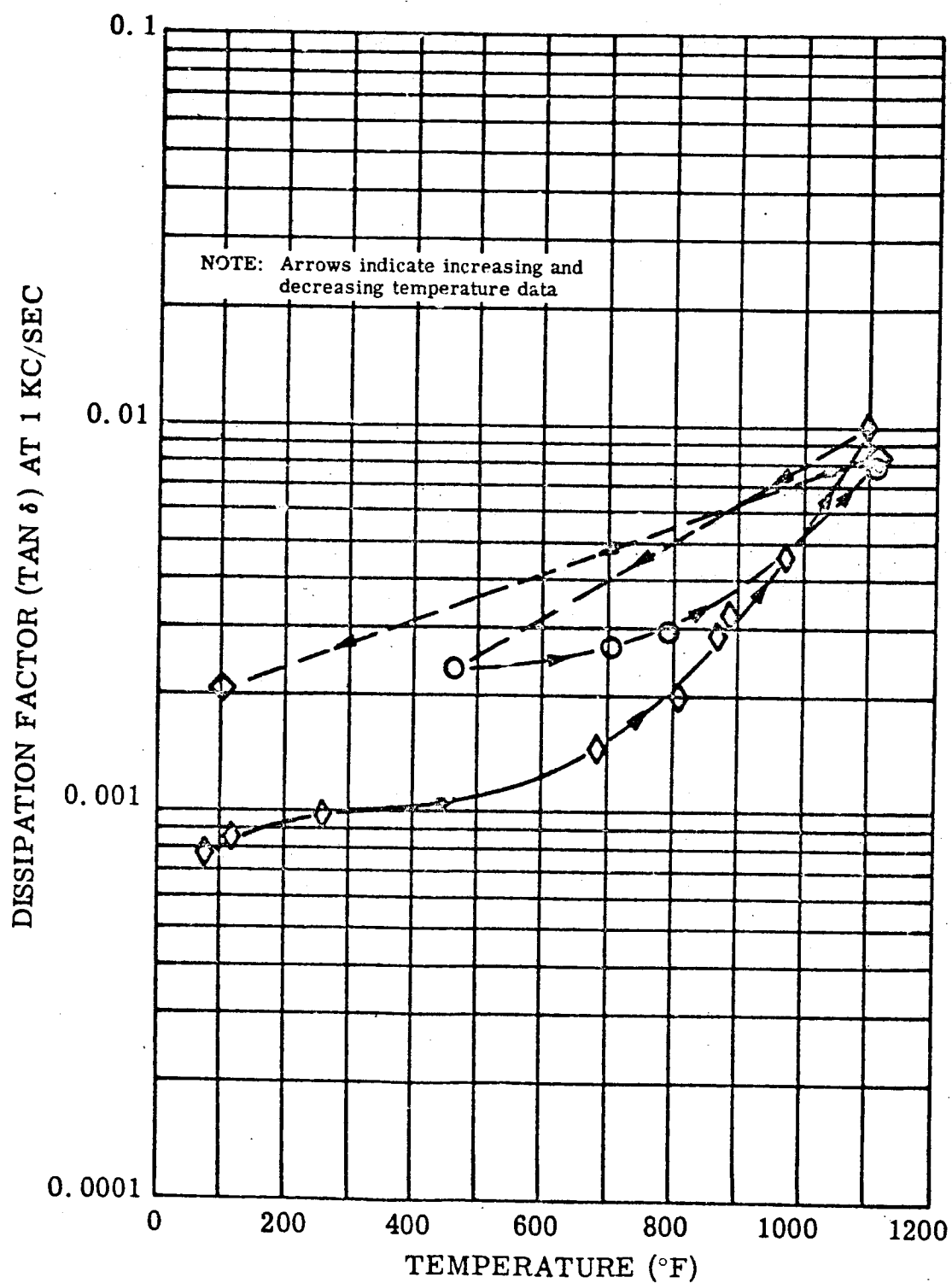


FIGURE III-16. Tan δ Versus Increasing and Decreasing Temperature for Sapphire Capacitor No. 2 Measured in Vacuum at $1-4 \times 10^{-7}$ torr, 1 kc/sec

Figure III-16. Tan δ versus Increasing and Decreasing Temperature for Sapphire Capacitor No. 2

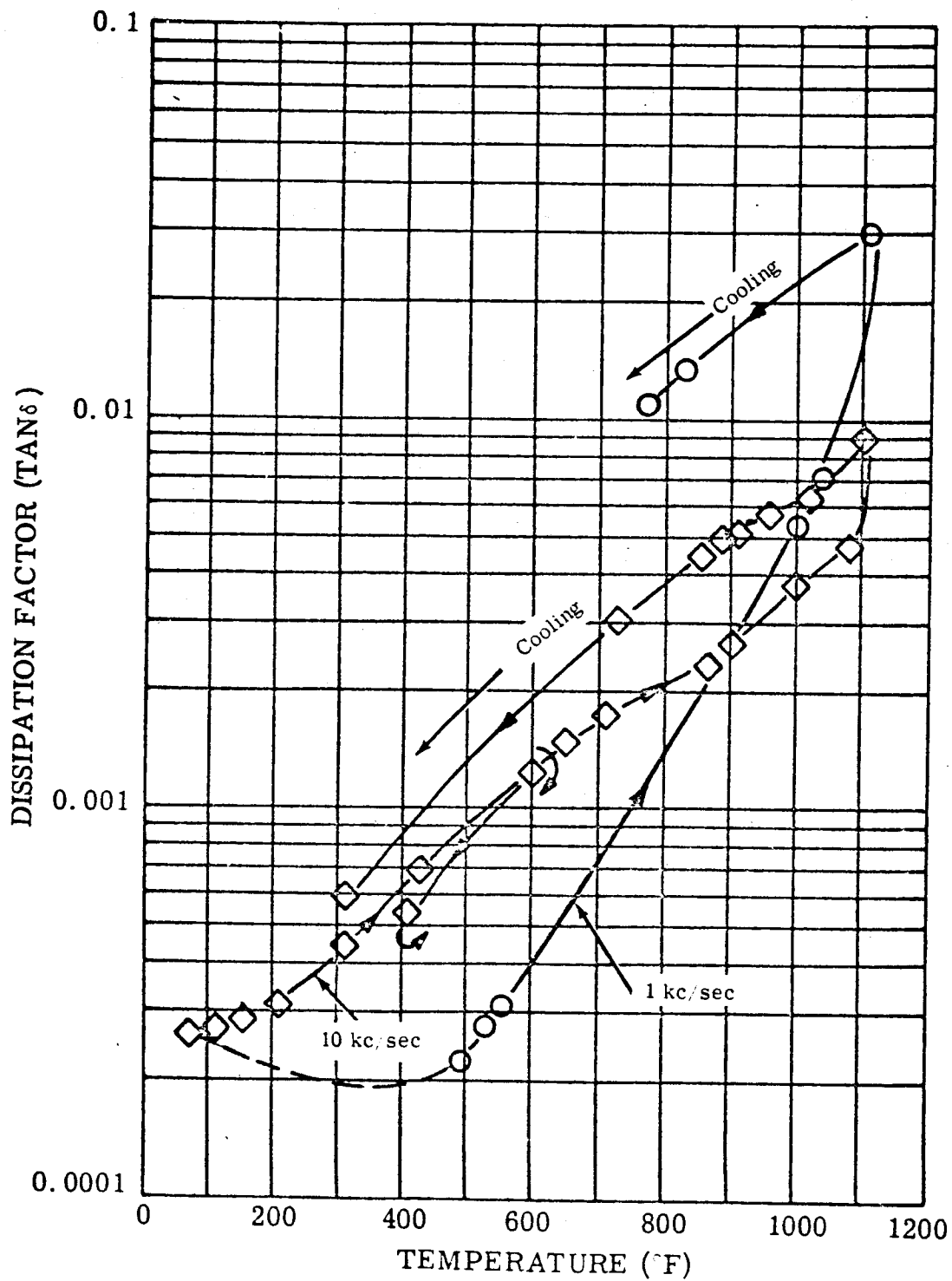


FIGURE III-17. $\tan \delta$ Versus Temperature for Sapphire Capacitor No. 1
Showing Hysteresis Effects on Cooling

Figure III-17. $\tan \delta$ versus Temperature for Sapphire Capacitor No. 1
Showing Hysteresis Effect

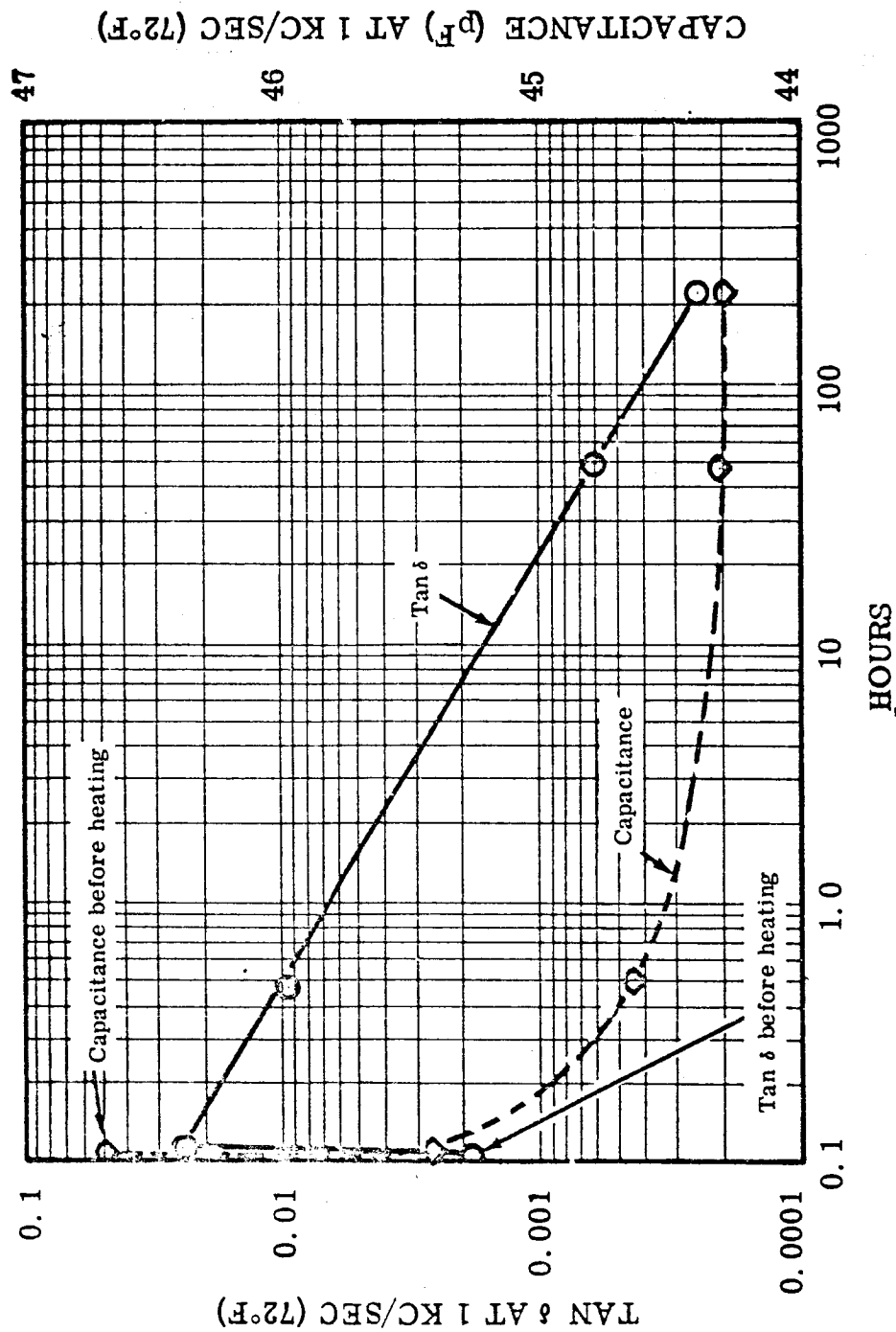


FIGURE III-18. Tan δ and Capacitance Versus Time After Heat Treating BeO Capacitor No. 2 in Air to 960°C (Cooled and Aged in Air Ambient, 72°F)

Figure III-18. Change in Tan δ and Capacitance versus Time for BeO Capacitor No. 2 After Heating to 960°C

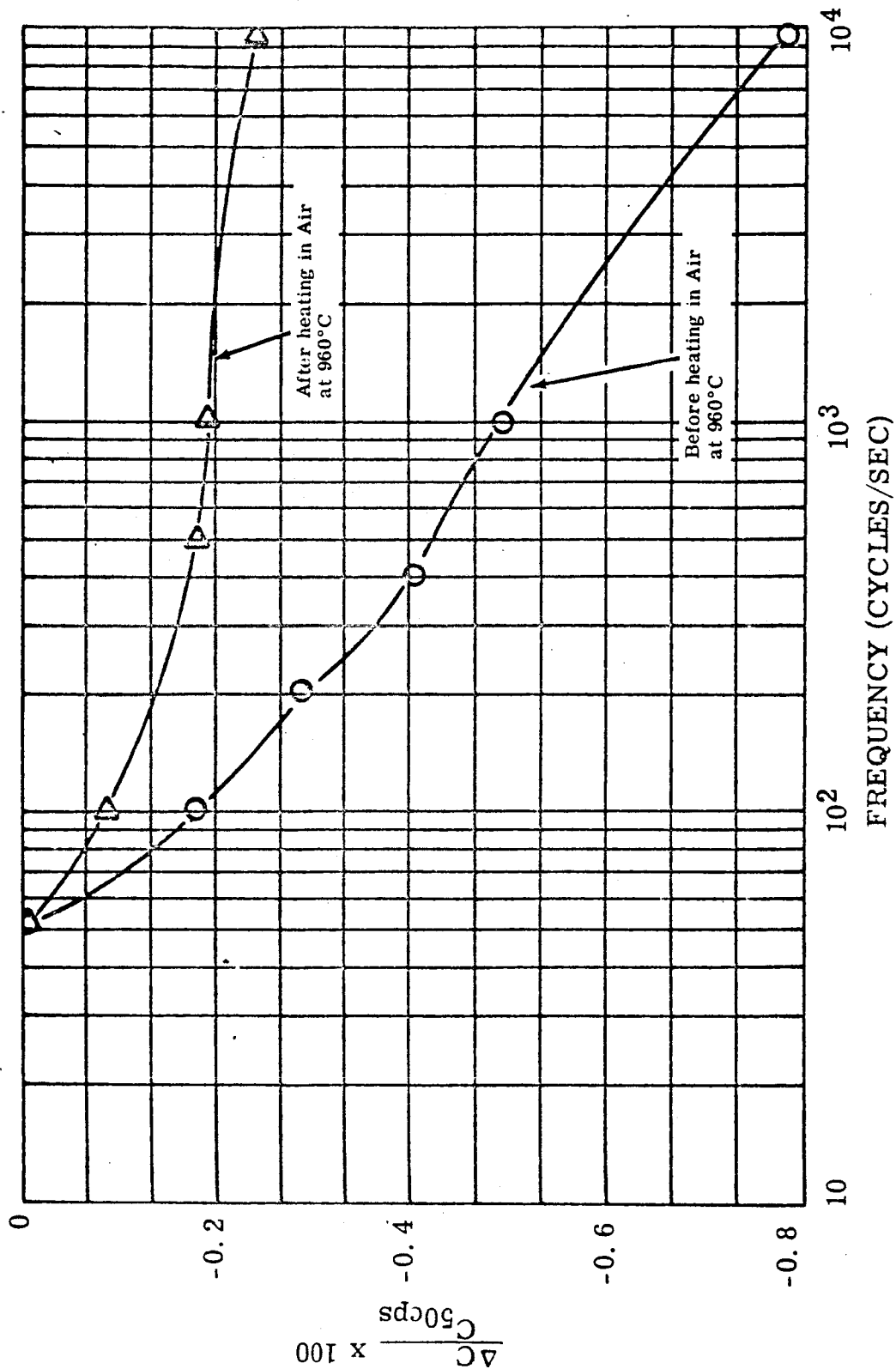
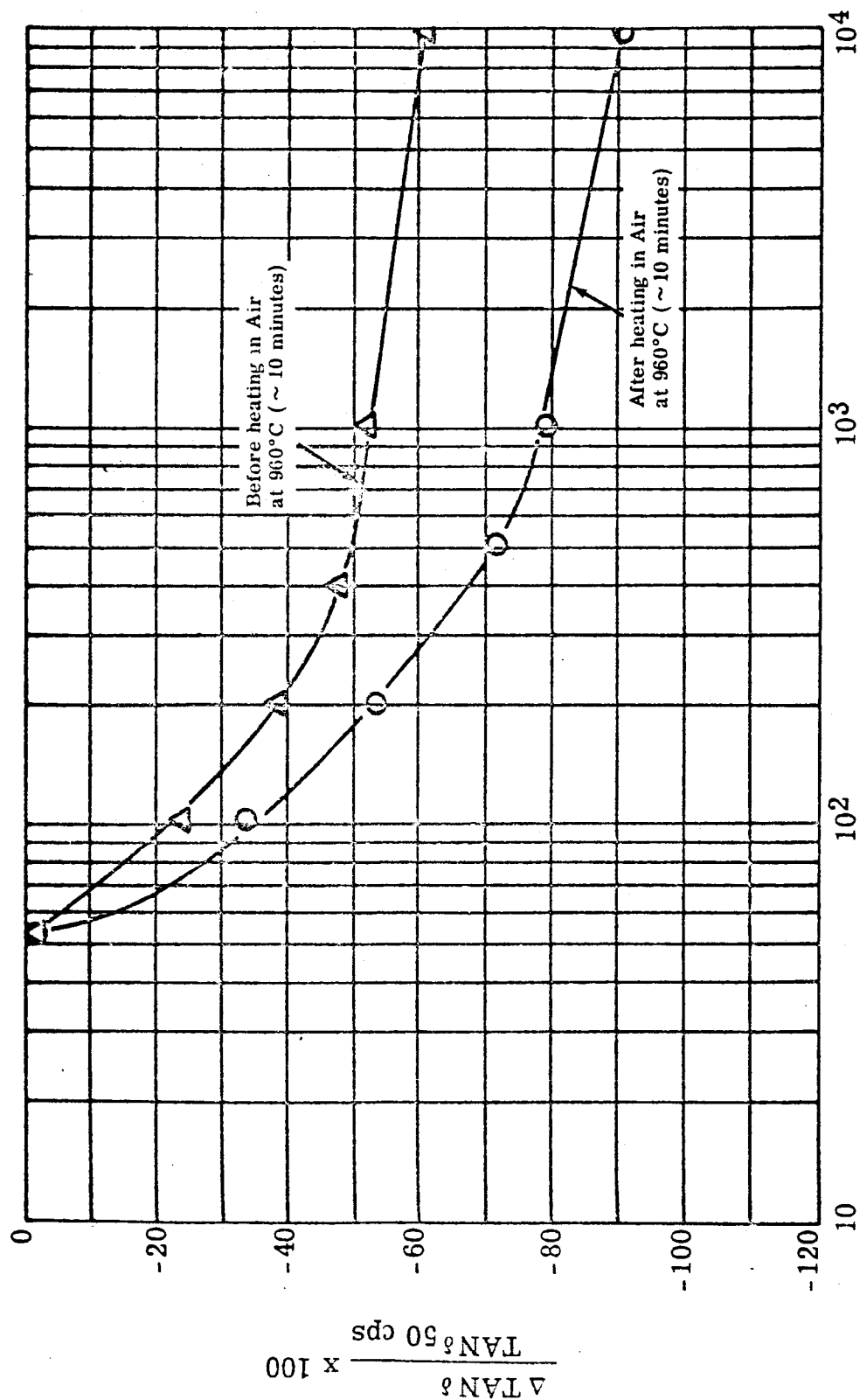


FIGURE III-19. Effects of Heating BeO Capacitor No. 2 in Air at 960°C on the Ratio of $\frac{\Delta C}{C_{50 \text{ cps}}} \times 100$ Versus Frequency (Measured in Air at 72°F)

Figure III-19. Effects of Heating BeO Capacitor No. 2 in Air at 960°F on the Ratio of $\frac{\Delta C}{C_{50 \text{ cps}}} \times 100$ Versus Frequency



FREQUENCY (CYCLES/SEC)

FIGURE III-20. Effects of Heating BeO Capacitor No. 2 in Air at 960°C on the Change in the Ratio of $\frac{\Delta \tan \delta}{\tan \delta 50 \text{ cps}} \times 100$ Versus Frequency (Measured in Air at 72°F)

Figure III-20. Ratio of $\frac{\Delta \tan \delta}{\tan \delta 50 \text{ cps}} \times 100$ Versus Frequency for BeO Capacitor No. 2 Before and After Heating to 960°C

effective series resistance of the electrodes may have been decreased.

e. DC RESISTANCE VS. TEMPERATURE

The d-c resistivity was calculated using the relationship:

$$(1) \quad \sigma = RA/t$$

where:

σ = resistivity (ohm-cm)

R = measured d-c resistance (volume and surface contributions)

A = area of capacitor electrodes (cm²)

t = thickness of dielectric (cm)

Resistivity values were calculated for pyrolytic boron nitride (BN Capacitor No. 3), single crystal Al₂O₃ (Sapphire Capacitor No. 2), hot pressed polycrystalline BeO (BeO Capacitor No. 2), and polycrystalline Al₂O₃ (Lucalox Capacitor No. 1). These data are shown as a function of increasing temperature in vacuum (1-4 x 10⁻⁷ torr) in Figure III-21. Capacitor wafer dimensions and electrode sizes used to calculate σ are listed in Table III-1 for each of these capacitors. The d-c resistance was measured with a Keithly Model 610B Electrometer and a Keithly Regulated D-C Power Supply. In most instances 200 V d-c was applied to the specimens.

The values obtained for d-c resistance include the shunt effects of surface leakage currents. The magnitude of these currents is a variable that must be considered for a more detailed analysis. However, for comparison purposes, the curves shown in Figure III-21 indicate that pyrolytic boron nitride has a higher d-c resistivity over most of the temperature range. At temperatures in the neighborhood of 1100°F, the resistivities of all the materials does not show as wide a divergence as indicated for temperatures in the 300 to 900°F range. This is particularly evident for pyrolytic boron nitride which has resistivities several order of magnitude greater than the other materials tested in this range of temperatures.

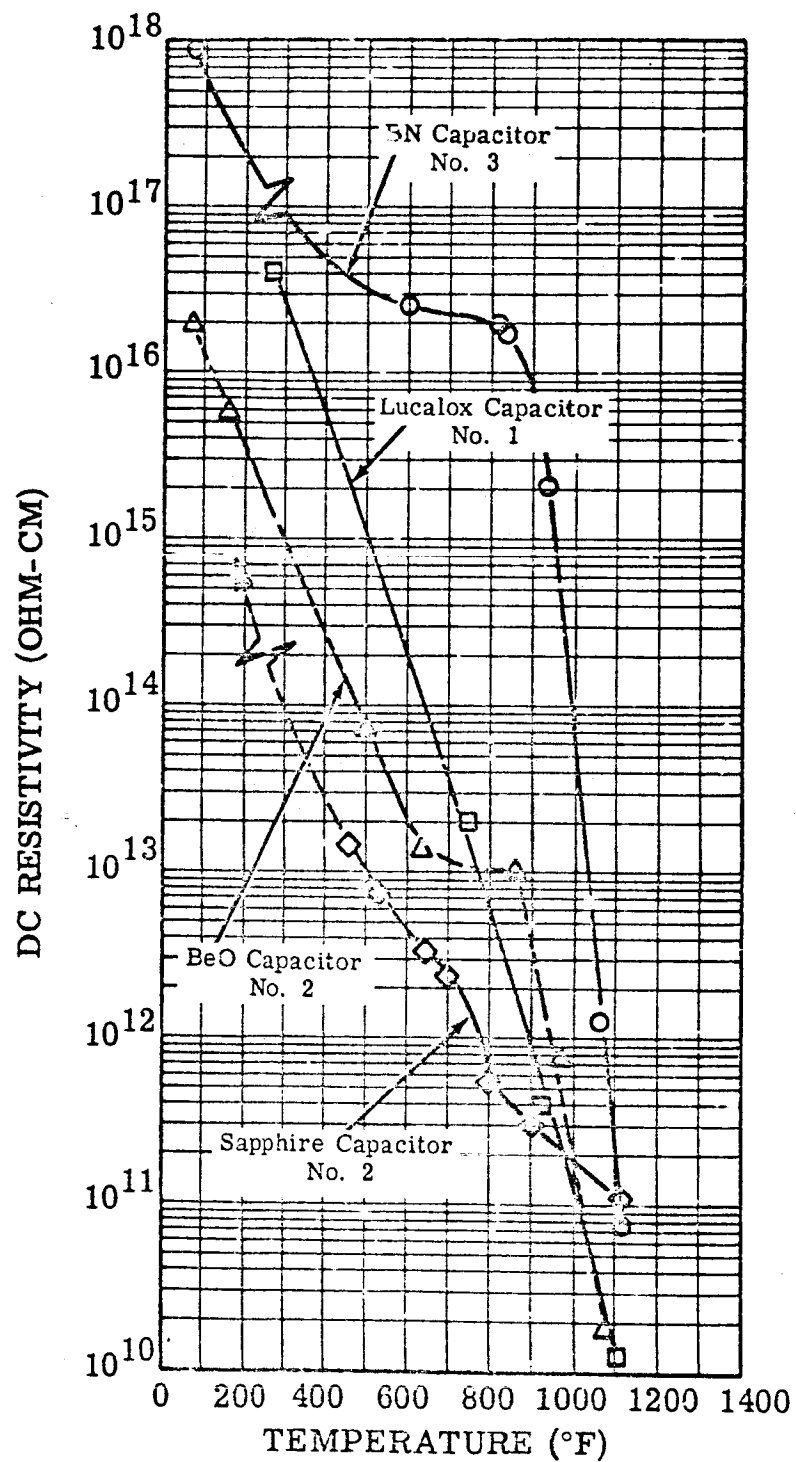


FIGURE III-21. DC Resistivity (ohm-cm) vs. Temperature in Vacuum (1-4 x 10⁻⁷ torr) For Pyrolytic Boron Nitride (BN Capacitor No. 3), Single Crystal Al₂O₃ (Sapphire Capacitor No. 2), Hot Pressed BeO (BeO Capacitor No. 2), and Polycrystalline Al₂O₃ (Lucalox Capacitor No. 1)

Figure III-21. Comparison of DC Resistivity vs. Temperature for Four Different Capacitor Materials

f. DC BREAKDOWN VOLTAGE AT 1100°F IN VACUUM

A final version of the test set up is now being made based on the results discussed below. The problem is essentially one of analyzing a series of breakdown voltages because the thin film electrodes used on the test capacitors volatilize at each breakdown. This "self healing" effect makes it difficult to determine the precise voltage at which an actual breakdown occurred. In addition, it is not possible to determine whether the first breakdown is an actual puncture through the bulk of the dielectric or whether it is a surface discharge (unless the test was shut down and the capacitor removed and examined).

The first test performed at 1100°F in vacuum ($1-3 \times 10^{-7}$ torr) showed a d-c breakdown voltage for Sapphire Capacitor No. 1 (3.25 mils thick) of approximately 6000 volts (1840 volts/mil). This value is based on the indicated supply voltage (meter reading) corresponding to the point where the relay tripped the power supply output (10 ma). The next test was performed on a one mil thick pyrolytic boron nitride capacitor at 1100°F (Table III-1, Group 8). A Brush Model RD 2662 Oscillograph was used on this test to indicate the level of voltage applied to the test specimen. The first indication of a voltage drop occurred at 7000 volts (7000 volts/mil). However, the power supply relay did not trip the power supply until an indicated level of about 10,000 volts was recorded. BeO Capacitor No. 2, was tested in a similar manner. The first indication of a voltage drop occurred at 3250 volts (762 volts/mil). The next indication occurred at 5250 volts (1167 volts/mil). The power supply was then manually turned off and the voltage was again increased with the first indication of a voltage drop occurring at 7500 volts (1665 volts/mil).

Examination of the boron nitride capacitor and the beryllium oxide capacitor after these tests showed a number of puncture holes directly through the material and volatilization of the electrodes at these points. The capacitors were still good when contact was made to the remaining portion of the electrodes (From 20 to 30% reduction in capacitance).

This series of preliminary tests has demonstrated the need for a more sophisticated test and measuring setup. It will be necessary to record each breakdown as a function of voltage with the

voltage raising as a linear function of time. The breakdown voltages for boron nitride and beryllium oxide are probably more accurate than the value indicated for sapphire. The sapphire value appears to be somewhat high. However, for comparative purposes, these results show that boron nitride has a volts/mil breakdown strength which is at least four times greater than any of the other materials tested at 1100°F.

g. RELATIVE FIGURE OF MERIT

Most of the data which has been discussed in previous sections for each dielectric material can be condensed into a synthetic number. This number can be obtained in a variety of ways; however, the following relationship has been used to generate a so-called "figure of merit" (M).

$$(1) \quad M = \frac{MF}{IN^3} \times \frac{1}{\tan \delta (1100^\circ F)} \times \frac{1}{\Delta C / C_{72^\circ F}}$$

where:

M = Figure of Merit

MF = Measured Capacitance (pF x 10⁻⁶) in micro-farads at room temperature (1 kc/sec)

IN³ = Volume (electrode area x thickness) of dielectric material included between electrodes (refer to Table III-1)

tan δ = Measured dissipation factor (tan δ) at 1100°F and 1 kc/sec

ΔC = Change in Capacitance from room temperature (72°F) to 1100°F

The value of M will be greater for capacitors that have a thinner dielectric, the lowest losses at 1100°F and show the least change in capacitance over the temperature range from room temperature (72°F) to 1100°F. Therefore, the ratio of M is an attempt to show the relative merits of each of the dielectric materials in terms of fabricability combined with measured 1100°F electrical data for specific single wafer capacitors. The bar graph shown in Figure III-22 has been prepared to illustrate the calculated values of M

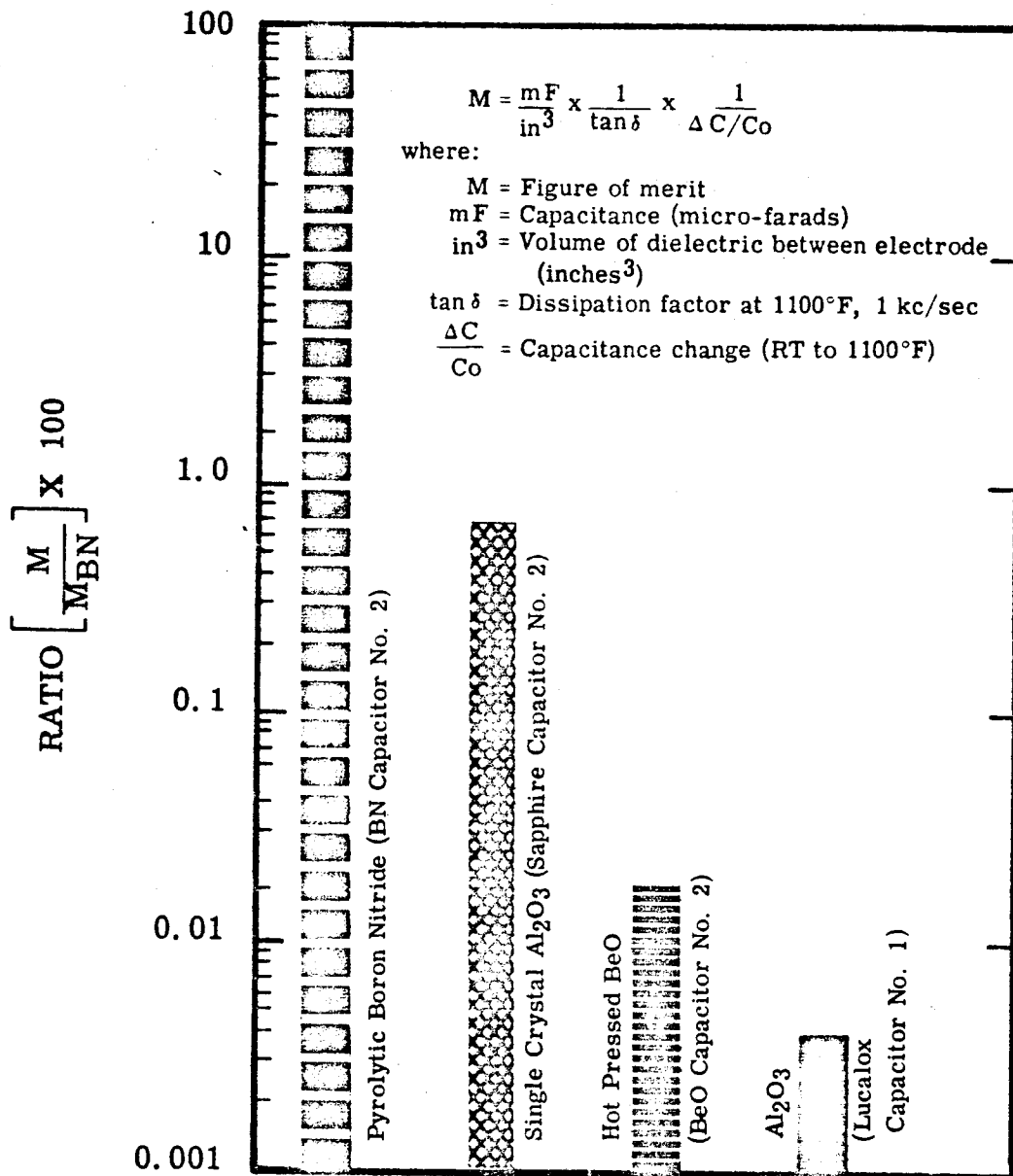


FIGURE III-22. Figure of Merit (M) for Four Different Dielectric Materials
Expressed as the Ratio $\frac{M}{M_{BN}} \times 100$.

M is calculated for 1 kc/sec Electrical Data

Figure III-22. Comparison of a Figure of Merit for Four Candidate
High Temperature Capacitor Materials

for each of the four dielectric materials investigated. These include pyrolytic boron nitride (BN Capacitor No. 2), single crystal Al_2O_3 (Sapphire Capacitor No. 2), polycrystalline beryllium oxide (BeO Capacitor No. 2) and polycrystalline alumina (Lucalox Capacitor No. 1). It is apparent from Figure III-22 that pyrolytic boron nitride is a logical first choice for a high temperature capacitor dielectric by a factor of at least 100.

Figure III-22 shows M converted into an index number using M for BN Capacitor No. 2 as the base and multiplying by 100. All the other capacitors are shown on a scale relative to 100 for pyrolytic boron nitride. The electrical data used in the calculations of M were taken from 1 kc/sec measurements and are selected "best values" for each material.

The volume parameter (MF/IN^3) used in these calculations does not include a voltage term because a true working voltage cannot be assigned at this point in the program. In fact, a working voltage could not be accurately determined unless extensive life testing were performed for each of the capacitor materials. In addition, the breakdown voltage for these materials is actually a statistical distribution of values with a mean and standard deviation. The breakdown strength that has been measured for only one capacitor per dielectric is not a satisfactory substitute.

C. PROGRAM FOR THE NEXT QUARTER

1. Preparation of pyrolytic boron nitride wafers will be continued.
2. An investigation of electrode materials, sheet resistivities and sputtering conditions will be completed.
3. A multi-layered capacitor with five or more wafers of pyrolytic boron nitride will be completed.

SECTION IV

PROGRAM III - BORE SEAL DEVELOPMENT AND COMBINED MATERIAL INVESTIGATIONS UNDER A SPACE-SIMULATED ENVIRONMENT

The bore seal effort under Task 1 will evaluate promising ceramic-metal sealing systems in potassium and lithium vapor at temperatures to 1600°F for 2000 hours. Elevated temperature seal strength and vacuum tightness will be determined. A four-inch diameter bore seal loaded with potassium will be incorporated in a stator design and evaluated in a 5000 hour endurance test at temperature and in a high-vacuum environment. This test will confirm data determined on smaller geometries.

Two five-thousand hour tests will be run under Task 2 on a stator which typifies the construction of an inductor alternator or a motor. The first will be run between 800 and 1100°F temperature. The second test will be run with a bore seal at temperatures between 1100 to 1600°F. All will be tested at a high-vacuum (less than 10^{-8} torr) under electric and magnetic stresses.

A transformer and two solenoids under Tasks 3 and 4 will be similarly tested under high vacuum and at elevated temperature. The purpose will be to evaluate the combined effects of electric and magnetic stresses, and high vacuum on combinations of materials suitable for application to advanced space electric power systems. One solenoid test will be under d-c excitation and the other under intermittent excitation so the effects of an invariant electric stress can be investigated.

The design features incorporated into the stator, transformer and bore seal were defined in detail in Appendixes A, B, and C of the first quarterly report.

A. TASK 1 - BORE SEAL DEVELOPMENT

1. Summary of Technical Progress

- a) Purity test capsules have been loaded with potassium during several loading runs under vacuum. Analyses of the oxygen content of the potassium in the capsules by neutron activation indicates high oxygen in the system. The amount of oxygen which can be attributed to the loading system or the weighted oxygen content of the capsules is not known. The oxygen content of the stainless steel capsules supplied for the analyses was higher than anticipated.
- b) The ceramic outgassing study has been completed. The present firing cycles applied to the ceramic in the clean fire at 2597°F (1425°C) in N₂-H₂ and the vacuum (5×10^{-6} torr) fire which they undergo during brazing is sufficient to maintain oxygen bearing outgassing products at a low level.
- c) The evaluation of active-metal brazes for ceramic-to-metal seals was continued. 99.8 percent beryllia modulus-of-rupture bars were brazed to columbium-1% zirconium metal members using five active metal brazing alloys. The brazed specimens exhibited high flexural strength. Test results ranged from 15,000 psi to nearly 25,000 psi.

2. Discussion

The program on ceramic-to-metal seals expands on the work initiated under NAS3-4162. On the current program alkali-metal loading will be conducted in potassium and lithium under vacuum ($< 1 \times 10^{-5}$ torr). The oxygen content in potassium will be less than 10 ppm as was observed during the previous program. The nitrogen level goal in lithium is 40 ppm.

Active-metal seals are being pursued since these offer less-brittle structures than refractory metal metalizings with thermodynamically stable second phases as observed in NAS3-4162. Small samples used in evaluations include modulus-of-rupture for flexural strength, tab-peel for brittleness and notch sensitivity and joined cylinders for leak tightness. Two-and-a-half-inch diameter ceramic-to-metal seals and a four-inch seal tested with saturated potassium vapor will complete the ceramic-to-metal seal investigations. Outgassing studies, mechanical strength and leak tightness at elevated temperature will complement the other investigations.

a. FACILITY CONSTRUCTION AND CHECK-OUT

Construction of the facility for fabricating, loading and exposure testing in vacuum of test capsules with alkali metal has been completed. The first and second quarterly reports included photos, diagrams and construction specifications and details.

The dual vacuum furnace equipment which will be used to carry out the 500 and 2000-hour capsule exposure tests at 1000 and 1600°F was completed. A vacuum of better than 8×10^{-10} torr has been achieved with the equipment cold, dry and empty.

To date, three potassium loadings have been made in the vacuum chamber for alkali-metal loading and electron beam welding. The mechanical problems of jiggling and fixturing to facilitate capsule handling in the vacuum chamber have been resolved. The recent effort has been in the direction of improving the loaded capsule potassium purity.

The evolution of fixturing and techniques is reflected in the reduced oxygen level in the second loading as compared to the first loading. The lower oxygen in the third of three capsules loaded during the second loading is largely attributed to flushing the tip of the potassium line with a few drops of potassium just prior to filling the capsule. The hot potassium (200°F) exposed at the tip of the fill line reacted with the partial pressure of oxygen in the loading chamber (vacuum approximately 4 to 6×10^{-6} torr) during the time between capsule fillings (10 to 15 minutes) and evidently became contaminated. The 55.1 ± 14.3 ppm oxygen probably represents the best loading possible with the system, as of that time. On the basis of the above analysis, it was decided that remedial action should be taken.

The potassium hot-trap container was returned to Mine Safety Appliance Corporation for oxygen analysis and refilling. The analysis showed the potassium to contain less than 10 ppm oxygen. Therefore, this was not a major contributing factor toward the high-oxygen level in the loaded capsule.

The second significant procedure modification taken prior to the third loading was the placement of polyethylene sleeves over the vacuum manipulator fittings and handles and pressurizing them with a continuous source of high-purity argon. This device does

not hinder manipulator capability and assures a reduction in the oxygen content of the gas by more than one order of magnitude if a leak should occur in the manipulator seals during the capsule handling.

The oxygen analyses of potassium in the capsules filled during the third loading indicated some improvement over the best results from the second loading. This is attributed to the flushing of the potassium fill line tip and to the use of argon filled polyethylene sleeves over the manipulators.

The oxygen level which can be achieved in a test capsule loaded in the vacuum loading facility remains questionable. A low oxygen level has not been achieved on the basis of the neutron activation analyses performed to date. However, the current neutron activation analyses have sufficient built-in errors that they must be resolved before further facility modifications are undertaken.

The potassium samples for neutron activation analyses are loaded into stainless steel capsules supplied by General Atomics, Division of General Dynamics Corp. The capsule material is assumed to contain 95 ppm oxygen, on the basis of a historical average by General Atomics. Since the average capsule weighs 14 grams and the average potassium sample weighs 4.5 grams, this means that, assuming 40 ppm oxygen in the sample and 95 ppm in the capsule, 0.18 mg of oxygen must be measured against a background of 1.33 mg of oxygen. The reproducibility of the oxygen content in the stainless steel capsules is therefore critical. On at least one occasion (Capsule No. 3 of the third loading) the total oxygen measured by neutron activation was less than the assumed 95 ppm oxygen content of the capsule material.

In order that the neutron activation analyses of low-oxygen bearing potassium be more accurate, the oxygen blank for the capsule should be below 10 ppm and preferably near 5 ppm oxygen. One source has been located for vacuum-melted type 304 stainless steel with oxygen content at the 5-12 ppm level. It is available in heat-size quantities only (1000 lbs.). Westinghouse and Eimac are considering sharing the cost of one 1000 pound heat in the form of bar. In addition, the test capsules from the third loading have been emptied and cleaned. After vacuum firing, the oxygen content will be determined. The MSA Research geometry stainless steel capsules (see the second quarterly report) loaded with potassium at the same time have been sent to MSA Research for mercury amalgamation analyses.

In the event the reported 40 ppm oxygen in the potassium is actually much less, the facility will be considered satisfactory and capsules for potassium exposure testing will be loaded. (Data obtained after the fourth quarterly report reporting period has indicated loading with less than 10 ppm of oxygen have been achieved as measured by MSA Research.)

b. CERAMIC OUTGASSING STUDY

Alumina and beryllia ceramics are normally fabricated by sintering the appropriate materials in an oxidizing atmosphere for 1/2 to 3 hours at temperatures in the 2700 to 3100°F (1500 to 1700°C) range. Dissolved, chemisorbed and occluded oxygen-containing gases (H₂O, CO, CO₂) are therefore released by the ceramics during subsequent treatment or use at elevated temperatures. The availability or presence of oxygen in alkali metal accelerates its corrosive effect toward refractory metals. The purpose of this study is to determine the species and amount of gaseous oxygen compounds remaining in selected bore seal ceramics (wall thickness 0.040 to 0.100 inch) after various processing schedules. Corrective action such as prolonged high-temperature vacuum firing can be programmed if shown necessary by this study. The equipment and methods employed in the outgassing study were described in detail in the second and third quarterly reports. A block diagram of the equipment is shown in Figure IV-1. The prepared samples are dropped into a precisely controlled, pre-conditioned vacuum furnace held at the test temperature. Selected m/e (mass to charge) ratios corresponding to the predominant gases as well as the overall fluctuations in furnace pressure are cyclically monitored. The pumping rate of the system for each gas component is known and outgassing rates and total evolved gas volumes can thus be computed. The sensitivity of the mass spectrometer is approximately 2×10^{-9} torr for nitrogen.

The residual bulk outgassing rates of similarly fabricated and sintered ceramics will be similar. For this study, ceramic materials which were representative of different fabricating and sintering procedures were chosen. The three materials selected for this series of measurements are listed with the systems which they represent:

- 1) Sapphire, (Linde Co.) single crystal 100 percent alumina; flame fusion grown in an oxy-acetylene flame; no grain boundaries, no voids, density 3.98 g/cc.
- 2) Lucalox, (G. E.) polycrystalline 99.8 percent alumina; sintered in hydrogen; with grain boundaries, but almost no voids; essentially 100 percent theoretical density, 3.98 g/cc.

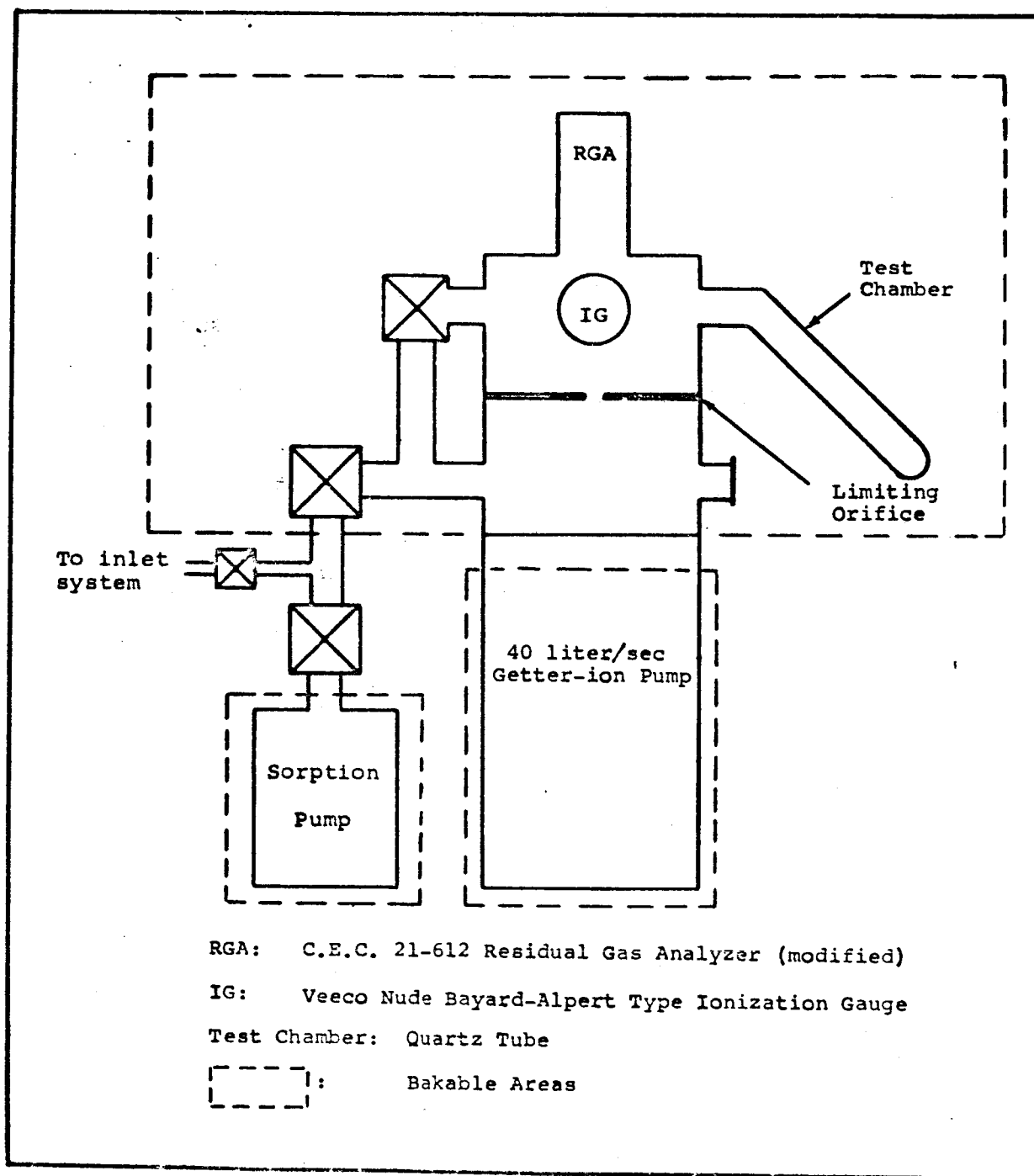


FIGURE IV-1. Block Diagram of Ceramic Outgassing Analysis System

- 3) Thermalox 998, (Brush Beryllium Co.) polycrystalline 99.8 percent beryllia; sintered in air atmosphere electric kiln; with grain boundaries and voids; 95-98 percent theoretical density, 2.86 - 2.95 g/cc.

The beryllia and Lucalox are representative bore seal ceramics and the sapphire is a control which will give an indication of the importance of grain boundaries and voids to residual outgassing. These three materials are not sintered in the same atmosphere.

Two outgassing temperatures and three different sample preparations were selected for the study. The two temperatures were 1000°F and 1600°F. The three preconditioning treatments were:

Precondition 1: After dye check and ceramic cleaning procedures. (See the second quarterly report).

Precondition 2: After dye check and ceramic cleaning procedures plus 10 minutes at 1832°F (1000°C) at less than 5×10^{-6} torr.

Precondition 3: After dye check and ceramic cleaning procedures plus 30 minutes at 2597°F (1425°C) in 75N₂ - 25H₂ with 100° F dew point, plus 10 minutes at 1832°F (1000°C) at less than 5×10^{-6} torr.

The preparations, consisting of cleaning, 1832°F vacuum firing and 2597°F 75% N₂-25% H₂ firing, are normal cleaning and firing procedures applied to all ceramics on this program prior to vacuum brazing. The composition of the furnace gas present during the 2597°F firing in N₂-H₂ atmosphere is given in Table IV-1. The beryllia is fired in a special furnace because of its toxic properties. The input gas to the two furnaces was identical. The CO in the tunnel furnace is due to the reaction of water vapor with the carbon boats along the length of the furnace.

The preconditioned samples were outgassed at 1000°F or 1600°F. The outgassing continued for 20 minutes. The evolved gases were monitored by a Bayard-Alpert-Ion gage and a CEC No. 21-612 mass spectrometer. Quantitative determinations of the evolved gases can be made since the pumping speed of the system for each gas is known. Total integrated amounts of gas evolved from the various preconditioned ceramics are summarized in Table IV-2. The sample surfaces areas and weights are given in Table IV-3.

TABLE IV-1. Typical Compositions of Nitrogen-Hydrogen Gas Atmospheres in Furnace Hot Zone During 2597°F Firing of Ceramics(a)

Furnace	Gas Composition(b)			
	N ₂	CO	A + O ₂	H
Tunnel Furnace	71.13%	3.02%	0.85%	balance
Ram Furnace	74.68%	0	0.31%	balance
<p>Notes: (a) Alumina parts are fired in a tunnel furnace and the beryllia parts in a ram furnace.</p> <p>(b) Averaged from data obtained with Burrell KROMO-TOG Model #K2 gas chromatograph.</p>				

TABLE IV-2. Total Gas Evolved From Sapphire, Lucalox and Thermalox 998 at 1000°F and 1600°F During an Outgassing Period of Twenty Minutes. See Text for Additional Details.

Material	Outgassing Temperature	Total Gas Evolved (Q_T)		
		Precondition 1(a)	Precondition 2(b)	Precondition 3(c)
Sapphire 100% Al_2O_3 Density - 3.98 g/cc	1000°F 1600°F	40 x 10 ⁻⁴ torr-liter/g 54 x 10 ⁻⁴ torr-liter/g	11 x 10 ⁻⁴ torr-liter/g 20 x 10 ⁻⁴ torr-liter/g	3.5 x 10 ⁻⁴ torr-liter/g 6.0 x 10 ⁻⁴ torr-liter/g
Lucalox 99.8% Al_2O_3 Density - 3.98 g/cc	1000°F 1600°F	40 x 10 ⁻⁴ torr-liter/g	18 x 10 ⁻⁴ torr-liter/g	10 x 10 ⁻⁴ torr-liter/g
Thermalox 998 99.8% BeO Density 2.90 g/cc	1000°F 1600°F	47 x 10 ⁻⁴ torr-liter/g	13 x 10 ⁻⁴ torr-liter/g	4 x 10 ⁻⁴ torr-liter/g 10 x 10 ⁻⁴ torr-liter/g
Notes: (a) Precondition 1 - after dye check and ceramic cleaning procedures. (b) Precondition 2 - after dye check and ceramic cleaning procedures and vacuum firing 10 minutes at 1832°F at less than 5 x 10 ⁻⁶ torr. (c) Precondition 3 - after dye check and ceramic cleaning plus 30 minutes at 2597°F in 75% N ₂ -25% H ₂ with 100°F dew point, followed by vacuum firing at 1832°F for 10 minutes at less than 5 x 10 ⁻⁶ torr.				

TABLE IV-3. Ceramic Outgassing Sample Weights and Surfaces Areas

Sample	1000°F			1600°F		
	Weight (grams)	Area (Cm ²)	Gas Evolved Q _T	Weight (grams)	Area (Cm ²)	Gas Evolved Q _T
Sapphire, 100% Al ₂ O ₃ (0.10 inch Round Rod) Precondition 1 (a) Precondition 2 (b) Precondition 3 (c)	0.2646	1.16	40 x 10 ⁻⁴ torr-liter/g	0.2644	1.16	54 x 10 ⁻⁴ torr-liter/g
	0.2497	1.12	>11 x 10 ⁻⁴ torr-liter/g	0.2697	1.17	20 x 10 ⁻⁴ torr-liter/g
	0.2637	1.06	3.5 x 10 ⁻⁴ torr-liter/g	0.2641	1.07	6 x 10 ⁻⁴ torr-liter/g
Lucalox, 99.8% Al ₂ O ₃ (0.10 inch Square Rod) Precondition 1 (a) Precondition 2 (b) Precondition 3 (c)						
				0.3764	1.69	40 x 10 ⁻⁴ torr-liter/g
				0.3404	1.59	18 x 10 ⁻⁴ torr-liter/g
				0.3764	1.69	10 x 10 ⁻⁴ torr-liter/g
Thermalox 998, 99.8% BeO (0.10 inch Square Rod) Precondition 1 (a) Precondition 2 (b) Precondition 3 (c)						
				0.3450	1.99	47 x 10 ⁻⁴ torr-liter/g
				0.3567	1.99	13 x 10 ⁻⁴ torr-liter/g
	0.3328	1.88	4 x 10 ⁻⁴ torr-liter/g	0.3495	2.19	10 x 10 ⁻⁴ torr-liter/g

Notes: (a) Precondition 1 - after dye check and ceramic cleaning procedures

(b) Precondition 2 - after dye check, ceramic cleaning and vacuum firing 10 minutes at 1832°F at less than 5 x 10⁻⁶ torr.

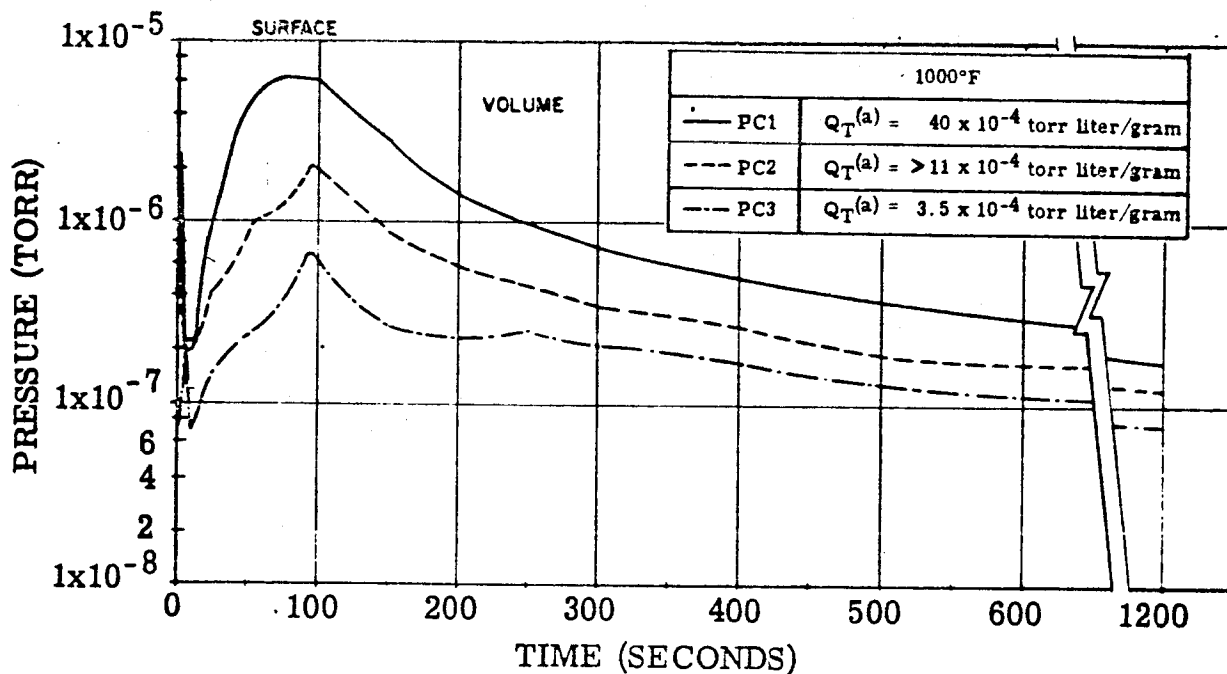
(c) Precondition 3 - after dye check, ceramic cleaning plus 30 minutes firing at 2597°F in 75 N₂-25H₂ followed by vacuum firing at 1832°F for 10 minutes at less than 5 x 10⁻⁶ torr.

The total evolved gas Q_T is expressed as 10^{-4} torr liters of gas evolved per gram of material. It is determined by first integrating the area under the curve of the "system pressure versus time". The resulting quantity is then divided by the time in seconds to obtain a mean pressure from which the background pressure is subtracted. This difference is then multiplied by the pumping speed of the system (one ℓ /sec for N_2). This number is the evolved quantity of gas, which is divided by the sample weight or surface area respectively, to give torr liter/gram or torr liter/cm².

The total pressure outgassing plots as a function of time are given in Figures IV-2, IV-3, IV-4 and IV-5. In Figure IV-6, the total pressure outgassing curves for the three materials at 1600°F after dye check and ceramic cleaning procedures (precondition 1) are shown.

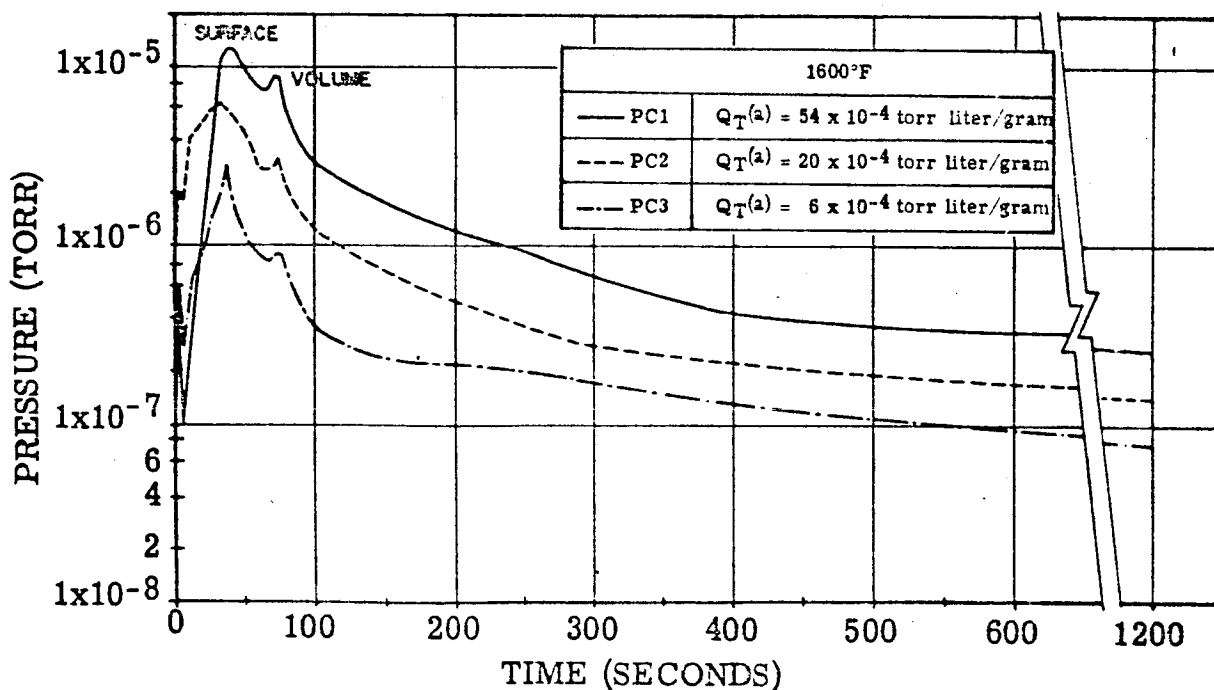
The partial pressures of selected gases as well as the total pressure were monitored on each outgassing run. The four specific gases monitored were hydrogen (H , $m/e = 2$), water vapor (H_2O , $m/e = 18$), nitrogen and/or carbon monoxide (N_2 , $m/e = 28$; CO , $m/e = 28$) and carbon dioxide (CO_2 , $m/e = 44$). These components account for essentially all of the evolved gases. This is confirmed by spot checks which showed that the partial pressures add up to the total pressure within experimental error. Methane (CH_4 , $m/e = 16$) was not monitored specifically, although it was always measured due to its proximity to water vapor, $m/e = 18$, which was monitored.

Partial pressure plots of representative gas determinations are given in Figures IV-7 to IV-12. The major item of interest in this work is the residual gas after reasonable vacuum processing. The partial pressure plots are those of the tails of the third and last outgassing peak representing bulk outgassing. The first two pressure peaks representing surface gas disturbed in sliding the sample into the furnace and surface gas from the sample itself occur within the first minute. During this time, the partial pressure excursions are so rapid that only one m/e ration can be satisfactorily monitored. The partial pressure monitored in all cases during this time was $m/e = 28$. This m/e peak was monitored continuously for the first 30 to 60 seconds of each run and the shape of the resulting curve duplicated the total pressure curve. The shape of the $m/e = 28$ curve for the first minute can therefore be checked by referring to the appropriate total pressure curve presented previously in this report.



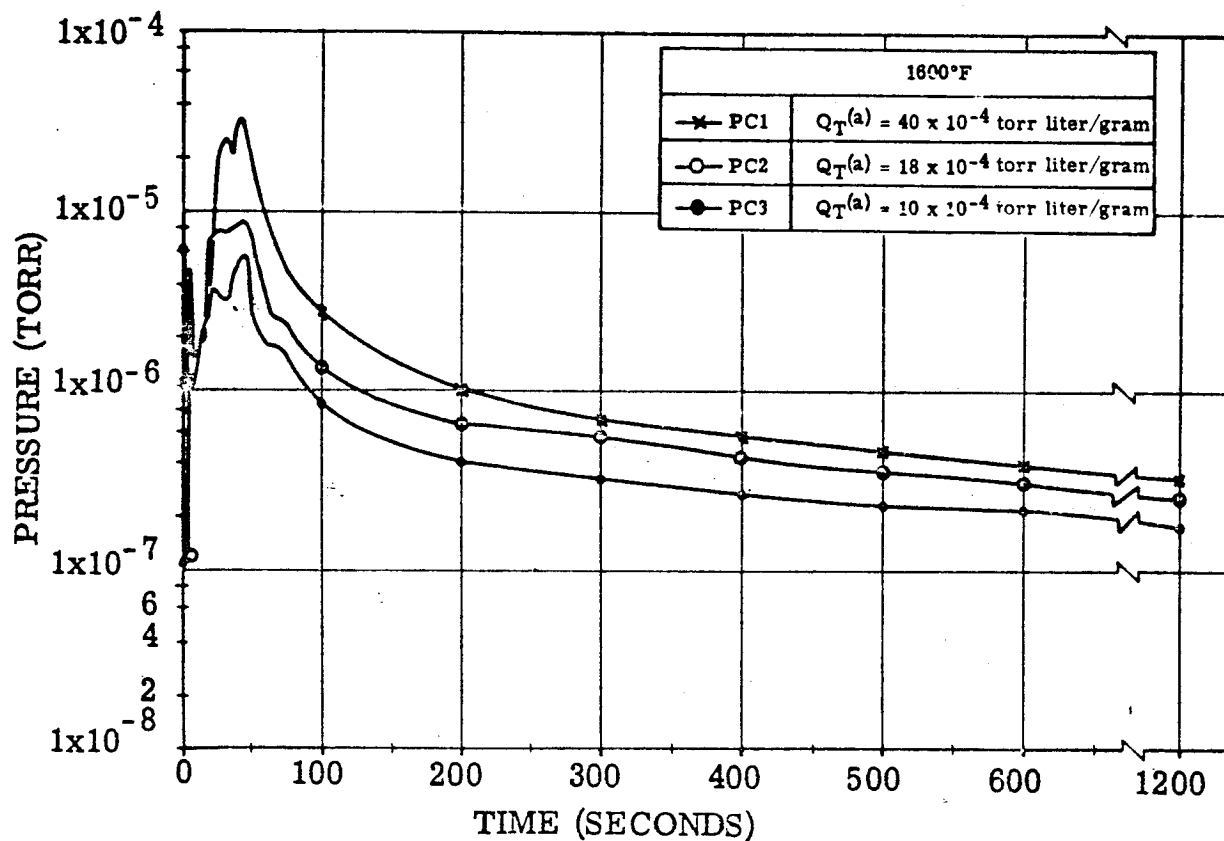
(a) Adjusted for calibrated pumping speed on the vacuum furnace.

FIGURE IV-2. Total (a) Pressure Outgassing Curves at 1000°F Furnace Temperature for Sapphire (100%Al₂O₃, density 3.98 g/cc) Samples for Preconditions 1, 2, and 3



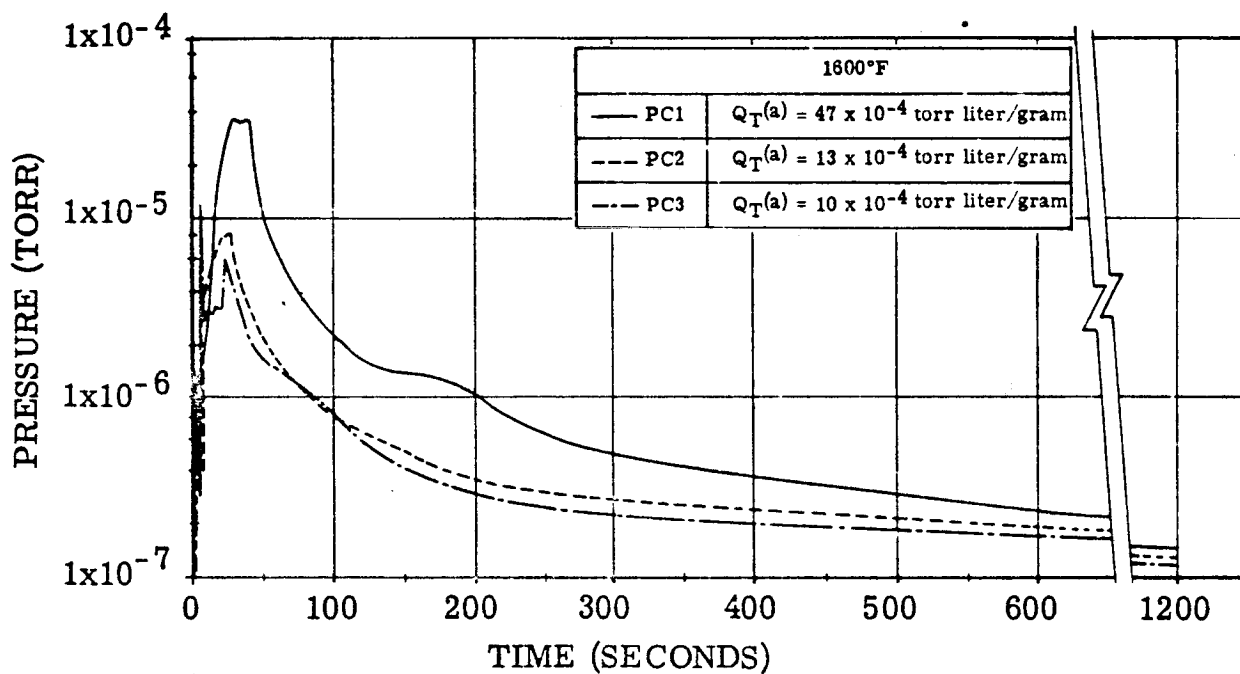
(a) Adjusted for calibrated pumping speed on the vacuum furnace.

FIGURE IV-3. Total (a) Pressure Outgassing Curves at 1600°F Furnace Temperature for Sapphire (100%Al₂O₃, density 3.98 g/cc) Samples with Preconditions 1, 2, and 3



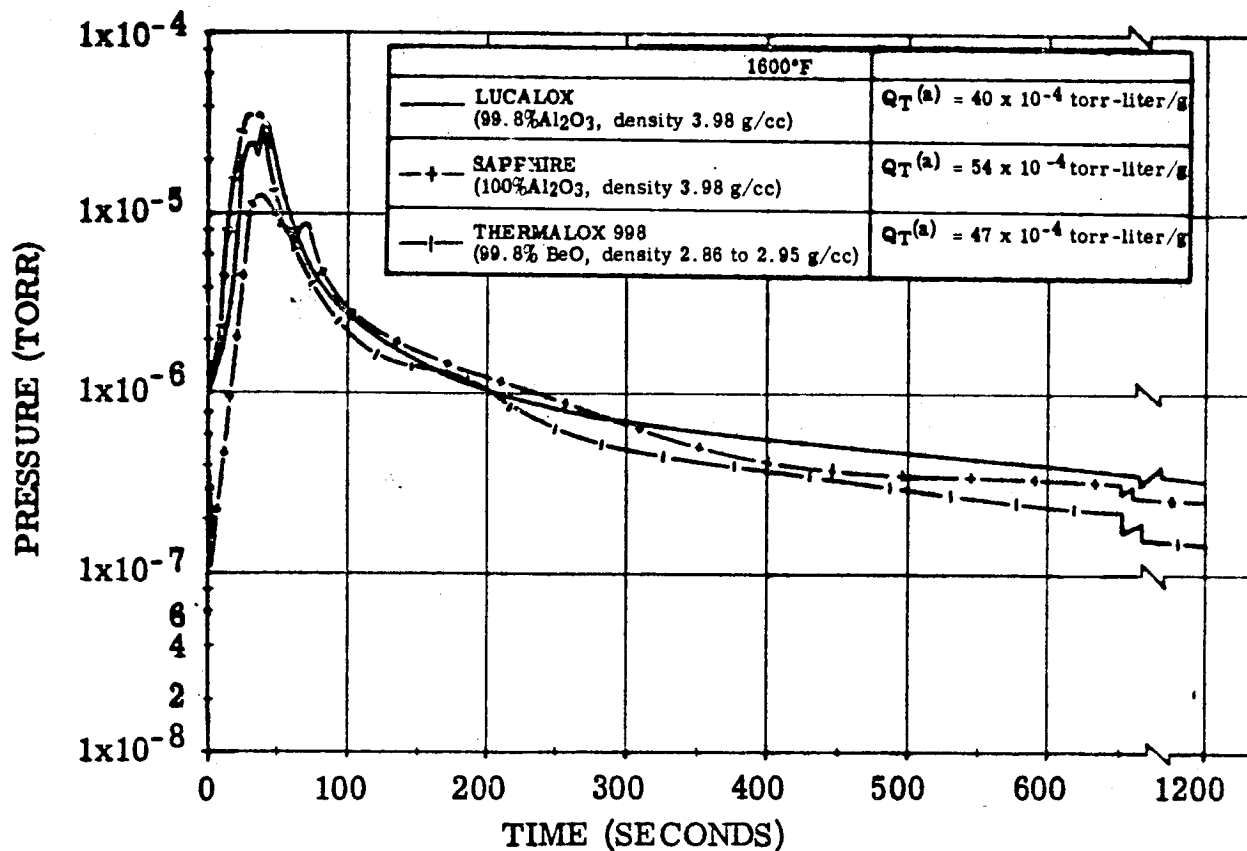
(a) Adjusted for calibrated pumping speed on the vacuum furnace.

FIGURE IV-4. Total (a) Pressure Outgassing Curves at 1600°F Furnace Temperature for Lucalox (99.8% Al_2O_3 , density 3.98 g/cc) Samples for Preconditions 1, 2, and 3



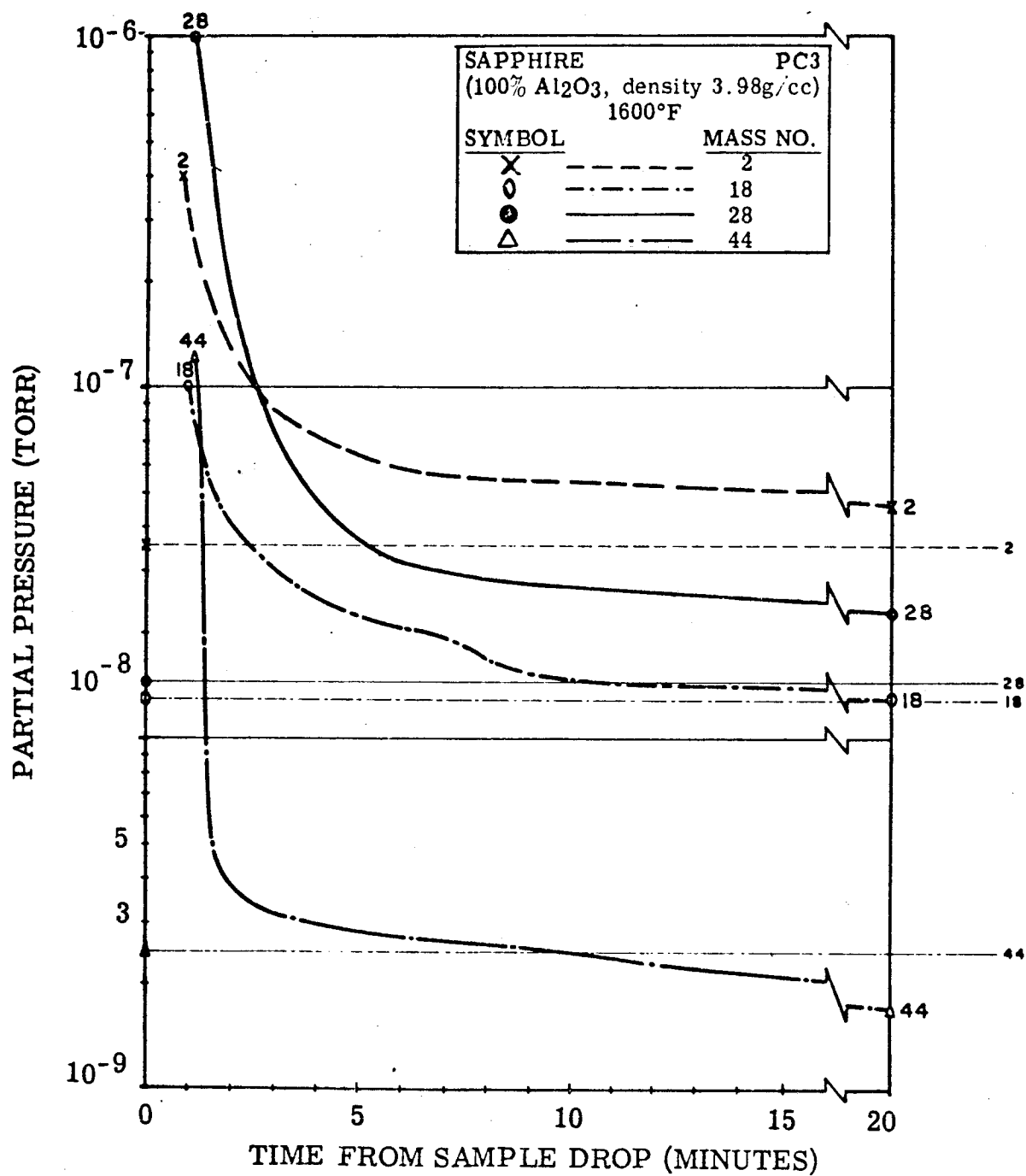
(a) Adjusted for calibrated pumping speed on the vacuum furnace.

FIGURE IV-5. Total (a) Pressure Outgassing Curves at 1600°F Furnace Temperature for Thermalox 998 (99.8%BeO, density 2.86 to 2.98 g/cc) Samples for Preconditions 1, 2, and 3



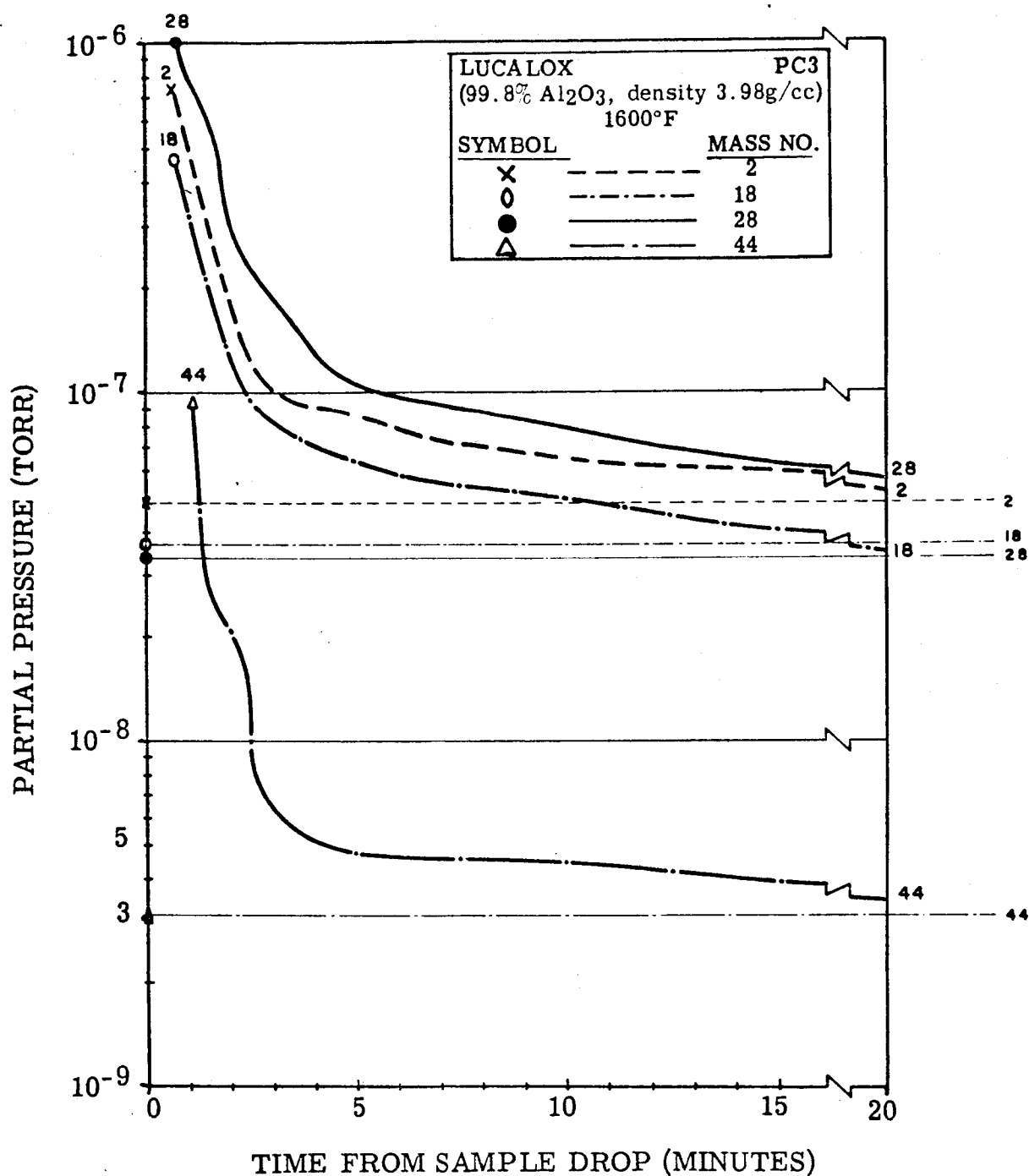
(a) Adjusted for calibrated pumping speed on the vacuum furnace.

FIGURE IV-6. Total (a) Pressure Outgassing Curves at 1600°F for Sapphire, Lucalox, and Thermalox 998 After Dye Check and Ceramic Cleaning Procedures (PC1)



Horizontal lines indicate the furnace background pressure for the gas with the designated mass number.

FIGURE IV-7. Partial Pressure Curves of Outgassed Products For Sapphire (100% Al₂O₃, density 3.98 g/cc) Precondition 3, Outgassed at 1600°F



Horizontal lines indicate the furnace background pressure for the gas with the designated mass number.

FIGURE IV-8. Partial Pressure Curves of Outgassed Products for Lucalox (99.8% Al_2O_3 , density 3.98 g/cc) with Precondition 3, Outgassed at 1600°F

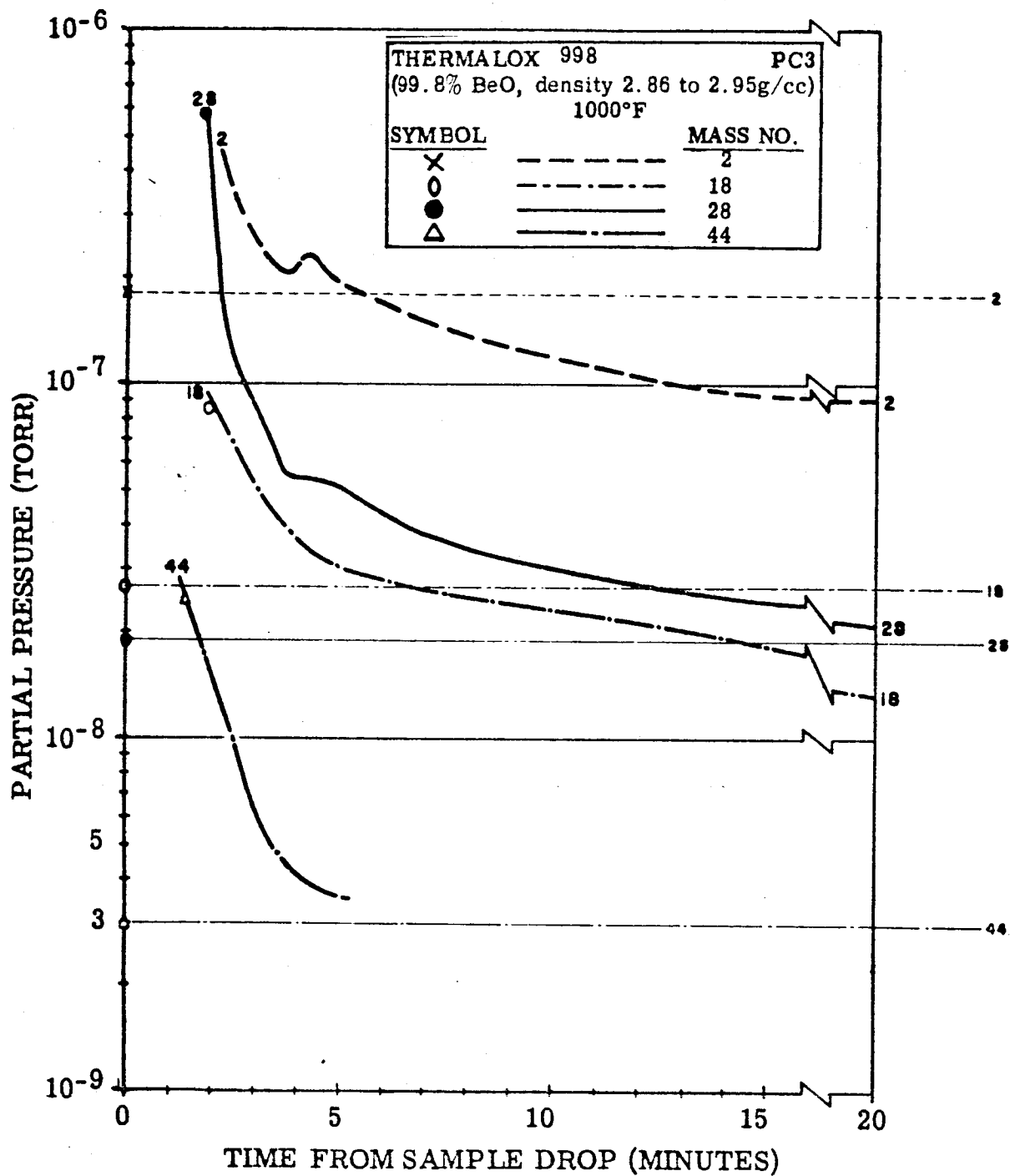


FIGURE IV-9. Partial Pressure Curves of Outgassed Products for Thermalox 998 (99.8% BeO, density 2.86 to 2.95 g/cc) Precondition 3, Outgassed at 1000°F

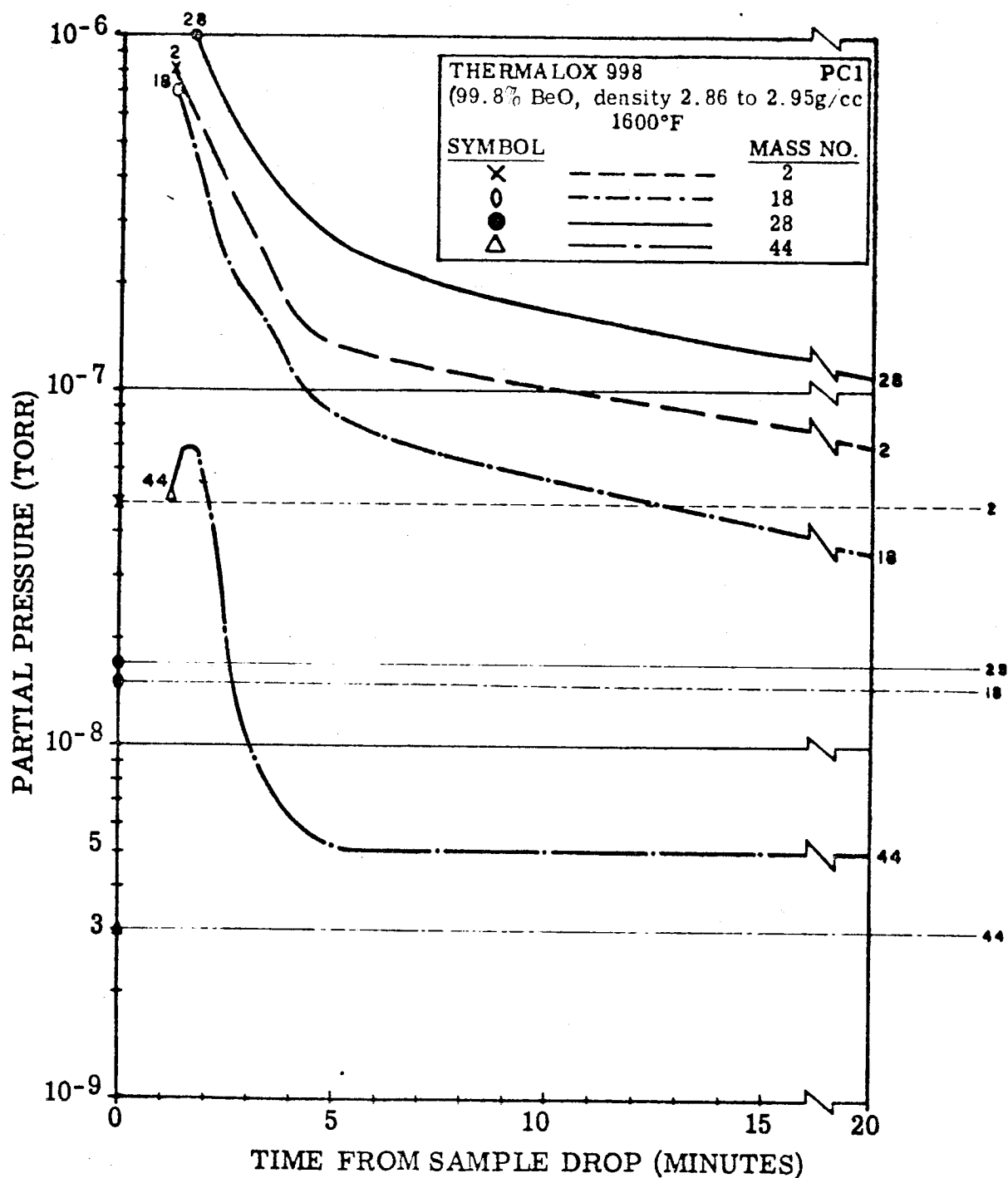


FIGURE IV-10. Partial Pressure Curves of Outgassed Products for Thermalox 998 (99.8% BeO, density 2.86 to 2.95 g/cc) with Precondition 1, Outgassed at 1600°F

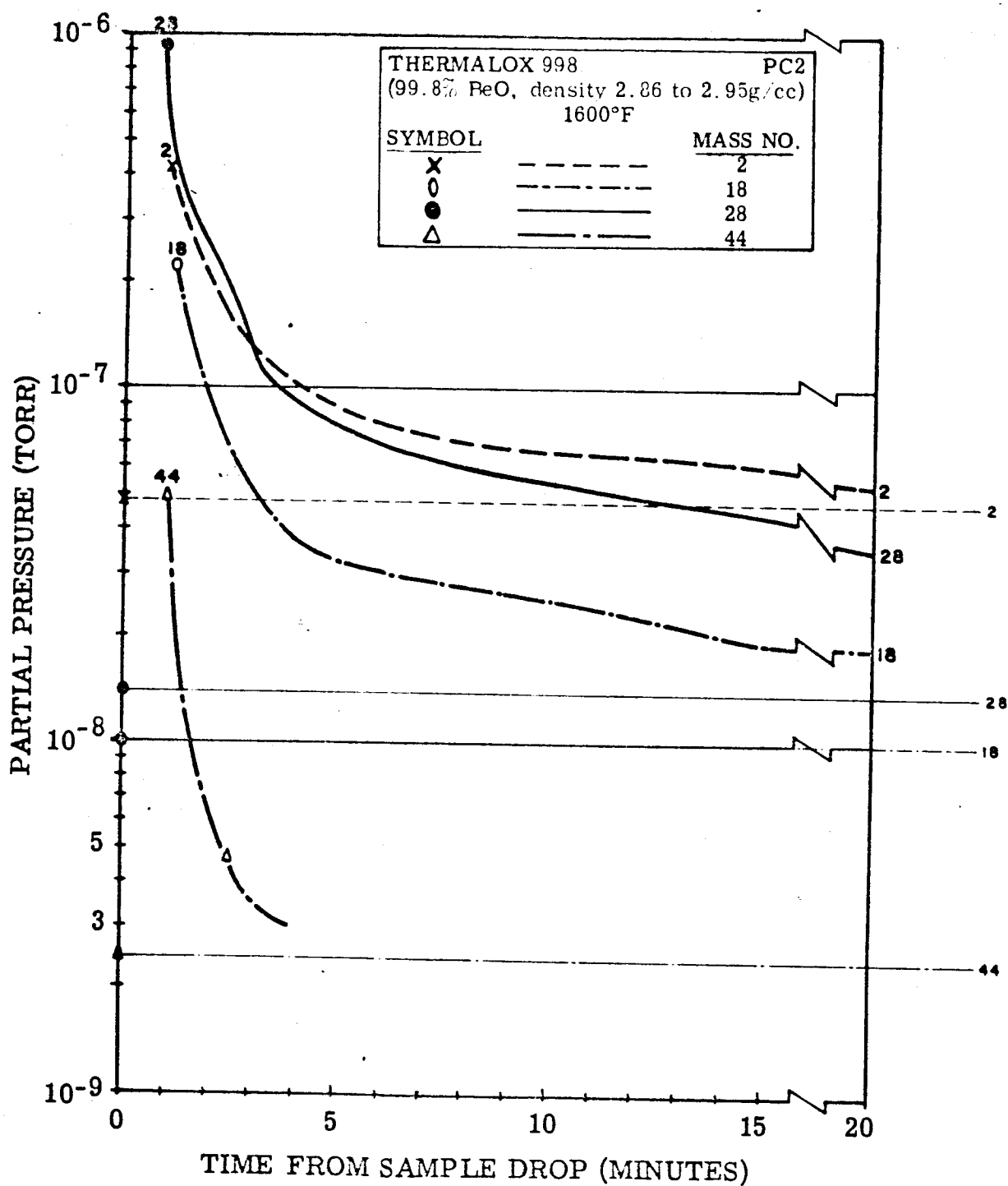


FIGURE IV-11. Partial Pressure Curves of Outgassed Products for Thermalox 998 (99.8% BeO, density 2.86 to 2.95 g/cc) with Precondition 2, Outgassed at 1600°F

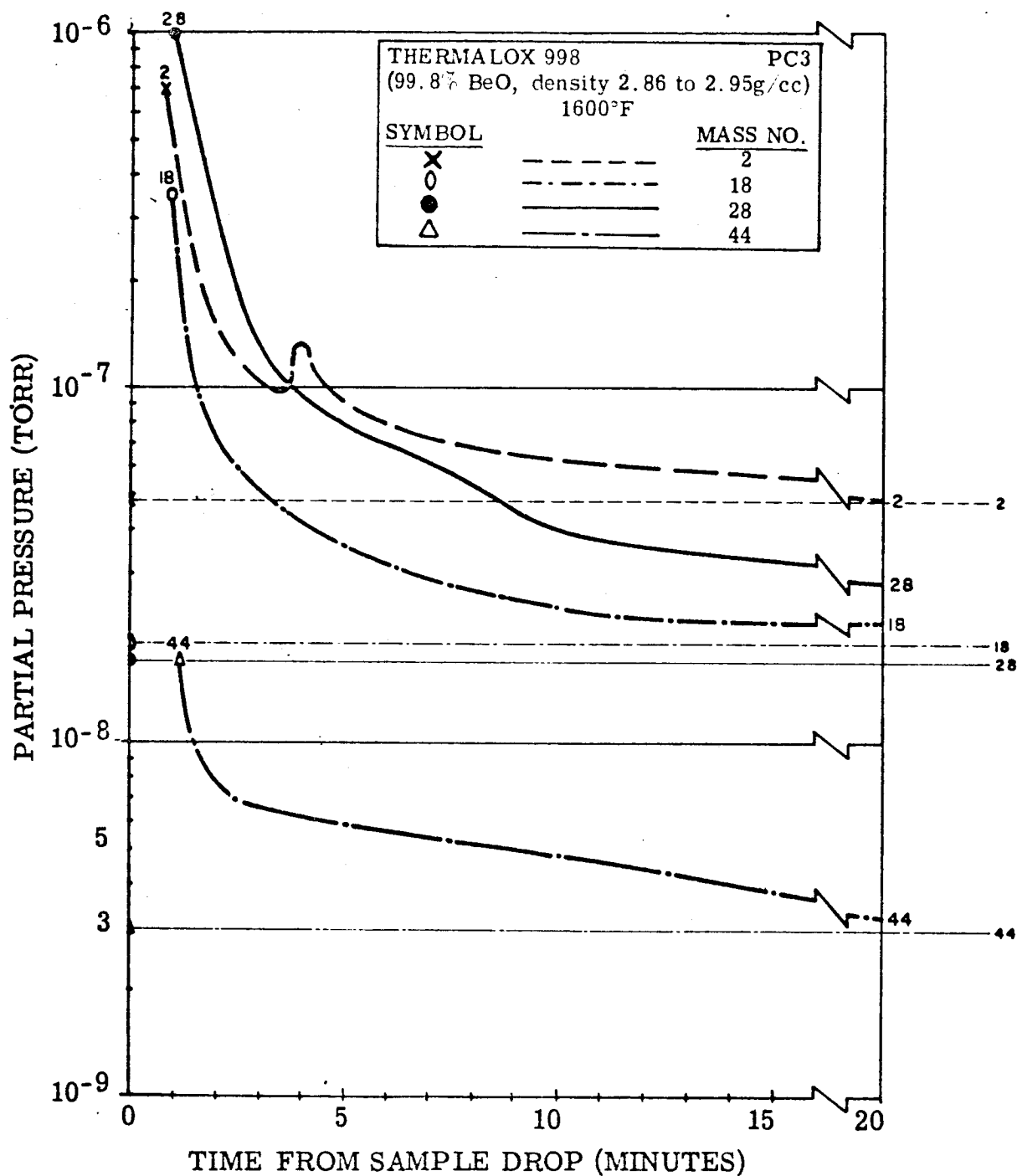


FIGURE IV-12. Partial Pressure Curves of Outgassed Products for Thermalox 998 (99.8% BeO, density 2.86 to 2.95 g/cc) with Precondition 3, Outgassed at 1600°F

The partial pressure curves have been smoothed out from the raw data and the remaining inflections are considered real and significant. For example, deviations from the normal uniform decay in pressure are noted such as the hydrogen peaks ($m/e = 2$) at 4 minutes on the Thermalox 998, in precondition 3 on the (Figures IV-9 and IV-12) 1000°F and 1600°F curves. Starting background levels for the individual gaseous components, just prior to sample drop, are noted on the left hand margins of the figures and by faint lines extending horizontally across the figures.

Table IV-2 shows that in all cases the total evolved gas from dye checked and cleaned ceramics (precondition 1) was significantly reduced by vacuum firing (precondition 2) and was reduced further when the vacuum firing was preceded by firing the samples at high temperature ($\sim 2600^\circ\text{F}$) in 75% N_2 -25% H_2 forming gas (precondition 3). The partial pressure curves (Figure IV-7, IV-8, and IV-12) show that after 20 minutes of outgassing at 1600°F, all three materials in the precondition 3 form indicate pressures within 2×10^{-8} torr of the furnace background pressure for each of the four monitored mass-to-charge ratios. An extrapolation of these curves shows that after an additional 20 minutes the partial pressures would fall below the corresponding starting pressures in all cases.

The most significant gases remaining after 20 minutes outgassing at 1600°F in all materials in precondition 3 are those with $m/e = 28$. The water vapor ($m/e = 18$) is essentially down to background level and the hydrogen ($m/e = 2$) is of lesser importance since it is not a liquid alkali metal corrosion accelerator. As stated previously, $m/e = 28$ represents nitrogen and/or carbon monoxide. To resolve the question of the ratio of nitrogen to carbon monoxide, it is necessary to measure other secondary m/e partial pressures which are over an order of magnitude less intense and are therefore at the sensitivity limit of the equipment used. As a result, only qualitative results were possible and these indicated a CO to N_2 ratio of approximately 7 to 1.

These data indicate that each gram of sapphire, Lucalox or Thermalox 998 which are given the treatment described as precondition 3 and outgassed at 1600°F for 20 minutes will evolve approximately 30 μg of oxygen (as Co) during the next 20 minutes at 1600°F. If the evolved gas during the second 20 minutes is assumed to consist entirely of nitrogen, then approximately 80 μg will be released from each gram of ceramic.

The evolved gases have been reported in units of gas per unit of weight for the ceramics, since it is believed the bulk gases are of more importance than the surface gases which can be removed from a completed structure with a relatively simple bakeout.

If the mass of the ceramic in a space electric power system were equal in weight to the mass of the alkali metal, the liquid alkali metal would be contaminated with 30 ppm oxygen or 80 ppm nitrogen, assuming the worst case for potassium and lithium respectively (e.g. 30 μ g oxygen per gram of ceramic transferred into each gram of alkali metal equals 30 ppm contamination). Since practical systems usually contain at least 10 times the mass of alkali metal than they do of ceramic, the contamination is reduced to less than 3 ppm and 8 ppm respectively.

Therefore, the present ceramic preparation procedure of dye checking, ceramic cleaning (in detergent) and clean firing at 2500°F in 75% N₂-25% H₂ is adequate if precautions in subsequent processing are followed.

The vacuum brazing operation (which is of longer duration and takes place at higher temperature than 10 minutes at 1832°F applied in the outgassing) is adequate as a vacuum firing step without a prior vacuum firing. A prior vacuum firing is useful only insofar as it permits the vacuum brazing operation to be carried out more rapidly.

Completed brazed assemblies should be stored in clean polyethylene bags. Handling with bare hands should not be permitted. If handling, which contaminates the ceramic, is necessary, it will prolong the vacuum firing of the completed system which must be carried out before the introduction of alkali metal into that system.

The completed system (loop, generator, etc.) should be vacuum outgassed at the operating temperature (1600°F in the case cited) for the time required to get the system pressure down to below 5×10^{-6} torr before introducing liquid metal.

c. BORE SEAL CERAMIC MATERIALS

A four inch beryllia bore seal containing potassium will be tested in a generator stator on this program. The test will be conducted at elevated temperature and under high vacuum. The final design is now being reviewed. A four inch diameter, four inch long Thermalox 998 beryllia tube with 0.100 inch wall flared to 0.250 inch at the ends has been ordered from the Brush Beryllium Company. Delivery is expected in January 1966.

Studies reported previously (NASA-CR-50493) showed that sapphire (Linde Co.), Lucalox (G.E.) and Thermalox 998 containing 80 ppm silica (Brush Beryllium Co.) retained their intrinsic strength and resisted attack by potassium after 500-hour exposure tests at 1600°F. Since actual bore seal ceramics will be required to operate for 10,000 hours or more, prolonged tests (2,000 hours) are to be carried out on this program. Additional ceramic bodies are to be tested for use in the event that the above materials prove unsatisfactory.

Yttria and Thermalox 998, both manufactured under special processes to limit the content of silica and other thermodynamically unstable constituent have been ordered from Coors Porcelain Company and Brush Beryllium Company, respectively, in the form of modulus-of-rupture bars and small cylinders.

The yttria ceramic has been delivered. The low silica Thermalox 998 was received from Brush. Samples of it and other lots of Thermalox 998 were subjected to neutron activation analysis. The neutron activation did not agree with the Brush Beryllium spectographic analyses, showing an excessive amount of silica. It has been returned for replacement and, at this time, the subject is under negotiation. Table IV-4 summarizes the analyses.

TABLE IV-4. Silica Analyses (as silicon) of Various Lots of Thermalox 998 Received from Brush Beryllium Co.

Silicon Content (ppm)	
Supplier Lot Analysis (a)	Neutron Activation Analysis (b)
30	149 ± 24
70	85 ± 21
150	207 ± 26
<p>(a) Spectrographic Analyses by Brush Beryllium Corporation, Elmore, Ohio</p> <p>(b) Neutron Activation Analyses utilizing Si28 (η, p) A128 Reaction by General Atomics, San Diego, California. Two samples from each lot were run. The \pm values represent one standard deviation estimated from counting statistics only.</p>	

d. ACTIVE METAL BRAZING ALLOYS

The task of screening braze filler alloys for use in joining beryllia ceramic to columbium-1% zirconium metal was continued during this period.

Six braze filler alloys were investigated in order to select three alloys for further evaluation by exposing to potassium vapor at 1600°F for 500 hours. The brazing data of the six braze alloys tested are given in Table IV-5. The three braze alloys selected from the screening are given below:

Alloy No. 5	- (46Ti-46Zr-4Be-4V)	Brazing temperature 1832°F (1000°C)
Alloy No. 9	- (60Zr-25V-15Cb)	Brazing temperature 2436°F (1330°C)
Alloy No. 12	- (35Ti-35V-30Zr)	Brazing temperature 2804°F (1540°C)

The strength data in Table IV-5 does not include all the brazing results because it was occasionally found that some joints in the same brazing run were abnormally low in comparison with the general strength level. It was possible to detect and reject the low strength brazed samples on the basis of visual appearance prior to testing. The causes for rejection were primarily due to faulty assembly which included misalignment, faulty pressure application, or loss of braze powder. A smooth well filleted braze was not possible in all instances, however, because certain alloys were characterized by incomplete and uneven wetting. It is probable that in these cases, the poor wetting could be alleviated by using a metallic wetting layer on the beryllia ceramic. Some process variations were carried out whenever the brazements appeared to be less than optimum.

In addition to the braze filler alloy evaluations, several beryllia ceramics were tested to obtain modulus-of-rupture strength of these bodies. The tested ceramic pieces were the end portions of modulus-of-rupture assemblies and had been exposed to the indicated brazing cycle as well as normal ceramic preparation procedures. The latter procedure was followed in order to include the possible influence of brazing temperature exposure on ceramic strength.

TABLE IV-5. Summary of Brazing Data for the Selection of Braze Alloys to Join Thermalox 998 Beryllia Ceramic to Columbium-1% Zirconium Metal

Braze Alloy No.	Nominal Alloy Composition (weight percent)	Brazing Conditions Time (minutes) Temperature (°F)		Strength of Brazed Specimens					Leak Test(e)			
				Modulus of Rupture			Tab Peel Strength					
				Number of Specimens	Remarks	Average Strength (psi)	Standard Deviation (d) (psi)	Number of Specimens		Average Strength (pounds/inch)	Standard Deviation (d) (pounds/inch)	
2	68Ti-28V-4Be	5	2372	14	(a)	17,465	1,900	6	(c)	9	2	6/8 VT
5	46Ti-46Zr-4Be-4V	5	1832	17	(a)	16,800	3,220	8	(a)	19	17	5/6 VT
6	50Zr-30V-20Cb	5	2516	6	(a)	15,150	2,160	4	(b)	21	3	2/2 VT
9	60Zr-25V-15Cb	5	2436	12	(a)	15,000	875	6	(b)	34	9	6/6 VT
10	50Zr-30Ti-20V	10	2732	4	(b)	15,225	3,140	2	(b)	21	±1 (f)	0/2 VT
12	35Ti-35V-30Zr	1	2804	3	(a)	24,433	1,380	2	(c)	16	±0 (f)	2/2 VT

Ceramic parts were Brush Beryllia's 99.8% BeO body containing 70 ppm SiO₂ (Lot No. 1) or 150 ppm SiO₂ (Lot No. 2). The parts were fabricated by dry pressing slabs, firing in electric kiln with subsequent cutting and grinding to shape. The ceramic bar size was 0.1 inch x 0.1 inch x 1 inch. Density was between 2.85 and 2.94 g/cc as specified by vendor. Average post-braze modulus-of-rupture strength of the ceramic was 25,000 psi. Ten bars from above assemblies were tested. The standard deviation was 3230 psi. The metal member was 0.015 inch thick Cb-1%Zr sheet.

Note:
(a) Good wetting, good fillet.
(b) Fair wetting, incomplete fillet.
(c) Poor wetting, incomplete, granular fillet.
(d) $S = \sqrt{\frac{\sum (x-\bar{x})^2}{(n-1)}}$
(e) VT indicates a leak rate $< 1 \times 10^{-9}$ std. cc/sec., 2/3 indicates 2 of 3 samples vacuum tight, etc.
(f) When there were less than three specimens, the standard deviation was not determined; the value shown indicates the spread of values from the average value.

Ceramic parts were Brush Beryllia's 99.8% BeO body containing 70 ppm SiO₂ (Lot No. 1) or 150 ppm SiO₂ (Lot No. 2). The parts were fabricated by dry pressing slabs, firing in electric kiln with subsequent cutting and grinding to shape. The ceramic bar size was 0.1 inch x 0.1 inch x 1 inch. Density was between 2.85 and 2.94 g/cc as specified by vendor. Average post-braze modulus-of-rupture strength of the ceramic was 25,000 psi. Ten bars from above assemblies were tested. The standard deviation was 3230 psi. The metal member was 0.015 inch thick Cb-1%Zr sheet.

Note:

- (a) Good wetting, good fillet.
 (b) Fair wetting, incomplete fillet.
 (c) Poor wetting, incomplete, granular fillet.

$$(d) S = \sqrt{\frac{\sum (x - \bar{x})^2}{(n-1)}}$$

- (e) VT indicates a leak rate $< 1 \times 10^{-9}$ std. cc/sec., 2/3 indicates 2 of 3 samples vacuum tight, etc.
 (i) When there were less than three specimens, the standard deviation was not determined; the value shown indicates the spread of values from the average value.

Braze alloy No. 2 (68Ti-28V-4Be) was the only braze alloy of the six tested that contained no zirconium. The average modulus-of-rupture strength was 17,465 psi. On the deficit side, the braze alloy showed poor wetting, forming isolated droplets, and had an average tab peel strength of only 9 psi. Of the six alloys tested this alloy showed a leakage incidence second only to that of alloy No. 10. The poor wetting was due in part to an increase in surface tension and melting point due to the loss of beryllium by volatilization. The vapor pressure is reported (ref. 1) to be near 10^{-2} torr at 2239°F (1226°C) which is less than the brazing temperature 2372°F (1300°C). Volatilization is not necessarily detrimental since it is a conventional method of raising the melting point of a braze by removing a melting point depressant, in this case, beryllium. The volatilization could be inhibited by brazing in an inert atmosphere, although contamination by reactive gases would be greater than that encountered in vacuum brazing. It is also possible that wetting and liquid spreading could be improved in this case by metallizing the ceramic or altering the braze cycle.

The low average tab peel strength for the 68Ti-28V-4Be braze alloy was apparently related to poor wetting of both the metal and ceramic. It was noted that an increase in applied pressure during brazing improved the peel strength slightly. It is possible that the low tab peel strength is indicative of the presence of a brittle layered phase, since a brittle layer would be conducive to crack propagation. It is planned to keep the 68Ti-28V-4Be braze as a back-up alloy.

Braze alloy No. 5, the 46Ti-46Zr-4Be-4V alloy, was particularly promising for bore seal applications in the 1000 to 1400°F temperature range because of its excellent wetting and relatively low brazing temperature (1832°F). In addition, one specimen had a tab peel strength of 53 lb/in. which was slightly higher than the 50 lb/in. encountered thus far. Like alloy No. 2, this alloy contains beryllium which would be expected to form a suitable joint with the beryllia. This alloy will be further evaluated by potassium exposure testing.

Braze alloy No. 9 (60Zr-25V-15Cb) was selected for potassium exposure testing over alloy No. 6 primarily on the basis of its lower brazing temperature 2436°F (1330°C) versus 2516°F (1380°C). The lower brazing temperature of alloy No. 9 is due to the lower columbium content. A low brazing temperature is desirable because various technical difficulties increase with an increase in brazing temperature. In addition, the average tab peel strength was 34 lb/in. and was the highest of all six alloys tested. In general, the braze alloy appeared to form a very satisfactory brazement. All leak test cylinders were vacuum tight.

Although preliminary test results using alloy No. 10 (50Zr-30Ti-20V) were very satisfactory, more recent results were not. The earlier average modulus-of-rupture strength was near 25,000 psi as opposed to a more recent value of 15,225 psi. The average tab peel results were similarly reduced from 49 lb/in. to 21 lb/in. Neither of the two cylindrical assemblies which were made in the first run was vacuum tight. This alloy will not be subjected to potassium exposure testing.

Braze alloy No. 12 (35Ti-35V-30Zr) was selected for potassium exposure testing because it exhibited the highest average modulus-of-rupture strength (24,437 psi) of the six alloys tested. In addition, in the test assemblies, the beryllia ceramic was coated with an evaporated molybdenum layer to promote wetting by the braze alloy. However, the brazing temperature 2804°F (1540°C) was the highest of the alloys tested and may be a prohibitive factor in making large assemblies because of distortion arising from relief of thermal stresses.

3. Program For The Next Quarter

- a) Complete 1600°F potassium exposure test of active metal-brazed ceramic-to-metal assemblies.
- b) Work on alternate seals particularly the application of metallic layers on ceramics by ion plating and chemical vapor deposition.
- c) Complete design of special test equipment for the high temperature testing of ceramic-to-metal seals.

B. TASK 2 - STATOR AND BORE SEAL

1. Summary of Technical Progress

- a) Stator model manufacturing and assembly was completed.
- b) Following assembly, the stator was given a 50 hour outgassing bake-out at 1100°F in a liquid-nitrogen-trapped diffusion-pumped vacuum furnace.
- c) Thermocouples were installed in the stator after the outgassing bake-out and then the stator assembly was installed in the thermal vacuum chamber.
- d) The logging of official endurance time at an 1100°F hot spot temperature began on November 19, 1965.
- e) Minimum cold chamber pressure attained after system bake-out was 1.1×10^{-10} torr. Chamber pressure when official endurance time was started was 4.2×10^{-7} torr. This pressure increased to 6.4×10^{-7} torr as final temperature stability in the stator was attained, and then began to decrease slowly.
- f) Final dimensions for the BeO bore seal tube and end plates were established with Eitel-McCullough.

2. Discussion

a. STATOR PHYSICAL AND ELECTRICAL DESIGN AND CONSTRUCTION

Figure IV-13 is a cutaway view of the stator assembly which shows the primary features of the design. The main frame is made from a Hiperco 27 (27% cobalt-iron) alloy forging, and the laminations are held in place in the frame by a retaining ring which is also made from a Hiperco 27 alloy forging. The magnetic stack consists of Hiperco 27 alloy laminations 0.008 inch thick, with a sapphire-like insulation coating of plasma-arc sprayed Linde A compound (99.995% Al_2O_3). Conductor wire is nickel-clad silver (20% nickel cross-section) coated with a 0.006 inch thick layer of Anadur, a refractory-oxide-filled E-glass fiber. Slot insulation is provided by ceramic (99% Al_2O_3) U-shaped channels (slot liners), spacers and wedges.

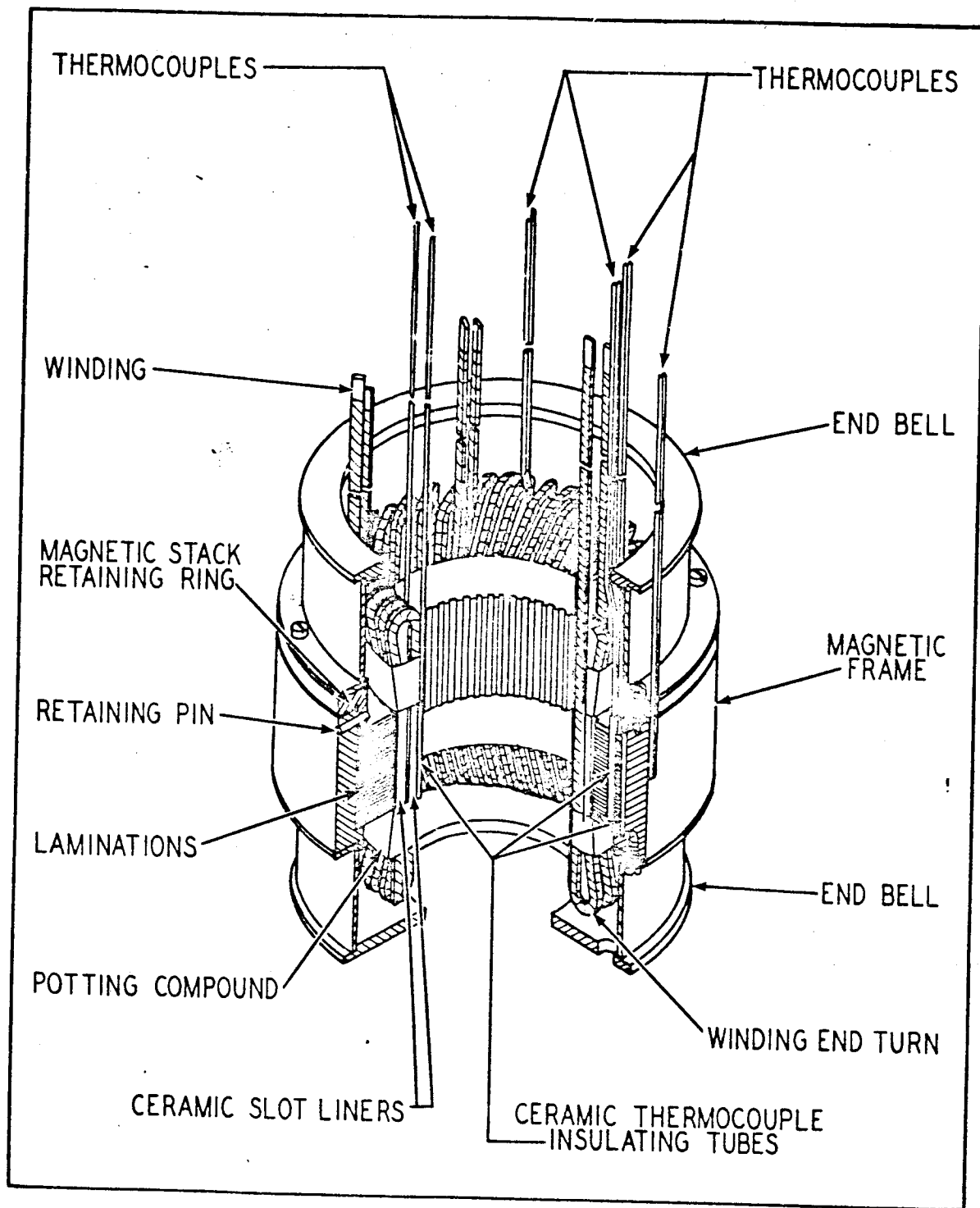


FIGURE IV-13. Cutaway View of Stator Without a Bore Seal

W-839 zirconia-base potting compound is used to fill small voids between the slot liners and the slots, and extends about 3/8 inch beyond the slot liner ends to provide winding support. Hollow ceramic tubes (99% Al_2O_3) are used as thermocouple insulators in the slot and stack areas. Two thermocouples are installed in slots in each winding. Additional pairs of thermocouples are located in the stack, between the stack OD and the frame, on the OD of the frame and on winding end turns. End bells are made from Hastelloy Alloy B, which is a non-magnetic material having a thermal expansion coefficient very similar to that of Hiperc 27 alloy. Average thermal expansion coefficient for Hiperc 27 from 72°F to 1100°F is 6.14×10^{-6} inch/inch - °F, while the coefficient for Hastelloy Alloy B from 72°F to 1200°F is 6.7×10^{-6} inch/inch - °F.

The lamination stack is representative of one of the two stator stacks of a 15 KVA, 12,000 rpm inductor generator and of the stator for a 12 horsepower, 12,000 rpm induction motor. The laminations have 36 teeth and slots which are proportioned approximately the same as those of an operating generator or motor. The a-c stator winding is similar to that in a three phase generator or motor. The winding is divided into three sections of twelve turns each, and the overlapping of the sections is similar to that which occurs between the phases of a generator or motor winding. Thus, it is possible to test the stator with a potential between windings and from winding to ground, the same as in an operating generator.

Rated frequency of the stator for design and test purposes is 400 cps to insure the availability of a reliable laboratory power supply for endurance testing. However, the stator could be tested at frequencies up to 1600 cps and higher, if required. The loss in the stator when current is passed through the winding is the I^2R loss plus a small amount of core loss. At frequencies higher than 400 cps, there will be a slight increase in losses, but at 1600 cps this increase will be less than 10 percent.

b. STATOR ASSEMBLY

After completion of all shop operations such as machining, punching, welding, plasma-arc spray and annealing, the detail stator parts were cleaned according to the cleaning specifications included in Appendix B of the third quarterly report. The only material not cleaned was the Anadur coated nickel-clad silver wire.

The stack was formed on a stacking arbor using 244, 0.008-inch thick, Hiperc 27 laminations with plasma-arc sprayed Al_2O_3 on one side of each lamination. The laminations were squeezed together by a 500 pound load and secured on the arbor. Total stack height after compression was 1.980 inches, giving a calculated nominal Al_2O_3 layer thickness of 0.000117 inch/lamination. Weight of the laminations was 12.6 pounds. The frame was heated to approximately 400°F and the stack was seated into place. After the frame had cooled to room temperature, the retaining ring was bolted and pinned in place. The stacking arbor was then removed from the stack. Figure IV- 14 shows the lamination stack installed in the frame with the retaining ring in place and the arbor removed (left assembly). The stack on the right side is the practice stack, showing one of the practice enamel covered copper wire windings in place. The cleaned tools in the foreground give some idea as to stack size. The stator frame outside diameter is eight inches. This picture was taken with the equipment sitting on the "clean" bench work table. Filtered air is blown across the work area from the filter bank visible in the upper part of the picture. Once parts had been cleaned, all further work on them was done at the clean bench, which provides a monitored atmosphere equivalent to or better than a Class 10,000 clean room as defined by Federal Standard No. 209, "Clean Room and Work Station Requirements, Controlled Environment".

Final coil forming procedures were developed using the Anadur insulated nickel-clad silver wire. Figure IV-15 shows the operator forming a winding with the test wire in front of the clean bench. The stiffness of the wire required shaping each coil to the installed radius prior to installation in the stator. W-839 potting compound was used to anchor the Al_2O_3 slot liners in the stack slots and to hold the Al_2O_3 thermocouple tubes in place. Figure IV-16 shows the windings installed in the stator prior to the Anadur insulation system bake-out

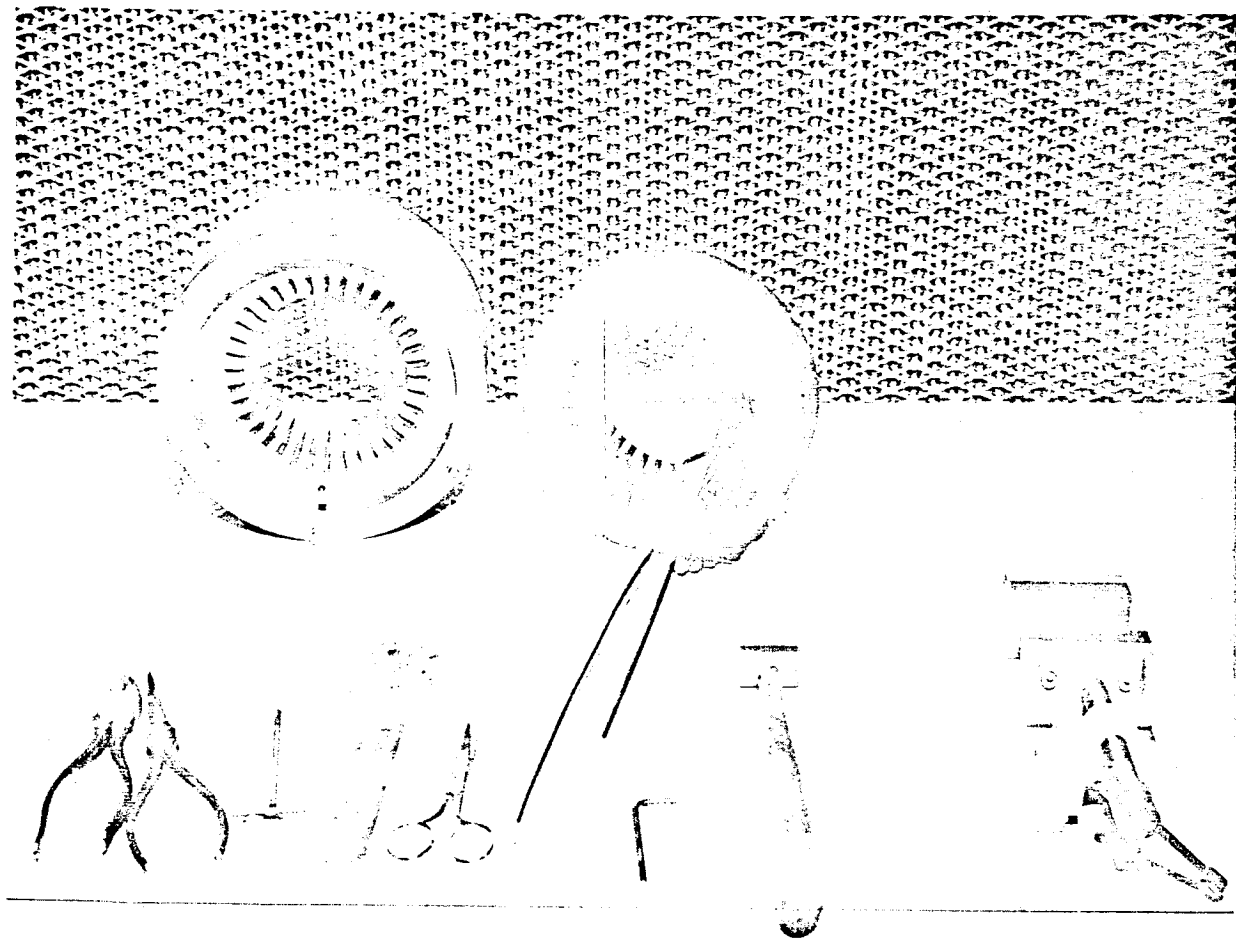


FIGURE IV-14. Test Stator Stack and Practice Winding Stator Stack

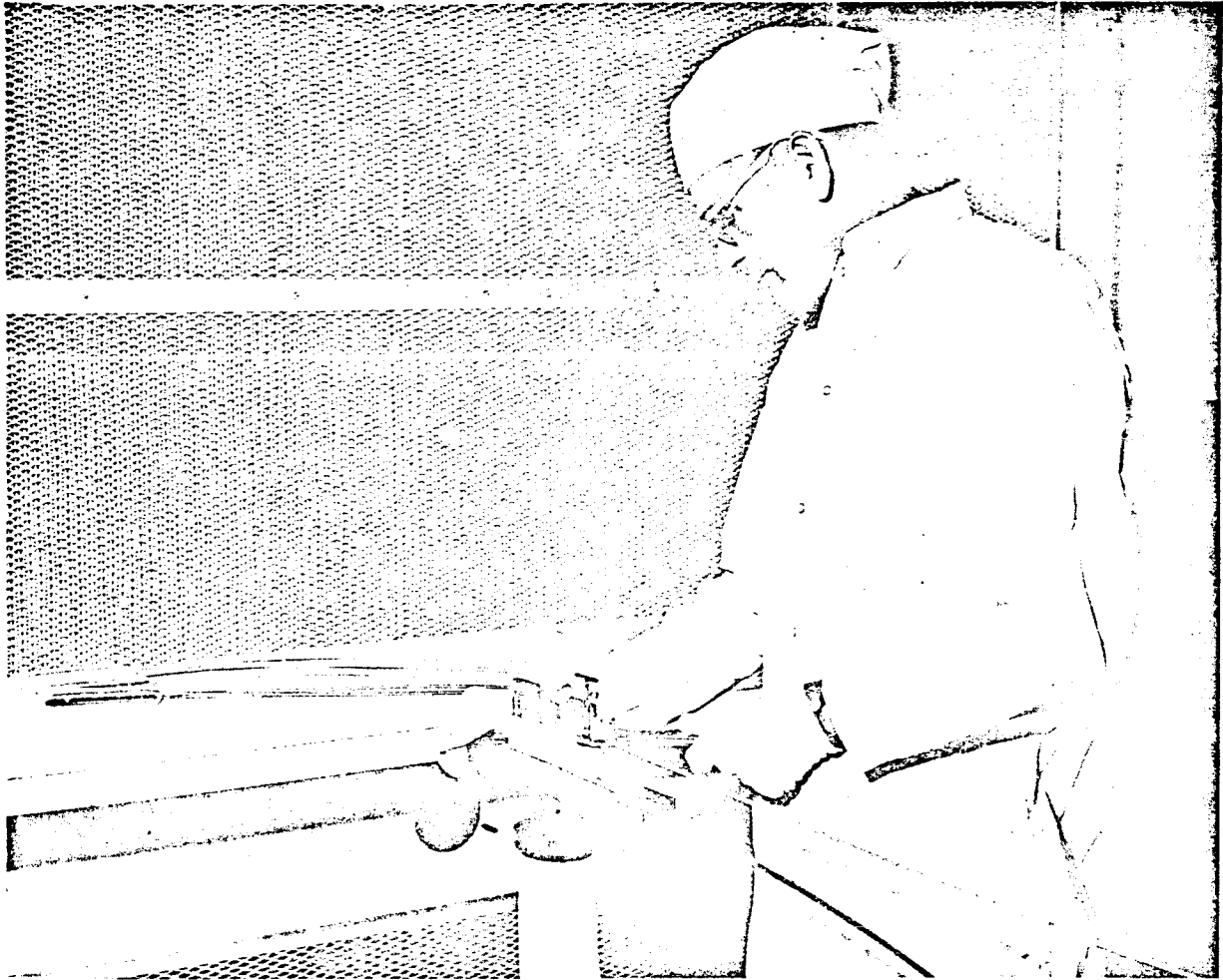


FIGURE IV-15. Operator Forming a Winding With Test Wire in Front of the Clean Bench

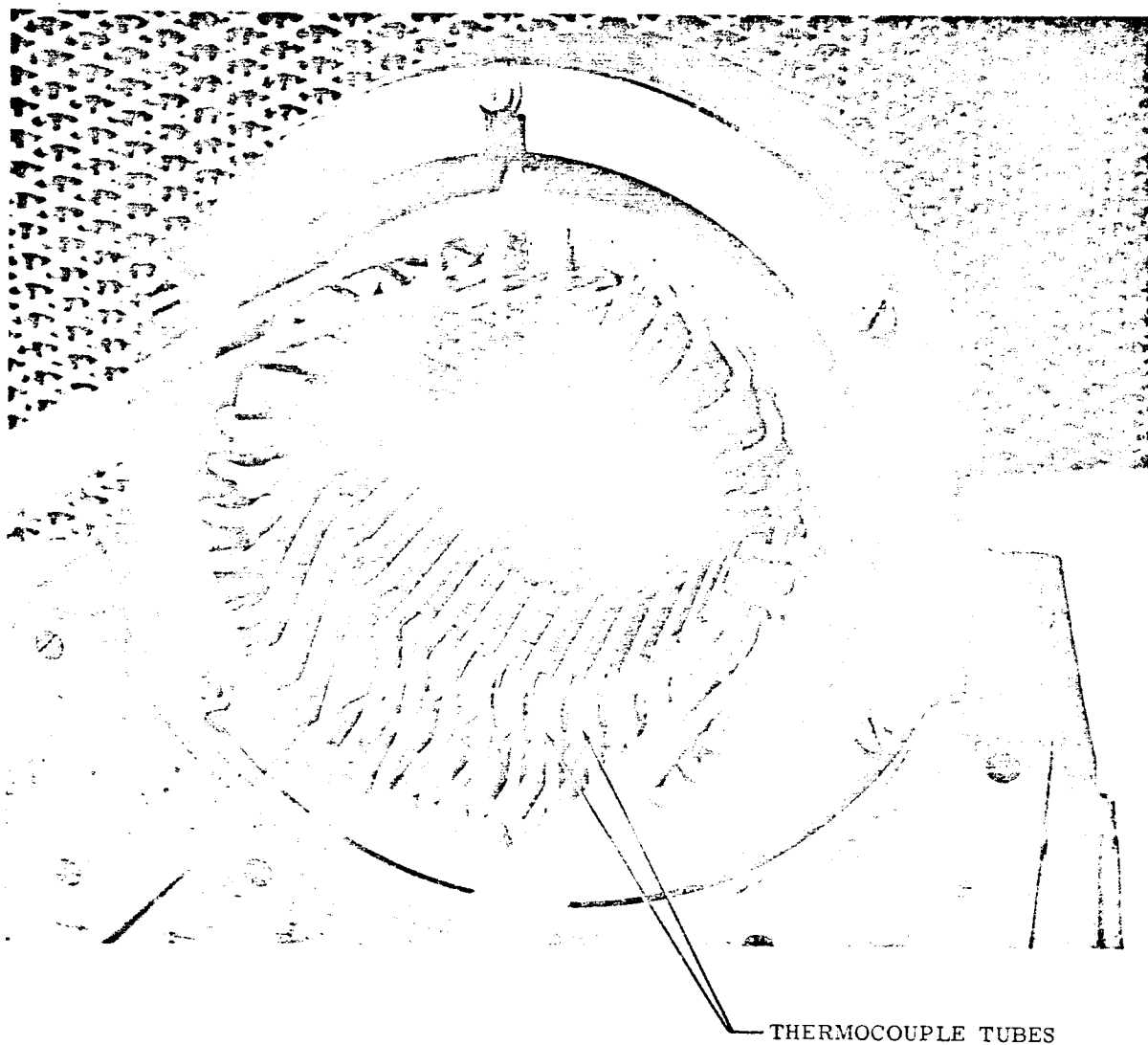


FIGURE IV-16. Test Winding Installed in Stator Prior to Anadur Bake-Out

cycle. The slot thermocouple tubes in one winding are indicated by arrows. The potting compound was baked out in air according to the following schedule:

Temperature (°F)	Time (hours)
Room Temperature	Overnight
125	1
150	1
190	2
220	2
350	2
450	2

This was followed by a bake-out and cure cycle for the Anadur insulation. This operation was carried out in air to the following time and temperature schedule.

Temperature (°F)	Time (hours)
350	2
550 - 600	16
750 - 800	4
1250 ± 25	1/2

Additional potting compound was added to the windings where they extended from the slot liners (approximately 3/8 inch out from the stack) and to hold alumina thermocouple tubes to four winding end turns. Thermocouple tubes were also added to the stack bore and in the lamination outside diameter marker slot. The stator was then put through another potting compound cure cycle.

The two Hastelloy Alloy B end bells were added to the stator assembly, along with the frame OD thermocouple retaining plate. Figure IV-17 shows the completed stator, except for the installation of thermocouples, sitting on three posts which were used to support the stator on the hearth plate in the thermal vacuum chamber. The discoloration of the stator frame occurred during the Anadur insulation bake-out period at 1250 ± 25°F in air. Stator assembly weight less thermocouples was 39.0 pounds.

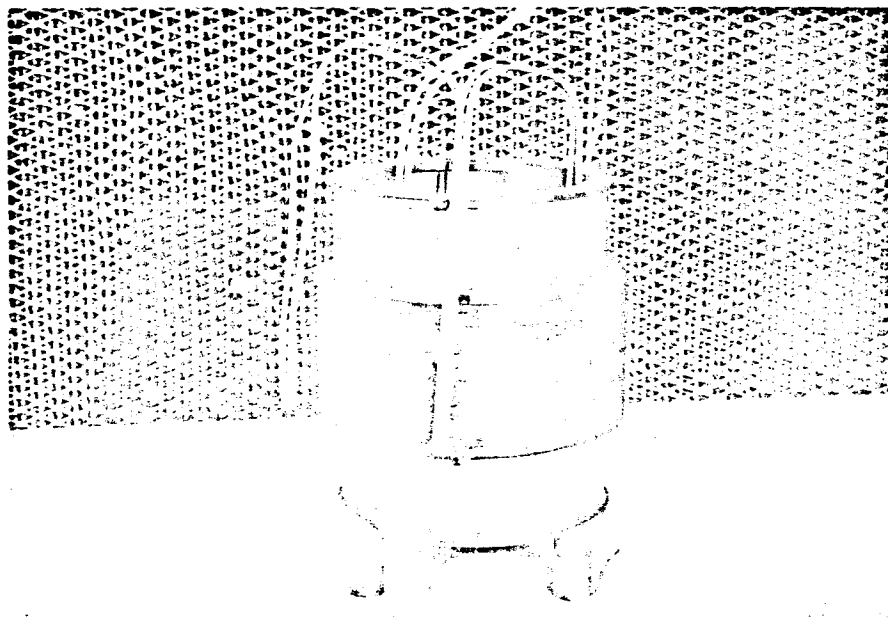


FIGURE IV-17. Stator Assembly on Furnace Supports

The stator assembly less thermocouples was installed in a liquid-nitrogen-trapped diffusion-pumped vacuum furnace for a preliminary degassing bake-out. After an equilibrium furnace temperature of 1100°F was established, the stator assembly was baked for 50 hours. Initial chamber pressure at equilibrium was 9.0×10^{-6} torr. At the end of 50 hours, the pressure had stabilized at 5.3×10^{-6} torr, at which point the furnace was turned off. After cooling down, the furnace pressure was 3.1×10^{-6} torr. The furnace chamber was back-filled with argon and then, for temporary storage, the stator was transferred to an argon filled bag containing dessicant envelopes, pending completion of a residual gas analysis scan on the No. 1 thermal vacuum chamber.

c. THERMOCOUPLE SYSTEMS

Thermocouples were positioned in the stator just before installation in the thermal vacuum chamber. Figure IV-18 shows the thermocouple dimensions. The reduced tip diameter version was used in the stator slots where space was at a premium. The wire system used was the Platinel II, a platinum-paladium-gold alloy manufactured by Engelhard Industries, Inc. The wires were encased in an Inconel sheath with 99% Al_2O_3 insulation between the wires and between wires and sheath. The thermocouple junction was isolated from the tip closure and the cold end terminals were vacuum sealed to the sheath. Before being shipped by the vendor, each thermocouple was pressurized externally with helium at 2000 psig, then leak checked with a mass spectrometer. This operation was followed by five thermal cycles to 750°F and individual thermocouple calibration. The welded thermal junction was also radiographed in two views 90° apart and perpendicular to the thermocouple axis. Except for the stator outside diameter thermocouples, each one was installed in an alumina tube in the stator to provide extra electrical insulation.

The vacuum chamber feedthroughs included one with a ceramic disc carrying 20 brazed-in hollow Kovar tubes having an inside diameter of 0.040 inch. After the stator assembly had been installed in the thermal vacuum chamber, each thermocouple was threaded out through a Kovar tube. An induction-brazed leak tight joint was formed between each thermocouple and its Kovar tube outside the furnace. Unused tubes were pinched off and sealed. This design resulted in a sealed thermocouple system with only the temperature junction located inside the thermal vacuum chamber. Thermocouple locations in the stator are discussed in Section IV.B.2.g.

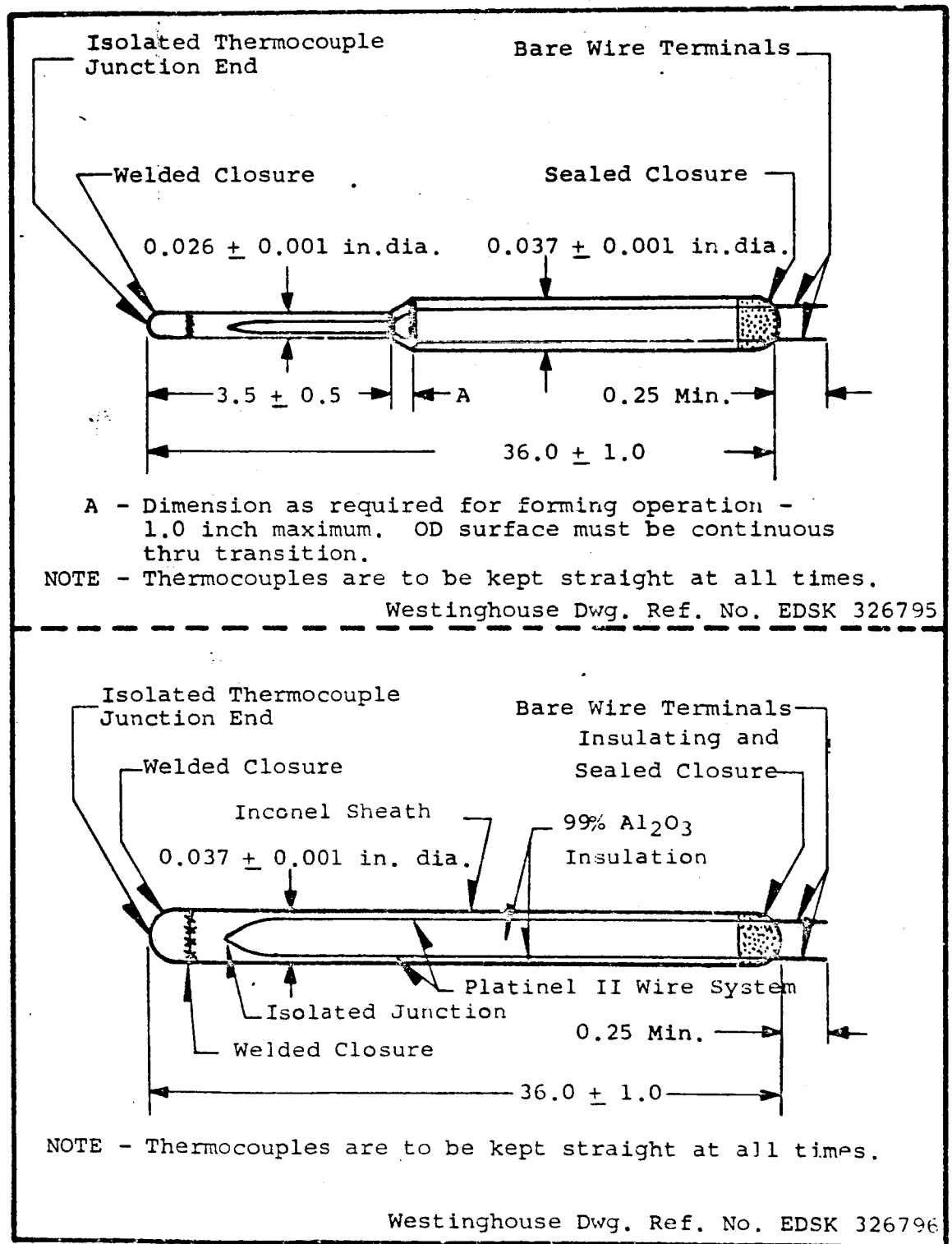


FIGURE IV-18. Single and Dual Diameter Sheathed Thermocouples
(Reference: Westinghouse D-Spec No. 709747)

d. THERMAL VACUUM CHAMBER INSTALLATION

The Varian No. 1 thermal vacuum chamber was evacuated in a clean, dry and empty condition and put through a 24 hour bake-out at 482°F (250°C). Residual gas analysis scans were taken with the chamber at 77°, 1100° and 1500°F to obtain background data. The chamber was then brought up to ambient pressure under argon preparatory to installing the stator assembly.

The clean bench was positioned in front of the chamber to serve as a work bench for the stator and to supply a filtered air flow across the chamber. Figure IV-19 is a cutaway drawing of the thermal vacuum chamber which shows the stator installed in the furnace hot zone. The chamber is of double wall construction with baffles between the walls to channel cooling water flow. The chamber top cover is also double walled to provide a path for cooling water. Thermocouples were installed in the stator at the clean bench, the stator support posts were bolted to the furnace hearth plate, and the stator was set in place on the posts inside the chamber. The stator winding leads were inserted in short lengths of hollow alumina tubing to insulate them as they passed through the top heat shields. Thermocouples and winding leads were then passed upward through perforations in the top heat shields, and the shields were set in place. The winding leads were brazed to OFHC copper feedthrough bus bars inside the furnace, using a bell jar with supporting frame and foil curtains to maintain an argon atmosphere for the brazing operation. Thermocouples were passed through the hollow Kovar tubes and brazed externally. Thermocouple and winding lead integrity was verified and the chamber was closed, evacuated and leak checked.

e. STATOR TEST CIRCUITRY

Figure IV-20 is a schematic showing the test circuitry for applying power to the stator windings. Three-phase power from a 400 cps, 292 volt a-c line-to-neutral generator capable of 312 KVA, is supplied into the test area through a 50 amp fuse in each phase. Voltage between phases is 505 volts a-c. Two three-phase reactive load banks are connected in phase series with each stator phase outside the test chamber to simulate the electrical load that normally would be supplied by a conventional generator. Each load bank has multiple taps to permit adjusting each phase current to the desired value.

Reactive loads are used rather than resistive loads so that stator winding current densities (amp/square inch) can be maintained at typical generator values without dumping an excessive amount of heat into the laboratory area.

Thermocouple leads are not shown in the schematic, but they were connected to a Honeywell multi-point recorder which can be set up to sequence readings continuously or on a timed cycle basis.

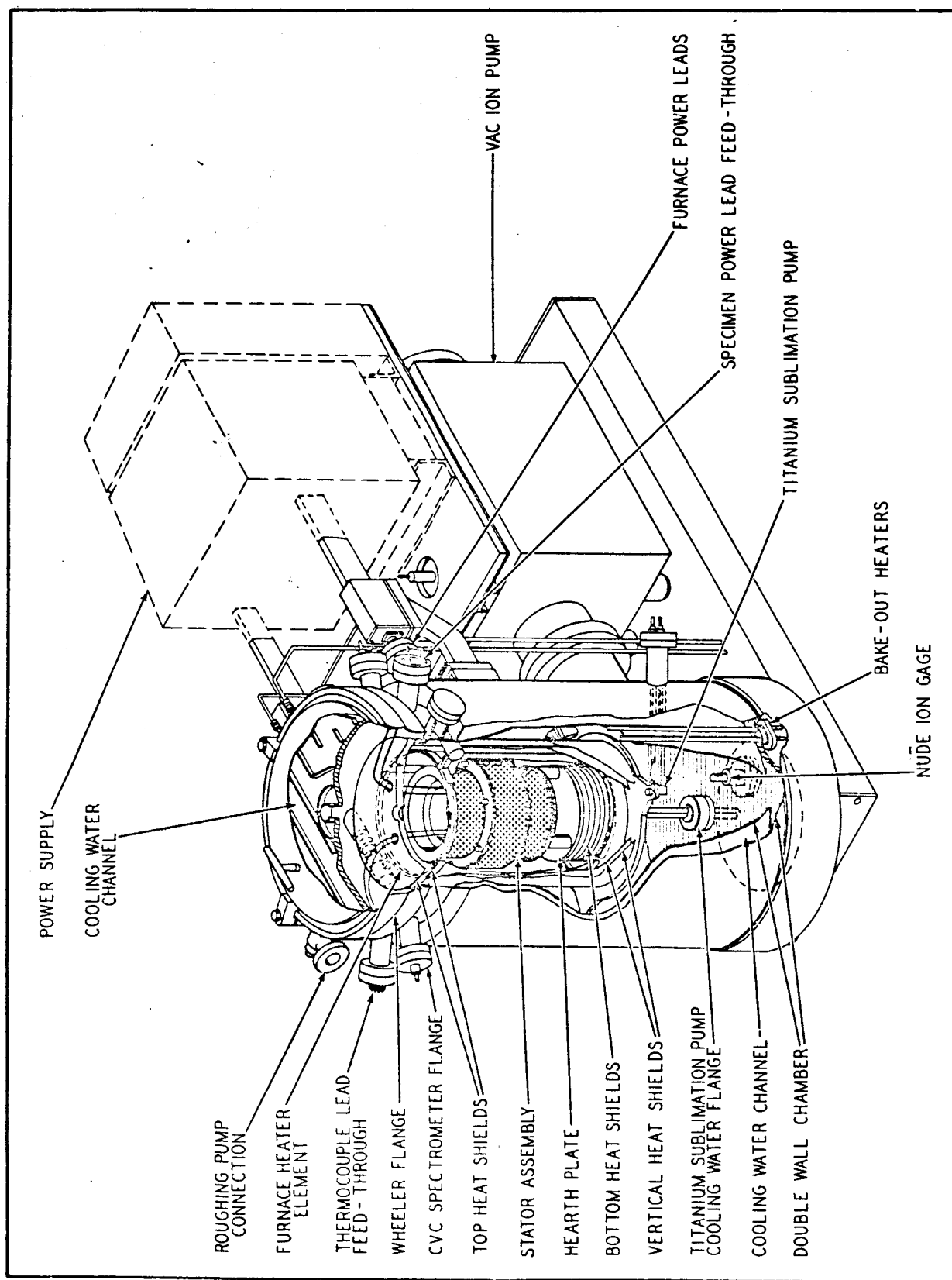


FIGURE I V-19. Cutaway View of Vacuum Furnace Showing the Stator Test Specimen Installed

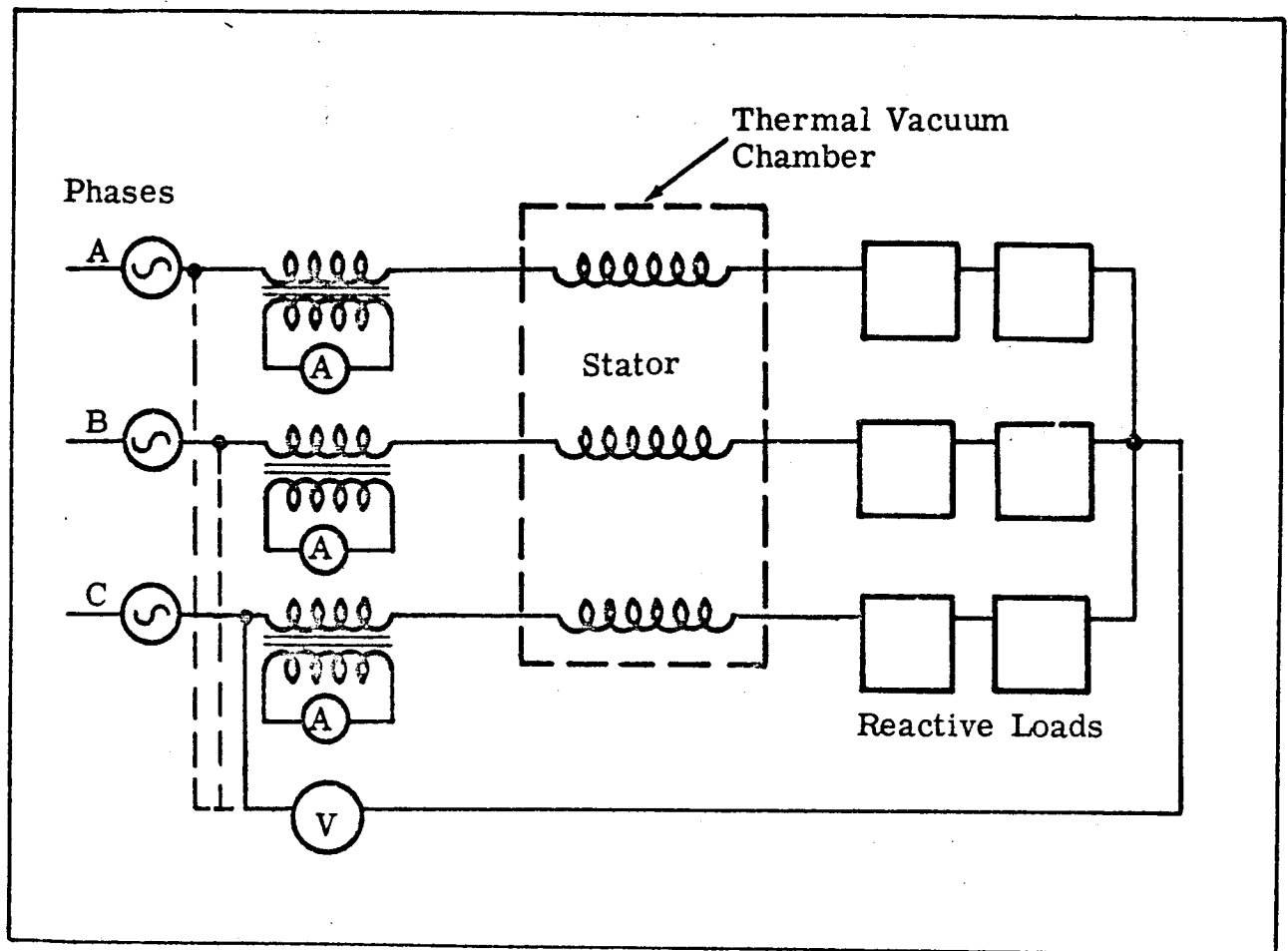


FIGURE IV-20. Schematic of Stator Electrical Hook-up

Figure IV-21 shows two Varian thermal vacuum chambers and a three element Varian Vac-Sorb roughing pump cart. Residual gas analyzer magnets and sensing elements are shown in their temporary position at each furnace. The stator assembly was installed in the furnace on the left. Figure IV-22 shows the control consoles for the two chambers. The residual gas analyzer is shown on the roll table to the left of the consoles.

f. STATOR TEST PROCEDURE

After electrical continuity of the winding leads and thermocouples was verified, the thermal vacuum chamber Wheeler flange was installed. The chamber was pumped down to approximately six microns and the ion-pump was started. Several titanium sublimation pump bursts were used to bring the chamber pressure down to the 10^{-6} torr range as indicated by a nude ion gauge. Thermocouple brazed joints were leak checked with helium and several joints required additional sealing. The titanium sublimation pump was then cycled, 40 seconds on, including warmup time, and 85 seconds off, for a nine hour period. System pressure continued to decrease after the leaks were sealed, and when the pressure reached a value of 3×10^{-8} torr, a 32-hour bake-out at 482°F (250°C) was started. The minimum cold pressure reached after bake-out was 1.1×10^{-10} torr. As mentioned earlier, residual gas analysis traces were taken with the chamber under vacuum at ambient temperature and at 1100° and 1500°F before the stator was installed. Additional traces were taken after stator installation at various stages of increasing stator temperature and corresponding chamber pressures. Traces are discussed in Section IV. B. 2. g.

Bench test static electrical measurements covering conductor resistance, d-c insulation resistance and a-c potential electrical leakage had been taken prior to installation of the stator in the chamber. (See Section IV. B. 2. g for data tabulations). These measurements were repeated at a cold chamber pressure of 1.1×10^{-10} torr to provide base line data under high vacuum conditions. Chamber pressure subsequently dropped to a minimum value of 8.2×10^{-11} torr before power was applied to the stator windings.

A current of 31.2 amps was applied to each winding with no furnace heater element power. When the average stator slot temperature reached a near-stable value of 450°F , static electrical tests were repeated. The average slot temperature (four thermocouples) leveled off at 451°F and a chamber pressure of 4.6×10^{-10} torr. With the stator winding current held constant, 400 amperes at 1.0 volt a-c was applied to the furnace heater element. This power setting turned out to

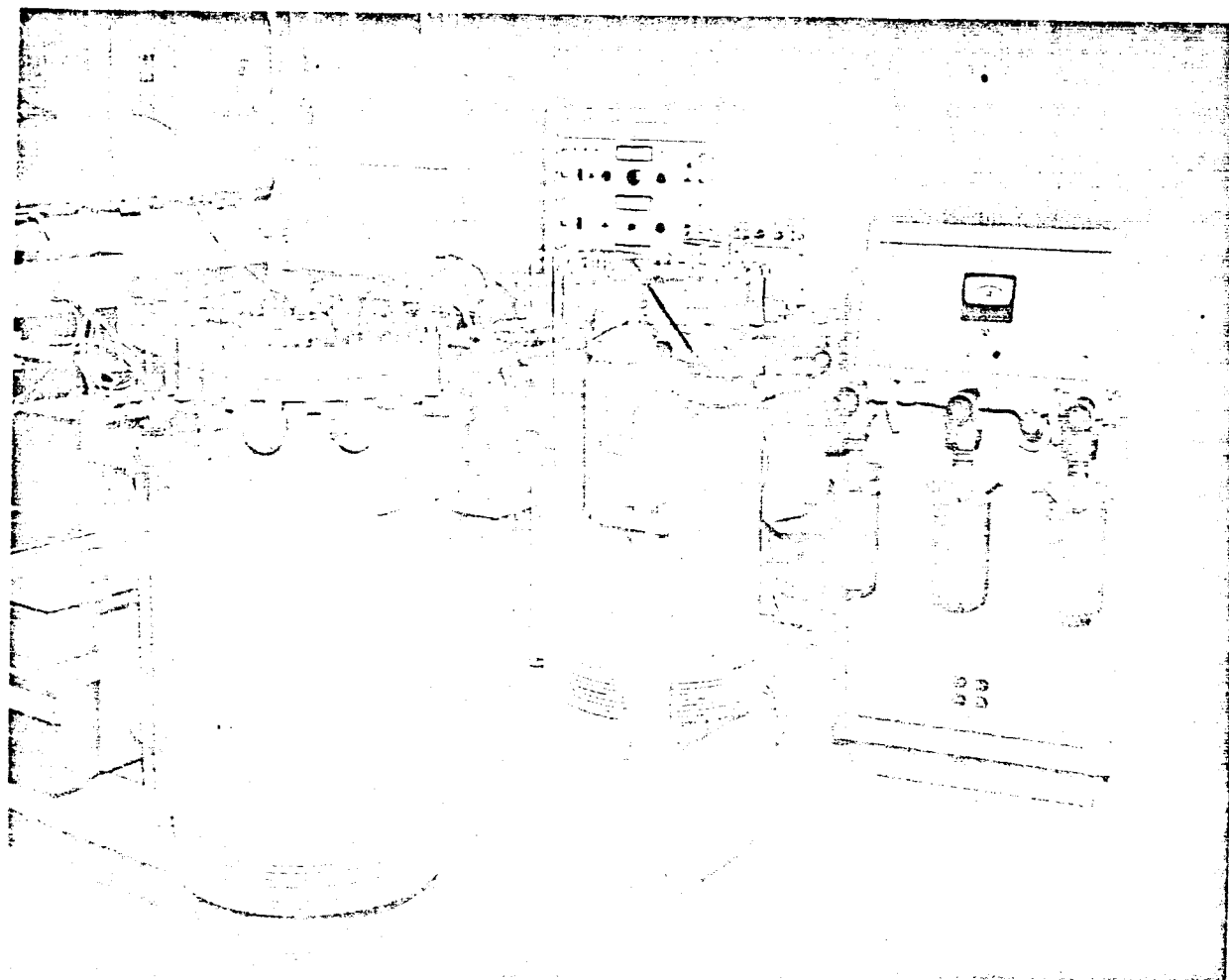


FIGURE IV-21. Two Varian Thermal Vacuum Chambers and a Three Element Varian Vac-Sorb Roughing Pump Cart

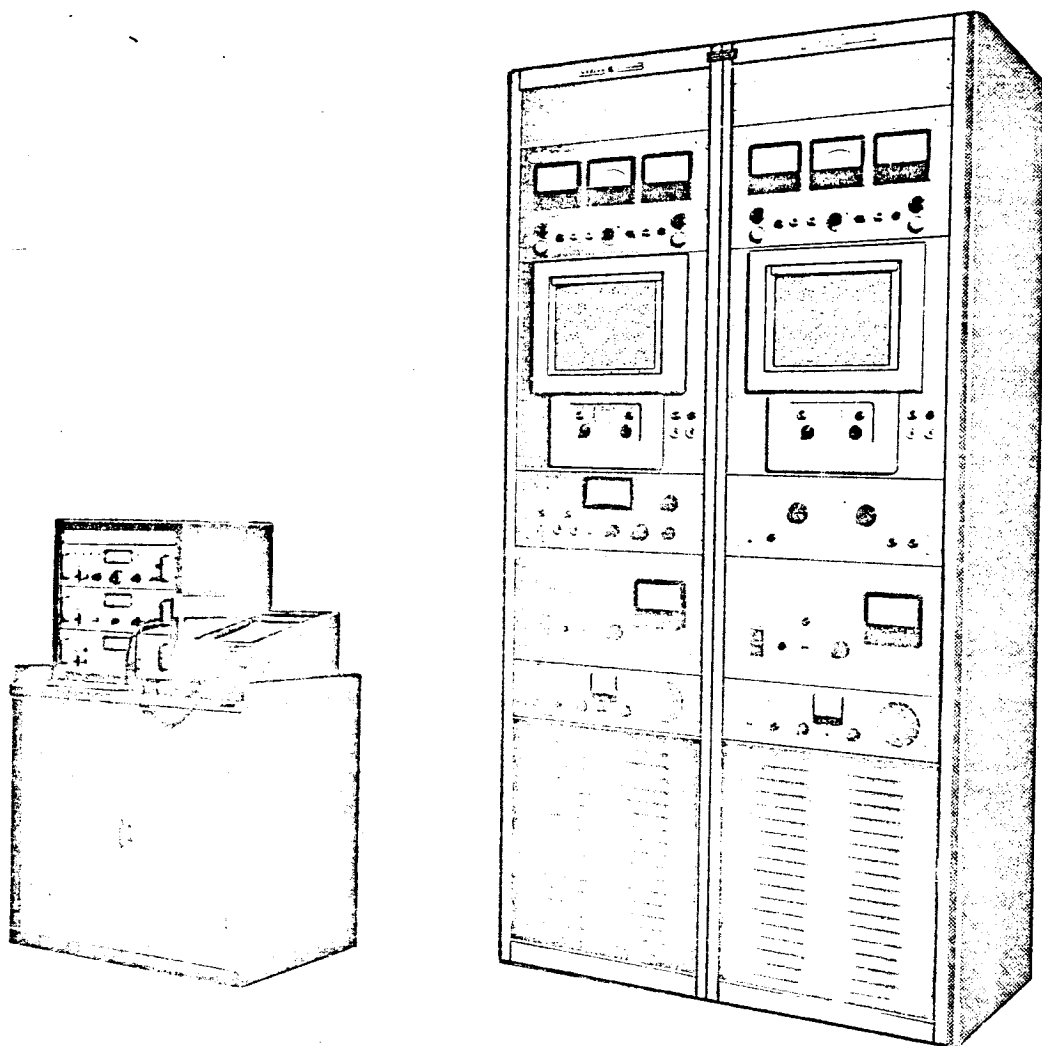


FIGURE IV-22. Varian Thermal Vacuum Chamber Control Consoles and Residual Gas Analyzer

be at the low end of the automatic temperature controller range, and current fluctuations were troublesome. Furnace power was subsequently increased to 440 amps at 1.4 volts which improved the controller stability. A set of static electrical readings was taken at a stable average slot liner temperature of 985°F.

The furnace power setting was maintained constant at 616 watts and the stator winding current was increased to 35.6 amperes per phase. In approximately 18 hours, all the stator thermocouples were showing stable readings, with a hot spot reading of 1040°F. Winding current was increased to 41.2 amperes per phase with furnace power held constant at 616 watts. When the hot spot temperature (average of four slot liner readings) reached 1092°F and was approaching stability, the logging of official endurance time at temperature was initiated. Static electrical measurements were taken when the hot-spot temperature reached 1098°F. Endurance time accumulated in the last month of the fourth program quarter amounted to 172 hours.

g. DATA EVALUATION

The primary purpose of this test is to evaluate generator materials under high-temperature and high-vacuum conditions. Power losses associated with a conventional generator should be duplicated or synthesized when testing a stator only, if the materials evaluation data is to be useful for generator design.

Winding joule heating (I^2R) losses in a conventional machine can be duplicated in the stator. The test current being used gives a phase current density of 41.2 amperes divided by a conductor cross-section area (silver and nickel) of 0.0123 square inches, or 3350 amperes per square inch. Higher current densities are used in stationary and aircraft type generators, but the increase in conductor resistance with increased wire temperature must be considered. The I^2R loss in the test stator is comparable to that found in a conventional machine.

Another power loss associated with a conventional generator is magnetic core loss. In a stator alone, the core loss is less than in an operating generator, because it is not possible to have normal flux density without a rotor. Reduced core losses and other minor losses that could not be duplicated in the stator alone are compensated for by additional heat supplied by the furnace heater element.

The heater element serves a second function, in that it is the primary radiation shield that establishes the desired hot spot test temperature.

Figure IV-23 is a plot of thermal vacuum chamber nude ion gauge pressure against time, from start-up of the ion pump after chamber evacuation until stator hot-spot temperatures became stable and official endurance time was started. The first 65 hours after pump-down were involved in leak checks and in putting the system through a 32 hour bake-out cycle at 250°C. Chamber pressure decreased slowly during bake-out and at a more rapid rate during the cooling down period. For the next 45 hours, chamber pressure was pulled down using the ion pump only. Several leak checks were made during this period. At approximately 110 and 115 hours, titanium sublimation pump bursts (TSP) were applied to help establish a base pressure level. The ion pump was turned off briefly at 133 hours so recorder control jacks could be attached to the back of the ion pump control unit. This shutdown resulted in a 2-1/2 decade pressure burst, but recovery was rapid when the pump was turned back on. At 136 hours, a current of 41.2 amps at 290 volts a-c was applied to each stator phase winding. After 2-1/2 hours, the average stator slot temperature (average of four thermocouples) has risen to 303°F and did not show any indication of leveling off. Stator power was shut off and reapplied the next morning (155th hour). When slot temperature reached 400°F, the stator power was shut off briefly to adjust the load banks for phase currents of 31.2 amps per phase. The slight drop in slot temperature which occurred while the power was off shows as a small and temporary decrease in chamber pressure. Slot temperature leveled off at 445°F and chamber pressure rose slowly with time to a value of 1×10^{-9} torr (200th hour). Two titanium sublimation pump bursts were followed by a brief stator power shutdown to obtain stator electrical measurements. In the 209th hour, 400 watts of power was applied to the chamber heater element. Chamber pressure rose quite rapidly and a titanium burst was used to speed up stabilization. In the 212th hour, an unplanned heater element power excursion occurred which caused a further chamber pressure increase. Heater power was reset to 616 watts and the furnace control was shifted from manual to automatic. A low "on" time TSP cycle was initiated to help reduce chamber pressure. At 288 hours, stator power was shut off for electrical measurements. This was followed by a winding current increase from 31.2 amps to 35.6 amps. The pressure rose as the average stator slot temperature increased. In the 307th hour, the stator phase winding current was increased to 41.2 amps per phase, which was the planned test value. When the average stator slot temperature reached a value of 1092°F, official endurance time was started.

Figure IV-24 is a plot showing chamber pressure vs. time during the 172 official test hours completed in the fourth program quarter. The points which were plotted were for stable conditions, to show the trend

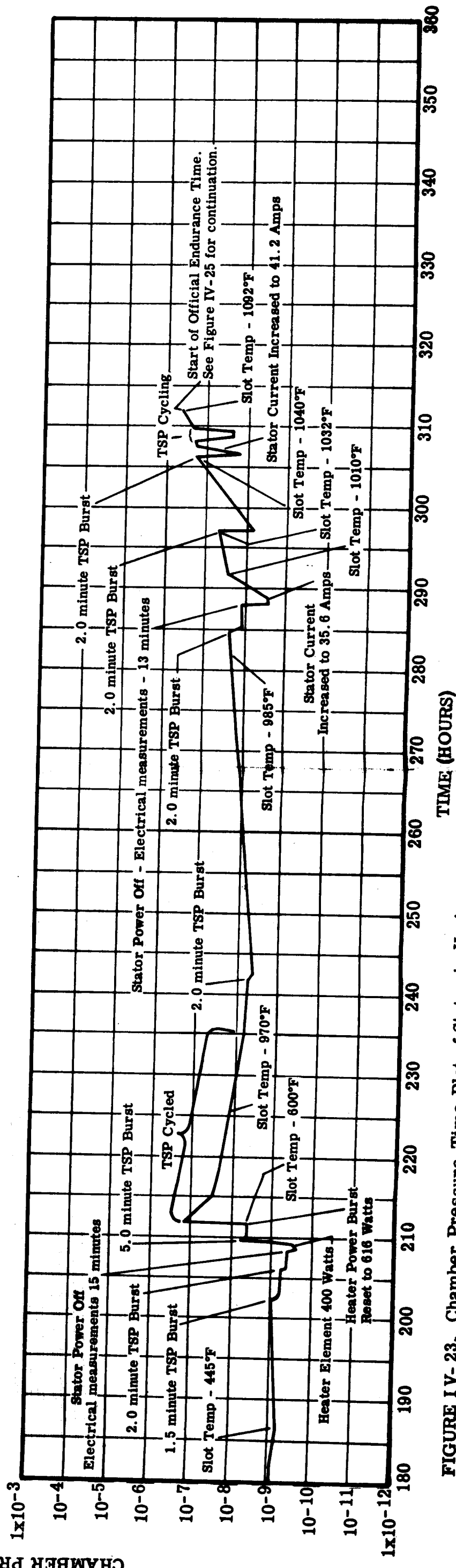
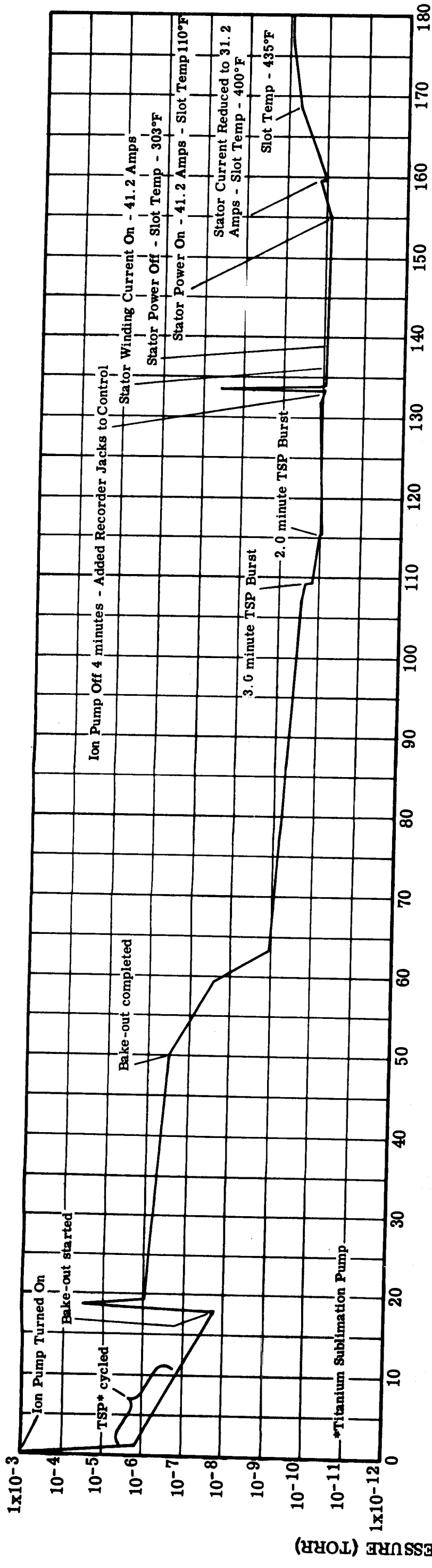


FIGURE IV-23. Chamber Pressure-Time Plot of Stator in Varian Chamber No. 1

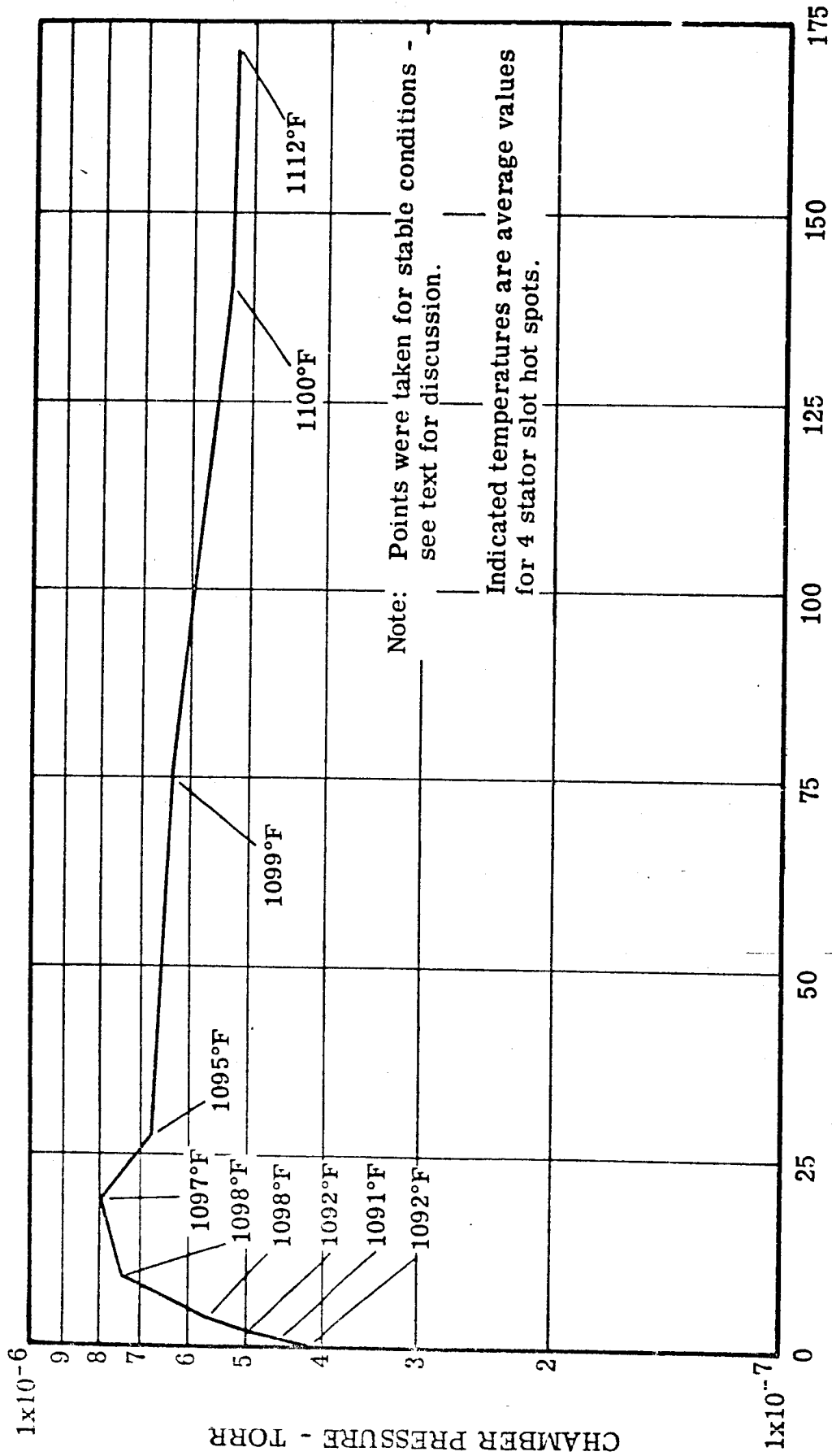


FIGURE IV-24. Chamber Pressure - Endurance Time Plot for Stator

of pressure level with time. Brief pressure transients were introduced from time to time by applying titanium bursts, which caused a rapid pressure reduction of as much as a decade. In every case, the pressure increase was as rapid as the reduction, as soon as the titanium was used up, with no apparent change in the existing stable pressure level.

Table IV-6 is a tabulation of electrical measurements taken at various times as the stator assembly was completed and then brought up to temperature in the thermal vacuum chamber. The conductor resistance increased approximately 2.5 times in going from room temperature to an average slot temperature of 1098°F. The conductor insulation resistance improved considerably, both phase-to-phase and phase-to-ground, in going from room ambient pressure and temperature to high vacuum at room temperature. The a-c potential test leakage current also showed a marked reduction in going from room ambient to vacuum conditions. The major reason for these changes was the elimination of most of the water vapor which was present during bench testing. The first set of vacuum readings was taken after system bake-out at 482°F (250°C). The insulation resistance decreased as the stator temperature was increased. The a-c leakage current increased as stator temperature increased. All these electrical tests will be repeated on a regular basis to observe changes in operation at high-temperature and under high-vacuum conditions.

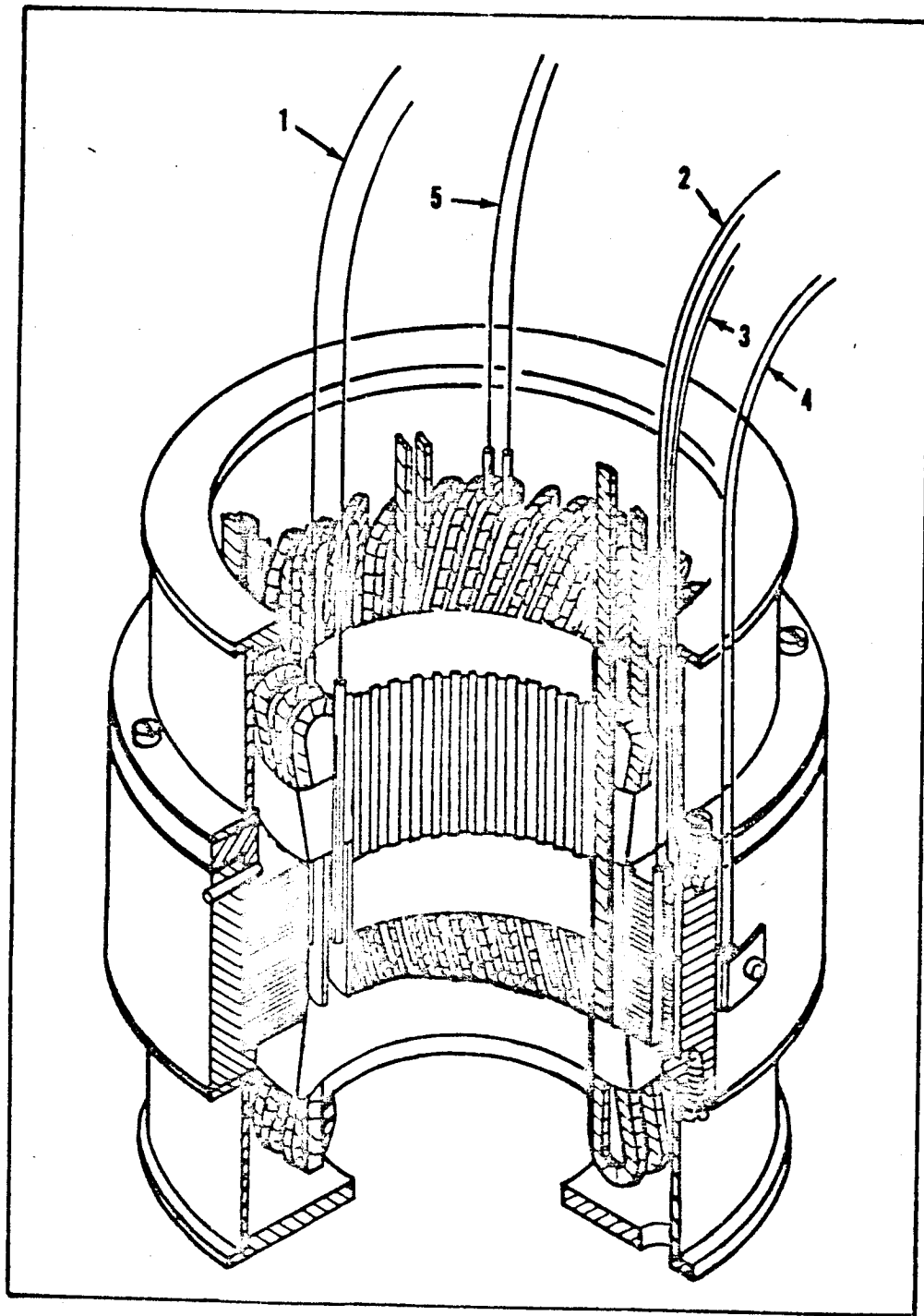
The calculated winding I^2R loss at 1098°F is 61.2 ohms per phase, or 183.6 ohms total for the stator. This is based on a winding current of 41.2 amps per phase and a resistance of 0.036 ohms per phase.

Figure IV-25 is a sketch showing the location of thermocouples in the stator. Sixteen thermocouples were installed before the stator was put into the thermal vacuum chamber. Six were lost during installation, primarily because of difficulties in obtaining good induction brazed joints between the thermocouples and Kovar tubes in the 20-tube chamber feedthrough. Changing to an 8-tube feedthrough on the second test has eliminated most of these difficulties. Pairs of thermocouples had been installed at each location as a precaution in case of installation problems, and each sensing location has at least one good sheathed thermocouple.

Table IV-7 is a tabulation of temperature distributions that occurred as stator winding current was increased and power was added to the furnace heater element. The table also covers the first 172 hours of endurance time. For every condition shown, the stator slot thermocouples recorded the highest temperatures. It had been anticipated that winding end turn temperatures would be nearly as high as slot temperatures. Radiation from the end turns to the furnace top heat shields is sufficient

TABLE IV-6. Electrical Measurements of Stator Assembly

Measurement	Bench Test Room Ambient Pressure 82°F		In Thermal Chamber 1.1x10 ⁻¹⁰ torr 78°F		In Thermal Chamber 5.4x10 ⁻¹⁰ torr 425°F Hot Spot		In Thermal Chamber 1.2x10 ⁻⁸ torr 995°F Hot Spot		In Thermal Chamber 8.6x10 ⁻⁹ (After TSP Burst (a) 1100°F Hot Spot	
	Ohms	Megohms	Ohms	Megohms	Ohms	Megohms	Ohms	Megohms	Ohms	Megohms
Winding Resistance										
Phase A-A	0.0145	10	0.0135	>2x10 ⁶	0.0195	>2x10 ⁶	0.0356	1.25x10 ⁴	0.036	7
Phase B-B	0.0144	10	0.0132	>2x10 ⁶	0.0205	>2x10 ⁶	0.0355	1.25x10 ⁴	0.036	6.5
Phase C-C	0.0145	9	0.0135	>2x10 ⁶	0.020	>2x10 ⁶	0.0356	1.25x10 ⁴	0.0358	7
Insulation Resistance										
Phase A-B	500	4.6	500	2x10 ⁶	500	1.2x10 ⁴	500	8	500	3.5
Phase A-C	500	5	500	2x10 ⁶	500	1.2x10 ⁴	500	10	500	3.8
Phase B-C	500	4.7	500	2x10 ⁶	500	1.2x10 ⁴	500	8	500	3.4
A-Ground	500		500		500		500		500	
B-Ground	500		500		500		500		500	
C-Ground	500		500		500		500		500	
Potential Test										
Phase A-B	60 cps Volts a-c 500	μA 94	60 cps Volts a-c 500	μA 6	60 cps Volts a-c 500	μA 2	60 cps Volts a-c 500	μA 88	60 cps Volts a-c 350	μA 98
Phase A-C	500	94	500	7	500	2	500	88	350	98
Phase B-C	500	98	500	7	500	1	500	86	350	98
A-Ground	500	175	500	16	500	6	250	82	150	93
B-Ground	500	170	500	16	500	6	250	80	175	94
C-Ground	500	175	500	18	500	6	250	84	150	94
(a) Titanium Sublimation Pump										



Legend - Page 207

FIGURE IV-25. Stator Cross Section Showing Thermocouple Locations and Junction Positions

KEY TO FIGURE IV-25

No.	Qty. Installed	Description
1	6	Slot Liner - 2 per phase "B" Phase Thermocouple lost during assy.
2	2	Stack Bore Tube
3	2	Lamination - Frame Slot One lost during assy.
4	2	Frame OD One lost during assy.
5	4	"B" and "C" Phase End Turns "B" phase lost during assy.

TABLE IV-7. Stator Temperature Distributions

Winding Current - AC Amps/ Winding	Volts AC Per Winding	Stator Thermocouple Temperatures - °F						Chamber Pressure (torr)	Furnace Power (watts)	Date	Endur- ance Time (hours)
		Stator Slot . (average)	Winding End Turn (average)	Stack Bore Tube (average)	Lamina- tion Frame Slot	Frame OD	Δ T Slot to Frame OD				
31.2	290	451	437	430	415	415	36	4.6x10 ⁻¹⁰	0	11-19-65	
31.2	290	986	980	980	975	980	6	1.2x10 ⁻⁸	615	11-22-65	
35.6	290	1041	1008	1021	1022	1022	19	1.9x10 ⁻⁸	615	11-23-65	
41.2	290	1092	1060	1067	1065	1065	27	4.2x10 ⁻⁷	615	11-23-65	0
41.2	290	1099	1069	1075	1074	1071	28	6.4x10 ⁻⁷	615	11-26-65	75
41.2	290	1112	1078	1090	1091	1082	30	5.4x10 ⁻⁷	615	11-30-65	172

to reduce temperature by approximately 30°F at the 1100°F hot-spot operating temperature. The frame outside diameter temperature was higher than the end turn temperature because the frame is radiating primarily to the furnace heater element rather than to unpowered heat shields. The first line of the data, taken before power was applied to the furnace element, shows a ΔT of 36°F between slot and frame outside diameter. Further temperature distribution analysis and an effort to calculate heat flow and heat transfer coefficient from the slot will be included in the next quarterly report.

Analysis of the residual gases in the stator chamber, as well as the chamber used for the transformer and solenoids in Tasks 3 and 4, was conducted using a Consolidated Electrodynamic Corporation Model 21-614 residual gas analyzer (RGA). Two analyzer tubes were used, one connected to each chamber. Traces of peaks in the mass range from 2 to 150 were obtained for furnace atmospheres at different temperatures and pressures. As mentioned previously, RGA peak traces were obtained with the furnaces empty at temperatures of 77°, 1100° and 1500°F. The test specimens were then installed in their respective furnaces and residual gas mass peak traces were taken at temperatures up to the 1100°F hot-spot level, with the specimens energized and non-energized.

The residual gas mass spectra obtained are complex in some scans. A computer matrix program is presently being programmed to identify and assign values to the mass peaks observed. The principal mass peaks contributing to the total pressures measured on the chamber nude ionization gauges are due to CO₂, N₂, A, H₂O, and H₂. Masses beyond the 44 m/e of CO₂ indicate the presence of some organic materials. The occurrence of the higher masses necessitates a more thorough mathematical treatment before numerical partial pressure values can be assigned.

3. Program for Next Quarter

- a) Continue the stator endurance test with a hot spot temperature of 1100°F.
- b) Develop a residual gas analysis computer matrix to better identify constituents.
- c) Work on a stator heat flow model within the limits of temperature instrumentation.

- d) Review the stator design for changes needed in a 1400°F hot-spot stator model.
- e) Review the bore seal and 1400°F stator designs for compatibility.
- f) Begin construction of a 1400°F stator model.

C. TASK 3 - TRANSFORMER

1. Summary of Technical Progress

- a) Transformer model manufacture and assembly was completed.
- b) After assembly, the transformer was given a 43 hour outgassing bake-out at 1100°F in a liquid-nitrogen-trapped diffusion-pumped vacuum furnace.
- c) Thermal vacuum chamber installation of the transformer was completed and chamber pump-down and bake-out were carried out.
- d) Minimum cold chamber pressure attained after system bake-out was 4.6×10^{-10} torr.
- e) Base line transformer electrical measurements and chamber residual gas analysis scans were obtained.

2. Discussion

a. TRANSFORMER PHYSICAL AND ELECTRICAL DESIGN AND CONSTRUCTION

Figure IV-26 is a cutaway view of the transformer which shows the basic design features. The core is made from E-I style Hiperco 27 alloy laminations 0.008 inch thick, with plasma-arc sprayed alumina (Linde A - 99.995% Al_2O_3) as the interlaminar insulation (same as used on stator laminations). The windings are formed around a ceramic 99.5% Al_2O_3 spool which provides insulation between the windings and the center leg of the core. Alumina end plates and channels provide insulation between the winding ends and sides and the laminations. Non-magnetic alloy strips are used outside the laminations to provide lamination support. The laminations and support strips are held together by through-studs, ceramic washers and lock nuts.

Pairs of thermocouples are installed between the primary winding and ceramic spool and between the two windings. The stack has been divided into two halves by ceramic strip spacers so that thermocouples can be buried in the core.

The transformer design is rated at 1 KVA at 400 cps with 600 volts on the primary and approximately 30 volts on the secondary. A frequency of 400 cps was chosen because of the availability of 400 cps power for

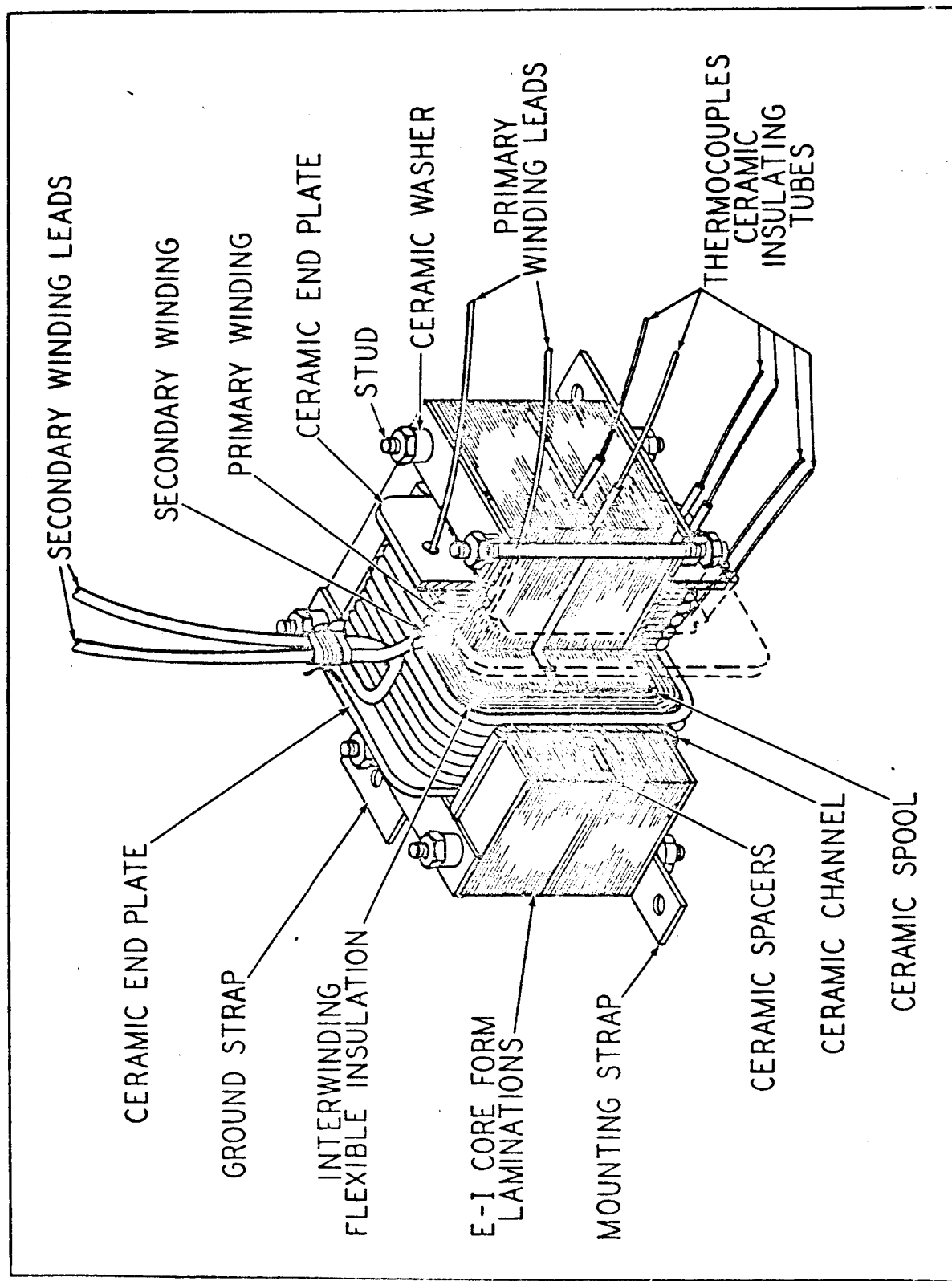


FIGURE IV-26. Cutaway View of Transformer

lab testing, and because Hiperco 27 alloy was available in 0.008 inch thickness only, a thickness best suited for 400 cps. The transformer can be operated at higher frequencies with little change in losses provided the voltage is maintained at rated value. This 600 volt a-c single-phase design is representative of the technology for a three-phase transformer having the same phase voltage which, when coupled in a wye network with a full-wave rectifier system, would provide 1400 volts d-c.

b. TRANSFORMER ASSEMBLY

When all shop operations had been completed, the transformer parts were cleaned according to the cleaning specifications included in Appendix B of the third quarterly report. The only material not cleaned was the Anadur coated nickel-clad silver wire.

The first transformer subassembly required was the winding spool. Figure IV-28 shows the 99% alumina spool, alumina end plates, alumina thermocouple tubes and the primary and secondary windings in place. The end plates were attached to the spool by means of Pyrocera #45 cement, a nucleating glass that fuses at approximately 1225°F and changes to a polycrystalline structure at 1400°F. The spool subassembly was fitted to a rectangular winding arbor to provide support for the ceramic spool and end plates during the winding operation.

The primary winding was wound by hand using 0.032 inch diameter nickel-clad silver wire coated with Anadur insulation 0.006 inch thick. The winding consisted of four layers with 37 turns in each layer plus one layer with 26 turns. Winding layers were separated by 0.010 inch thick layers of 3M Company Burnil CM-2 flexible sheet insulation which is a synthetic fluorophlogopite mica paper. Four layers (0.040 inch total) were used between the primary outer layer and the secondary winding. The secondary winding consisted of one 10 turn layer of 0.144 inch diameter nickel-clad silver wire with a 0.006 inch thick coating of Anadur insulation. The large outside diameter ceramic thermocouple tubes (99% Al_2O_3) were wound in place inside the innermost primary winding layer and the smaller tubes were installed at the secondary winding inside diameter.

E-I core form Hiperco 27 laminations 0.008 inch thick were plasma-arc sprayed with alumina (Linde A) on one side prior to assembly into the stack. This is the same interlaminar insulation system that was used on the stator laminations with a coating thickness of approximately 0.0001 inch. Figure IV-28, which was taken after the Anadur insulation bake-out, shows the laminations installed in the winding as-

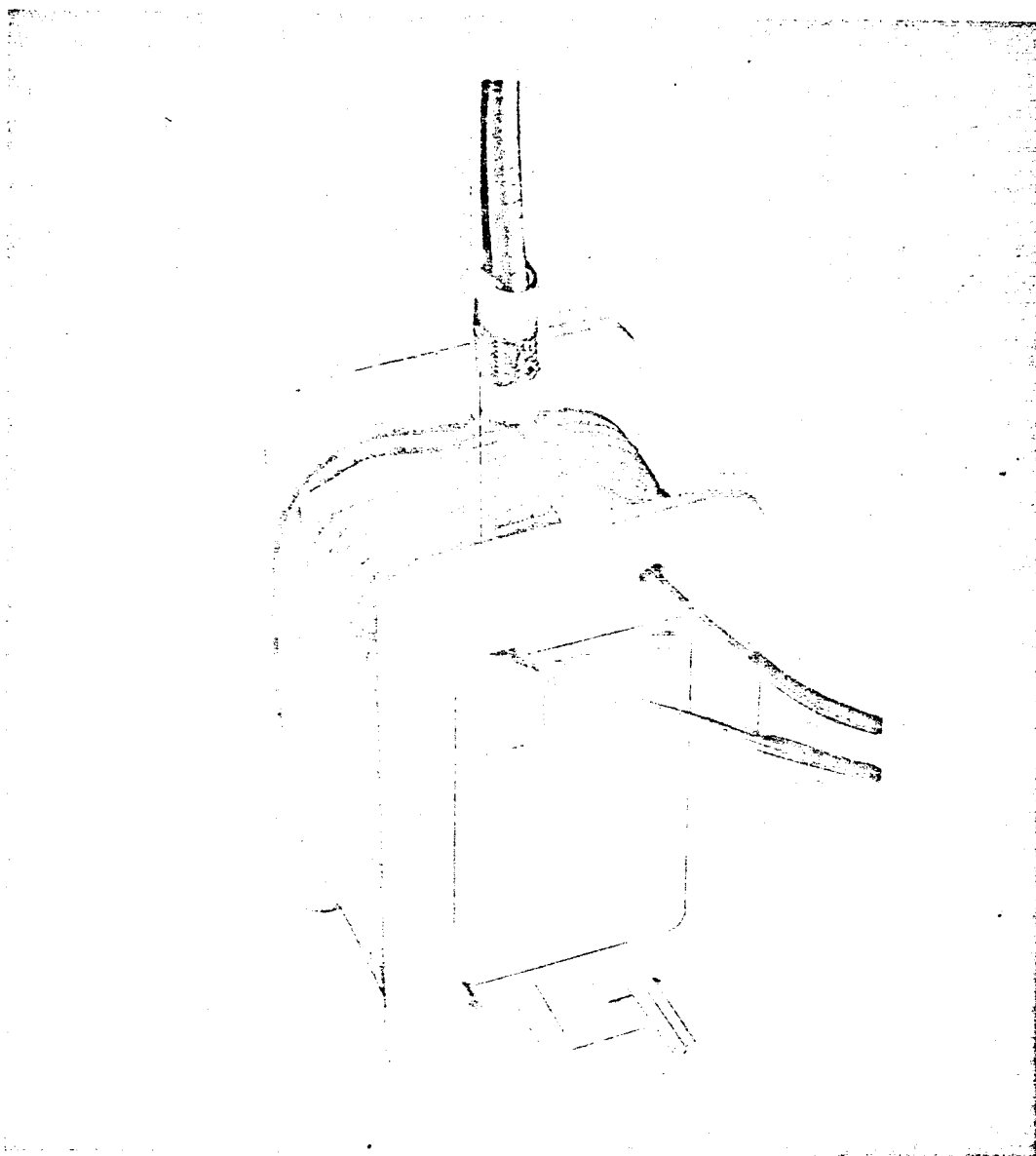


FIGURE IV-27. Transformer Spool Assembly and Windings

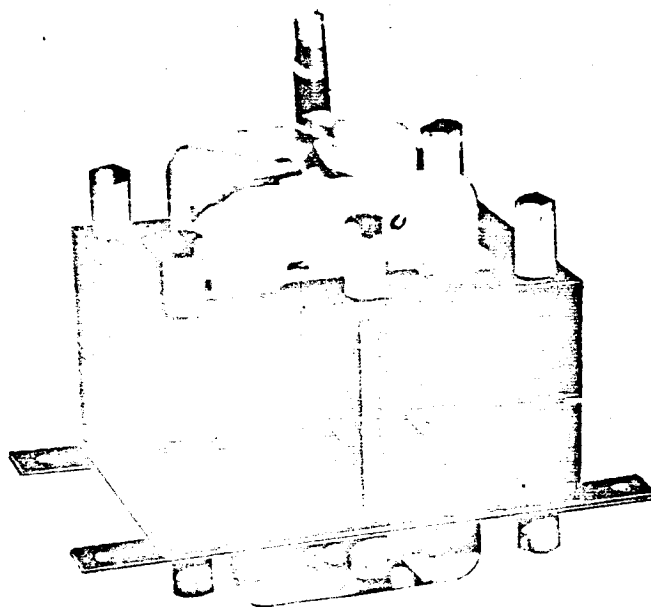


FIGURE IV-28. Transformer Assembly Less Thermocouples

sembly. The stack consisted of 230 laminations divided into two sections by alumina spacers and thermocouple tubes. Hastelloy Alloy B plates 0.063 inch thick were used on each side of the stack to provide stiffness. Through-studs, alumina washers and nuts were used to hold the stack together. The studs were plasma-arc sprayed with alumina insulation (Linde A) and the nuts were heliarced to the studs after assembly. The weight of laminations built into the stack was 5.75 pounds. Total transformer weight was 8.47 pounds.

After assembly, the transformer was put through an Anadur insulation bake-out using the same time-temperature schedule as was used for the stator. Following this, a small amount of W-839 potting compound was added at the stack midpoint to retain the alumina spacers and thermocouple tubes. Potting was baked-out according to the same schedule used for the generator. Figure IV-29 shows some of the potting details and also shows the transformer resting on the frame which supports it in the thermal vacuum chamber.

The transformer assembly less thermocouples was installed in a liquid-nitrogen-trapped diffusion-pumped vacuum furnace for a preliminary degassing bake-out. The two solenoids covered under Task 4 were put through the same bake-out. After an equilibrium furnace temperature of 1100°F was established, the assemblies were baked for 43 hours. Initial chamber pressure at equilibrium was 4×10^{-6} torr and at the end of the bake-out it had decreased to 2.6×10^{-6} torr. After cooling off, the furnace chamber was back-filled with argon and the assemblies were stored this way until installation in the thermal vacuum chamber.

c. THERMOCOUPLE SYSTEM

Thermocouples were positioned in the transformer just before installation in the thermal vacuum chamber. The same thermocouple system used with the stator was used with the transformer including the vacuum chamber hollow Kovar tube feedthroughs.

d. THERMAL VACUUM CHAMBER INSTALLATION

Residual gas analysis scans were taken with the Varian No. 2 thermal vacuum chamber evacuated and at chamber temperatures of 77°, 1100° and 1500°F to obtain background data. The chamber was then brought up to ambient pressure under argon preparatory to installing the transformer assembly and the two solenoid assemblies from Task 4.

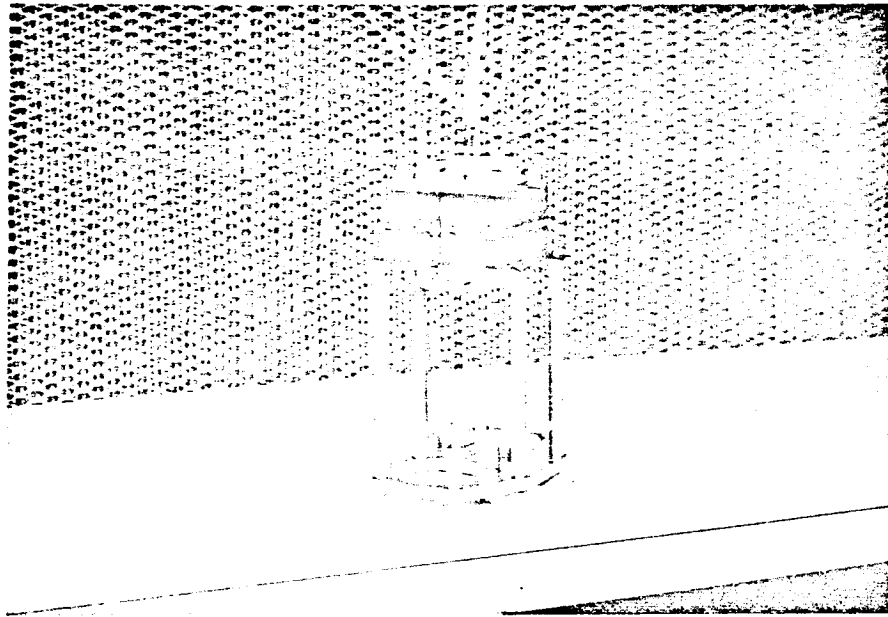


FIGURE IV-29. Transformer in Position on Furnace Mounting Frame

The installation procedure for the transformer and solenoids was the same as that used for the stator. The clean bench was moved up to the chamber to supply filtered air, and after installation of thermocouples the models were moved into the test chamber. Figure IV-30 is a cutaway drawing of the thermal vacuum chamber showing the transformer and solenoids installed in the furnace hot zone. After brazing of model power leads and thermocouples, lead integrity was verified and the chamber was closed, evacuated and leak checked.

e. TRANSFORMER TEST CIRCUITRY

Figure IV-31 is a schematic showing the test circuitry for applying power to the transformer primary winding and loading the secondary winding. Single-phase power from a 400 cps, 292 volt a-c line-to-neutral three-phase generator was brought into the test area. A variac and a 1:4 step-up transformer were used to provide a 600 volt a-c source for the test transformer primary winding. A resistive load bank with multiple series switches was used as an adjustable load for the secondary winding.

f. TRANSFORMER TEST PROCEDURE

After electrical continuity of the thermocouples and winding leads had been checked (transformer and solenoids), the thermal vacuum chamber was closed up and pumped down using a cryogenic pump. When the thermocouple gauge reached 7 to 8 microns pressure, the ion pump was energized. Several titanium sublimation pump bursts were used to help the pump get started. Thermocouple brazed joints were leak checked and several required additional sealing to form vacuum tight joints.

When chamber pressure reached a value of 8×10^{-7} torr, room temperature base-line static electrical measurements were made on the transformer and solenoids, and the transformer secondary load bank was adjusted. The titanium sublimation pump was cycled for an hour and when the pressure decreased into the 10^{-8} torr range, a 24 hour chamber bake-out at 250°C was started. Cold chamber pressure after the bake-out was 9.3×10^{-10} torr.

In an effort to reduce the base pressure, a second 24 hour bake-out cycle was initiated. Cold chamber pressure, after this cycle, reached a value of 4.6×10^{-10} torr, and the chamber was judged ready for the application of model test loads and furnace heater power to bring the test models up to test temperature. This event coincided with the completion of the fourth program quarter.

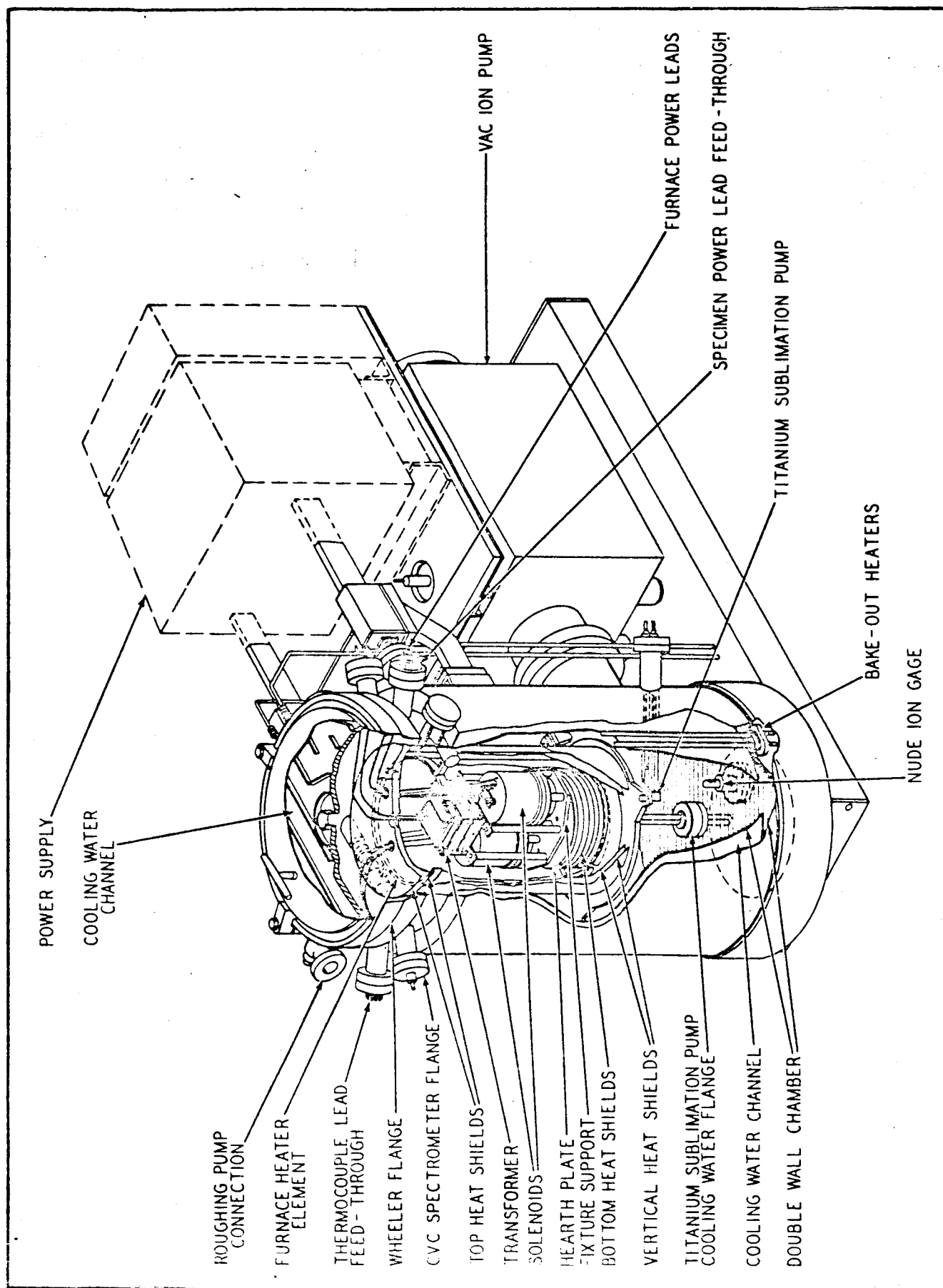


FIGURE I V-30. Cutaway View of a Vacuum Furnace Showing Installation of Two Solenoids and a Transformer

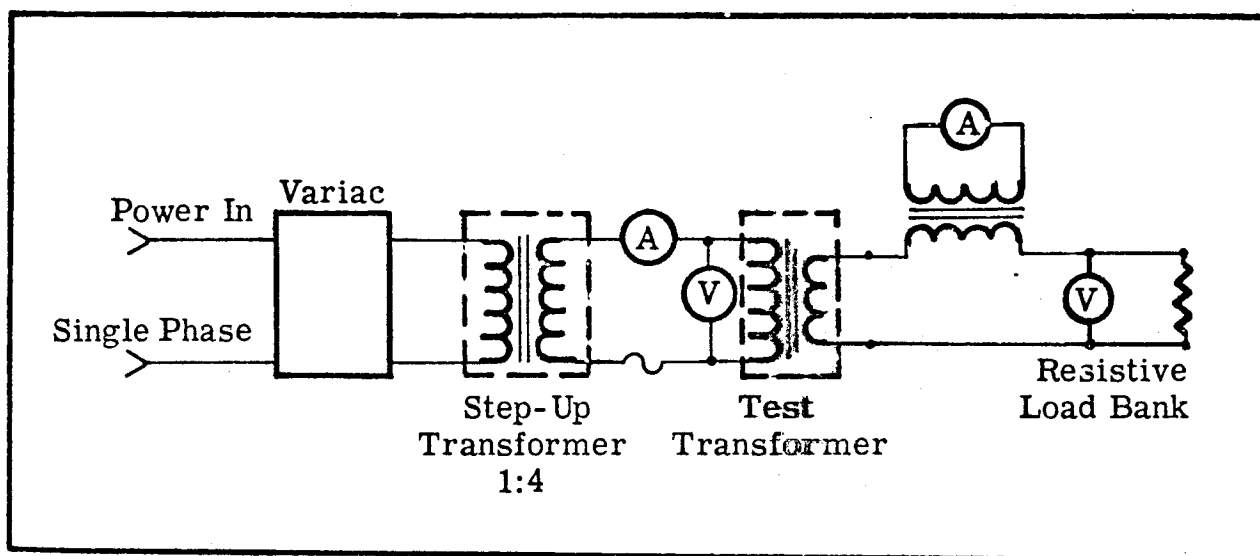


FIGURE IV-31. Electrical Test Schematic for the 1 KVA Rated Transformer

Bench test electrical measurements covering conductor resistance, d-c insulation resistance and a-c potential electrical leakage had been taken prior to installation of the transformer and solenoids in the chamber. As mentioned previously, these measurements were repeated at room temperature under vacuum conditions, and they will be repeated periodically as the test progresses. Residual gas analysis scans will also be taken periodically.

g. DATA EVALUATION

The transformer was designed to be a 1 KVA working model. The resistive load banks outside the vacuum chamber were adjusted for a secondary winding load of 29.8 amperes at 29.1 volts. The primary winding input was 1.84 amps at 600 volts a-c, giving an input power of 1104 volt-amperes and a load of 867 watts on the secondary.

Figure IV-32 is a plot of thermal vacuum chamber nude ion gauge pressure against time, from start-up of the ion pump after chamber evacuation through two 24 hour system bake-outs at 482°F (250°C). Pressure readings were monitored periodically, but not recorded during the bake-out cycles. Thus the plot shows dotted lines rather than the pressure transients that occur during bake-out. The titanium sublimation pump was cycled several times to help reduce chamber pressure. The plot covers time up to the end of the reporting period.

Table IV-8 is a tabulation of electrical measurements taken during bench test and with the transformer installed in the chamber. The decrease in winding resistances between the bench and chamber tests occurred because some lead length was removed to fit the leads to the power feedthroughs in the vacuum chamber. Insulation resistance improved under vacuum conditions, as was noted in the stator test. There was also some reduction in leakage current under vacuum conditions.

Figure IV-33 is a sketch showing the location of thermocouples in the transformer. Eight thermocouples were installed before the transformer was put into the thermal vacuum chamber, two of which were lost during brazing. However, each sensing location has at least one good thermocouple because dual instrumentation was incorporated in the buildup in anticipation of possible thermocouple breakage.

3. Program for the Next Quarter

- a) Use transformer load and furnace power to establish a hot spot temperature of 1100°F.

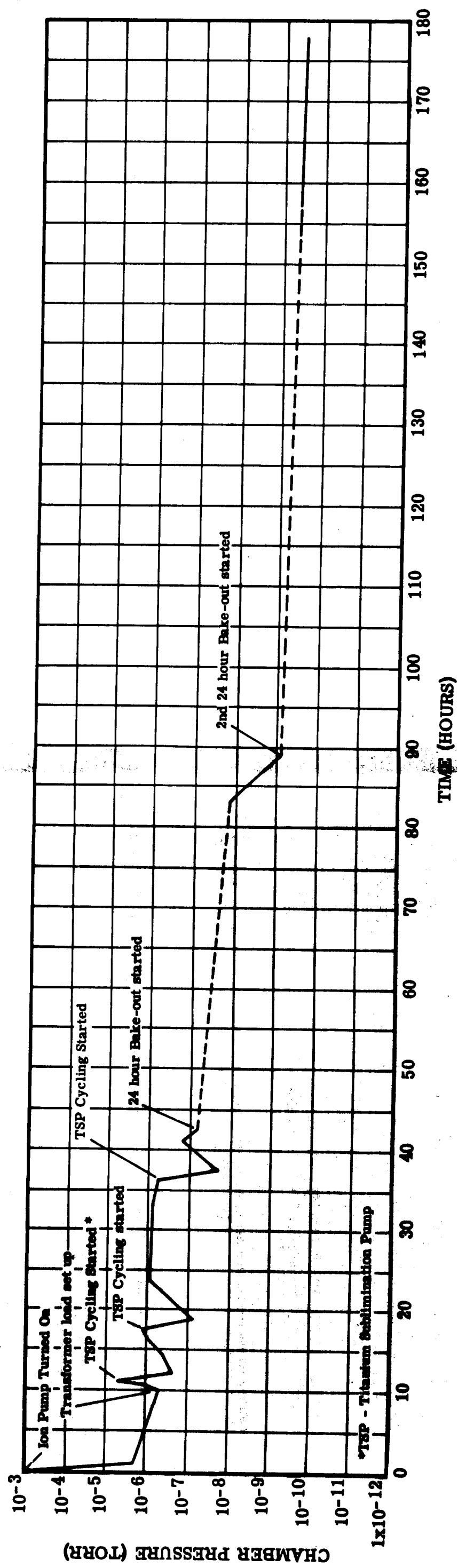


FIGURE IV-32. Chamber Pressure-Time Plot of Transformer and Solenoids in Varian Chamber No. 2

TABLE IV- 8. Tabulation of Transformer Electrical Readings

Measurement	Bench Test Room Ambient Pressure 81°F		In Thermal Chamber 6x10 ⁻⁷ torr 78°F	
<u>Winding Resistance</u>	<u>Ohms</u>		<u>Ohms</u>	
Primary	1.68		1.58	
Secondary	0.0074		0.0055	
<u>Insulation Resistance</u>	<u>Volts d-c</u>	<u>Megohms</u>	<u>Volts d-c</u>	<u>Megohms</u>
Primary to Secondary	500	5x10 ²	500	2x10 ⁶
Primary to Ground	500	1.5x10 ⁴	500	2x10 ⁶
Secondary to Ground	500	1.5x10 ⁴	500	2x10 ⁶
<u>Potential Test</u>	60 cps <u>Volts a-c</u>	<u>μ A</u>	60 cps <u>Volts d-c</u>	<u>μ A</u>
Primary to Secondary	750	20	750	20
Primary to Ground	750	54	750	20
Secondary to Ground	750	48	750	22

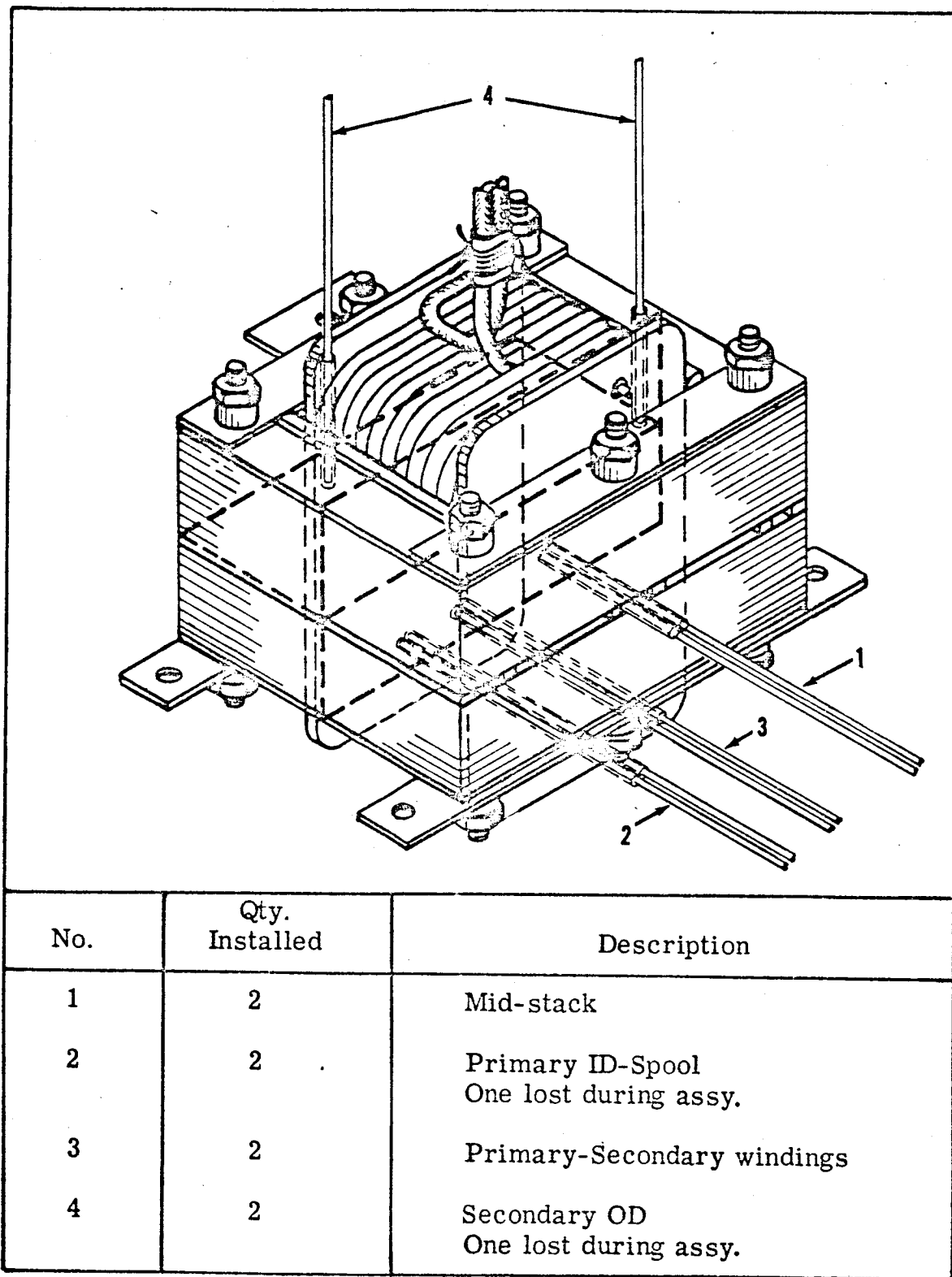


FIGURE IV-33. Transformer Assembly Showing Thermocouple Locations and Junction Positions

- b) Develop a residual gas analysis computer matrix to identify components.
- c) Work on a transformer heat flow model within the limits of temperature instrumentation.
- d) Review the transformer design for changes needed in a 1400°F hot spot model.

D. TASK 4 - SOLENOID

1. Summary of Technical Progress

- a) The manufacture and assembly of two solenoids was completed.
- b) After assembly, the solenoids were given a 43 hour outgassing bake-out at 1100°F in a liquid-nitrogen-trapped diffusion-pumped vacuum furnace.
- c) Thermal vacuum chamber installation of the solenoids was completed and chamber pump-down and final bake-out was carried out.
- d) Minimum cold chamber pressure attained after system bake-out was 4.6×10^{-10} torr.
- e) Base line solenoid electrical measurements and chamber residual gas analysis scans were obtained.

2. Discussion

a. SOLENOID PHYSICAL AND ELECTRICAL DESIGN AND CONSTRUCTION

Figure IV-34 is a cutaway view of the solenoid showing the location of the coil leads and thermocouples. A weight of three pounds is suspended on the plunger, and when the solenoid is activated, the weight is lifted approximately 0.050 inch and held in that position. The solenoid magnetic housing, cover and plunger are made from Hiperc 27 alloy forged material. The coil is wound on an alumina spool which provides insulation between the winding and the plunger and housing center core. Alumina end plates insulate the sides of the winding from the housing and cover. Bearing surfaces for the plunger consist of an alumina guide rod at one end of the plunger and an alumina bushing at the opposite end.

Electrically, the solenoid design is rated at 1530 ampere turns with 28 volts d-c applied to the winding at a winding temperature of 1100°F.

b. SOLENOID ASSEMBLY

When all shop operations had been completed, the solenoid parts were cleaned according to the cleaning specifications included in Appendix B of the third quarterly report. The only material not cleaned was the Anadur coated nickel-clad silver wire.

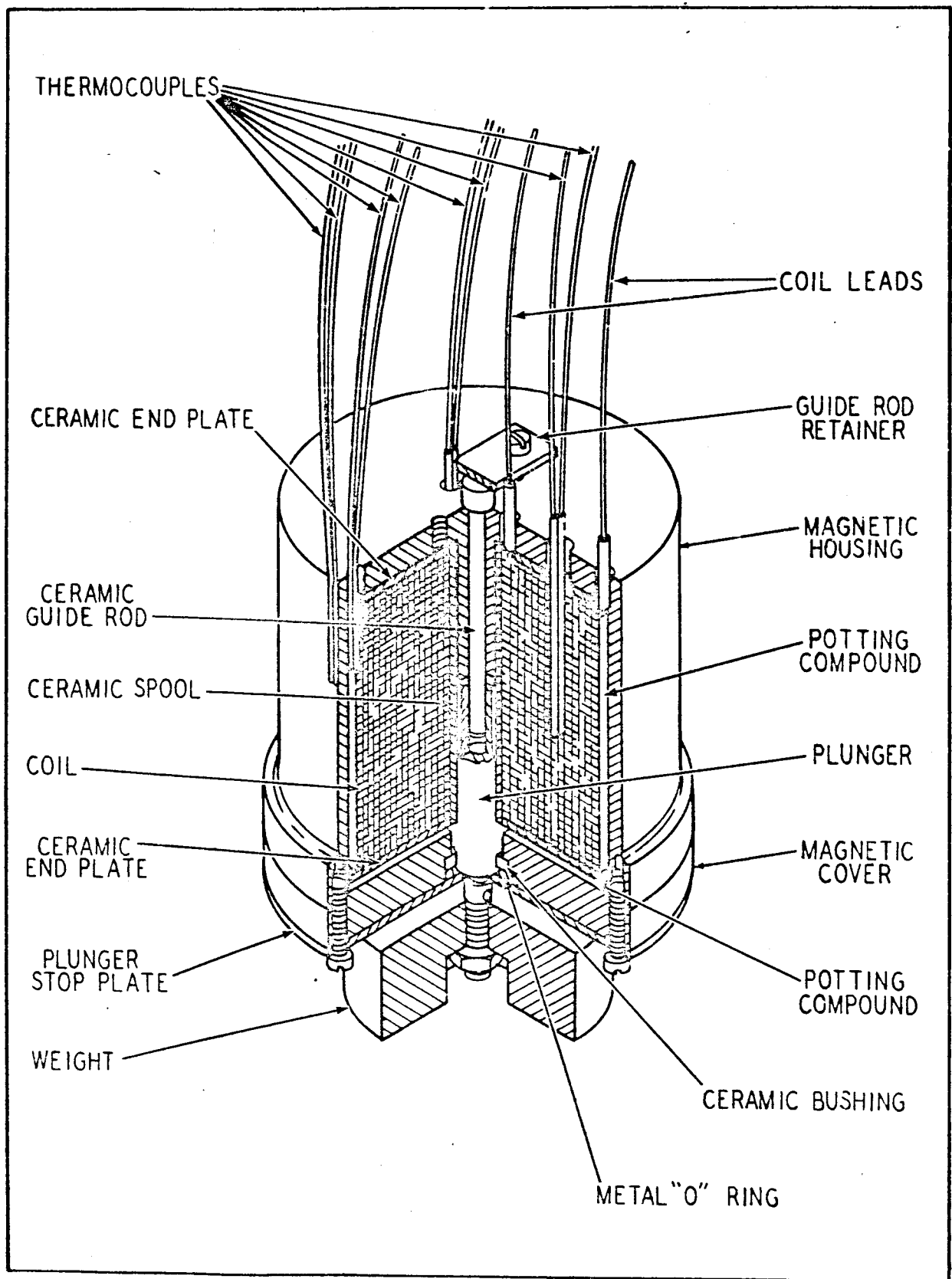


FIGURE IV-34. Cutaway View of Solenoid

The solenoid windings were formed on a winding arbor which was mounted on a winding machine, but the machine spindle was turned by hand and the wire was guided by hand. Eighteen hundred and sixty turns were put on each coil. Figure IV-35 shows a completed winding on the winding arbor. Alumina thermocouple tubes can be seen protruding through the top arbor plate. Figure IV-36 shows one winding on the arbor after the Anadur bake-out cycle. The other winding has been removed from the arbor and the alumina end plates have been installed and held in place with W-839 potting compound. The weight of the winding as shown is 4.0 pounds. The fragility of the Anadur conductor insulation after bake-out can be seen by noting the bare spots on the lead wires.

Figure IV-37 is an exploded view of a solenoid housing, plunger and weight assembly. The completed winding assembly shown in Figure IV-36 fits over the center post inside the housing, which also serves as a stop for the plunger. The end of the post has been plasma-arc sprayed with alumina to prevent "cold welding" between the plunger and post. Holes for the thermocouple tubes and lead wires can be seen in the bottom of the housing. The end bell shows the counterbore for the alumina bushing and metal O-ring. The end plate acts as a stop for the plunger when the solenoid is not energized. The alumina guide rod fits the hole in the housing center post and extends beyond it to provide a bearing guide for a close tolerance hole drilled in the plunger. The opposite end of the plunger rides in the alumina bushing which acts as a second bearing for the plunger. The metal O-ring is used as a semi-flexible ring to load the bushing at low temperatures and compensate for differential thermal expansion at high temperatures. The end of the plunger which rests against the end plate is coated with plasma-arc sprayed alumina, again to prevent cold welding with the end plate. Both the plunger and weight are threaded and a lock nut (not shown) is added after the weight is installed.

Before the installation of the winding assembly into the housing, four axial strips of W-839 potting compound were added to help keep the windings in place. After installation, four radial strips of potting compound were added to the alumina winding end plate adjacent to the end bell to take up the axial slack with the end bell in place. The end bell was installed and this portion of the solenoid assembly was given a potting compound bake-out. Then the plunger and bearing system was installed and the end plate was added. The last part to be added to the assembly was the weight.

Figure IV-38 shows a photograph of both solenoids complete, except for the thermocouples, just before being put through a 43 hour outgassing bake-out with the transformer.

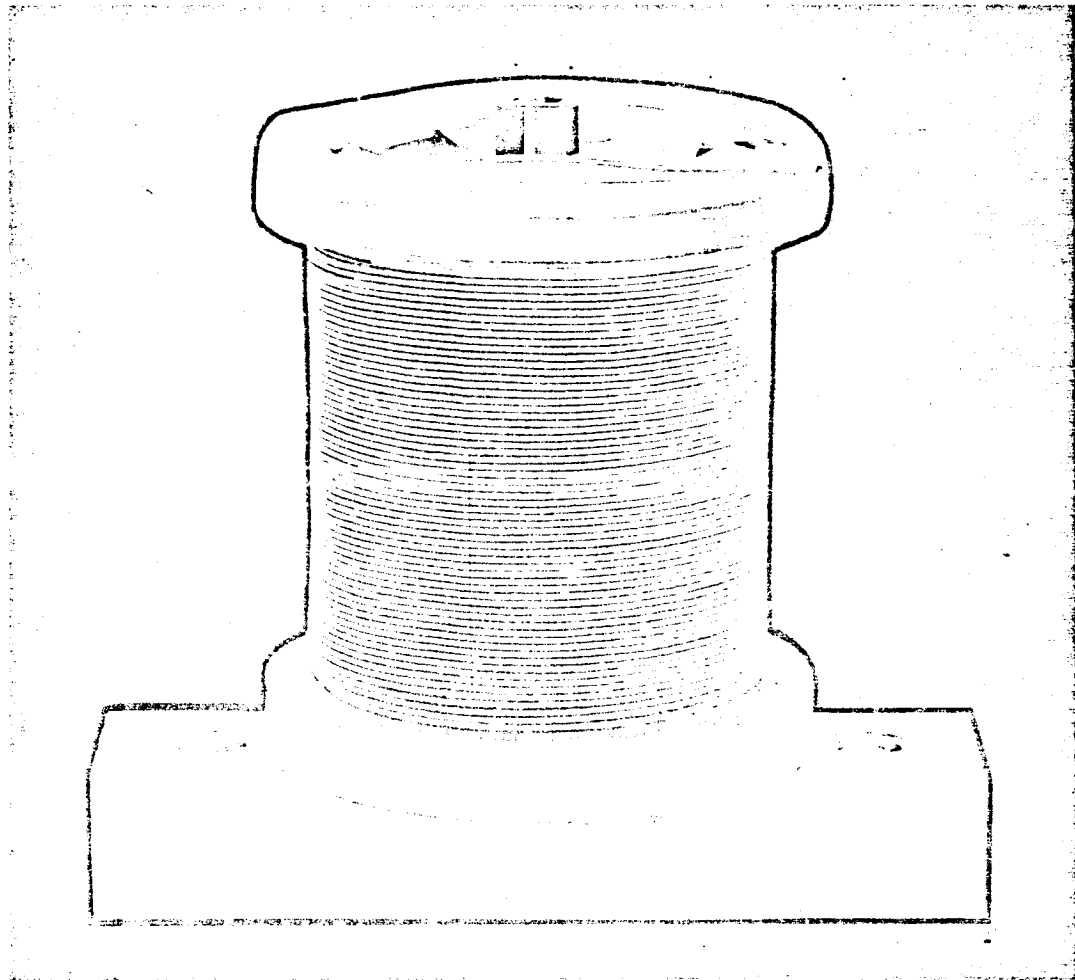


FIGURE IV-35. Solenoid Winding on Arbor Before Anadur Bake-Out

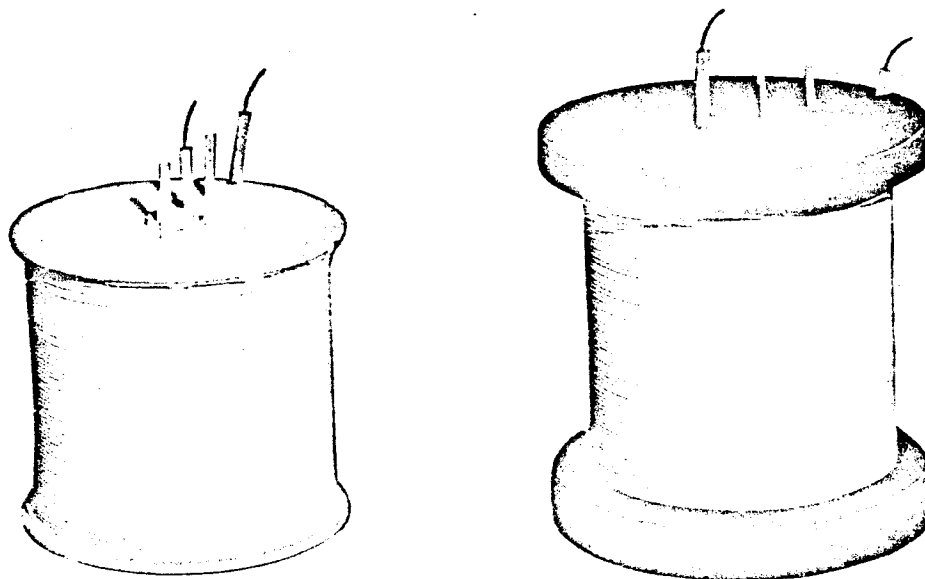


FIGURE I V-36. Solenoid Winding Assembly and Solenoid Winding on Arbor After Anadur Bake-Out

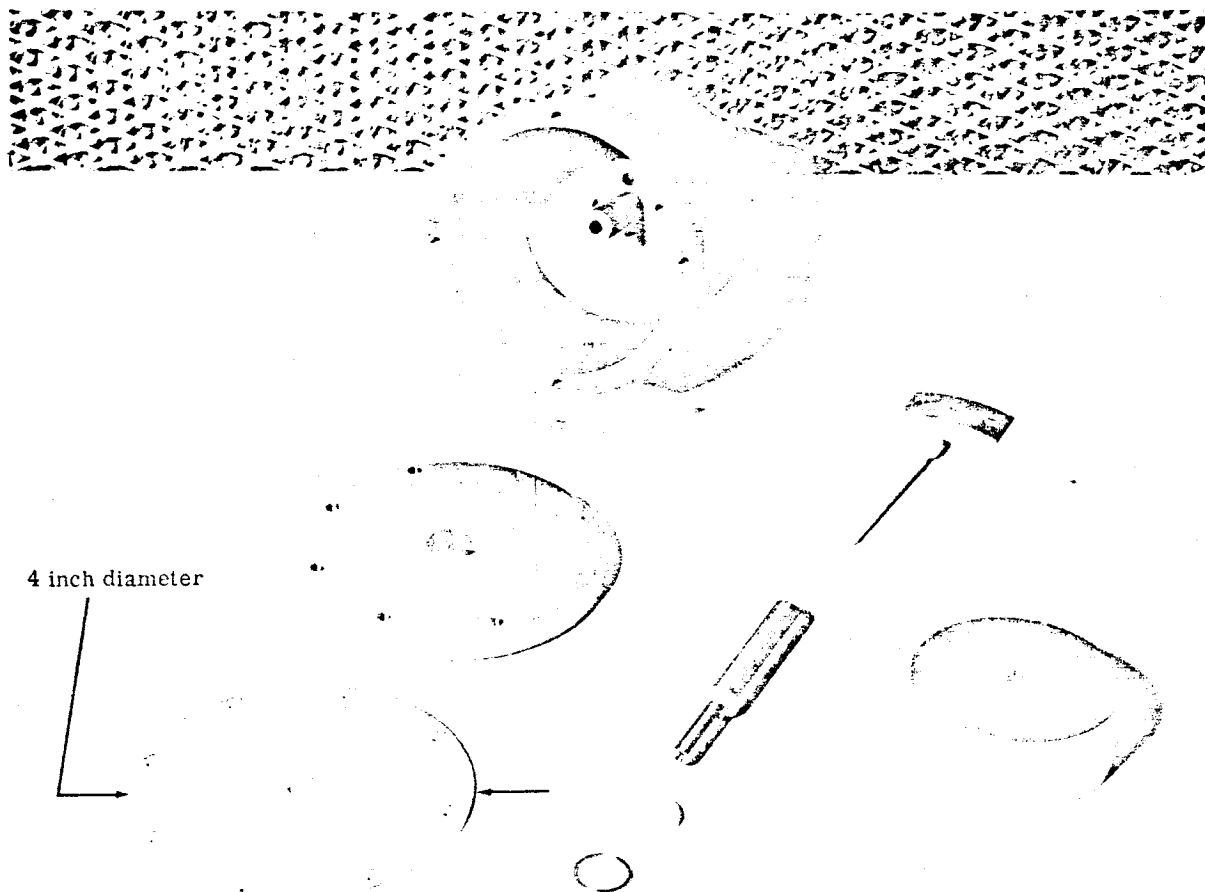


FIGURE IV-37. Solenoid Housing Assembly

Figure IV-39 shows a photograph of the solenoids and transformer in place on the frame which supports them when installed in the thermal vacuum chamber.

One potential problem occurred with the solenoids as well as with the stator and transformer. The threads in threaded holes and on screws and studs went together easily before parts were cleaned. The cleaning procedures used removed all traces of lubricant and extreme caution was required when assembling threaded parts to prevent galling and seizing.

c. SOLENOID TEST CIRCUITRY AND TEST PROCEDURE

Figure IV-40 is a schematic showing the test circuitry for applying d-c power to the solenoid windings. Only one d-c power supply was required, as one solenoid is energized continuously except for periodic electrical measurements and the other is only actuated periodically to verify operation. The variable d-c power supply allows the winding current to be adjusted as required to match the energized solenoid hot-spot temperature with that of the transformer.

Since the two solenoids were installed in the same thermal vacuum chamber as the transformer, solenoid test procedure coincides with the transformer procedure, Section IV. C. 2. f.

d. DATA EVALUATION

The two solenoids were identified as Serial No. 1 and Serial No. 2 for data recognition purposes. The weight of the plunger, weight and lock nut was 2.98 pounds for each solenoid. Electrical measurements were made to find the minimum weight pick-up voltage and current and minimum holding current and voltage for each solenoid.

	<u>Serial No. 1</u>	<u>Serial No. 2</u>
Minimum Pick-up Voltage - d-c	4.9	3.9
Minimum Pick-up Current - Amps	0.41	0.34
Minimum Holding Voltage - d-c	0.9	0.85
Minimum Holding Current - Amps	0.065	0.056

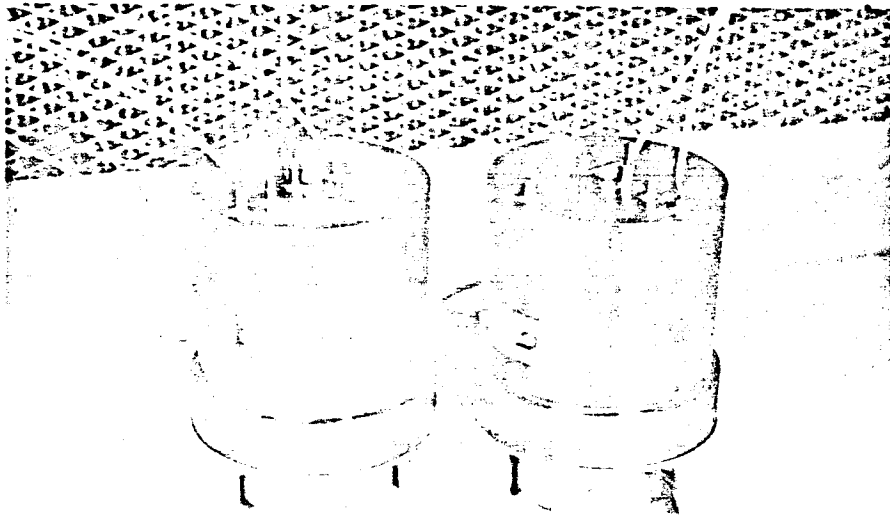


FIGURE IV-38. Solenoid Assemblies Complete Except for Thermocouples

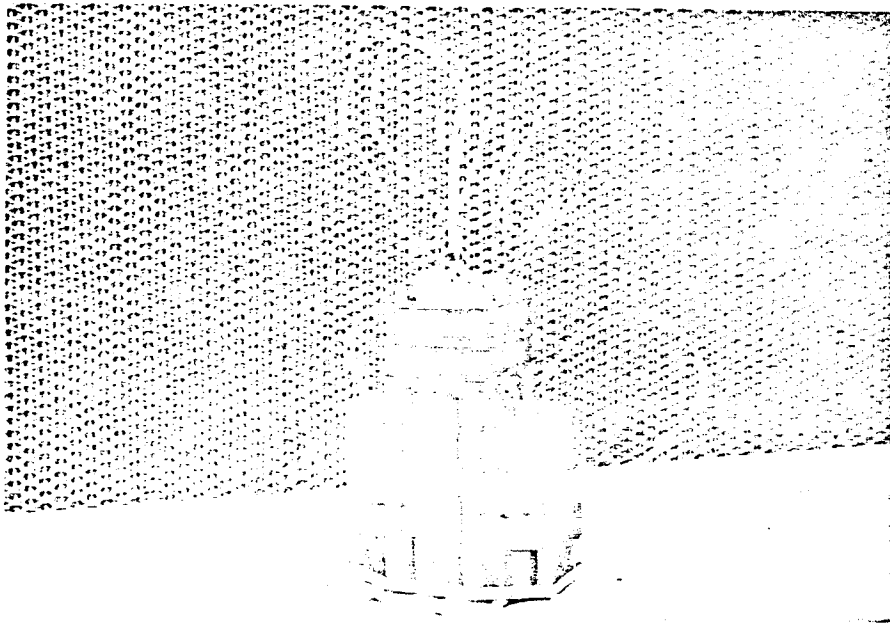


FIGURE IV-39. Transformer and Solenoids on Furnace Mounting Frame

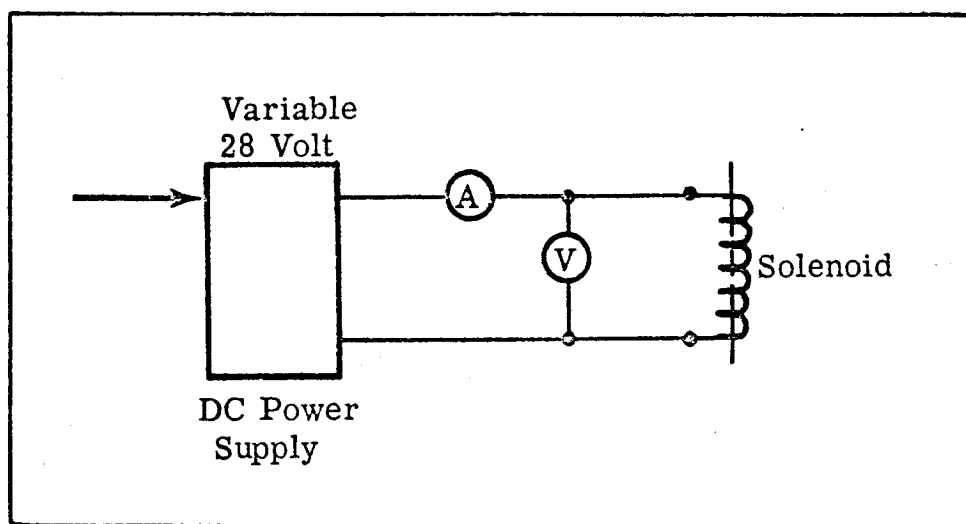


FIGURE IV-40. Solenoid Circuitry

The variation in minimum pick-up voltage between the solenoids was attributed to differences in friction between the plunger and the 99% Al_2O_3 bushing and guide rod which serve as bearings.

Winding resistance and insulation resistance measurements were made on both solenoids at the clean bench and again after installation in the thermal vacuum chamber. Readings are tabulated below.

<u>Serial No. 1</u>	<u>Room Ambient Bench Test 79°F</u>	<u>Chamber at 6×10^{-7} torr 78°F</u>
Winding Resistance	12.05 Ohms	13.74 Ohms
Insulation Resistance - Winding to Ground at 500 V d-c	7×10^4 Megohms	15×10^5 Megohms
<u>Serial No. 2</u>		
Winding Resistance	11.43 Ohms	13.04 Ohms
Insulation Resistance - Winding to Ground at 500 V d-c	14×10^4 Megohms	15×10^5 Megohms

Winding resistance for both solenoids increased after chamber installation and evacuation of the thermal vacuum chamber. Resistance decreased after installation of the stator and transformer, because in each case some lead length was removed to fit the leads to the chamber feedthroughs. The solenoid bench and chamber readings were made by two different operators using a Wheatstone bridge, and instrument accuracy and application may account for the difference.

Insulation resistance improved under vacuum conditions as was noted with the stator and transformer.

Figure IV-41 is a sketch showing the location of thermocouples in each solenoid. Eight thermocouples were installed in each solenoid before chamber installation, and of the sixteen, one was lost during brazing.

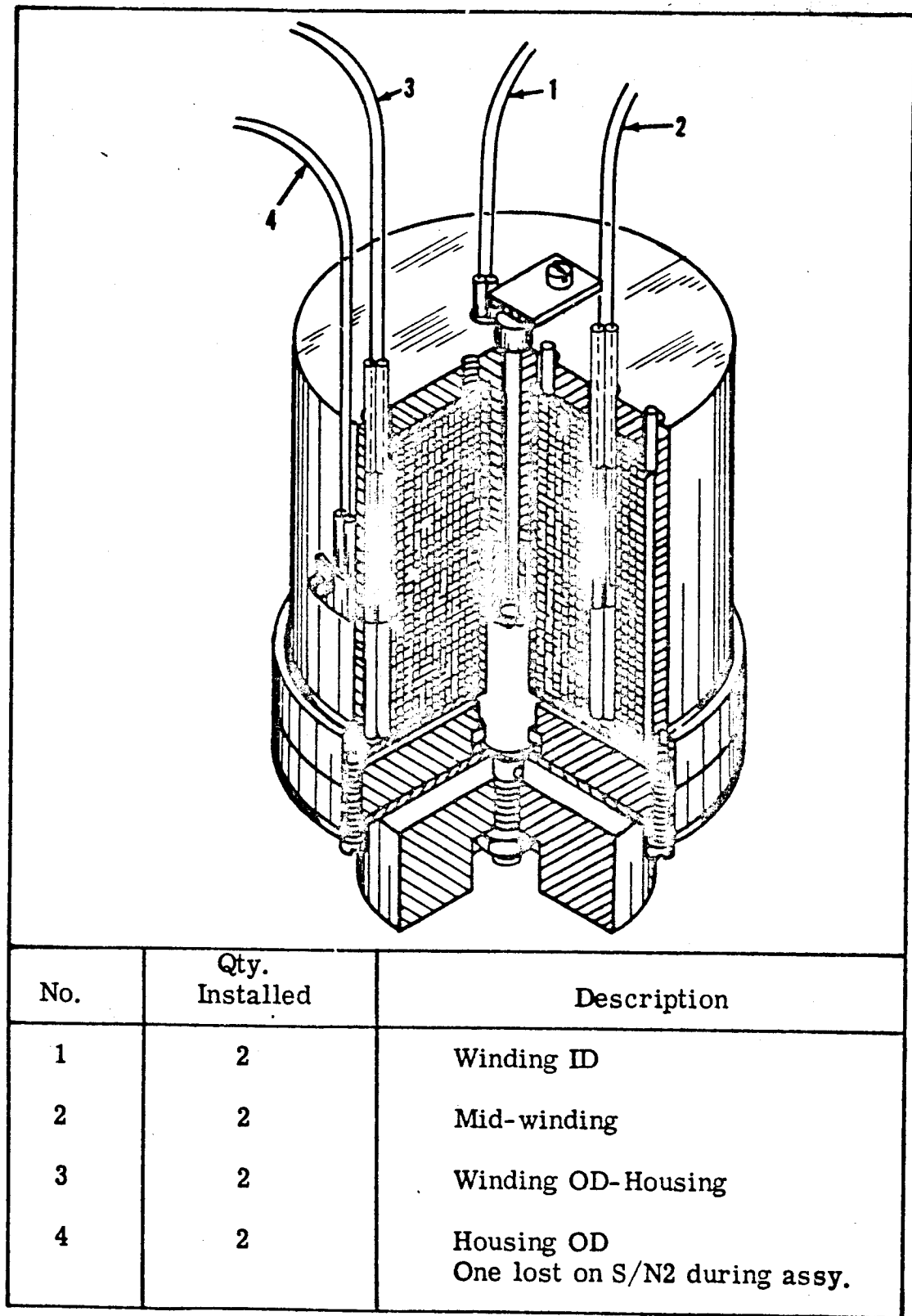


FIGURE IV-41. Solenoid Assembly Showing Thermocouple Locations and Junction Positions

3. Program for the Next Quarter

- a) Use the energized solenoid and furnace power to establish a hot-spot temperature of 1100°F.
- b) Work on a solenoid heat flow model within the limits of temperature instrumentation.
- c) Review the solenoid design for changes needed in a 1400°F hot-spot model.

SECTION V

REFERENCES

Reports published on this program are:

Kueser et al, P. E., "Development and Evaluation of Magnetic and Electrical Materials Capable of Operating in the 800° to 1600°F Temperature Range, "First Quarterly Report, NASA-CR-54354, March 1965.

Kueser et al, P. E., "Development and Evaluation of Magnetic and Electrical Materials Capable of Operating in the 800° to 1600°F Temperature Range, "Second Quarterly Report, NASA-CR-54355, June 1965.

Kueser et al, P. E., "Development and Evaluation of Magnetic and Electrical Materials Capable of Operating in the 800° to 1600°F Temperature Range, "Third Quarterly Report, NASA-CR-54356, September 1965.

References cited in this report follow and are grouped by Program and Task.

Section II

Program I - Magnetic Materials for High-Temperature Operation

References for Task 3 - Dispersion-Strengthened Magnetic Materials for Application in the 1200-1600°F Range.

1. R. C. Haverstraw, "Final Report On High Temperature Extrusion Lubricants", Technical Documentary Report NR ML-TDR-64-256, July 1964, Contract AF 33(657)-9141, Air Force Materials Laboratory, Wright-Patterson Air Force Base, Ohio (AD-606243).
2. T. W. Black, "Better Forging Lubricants Double Die Life", Machinery, October 1965, pp. 99-102.

3. I. Perlmutter and V. De Pierre, "Extruding Refractory Metals", Metal Progress, November 1963, pp. 90-95, 128-136.
4. A. M. Sabroff, "Lubricants For High-Temperature Metalworking Process", Metals Engineering Quarterly, May 1963, V. 3, No. 2, pp. 31-35.
5. "Product Information - Glass Lubricants for Metal Forming", Bulletin IC-18, June 15, 1961, Corning Glass Works, Corning, New York.
6. R. T. Howard and M. Cohen, "Quantitative Metallography by Point Counting and Lineal Analysis", Trans. AIME, v. 194, 1947, pp. 413-426.
7. C. S. Smith, "Microstructure", Trans. ASM, v. 45, 1953, pp. 533-575.
8. C. S. Barrett, Structure of Metals, Second Edition, 1952, McGraw-Hill, p. 86.
9. A. Taylor, X-ray Metallography, 1961, John Wiley & Sons, p. 663.
10. H. H. Stadelmaier, "Ternary Borides with the Cubic Chromium Carbide Structure", Met. Soc. AIME, Nuclear Metallurgy, v. 10, 1964, pp. 159-166.
11. H. H. Stadelmaier and G. Hofer, "Cobalt-Rich Corner of the Cobalt-Tantalum-Boron System and the $\text{Co}_{21}\text{Ta}_2\text{B}_6$ Phase", Metall, v. 18, no. 5, May 1964, pp. 460-462.
12. K. Detert and B. Ballough, private communication.
13. F. Förster, "Production Unit for the Rapid and Accurate Measurement of the Coercive Force and Its Temperature Dependence", Zeit Metallkunde, v. 46, no. 4, 1955, p. 359.

14. K. Hoselitz, Ferromagnetic Properties of Metals and Alloys, Oxford, Clarendon Press, 1952, p. 131.
15. R. Pauthenet "Magnetic Properties of Cobalt and of some Cobalt Alloys and Ionic Compounds", Cobalt, no. 26, March 1965, pp. 3-9.
16. A. S. Bufferd and N. J. Grant, "Oxide Dispersion Strengthening of Cobalt-Base Alloys", Journées Internationales des Applications du Cobalt, June 9-11, 1964, pp. 1-11.
17. B. Triffleman, "A New Pre-Alloyed Powder Process and Products", Progress in Powder Metallurgy 1962, v. 18, Metal Powder Industries Federation, New York, N. Y.

Reference for Task 4 - Creep Testing

18. Spur Generator Development Program. July 15, 1964, Westinghouse Electric Corp., Aerospace Electrical Division, Lima, Ohio.

Section III

Program II - High Temperature Capacitor Feasibility References

1. Anon, General Radio Catalog S. Standard Capacitors pp. 184-85, General Radio Company, West Concord, Mass, July 1965.
2. von Hippel A. R., "Mobilization of Charge Carriers in Liquids and Solids", Chapter 21, pp. 363-64; Molecular Science and Molecular Engineering, A. R. von Hippel et al. John Wiley and Sons, 1959.

Section IV
Program III - Bore Seal Development and Combined Material
Investigation under a Space-Simulated Environment

References for Task 1 - Bore Seal Development

1. Honig, R. E., "Vapor Pressure Data for the Solid and Liquid Elements",
Reprint from RCA Review, XXIII, 567 (1962).